

Vibration Analysis of Perforated Plates

THESIS

Submitted in partial fulfilment
of the requirements for the degree of

DOCTOR OF PHILOSOPHY

by

MALI KIRAN DINKAR

Under the Supervision of

Prof. Pravin M. Singru



BITS Pilani
Pilani | Dubai | Goa | Hyderabad

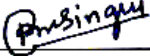
BIRLA INSTITUTE OF TECHNOLOGY AND SCIENCE, PILANI

2015

BIRLA INSTITUTE OF TECHNOLOGY AND SCIENCE, PILANI

CERTIFICATE

This is to certify that the thesis entitled “**Vibration Analysis of Perforated Plates**” and submitted by **MALI KIRAN DINKAR** ID No. **2008PHXF012G** for award of Ph.D. of the Institute embodies original work done by him/her under my supervision.

Signature of the Supervisor: 

Name: **Dr. PRAVIN M. SINGRU**

Designation: **Associate Professor**

Dept. of Mechanical Engineering,

K.K. Birla Goa Campus, Goa

Date: **29/09/2015**

ACKNOWLEDGEMENTS

I would like to express my sincere appreciation to all those people who made this research possible.

First and foremost I owe my deepest gratitude to my supervisor, Dr. Pravin M. Singru Associate Professor of Mechanical Engineering. He has been supportive since the days I began working on this research. He has supported me not only by providing a research inputs, but also academically and emotionally through the road to finish this work. His stimulating suggestions and encouragement helped me to develop new analytical models and writing of this thesis.

I am grateful to Prof. V.S. Rao Vice Chancellor, Prof. B. N. Jain, Ex-Vice Chancellor and Prof. L.K. Maheswari, Advisor to Chancellor, and Prof. S. K. Verma, Dean, Research and Consultancy Division, BITS Pilani, for granting me an opportunity to conduct research at this renowned institute and also for assuring the availability of necessary infrastructure and facilities to carry out my work. I wish to offer my sincere thanks to Prof. Sasikumar Punnekkat, Director, BITS Pilani-K. K. Birla Goa Campus, for his constant encouragement and support. Sincere thanks are also due to Prof. K.E. Raman and Late Prof. T. C. Goel, former Director, BITS Pilani-K. K. Birla Goa Campus, for his valuable motivation and inspiration to the work towards my Ph.D. degree.

I would like to extend my sincere gratitude to Prof. Prasanta Kumar Das , Associate Dean, ARD, BITS Pilani-K. K. Birla Goa Campus and Prof. S. D. Manjare, Faculty In-charge, Research and Consultancy and Education Development Division, BITS Pilani-K. K. Birla Goa Campus, for helping me through out with their valuable inputs on this research and thesis.

All the relevant facilities such as computing facilities, workshop facilities and laboratories associated with Department of Mechanical Engineering, BITS Pilani-K.K. Birla Goa campus are appreciated and acknowledged.

I would like to thank Prof. B. J. C. Babu and Prof. D. M. Kulkarni for graciously agreeing to be a part of my DAC committee and for their valuable suggestions. Especially suggestions given by Dr. B.J.C. Babu to carry out experimentation were very helpful and suggestion given by Dr. D.M. Kulkarni regarding inclusion of rectangular perforations and staggered pattern in the study was helpful to make sound analytical models.

Special thanks are due to Prof. Shibu Clement, Dr. Rakesh Mote and Dr. Sachin Waigaonkar for their encouragement and for sharing with me things related to thesis organization.

A special acknowledgement goes to Assistant Workshop Superintendent Mr. Vijay Suryawanshi, Technician Mr. Viraj Gaonkar and all technical and supporting staff of workshop for providing me helps in preparation of experimental set up.

I would also like to extend my thanks to all my colleagues and friends Dr. Rajaram, Dr. Abhishek Kumar, Dr. Vikas, Mr. Sreedhar, Mr. Ramkumar, Dr. C. P. Kiran , Dr. Varinder Singh and Mr. Pravin Mane for their, support and encouragement that gives me more confidence and motivate. Over the period of this research, I have shared happy moments and tough times with my friends and colleagues Dr. Raghavendra Naik and Dr. Dillipkumar Mohanty, I am grateful for this.

Heartfelt thanks to my father, mother, brothers and parents in law for their affectionate support and unconditional love. Last but not least, I want to thank my wife Priya for all the support that she gave me during the period of this research, especially all the holidays that she arranged to give me time to write, to think. I would like to express my deepest appreciation and love to my lovely son Advay. Thank you for blessing me with your presence, patience and good humour. Without them, I would not have been able to achieve what I have today.

Finally, I sincerely thank all those, who have helped, encouraged and supported me either directly or indirectly during my research work.

Above all, I give thanks to God.

Kiran Dinkar Mali

April, 2015

Abstract

Plates are used as structural elements in major engineering applications. It is common to see openings in these plated structures for various reasons. For example, openings are needed for electric wiring, water pipes, plumbing etc. In case of the perforated plates, openings are often introduced in the regular array. Industrial applications use both the rectangular and triangular array of the perforations. The existence of large open area can change the mass distribution and stiffness around the opening regions, thus changing the vibration characteristics of the plates. The extent to which the perforations can change the vibration behavior of the plated structures depends on the size, shape, locations, numbers and type of the perforation pattern. Existing literature on free vibration of the perforated plate lacks formulation of the analytical models. Existing studies are more related to the determination of the equivalent material properties and their use in calculation of the fundamental frequency. In this thesis, analytical models are formulated to determine the fundamental frequency of the thin perforated plates. Approximate analytical methods such as the Rayleigh's method, Rayleigh's-Ritz method and the Galerkin method are used to formulate the analytical models. For analytical models different aspects are considered for plates with clamped all edges. Analytical models are formulated for the rectangular plates with circular/rectangular/square openings arranged in the regular array. Proposed analytical models are based on the special functions to express the variation of the material properties due to the perforations, negative mass concept for perforation and replacing circular perforation with the equivalent square perforation. Expression for modal constant for fundamental frequency of perforated plate is also determined. To establish this modal constant, experimental vibration data is used. The parameters of interest are the size of the opening, the ratio of the area of full solid plate to that of perforated plate, type of perforation pattern and the aspect ratio of the plate. A simple approximate formula for the fundamental natural frequency of flexural vibration of rectangular isotropic perforated plate is developed using this modal constant. New analytical models proposed for thin plates are validated by comparing numerical results with FEM (Finite Element Method) and experimental results. Also one analytical model is formulated for the moderately thick perforated plates by using the Mindlin plate theory. Results obtained are compared with those obtained from the Kirchhoff plate theory and FEM. It is observed from the validation, proposed models with proper cautions can be used to predict the fundamental frequency.

Contents

Acknowledgement	i
Abstract	iii
Table of Contents	iv
List of Tables	xi
List of Figures	xiii
List of Commonly Used Symbols and Abbreviations	xvi
Chapter 1	1
Introduction	1
1.1 Background	1
1.2 Advantages of the Perforated Plate	1
1.3 Perforation Types and patterns	2
1.3.1 Perforation Types	3
1.3.2 Perforation Patterns	3
1.4 Motivation and Research Hypothesis	4
1.4.1 Motivation	4
1.4.2 Research Hypothesis	4
1.5 Objective and Scope	4
1.6 Organization of the Thesis	5
Chapter 2	7
Literature Review	7
2.1 Introduction	7
2.2 Vibration of Plates with Cut Outs and Perforations	7
2.3 Vibration of the Plates with the Non Homogeneous Material Properties	14
2.4 Vibration of the Plates with the Added Concentrated Mass	15
2.5 Gaps in the Existing Research	16
2.6 Concluding Remark	17

Chapter 3	18
Governing Equations and Formulation of the Problem	18
3.1 Introduction	18
3.2 Governing Equation of the Free Vibration of the Plate	18
3.3 Approximate Solution Methods	19
3.3.1 Rayleigh’s Method	20
3.3.2 Rayleigh-Ritz’s Method	22
3.3.3 Galerkin Method	23
3.4 Formulation of the Problem	25
3.4.1 The Rectangular Plates with the Rectangular/Square Perforations	25
3.4.2 The Rectangular Plates with the Circular Perforations	26
3.5 Validation of the Results Obtained by the Analytical Models	27
3.5.1 Validation by the Experimental Results of the Fundamental Frequency	27
3.5.2 Validation by the FEM Results of the Fundamental Frequency	27
3.6 Concluding Remark	27
Chapter 4	29
Experimental Determination of the Fundamental Frequency	29
4.1 Introduction	29
4.2 Parameters of the Perforated Plate Specimens	29
4.3 Details of the Fixture Used for Clamping the Plate Specimens	30
4.4 Experimental Set up and Procedure	32
4.5 Clamped All Edges Boundary Condition	33
4.5.1 Effect of Fit of the Bolts in the Plate-Fixture Assembly, On the Natural Frequency	33
4.5.2 Results and Discussions	34
4.5.3 Effect of the Spacing and the Number of Bolts Used To Clamp the Plate-Fixture Assembly, On the Natural Frequency	35
4.5.3 Results and Discussion	37

4.6 Effect of the Impact Location and the Hammer Tip on the Frequency Response Function (FRF)	39
4.6.1 Effect of the Impact Location:	39
4.6.2 Results and Discussion	40
□ Some Key Observations:	42
4.6.3 Effect of the Impact Hammer Tip:	42
4.7 Calculation of the Damping by Half Power Bandwidth Method	44
4.8 Concluding Remark	46
Chapter 5	47
Analytical Models for the Rectangular Plate with the Rectangular and Square Patterns of the Perforations	47
5.1 Introduction	47
5.2. Analytical Formulation	47
5.3 Rectangular Plates with the Square/Rectangular Perforations Arranged In the Square/Rectangular Array	48
5.4 Numerical Analysis	51
5.5 Validation of the Approach	51
5.6 Results and Discussions	52
5.6.1 Inferences About the Experimental Results	55
5.6.2 Comparison of the Analytical and FEM Mode Shapes	56
5.7 Square Plates with the Square Perforations Arranged In the Square Array	58
5.8 Numerical Analysis	61
5.9 Model Validation with the FEM Results	61
5.10 Results and Discussions	62
5.10.1 Comparison of the Analytical and FEM Mode Shapes	62
5. 11 Concluding Remarks	63
Chapter 6	64
Analytical Model for the Rectangular Plate with the Triangular	64

Pattern of Perforations	64
6.1 Introduction	64
6.2 Clamped Rectangular Plates with the 60 ° Triangular Perforation Pattern	64
6.3 Numerical Analysis	67
6.3.1 Analysis of the Plates with a Unit Cell of the Square Perforations	68
6.3.2 Analysis of the Plates with Fixed Outer Dimensions and Varying the Perforation Size	70
6.4. Validation of the Approach	70
6.5 Results and Discussion	71
6.5.1 Inferences about Experimental Readings	73
6.5.2 Comparison of the Analytical and FEM Mode Shapes	74
6.6 Clamped Rectangular Plates with the 45 ° Triangular Perforation Pattern	77
6.6.1 Plates with the square perforations in a staggered 45 ° perforation pattern:	77
6.6.2 Construction of the Material Property Variation Function	78
6.7 Numerical Analysis and Validation	80
6.8 Results and Discussion	81
6.8.1 Comparison of the Analytical and FEM Mode Shapes	82
6.9 Concluding Remark	82
Chapter 7	84
The Concentrated Negative Mass Approach	84
7.1 Introduction	84
7.2 Analytical Formulations	84
7.2.1 Equation of the Motion for an Isotropic Rectangular Plate	84
7.2.2 Determination of the Fundamental Frequency of the Plates with the Circular Perforations	87
7.3 Numerical Simulation	89
7.4 Validation of the Proposed Approach	89
7.5 Results and Discussions	90

7.6 Concluding Remarks	93
Chapter 8	94
An Equivalent Square Perforation Approach	94
8.1 Introduction	94
8.2. Analytical Formulation	94
8.2.1 Concept of an equivalent Square Hole for the Circular Perforation	94
8.2.2 Formulation of the Function to Express Non-Homogeneity in the Material Properties of the Plates with the Circular Perforations	95
8.2.3 Determination of the Fundamental Frequency of the Plates with the Circular Perforations	101
8.3 Numerical Simulation	103
8.4 Validation of the Proposed Approach	103
8.5 Results and Discussion	104
8.5.1 Comparison of the Analytical and FEM Mode Shapes	105
8.6 Concluding Remark	110
Chapter 9	111
Determination of the Modal Constant for the Fundamental Frequency	111
9.1 Introduction	111
9.2 Analytical Formulation	111
9.2.1 Analytical Solution	112
9.2.2 Geometry of the Perforated Plate with the Rectangular Perforation Pattern	113
9.3 Materials and methods	114
9.3.1 Experimental Analysis	115
9.3.2 FE Analysis	115
9.4 Results and Discussion	116
9.4.1 Determination of the Modal Constant	118
9.5 Application and Accuracy of the Approach	119
9.6 Concluding Remark	120

Chapter 10	121
Plates with the Circular Perforations in the Rectangular Array	121
10.1 Introduction	121
10.2 Analytical formulation	121
10.3 Numerical Analysis and Validation	124
10.4 Results and Discussion	125
10.4.1 Comparison of the Analytical and FEM Mode Shapes	126
10.5 Concluding Remark	126
Chapter 11	130
Vibration Analysis of the Mindlin Perforated Plates	130
11.1 Introduction	130
11.2 Theoretical formulation for the Mindlin Plate	130
11.3 Formulation for the material properties of the perforated Mindlin plate	132
11.4 Determination of the fundamental frequency of the perforated Mindlin plate	133
11.5 Numerical Analysis	135
11.6 Results and Discussion	135
11.5.1 Comparison of the Analytical and FEM Mode Shapes	141
11.6 Concluding Remark	141
Chapter 12	142
Conclusions	142
12.1 Specific Contributions	142
12.2 Conclusions	142
12.2.1 The Rectangular Plates with the Square/Rectangular Perforations	143
12.2.2 The Rectangular Plates with the Circular Perforations	144
12.3 Note on the Accuracy of the Analytical Models Proposed	146
12.4 Effect of Perforations on the Damping	146
12.5 Recommendations for Future Research	147

References	148
Appendix: A	157
Appendix: B	161
Appendix: C	168
Appendix: D	172
List of Publications	173
Brief Curriculum Vitae	174

List of Tables

Table No.	Caption	Page No.
Table 2.1	Coefficients for the cubic function in equation 2.6.....	10
Table 3.1	Summary of the problems considered.....	28
Table 4.1	Material properties assumed for the steel plate (Armenakas, 2006).....	29
Table 4.2	Details of the dimensions of M12 course bolt	34
Table 4.3	Details of the nominal diameter dimensions of the bolts for three sets	34
Table 4.4	Fundamental frequency results for the solid rectangular plate	35
Table 4.5	Experimental natural frequencies with the different bolt spacing	37
Table 4.6	Damping factors for the first two modes of the solid plate specimen.....	45
Table 5.1	Specimen parameters	51
Table 5.2	Comparison of the FEM and analytical results.....	54
Table 5.3	Comparison of the experimental and analytical results	55
Table 5.4	Comparison of the mode shapes obtained from analytical and FEM analysis	57
Table 5.5	Specimen parameters	61
Table 5.6	Comparison of the FEM and analytical results.....	62
Table 5.7	Comparison of the analytical and FEM mode shapes.....	63
Table 6.1	Results of the numerical and FE analysis for the plates with a single unit cell of 60^0 staggered perforation pattern	72
Table 6.2	Results of the numerical and FE analysis for the plates with the fixed outer dimensions	72
Table 6.3	Results of the numerical and experimental analysis for the plates with the fixed outer dimensions	73
Table 6.3a	Comparison of the analytical and FEM mode shapes for unit cell of 60^0 staggered perforation pattern.....	75
Table 6.3b	Comparison of the analytical and FEM mode shapes for the plates with the fixed outer dimensions	75
Figure 6.4	Geometry of the 45^0 staggered pattern	77
Table 6.4	Numerical and FEM analysis results for the 45^0 staggered pattern	81
Table 6.5	Comparison of the analytical and FEM mode shapes for a unit cell of 60^0 staggered perforation pattern.....	82
Table 7.1	Co-ordinates of the perforation centers.....	89

Table 7.2 Fundamental frequency results of the numerical and FE simulations	91
Table 7.3 Fundamental frequency results of the numerical and experimental analysis.....	92
Table 8.1 Fundamental frequency results obtained by the numerical and FE simulations....	105
Table 8.2 Comparison of the analytical and FEM mode shapes.....	107
Table 8.3 Fundamental frequency results obtained by the numerical and experimental analysis.....	110
Table 9.1 Details of the specimens analyzed	115
Table 9.2 Natural frequencies of the fundamental mode by the FE and experimental analysis	116
Table 9.3 Values of the correction factor for the different specimens.....	118
Table 9.4 Comparison of the results obtained by the proposed approach with the experimental and FE simulation results.....	120
Table 10.1 Numerical and FEM analysis results	125
Table 10.2 Analytical and FEM mode shapes	127
Table 11.1 Results obtained from the MPT, CPT and FEM.....	136
Table 11.2 Mode shapes obtained from the MPT and FEM for the specimen 11.10	140

List of Figures

Figure No.	Caption	Page No.
Figure 1.1	Perforation patterns (a) Staggered (b) Rectangular	3
Figure 2.1	Effective elastic constants given by O'Donnell and Langer (1962).....	8
Figure 2.2	Schematic of the perforated plate with 60° staggered patterns (Wang and Lai, 2003)	12
Figure 2.3	Effective elastic constants of perforated plates (Hung and Jo, 2006).....	14
Figure 3.1	Rectangular plate co-ordinates	19
Figure 4.1	Schematic of fixture the plate and the representative specimen used for experimentation	31
Figure 4.2	The fixture and specimen	31
Figure 4.3	Experimental set up	31
Figure 4.4	Schematic of the experimental set up	32
Figure 4.5	Diagram of the frame (side view) for the clamped boundary condition.....	33
Figure 4.6	Solid plate specimen used in the experiments	34
Figure 4.7	Frequency response Function (FRF) obtained with the Set1 Bolts	35
Figure 4.8	Bolt spacing arrangement first.....	36
Figure 4.9	Bolt spacing arrangement second	36
Figure 4.10	Bolt spacing arrangement third.....	36
Figure 4.11	Sample frequency response function (FRF) obtained with the bolts spacing arrangement first	38
Figure 4.12	Sample frequency response function (FRF) obtained with the bolts spacing arrangement second	38
Figure 4.13	Sample frequency response function (FRF) obtained with the bolts spacing arrangement third	38
Figure 4.14	Layout of the experimental grid points on the plate	39
Figure 4.15	The experimental set up.....	39
Figure 4.16	FRF's for different accelerometer locations on the plate	41
Figure 4.17	Force pulse with the different impact tips on the impact hammer	43
Figure 4.18	Force spectrums with the different impact tips on the impact hammer.....	44
Figure 4.19	Half power bandwidth method	45
Figure 5.1	Coordinates of the perforated plate.....	49

Figure 5.2 Perforated plate specimens no. 5.6 ($d = 16$ mm) tested experimentally.....	52
Figure 5.3 Plot of the unit step functions $f(x)$ and $g(y)$ for plate of size 700 mm X 700 mm ..	53
Figure 5.4 Plot of the functions $F(x,y)$ for the plate of size 700 mm X 700 mm.....	53
Figure 5.5 Orientation of the co-ordinates of the perforated square plate	59
Figure 5.6. Plot of the greatest integer functions $f(x)$ and $g(y)$	60
Figure 5.7. Density plot of the greatest integer function $f(x,y)$	60
Figure 6.1 Generalized triangular perforation pattern.....	65
Figure 6.2 Unit cell of the 60° staggered pattern	68
Figure 6.3 Density plot of the function $F(x, y)$	69
Figure 6.4 Perforated plate specimens with the staggered pattern tested experimentally	71
Figure 6.5 Frequency response function for the Specimen no. 6.14 ($d = 7.33$ mm).....	74
Figure 6.6 Frequency response function for the Specimen no. 6.15 ($d = 30.86$ mm).....	74
Figure 6.5 Density plot of the function $F(x, y)$ for the 45° staggered pattern	80
Figure 7.1 Rectangular plate co-ordinates	85
Figure 7.2 Co-ordinates of the plate clamped on all edges carrying circular holes	87
Figure 7.3 Perforated plate specimens used in the experiment.....	90
Figure 7.4 Variation of the percent error in the fundamental frequency with A/A_p ratio.....	92
Figure 7.5 Frequency response function for the Specimens no. 7.11 ($d = 5$ mm).....	93
Figure 7.6 Frequency response function for the Specimens no. 7.12 ($d = 10$ mm)	93
Figure 8.1 An equivalent square hole for the circle of radius r_c	94
Figure 8.2 Orientation of the perforated plate with equivalent square perforations.	96
Figure 8.3 Plot of the function $f(x)$ for the specimen 276 mm x 432 mm with.....	98
$r_c = 25$ from equation (8.7).....	98
Figure 8.4 Plot of the function $g(y)$ for the specimen 276 mm x 432 mm with.....	98
$r_c = 25$ from equation (8.8).....	98
Figure 8.5 Density plot of the function $F(x, y)$ for the specimen 276 mm x 432 mm with	99
$r_c = 25$ with corner origin	99
Figure 8.6 Plot of the function $f(x)$ for the specimen 276 mm x 432 mm with.....	99
$r_c = 25$ from equation (8.7a).....	99
Figure 8.7 Plot of the function $g(y)$ for the specimen 276 mm x 432 mm with.....	100
$r_c = 25$ from equation (8.8a).....	100
Figure 8.8 Density plot of the function $F(x, y)$ for the specimen 276 mm x 432 mm with ...	100
$r_c = 25$ with center origin.....	100
Figure 9.1 Co ordinates of the plate	112

Figure 9.2 Geometry of the perforated plate	113
Figure 9.3 Sample frequency response function (FRF) obtained for the Specimen No. 9.1 .	116
Figure 9.4 Sample frequency response function (FRF) obtained for the Specimen No. 9.2 .	117
Figure 9.5 Sample frequency response function (FRF) obtained for the Specimen No. 9.3 .	117
Figure 9.6 Sample frequency response function (FRF) obtained for the Specimen No. 9.4 .	117
Figure 10.1 Co-ordinates of the plate clamped on all edges carrying circular holes	123
Figure 10.2 Density plot of the function $F(x, y)$ for the specimen size 138 mm × 216 mm and $d = 25$ mm	124
Figure 11.1 Geometry and the coordinate system of the perforated rectangular plate	132
Figure 11.2 Results obtained from the MPT, CPT and FEM for all the specimens	137
Figure 11.3 Results from the MPT, CPT and FEM for the specimens with	137
$a/h \leq 33.333$	137
Figure 11.4 Results from the MPT, CPT and FEM for the specimens	138
with $10 \leq a/h \leq 20$	138
Figure 11.5 Plot of the % error vs. a/h ratio for the specimens with $6 \leq a/h \leq 14.285$	139
Figure 11.6 3D mode shape for the specimen 11.10 ($h = 0.045$ and $a/h = 11.111$)	140

List of Commonly Used Symbols and Abbreviations

Symbol/Abbreviation	Meaning
A	Area of perforation
a	Effective outer dimension along x axis
b	Effective outer dimension along y axis
D	Flexural rigidity of plate $D = \frac{Eh^3}{12(1-\nu^2)}$
AR	Aspect ratio = L_y/L_x
FE	Finite element
FEM	Finite element method
L_h	Centre to centre distance between holes along width in mm
L_v	Centre to centre distance between holes along length in mm
L_x	Effective plate width in mm
L_y	Effective plate length in mm
h	Effective plate thickness in mm
hr	Ligament width in mm
η_l	Ligament efficiency
MRR	Mass remnant ratio
ω_n	Natural Frequency of perforated plate in Hz
ν	Poisson's ratio
r	Radius of perforation hole in mm
d	Diameter of circular perforation/ size of square perforation in mm
E	Young's modulus in N/m^2
ρ	Density of material in kg/m^3
$(D + hr)$	Center to center distance in mm
d_c	Side length of square perforation
r_c	Radius of circular perforation
∇^2	Two-dimensional Laplacian operator
u_{max}	Maximum Kinetic Energy

T_{max}	Maximum Strain Energy
W	Deflection of the mid plane of the plate
$f(x)$	Function representing variation of material properties along x axis
$f(y)$ or $g(y)$	Function representing variation of material properties along y axis
$F(x, y)$	Function representing variation of material properties along x and y axes
λ_{1P}	Modal constant for perforated plate
ζ	Damping ratio

Dedication

This thesis is dedicated to my parents and family who provided unconditional love, emotional support and has been a source of strength and comfort throughout my life. Their faith in me and encouragement has been a major contributing factor in my achievements.

Chapter 1

Introduction

1.1 Background

Plates are important structural elements in engineering applications such as pressure vessels, missiles, liquid containers, ship structures, and nuclear power equipments. Since perforated products reduce the weight and improve certain properties, they are used in the products. The perforated plates are used in the construction of heat exchangers where these are called as tube sheets. The boiler is a well-known example for industrial application of the perforated plates. The perforated sheets have a multitude of functions. Their versatility includes screening, filtering, apportioning, ventilating, deflocculating, regulating, protecting, rasping, ordering and forming. Cutouts are found in mechanical, civil, marine and aerospace structures commonly as access ports for mechanical and electrical systems, or simply to the reduce weight. Cutouts are also made to provide ventilation and for modifying the resonant frequency of the structures. In addition, the designers often need to incorporate cutouts or openings in a structure to serve as doors and windows.

The holes in plate are arranged in various regular perforation patterns. Industrial applications include both square and triangular array perforation patterns. Behavior of the perforated component is drastically different from those of non-perforated component. Since the dynamic performance is always of interest, perforated rectangular plates having rectangular/triangular pattern with the circular/rectangular/square perforations are chosen and analytical, experimental models are formulated to find the fundamental frequency.

1.2 Advantages of the Perforated Plate

Advantages of perforated plates are discussed below (Europerf, 2013).

- **Enhanced Acoustic Performance**

The Perforated plate is used for soundproofing and for reducing acoustic emissions. Almost all results required can be achieved by defining the open area accurately. The perforated sheet is even ideal as a supporting material for other sound-insulating applications.

- **Radiation Containment**

The Perforated plate is used to enclose electrical appliances in order to attenuate the emitted EMI /RFT radiation and to ventilate the appliances at the same time. Test results show that a shielding effectiveness of 40 dB provides 99% percent attenuation of the electromagnetic radiation while a shielding effectiveness of 92 dB – the highest one in the tests – provides 99.997 percent attenuation.

- **Reduction in Weight**

Reducing weight is becoming more and more important in areas such as the aerospace industry. The perforated metal is the ideal way to meet this requirement. In addition, machining a perforated plate (bending etc.) does not leave its load-carrying capacity at a disadvantage compared to the unperforated specimen.

- **Ease in Separating Materials**

The perforation and open area can be specified exactly, making the perforated sheet ideal for filtering, separating, or sorting goods. The open area can be varied in numerous ways to affect the flow rate, size sorting etc. accurately. Filter elements made from perforated metal are of major benefit to the user.

- **Enhanced Heat Dissipation**

Components made from perforated plate play a valuable role in regulating temperature by heat dissipation in cold shelves, hot-air ventilators or complex heating units. The combination of useful functions with an appealing design gives rise to solutions in which a unique aesthetic touch complements the actual function of the application.

- **Improved Skid Resistance / Anti-Skid**

Floor coverings made from the perforated or stamped plates have special anti-skid properties to ensure safety in many areas. Especially in areas with high exposure to wetness, dirt etc., perforated floor coverings and steps etc. offer excellent skid-resistance so you can walk across these dangerous surfaces safely.

The uses of perforated metal plates are given in Appendix ‘A’

1.3 Perforation Types and patterns

Commonly used types of perforations and perforation patterns are discussed below (New Metals, Inc., 2013).

1.3.1 Perforation Types

- **Round:** Round perforations are produced with the greatest efficiency with less expensive and more durable tooling. Round holes are the most popular shape in the perforated metal industry. Round perforations are the strongest and most versatile of all perforation patterns.
- **Squares/ Rectangular:** These types of perforations are very useful in sorting and grading of solid objects, such as grains or minerals. It has most common use in ventilation and protective guards. Squares are the simplest of all decorative design perforations. The advantages that square and rectangular holes offer are maximum open area for ventilation, excellent visibility and excellent protection. Square/rectangular perforations are weaker than round ones.

1.3.2 Perforation Patterns

There are three types of standard distribution patterns. 60° Staggered, 45° staggered and rectangular/square (90°).

- **Staggered:** Distribution of perforations in a triangular pattern, forming a 45° or 60° angle when joining centre lines of three adjacent holes with a straight line (Figure 1.1a).
- **Rectangular/Square:** Distribution of perforations in a rectangular/square pattern, forming a 90° angle when joining centre lines of three adjacent holes with a straight line (Figure 1.1b).

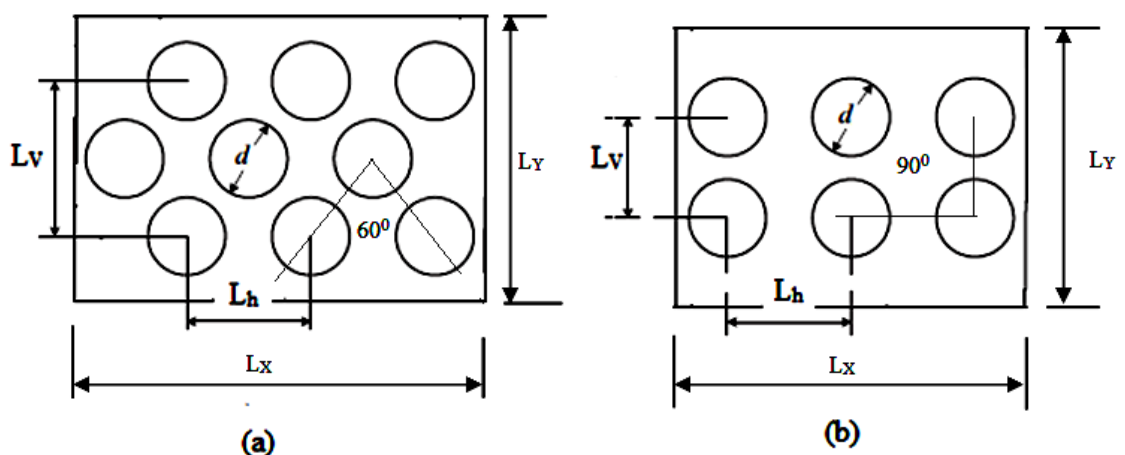


Figure 1.1 Perforation patterns (a) Staggered (b) Rectangular

These regular arrays are characterized by their ligament efficiency (η_l), which is defined as

$$\eta_l = \frac{(L_h - 2r)}{L_h} \quad (1.1)$$

1.4 Motivation and Research Hypothesis

1.4.1 Motivation

From above section 1.1 to 1.2 the problem of free vibration of plates with perforations/cutouts is very important since these plates are extensively used in various applications. The problems of plates with perforations are generally more difficult to be described easily and accurately. Moreover, there is little information about the free vibration problem of the plates having rectangular or triangular array of holes. Dynamic behavior of perforated plates is different from homogeneous isotropic plate structure. In order to understand the dynamic behavior of such a structure, a precise and efficient method is needed for the thin plate. Thus to design and manufacture these new types of structural components safely and economically, it is important to develop a simple and quick method for determining the fundamental frequency.

1.4.2 Research Hypothesis

It is possible to determine the fundamental frequency of perforated plates by considering the variation in its material properties due to holes. The fundamental frequency is a function of the perforated plate material properties such as Young's modulus and density distribution.

1.5 Objective and Scope

In the present research, the problems of the “free flexural vibrations of thin rectangular perforated plates with circular/rectangular/square perforations” are formulated for determining the fundamental frequency. The parameters like, size of perforation hole, ligament efficiency and perforation pattern are considered in the problem formulation. The theoretical formulations of the problem are based on the classical thin plate theory. Thus, the transverse shear deformations, the transverse and the rotary moments of inertia of the plates are not included in the formulation. The damping effects in the plates are neglected. In this study boundary condition considered is all edges clamped. However, the analytical models formulated for the material property variation in this thesis can be extended to other edge conditions. Also one extensional model is given for the moderately thick plates by using Mindlin plate theory. In all the analytical models standard available shape functions are used

in the approximate methods suitable for the boundary condition. The formulation of new shape function is not within the scope of this work. The main objectives of the present work are as follows:

1. To formulate the functions to express the variation of the Young's modulus and the density of the perforated plate having rectangular/square and staggered pattern (60° and 45°) of the perforations.
2. To develop an analytical model for determining the fundamental frequency of the perforated plate by incorporating the special functions to express the non homogeneity in the Young's modulus and density with approximate methods such as Rayleigh's method, Rayleigh's-Ritz method.
3. To develop an analytical model for determining the fundamental frequency of perforated plate by using the "added concentrated negative mass" approach to express the effect of the perforation.
4. To obtain an expression for the modal constant of the fundamental frequency of the perforated plate experimentally. Modal constant will permit the ready determination of the natural frequencies for a plate involving any combination of ligament efficiency and perforation diameter.
5. To analyze the dynamic behavior of the rectangular perforated plates with the rectangular or triangular perforation pattern for the varying sizes of the circular perforation holes and the ligament efficiencies.
6. To validate the analytical models developed by comparing results of the numerical analysis with the FEM simulations and the experimental results for representative specimens

1.6 Organization of the Thesis

This thesis is organized as follows. The Chapter 2 describes the existing work in the areas relevant to this thesis. At the end of the chapter gaps existing in the current literature are given. In the Chapter 3 the equation of motion governing the free vibration of the isotropic plates is given based on the classical plate theory, assumptions used in the derivation are also given. Further approximate methods i.e. Rayleigh's method, Rayleigh's-Ritzs method and Galerkin method used for obtaining the fundamental frequency are discussed. The theoretical models which are explained in the subsequent chapters are based on these methods. In this chapter problem formulation is also discussed in detail. Chapter 4 is devoted to the

experimental details to obtain the fundamental frequency, as the results of this analysis are used to validate proposed analytical models. This chapter gives details of the test fixture, specimen dimensions, experimental set up and test procedure.

Further work in thesis related to the formulation of analytical models to determine the fundamental frequency is categorized in three parts

- i) Thin rectangular plates with the rectangular/square perforations (Chapter 5 and 6)
- ii) Thin rectangular plates with the circular perforation (Chapter 7,8 9 and 10)
- iii) Moderately thick rectangular plates with the rectangular/square perforations (Chapter 11)

The Chapter 5 presents the analytical models to determine the fundamental frequency of plates with rectangular/ square array of perforations where as the Chapter 6 presents analytical models for plates with staggered array of perforations. In the Chapters 7, 8, 9 and 10 the models are formulated to determine the fundamental frequency of plates with rectangular array of perforations. In the Chapter 7 analytical model is formulated by using concept of negativ concentrated mass for the perforations. In Chapter 8 analytical model is formulated by using concept of equivalent square perforation to replace the circular perforation. The Chapter 9 presents the hybrid method to obtain expression for modal constant for the fundamental frequency. In the Chapter 10 analytical model is formulated by considering unit step function to map exactly the circular perforations. Extension of the approach presented in the chapter 5 is given in the chapter 11 for moderately thick plates. Mindlin plate theory is used in this chapter for the analytical modeling. Finally conclusions about the work presented in thesis along with the recommendations for the future work to extend this research are given in the Chapter 12.

Chapter 2

Literature Review

2.1 Introduction

Many researchers have studied vibration behavior of the plates, using a wide range of methods. However, for the rectangular plates having rectangular or triangular array of perforations, published literature is limited. This may be because of the complications involved due to geometry. Focusing our attention on the available literature on the perforated plate vibration, it is convenient to classify it into three categories based on the analytical models formulated in this thesis. Thus this chapter gives detailed review of the literature related to the analytical models formulated in the further chapters. The literature review is classified in to the following categories

1. Work directly dealing with the vibration of plates having cut outs and the perforated plates
2. Work dealing with the vibration of plates with the non homogeneous material properties.
3. Work dealing with the vibration of plates with the added concentrated mass.

2.2 Vibration of Plates with Cut Outs and Perforations

The problem of free vibration of the plates with the cut outs and perforations has attracted many researchers and engineers; hence many relevant papers have been published. Majority of the literature reviewed utilize approximating techniques to formulate the problem of free vibration of the plates with cut out or perforations. Most of the studies have been directed towards the plates with simply supported edges and very little regard is given to the clamped edges. O'Donnell and Langer (1962) obtained values of effective elastic constant for the plates having triangular perforation pattern of circular holes. Effective elastic constants were derived from strain measurement and photo-elastic tests. It was then proposed that these equivalent elastic constants can be used for analyzing perforated plates with concept of an "equivalent" solid plate. Equivalent plate is same as the solid plate, but it has fictitious elastic constants E^* and ν^* instead of actual constants of the material E and ν . Figure 2.1 shows variation of the ratio of the effective elastic constants (values with * as superscript) with the ligament efficiency.

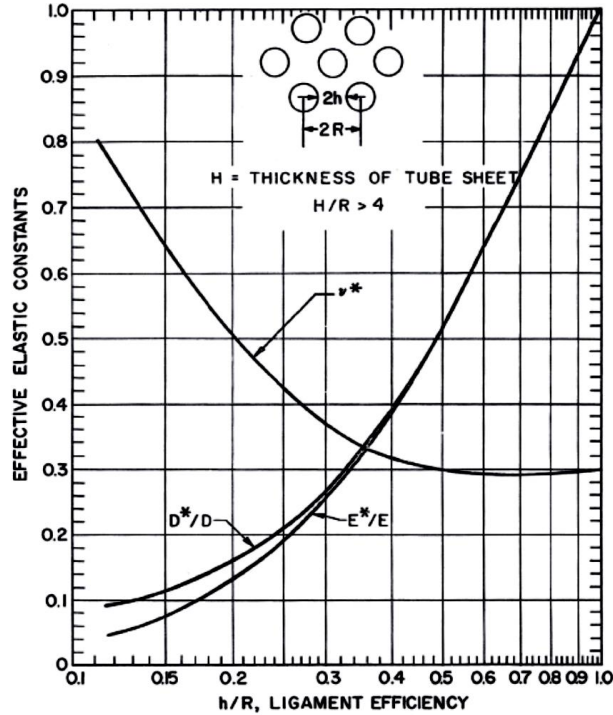


Figure 2.1 Effective elastic constants given by O'Donnell and Langer (1962)

Meijers (1967) also determined from experimental measurement of strain, values of the effective elastic constants for the rectangular plates having circular holes in rectangular array and diagonal array. Finite element analysis of a clamped plate with different cutout sizes, along with experiments using holographic interferometry, was carried out by Monahan (1970) et al. Paramsivam (1970) used a finite difference approach in analyzing the effects of openings on the fundamental frequencies of the plates with simply supported and clamped boundary conditions. O'Donnell (1973) determined the effective elastic constants for the thin perforated plates with the triangular and the square perforation patterns by equating the strains in an equivalent solid material to the average strains in the perforated material.

Free vibrations of the rectangular elastic plate, either clamped or simply supported, with a central circular hole has been investigated by Hegarty (1975) using least-squares point-matching method. Soler and Hill (1976) proposed a simple analytical expression which is suitable for determination of the effective bending stiffness of a perforated circular plate having both rectangular and triangular array of circular holes. Aksu and Ali (1976) obtained dynamic characteristics of the rectangular plates with one or two cutouts using a finite difference formulation along with experimental verifications. Ali and Atwal (1980) studied the natural frequencies of the simply supported rectangular plates and rectangular cutouts using the Raleigh Ritz method. Reddy (1982) studied linear and large amplitude

flexural vibration of the isotropic and the composite plates with cutout by using the finite element method. Chang and Chiang (1988) studied the vibration of the rectangular plate with an interior cutout by using the finite element method. Lam et al. (1989) presented an efficient and accurate numerical method in the study of the vibration of the rectangular plates with cutouts and non-homogeneity. The deflection function for the originally complex domain was found by dividing the problem domain into appropriate rectangular segments. Lam and Hung (1990) investigated flexural vibrations of the plates with discontinuities in the form of the cracks and the cutouts using a scheme which combines the flexibility of dividing the problem domain into appropriate segments and the high accuracy resulting from the use of orthogonal polynomial functions, generated using the Gram-Schmidt process. Lee, Lim and Chow (1990) predicted the natural frequencies of the rectangular plates with an arbitrarily located rectangular cutout. Forskitt et. al. (1991) introduced the concept of perpendicular and parallel ligament efficiency, XLE and YLE respectively to allow for different spacing between the layers of the holes in an array of perforations. For a diagonal array of circular holes of diameter d , perpendicular pitch L_h and parallel pitch L_v as shown in Figure 1.1, the perpendicular and parallel ligament efficiencies, XLE and YLE are defined as

$$XLE = \frac{(L_h - 2r)}{L_h} \quad (2.1)$$

$$YLE = \frac{(L_v - 2d)}{L_v} \quad (2.2)$$

The effective density ρ^* according to Forskitt et. al.(1991) is based on the solid area fraction of the plate and can be expressed by a function of XLE and YLE as given by equation (2.3) and (2.4) for the regular triangular and rectangular array respectively.

$$\frac{\rho^*}{\rho} = 1 - \left[\frac{\pi}{8} (1 - XLE)(1 - YLE) \right] \quad (2.3)$$

$$\frac{\rho^*}{\rho} = 1 - \left[\frac{\pi}{16} (1 - XLE)(1 - YLE) \right] \quad (2.4)$$

It was then proposed for a simply supported rectangular perforated panel, the effective resonance frequency of the (m, n) mode can be given as below by introducing the effective material properties,

$$\omega^*_{mn} = \frac{1}{2\pi} \left(\frac{E^* h^2}{12\rho^*(1-\nu^{*2})} \right)^{1/2} \left(\left(\frac{m\pi}{L_x} \right)^2 + \left(\frac{n\pi}{L_y} \right)^2 \right) Hz \quad (2.5)$$

According to Burgemeister and Hansen (1994) equation (2.5) does not provide correct resonance frequencies when using the effective material properties. Burgemeister and Hansen (1994) showed that the effective material constants can not be used in the classical equations to predict accurately the resonance frequencies of the simply supported perforated panel. Instead it is much more accurate to fit the results from ANSYS to a simple cubic function. This function can be used to determine the effective resonance frequency ratio for large range of the panel geometries with an error of less than 3%. The cubic function is given by

$$\frac{\omega^*}{\omega} = a \times XLE^3 + b \times XLE^2 + c \times XLE + d \times YLE^3 + e \times YLE^2 + f \times YLE + g \quad (2.6)$$

Coefficients of above function are listed in Table2.1.

Table 2.1 Coefficients for the cubic function in equation 2.6

Coefficient	Value
<i>a</i>	0.0399
<i>b</i>	-0.0727
<i>c</i>	0.1161
<i>d</i>	-0.1295
<i>e</i>	0.1013
<i>f</i>	0.1096
<i>g</i>	0.8395

Mundkur et al. (1994) studied the vibration of the square plate with the square cutouts by using boundary characteristics orthogonal polynomials satisfying the boundary conditions. Young et al. (1996) presented the free vibration of the thick rectangular plates with depression, grooves or cutouts using three-dimensional elasticity and Ritz method. Kaap's (1997) literature review of the methods for predicting the perforated plate vibrations showed that no design curves for this analysis have been developed. He showed from the review of literature that, there are no analytical, numerical, or experimental data available that would

enable a designer to predict the dynamic response of the perforated plates. Choi et al. (1998) performed the finite element modal analysis for the perforated plates having square and triangular hole patterns. Choi et al. (1998) studied vibration of the simply supported perforated plates by using the concept of the equivalent solid plate. They found that the values of equivalent elastic constants are different from the static problems to get accurate results. Further they noticed the difference between equivalent elastic properties for the static and dynamic analysis become significant as the ligament width gets smaller.

Sivasubramonian et al. (1997,1999) investigated the free vibration characteristics of the unstiffened and longitudinally stiffened square panels with the symmetrical square cutouts by using the finite element method. The optimized Rayleigh-Ritz method was applied by Ricardo et al. (1997) to generate values of the fundamental frequency coefficient and the one corresponding to the first fully antisymmetric mode for the rectangular plates elastically restrained against rotation and with located circular holes. Huang and Sakiyama (1998) analyzed the free vibration of the rectangular plates with variously shaped holes. Sahu and Datta (2003) studied the parametric instability behavior of the curved panels with cutouts subjected to the in-plane static and periodic compressive edge loadings using the finite element analysis. The first order shear deformation theory was used to model the curved panels, considering the effects of transverse shear deformation and rotary inertia. Avalos and Laura (2003) performed series of the numerical experiments on the vibrating simply supported rectangular plate with two rectangular holes and free edges. Liew et al. (2003) presented analysis of free vibration of the plates with internal discontinuities due to central cut-outs. A numerical formulation for the basic L-shaped element which was divided into the appropriate sub domains that were dependent upon the location of cut out was used as the basic building element. Wang and Lai (2003) adopted the hybrid method, which combines the experimental and the numerical methods, to investigate the dynamic behavior of the perforated plates. The equivalent material properties of the perforated plates were also obtained by the hybrid method. In addition, the curve-fitting technique was utilized to find the relationship of the mass remnant ratio (i.e. the ratio of surface area of the perforated plate to that of the solid plate for the same dimension) with the parameter ratio. Since the equivalent material properties of the perforated plate can be determined via the specimen dimensions, hole size, and hole arrangement, the mass remnant ratio (MRR) was defined in terms of the geometric parameters shown in Figure 2.2, and expressed as

$$MRR = 1 - \frac{\pi r^2}{2L_v L_h} \quad (2.7)$$

Here L_x and L_y are the horizontal and vertical lengths of the plate, respectively; L_h and L_v are the horizontal and vertical spacing between the centers of the holes of two neighboring columns and rows, respectively; r is the radius of a hole.

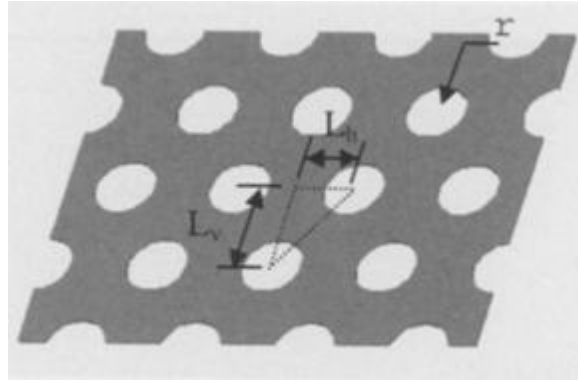


Figure 2.2 Schematic of the perforated plate with 60° staggered patterns (Wang and Lai, 2003)

They (Wang and Lai, 2003) obtained functions from the curve fitting and used, to predict accurately the equivalent material properties and the resonant frequencies of the perforated plates of the diagonal array. Sinha et al. (2003) suggested a formula for added mass of the vibrating perforated plate-type structures submerged in the fluid based on the experimental and the analytical studies on a number of test specimens. Wu et al. (2003) developed a mathematical model of the axisymmetric elastic/plastic perforated circular plate for the bending and stretching. Bhattacharya and Venkat Raj (2003) analyzed a quarter symmetric part of a perforated plate containing a 3×3 square array of the circular holes by the finite element method (FEM) to obtain the peak stress multipliers under membrane and bending loads for different biaxiality ratios. Britan and Karpov et al. (2004) studied experimentally and theoretically/numerically the flow and wave pattern resulted from the interaction of an incident shock wave with a few different types of barriers, all having the same porosity but different geometries. Bhattacharya, Venkat Raj (2004) developed second and fourth order polynomials describing the yield criterion for the perforated plates with square perforation pattern. They have not considered the effect of out-of-plane stresses in the investigation as these are found to be negligible in case of the thin perforated plates, for which plane stress condition was assumed in the finite element formulation. Pedersen (2004) studied the optimization of a hole of given area which is placed in the interior of a plate with an arbitrary

external boundary. The objectives of the optimization were the eigenfrequencies of the plate with the hole. The optimization was performed in relation to maximizing the first eigenfrequency or maximizing the gap between the first and second eigenfrequency. Lee and Kim (2005) studied the validity of the Eshelby-type model for predicting the effective Young's modulus and in-plane Poisson's ratio of the two dimensional perforated plates in terms of the porosity size and its arrangement. Rezaeepazhand and Jafari (2005) used analytical investigation to study the stress analysis of the plates with different central cutout. Particular emphasis was placed on the flat square plates subjected to a uni-axial tension load. They compared results based on the analytical solution with the results obtained using the finite element methods. Hung and Jo (2006) studied free vibration characteristics of a circular perforated plate submerged in the fluid with the rectangular and square perforation patterns. The natural frequencies were obtained by the theoretical calculations and three dimensional finite element analysis. The effect of holes on the modal characteristics was investigated; they also proposed new equivalent elastic constants for the modal analysis of a perforated plate. Figure 2.3 shows the effective elastic constants proposed for the modal characteristics of a perforated plate with triangular and square perforation patterns. The Young's moduli proposed by Hung and Jo (2006) for the modal analysis of the perforated circular plates with triangular and square perforation patterns are as follows ,where η is ligament efficiency and E^* is equivalent Young's Modulus.

$$\frac{E^*}{E} = 0.6106 + 1.1253\eta - 2.7118\eta^2 + 4.0812\eta^3 - 2.1128\eta^4 \quad (2.8)$$

$$\frac{E^*}{E} = 0.5280 + 2.0035\eta - 5.478\eta^2 + 7.7474\eta^3 - 3.8968\eta^4 \quad (2.9)$$

Work of Kathagea et. al. (2006) deals with the design of perforated trapezoidal sheeting. They calculated the effective stiffness values for the perforated sheeting with different arrays of the holes based on the numerical analysis and graphs. Patil et al. (2007) also gave an expression for the effective resonance frequency of the rectangular perforated plate with the staggered perforation pattern. They used curve fitting technique to obtain an expression for the effective resonance frequency. They used the FEM (Finite Element Method) simulation data of resonance frequencies for the five perforated plates. The formula is a function of the mass remnant ratio.

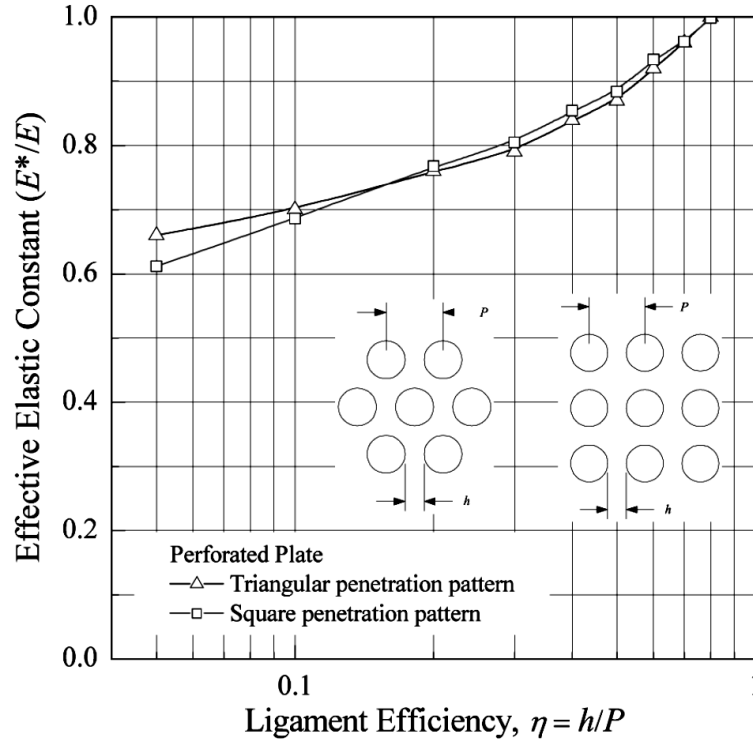


Figure 2.3 Effective elastic constants of perforated plates (Hung and Jo, 2006)

Tong Liu et al. (2009) studied effect of the cracks on the natural frequencies and modal strain energy of a perforated plate with ligament fractured cracks by the finite element analysis. Romero et al. (2010) used digital speckle interferometry technique for tuning resonant frequencies of the vibrating plates in order to investigate the dynamical behavior of the perforated plates. Experimental natural frequencies and modal shapes were compared to those obtained by an analytical approximate solution. Analytical approximate solution was based on the Rayleigh–Ritz method with the use of orthogonal polynomials as coordinate function.

2.3 Vibration of the Plates with the Non Homogeneous Material Properties

Leissa (1969, 1977, 1981, and 1987) compiled some works done in the field of the homogeneous and the non-homogeneous plates. Sobczyk (1972) studied free transverse vibrations of elastic rectangular plates with random material properties. Laura et al. (1984) studied non-homogeneous rectangular plates. Mishra and Das (1971) proposed a method of the characteristic orthogonal polynomials in one dimension to handle the rectangular plates. Pan (1976) developed characteristic orthogonal polynomials in two variables to study the flexural vibrations of the polygonal plates. Rao et al. (1974, 1976) studied vibrations of the inhomogeneous thin plates using a high precision triangular element, and vibration of the

inhomogeneous rectangular plates by using perturbation solution. Tomar et al. (1982, 1983, and 1984) studied vibrations of the plates of variable thickness having non homogeneity. Chakraverty et al. (1999, 2007) used two-dimensional orthogonal polynomials as shape functions in the Rayleigh-Ritz method to study vibration of the non-homogeneous plates; they also studied effect of the non-homogeneity on the natural frequencies of vibration of elliptic plates. Lal et al. (2009) studied free transverse vibrations of the uniform nonhomogeneous rectangular plates using boundary characteristic orthogonal polynomials in the Rayleigh-Ritz method on the basis of the classical plate theory for four different combinations of clamped, simply supported and free edges. Lal and Dhanpati (2010) studied the effect of nonhomogeneity on the vibration of the orthotropic rectangular plates of varying thickness resting on the pasternak foundation.

2.4 Vibration of the Plates with the Added Concentrated Mass

Low (1993, 2001) determined the vibration frequencies of the rectangular plates with weights mounted at various locations. He also developed improved model to determine the frequency of the vibrating plates carrying multiple masses at various positions. Low et al. (1997, 1998) obtained natural frequencies of the rectangular plates carrying a single and multiple concentrated masses by using the Rayleigh-Ritz method for different boundary conditions. Results obtained from the analytical study using the energy method are compared with those measured experimentally. Chai Gin Boay (1995) analyzed free vibration of the rectangular isotropic plates carrying a concentrated mass. The Ritz approach is applied to the rectangular plates with various edge support combinations of clamped and simple support conditions. The effect of different locations of the concentrated mass on the fundamental frequency of the plate is presented in detail. Wu and Luo (1997) determined the natural frequencies and the corresponding mode shapes of a uniform rectangular flat plate carrying any number of point masses and translational springs by means of the analytical and the numerical combined method (ANCM). Avalos et al. (1997) studied transverse vibrations of the simply supported rectangular plates with rectangular cutouts carrying an elastically mounted concentrated mass. Ostachowicz et al. (2002) presented new results for the identification of the location of a concentrated mass on the isotropic plates by means of a genetic algorithm search technique based on changes in the natural frequencies. Li (2003) presented an exact approach for free vibration of an isotropic rectangular plate carrying a line-concentrated mass and with a line-translational spring support or carrying a line-spring-mass system. Altintas (2009) investigated the special behaviors of the linear vibrating plates

with the special parameters near degenerate modes. The special parameters considered in this study are the location and quantity of an additional mass, which have an effect on removing the system symmetry. Yin Zhang (2011) presented and compared different methods on the eigenfrequency computation of a beam and a plate carrying arbitrary number of concentrated mass/spring. The advantages and disadvantages of these methods are analyzed and discussed. Amabili (2010) studied nonlinear forced vibrations of the rectangular plates carrying a central concentrated mass. Amabili et al. (2006, 2012) studied effect of concentrated masses with rotary inertia on vibrations of the rectangular plates and large-amplitude vibrations of the rectangular plates carrying concentrated masses.

2.5 Gaps in the Existing Research

From review of the literature it is observed that, more studies have been done, especially on the subject of vibration of the plates with few cut outs in the plate than the perforated plates. Also design guidelines are available for the static problem of the perforated plates. According to these guidelines elastic modulus of the plate can be replaced by an artificial or an effective elastic constant to accommodate the average decrease in stiffness (Kaap, 1997). However such guidelines or procedures do not exist for the dynamic design of the perforated plates. There are no analytical, numerical, or experimental data available that would enable a designer to predict the dynamic response of the perforated plates (Kaap, 1997). The effect of hole geometry, hole size and the ligament efficiency on the dynamic behavior of the rectangular plates is not studied in combination so far experimentally and also by using the FEM.

The key findings from the literature leading the gap existing in the research are as follows:

1. The effects of cutout size, ligament efficiency, and the equivalent elastic properties on the natural frequencies of the plates for different boundary conditions by experimental analysis have been treated sparsely in the literature. In the literature, much of the research has discussed the analytical or the numerical solutions of the plate with few cut outs.
2. No literature is reportedly dealing with the analytical solutions of the plate with the rectangular/square perforations arranged in the rectangular/triangular perforation pattern.

3. Values of the effective elastic constants suggested by O'Donnell et. al. (1962, 1973) are not valid from the modal characteristic point of view for the perforated plate because these are applicable under certain conditions (Hung and Jo, 2006).
4. From review of the literature, authors have found no work dealing with the analytical formulation by considering unit step function or using greatest integer function i.e. floor function to express the non homogeneity due to the holes (in the Young's modulus and density).
5. From the literature on vibration of the perforated plates and vibration of the plates with the added concentrated mass, it is found that, there is no evidence on the analytical formulation for the perforated plate vibration problem by considering negatively added concentrated mass approach for the holes.
6. There is no evidence on formulation of the modal constants, functions from curve fitting or empirical equations to predict accurately the effective resonance frequencies of wide range of the perforation geometries, for the rectangular plates with the rectangular perforation pattern for all edges clamped support condition.

2.6 Concluding Remark

The studies demonstrating practical applicability of the analytical methods to vibration analysis problem of the plate with multiple perforations are lacking in the professional literature. Present approaches in the literature use homogenization which aims for the equivalent stiffness (e.g. E , G , EI) and strength properties that can be used in the assessment of the structural systems, the response of homogenized solution is often not accurate for the dynamic problem. Thus there is need of the some analytical approach that will lead to at least an estimate of the answer of the problem. Further, proposed analytical methods should be simple and quick for the solutions.

Chapter 3

Governing Equations and Formulation of the Problem

3.1 Introduction

The deflection of the thin plate is governed by the fourth order partial differential equation. In this chapter the equations of motion for free vibration of the plate is given with underlying assumptions. The order of mathematical complexity increases when the flexural rigidity, D varies for the plate. As in the present problem of the plate with perforations arranged in the rectangular/triangular array flexural rigidity do not remain same all over the plate domain. Thus approximate techniques for the solution of the problem are required. The approximate methods used in this thesis for the analytical modeling are discussed in this chapter. In section 3.4 of the present chapter detailed formulation of the problem is given.

3.2 Governing Equation of the Free Vibration of the Plate

The work presented in this thesis considers only the classical plate theory in the analysis along with the solution of the rectangular plates of various sizes of the perforations and the different perforation patterns. Here, first classical plate theory is addressed. Classical thin plate theory or Kirchhoff plate theory is based on the following assumptions (Chakraverty, 2009) known as the Love-Kirchhoff hypotheses.

- The plate material is linear elastic and follows Hooke's law.
- The plate material is homogeneous and isotropic. Its elastic deformation is characterized by the Young's modulus and the Poisson's ratio.
- The constant thickness of the plate is small compared to its lateral dimensions. That is, the smallest lateral dimension of the plate is at least 10 times larger than its thickness.
- The normal stress in the transverse direction can be neglected compared to the normal stresses in the plane of the plate.
- Points that lie on a line perpendicular to the center plane of the plate remain on a straight line perpendicular to the center plane after deformation.
- The deflection of the plate is small compared to the plate thickness. A maximum deflection of one-tenth of the thickness is considered the limit of the small-deflection theory.
- The center plane of the plate is stress free, i.e., we can neglect the membrane stresses

in the plate.

- Loads are applied in a direction perpendicular to the center plane of the plate
- Effect of rotatory inertia is negligible.

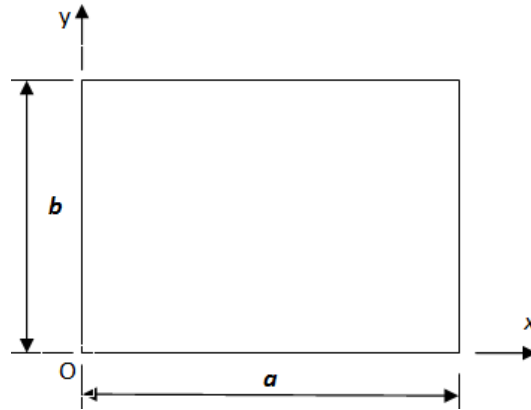


Figure 3.1 Rectangular plate co-ordinates

The partial differential equation governing the free transverse vibration of an isotropic thin plate with dimensions a , b and transverse dimension is h , the plate thickness shown in Figure 3.1, is (Ventsel and Krauthammer, 2001),

$$D\left(\frac{\partial^4 w}{\partial x^4} + 2\frac{\partial^2 w}{\partial x^2}\frac{\partial^2 w}{\partial y^2} + \frac{\partial^4 w}{\partial y^4}\right) + \rho h \frac{\partial^4 w}{\partial t^2} = 0 \quad (3.1)$$

$$D\nabla^2\nabla^2 w(x, y, t) + \rho h \frac{\partial^4 w}{\partial t^2}(x, y, t) = 0 \quad (3.2)$$

Where h is the uniform plate thickness, ρ is the density, w is transverse displacement, and D is the flexural rigidity, ∇^2 is two-dimensional Laplacian operator. D and ∇^2 are given as (Ventsel and Krauthammer , 2001; Chakraverty S., 2009),

$$D = \frac{Eh^3}{12(1-\nu^2)}, \quad \nabla^2 = \frac{\partial^2}{\partial x^2} + \frac{\partial^2}{\partial y^2} \quad (3.3)$$

where E is modulus of elasticity and ν is the Poisson's ratio.

3.3 Approximate Solution Methods

In the plate vibration problems, sometimes it is not possible to get the exact solutions due to the complexity of the domain occupied by the plate and sometimes specified boundary conditions make the problem more complex. Therefore, we need to use the approximate methods (Chakraverty, 2009). There exist various approximate methods to handle plate vibration problems. The approximate methods, viz., Rayleigh, Rayleigh–Ritz method and

Galerikin method, are discussed to handle the vibration of the plate problems in this section, because only these methods are mainly used in the rest of the chapters of this thesis by using a newly developed solution methodology for vibration of the perforated plate problems. These approximate methods have been emphasized in this work because of their relative ease in understanding in comparison with some of the other methods, their historical significance, and widespread usage in the published literature of free vibrations, and the capability to obtain truly accurate frequencies in majority of the cases.

3.3.1 Rayleigh's Method

The Rayleigh's method may be applied to all continuous systems. This method requires expressions for maximum kinetic and potential energies of a system. Rayleigh's principle is based on the statement 'If the vibrating system is conservative (no energy is added or lost), then the maximum kinetic energy, ' T_{max} ', must be equal to the maximum potential (strain) energy, ' u_{max} '. For applying this principle, elastic plate undergoing free vibrations, with fundamental mode, is considered as system with one degree of freedom. This gives us a quotient known as Rayleigh's quotient. This methodology for finding the fundamental frequency of the plate is shown below (Chakraverty, 2009).

Kinetic energy of the plate T is given as,

$$T = \frac{1}{2} \iint_R h \rho \dot{w}^2(x, y, t) dx dy \quad (3.4)$$

Assuming that the plate is undergoing harmonic vibrations, and then vibrating middle surface of the plate can approximated by equation),

$$w(x, y, t) = W_1(x, y) \cos \omega_1 t \quad (3.5)$$

Where $W_1(x, y)$ is a continuous function that approximately represents the shape of the plate's deflected middle surface and satisfies at least the kinematic boundary conditions and ω_1 represents the natural frequency of the plate pertinent to the assumed shape function. Assume $\omega = \omega_1$ be its fundamental frequency

Maximum value of Kinetic energy is obtained at,

$$\sin^2 \omega_1 t = 1 \quad (3.6)$$

$$T_{\max} = \frac{\omega_1^2}{2} \sin^2 \omega_1 t \iint_R h \rho W_1^2(x, y) dx dy = \frac{1}{2} \omega_1^2 \iint_R h \rho W_1^2(x, y) dx dy \quad (3.7)$$

Maximum Strain energy is given as,

$$u_{\max} = \frac{1}{2} \iint_R D[(\nabla^2 W_1)^2 + 2(1-\nu)\left\{\left(\frac{\partial^2 W_1}{\partial x \partial y}\right)^2 - \frac{\partial^2 W_1}{\partial x^2} \frac{\partial^2 W_1}{\partial y^2}\right\}] dx dy \quad (3.8)$$

For conservative system by the Rayleigh's principal,

$$T_{\max} = u_{\max} \quad (3.9)$$

From equation (3.7) and (3.8)

$$\omega^2 = \frac{u_{\max}}{T_{\max}^*} \quad (3.10)$$

where $T_{\max}^* = \frac{T_{\max}}{\omega^2}$ is the integral over the plate area without the frequency.

$$\omega_{21}^2 = \frac{\iint_R D[(\nabla^2 W_1)^2 + 2(1-\nu)\{W_{1,xy}^2 - W_{1,xx} W_{1,yy}\}] dx dy}{h\rho \iint_R W_1^2 dx dy} \quad (3.11)$$

where ,

$$W_{1,xy} = \frac{\partial^2 W_1}{\partial x \partial y} \quad W_{1,xx} = \frac{\partial^2 W_1}{\partial x^2} \quad W_{1,yy} = \frac{\partial^2 W_1}{\partial y^2} \quad (3.12)$$

Equation (3.12) is called as the Rayleigh's Quotient and gives the fundamental natural frequency of the plate. For constant thickness and homogeneous plate, D , ρ and h are constant. Hence the Rayleigh's Quotient becomes,

$$\omega_{21}^2 = \frac{D \int_0^a \int_0^b [(\nabla^2 W_1)^2 + 2(1-\nu)\{W_{1,xy}^2 - W_{1,xx} W_{1,yy}\}] dx dy}{h\rho \int_0^a \int_0^b W_1^2 dx dy} \quad (3.13)$$

If shape function W_1 satisfies boundary conditions of the problem, as well as if it happens to be a good approximation to the fundamental mode shape, then the first frequency as given by the Rayleigh's method will give better approximation of the fundamental frequency (Chakraverty, 2009).

3.3.2 Rayleigh-Ritz's Method

The Rayleigh's Ritz method utilizes a series of the admissible functions to represent the vibratory displacement of a two-dimensional continuous system. That is, $W_I(x, y)$ in the equation (3.5) is written as (Leissa and Qatu, 2011)

$$W(x, y) = \sum_{i=1}^n C_i \phi_i(x, y) \quad (3.14)$$

Each of the ϕ_i in above equations satisfies at least the geometric boundary conditions. Geometric boundary conditions for the plate are those imposed on the displacements and slopes. If the set of admissible function is capable of representing any arbitrary displaced shape consistent with the geometric boundary conditions as $n \rightarrow \infty$ in equation (3.14), then the Rayleigh-Ritz procedure will converge monotonically to the exact frequencies as sufficient terms in equation (3.14) are taken. If not, then it will converge to the frequencies which are upper bounds on the exact frequencies (Leissa and Qatu, 2011).

To use the Rayleigh's-Ritz method one formulates u_{\max} and T_{\max} in terms of C_i and ϕ_i of equation (3.14), and then minimizes the frequency with respect to C_i . That is, one lets the method determine C_i so as to obtain the best upper bounds for the frequencies. The frequency minimizing equations are

$$\frac{\partial(\omega^2)}{\partial C_i} = 0, (i = 1, 2, \dots, n) \quad (3.15)$$

Substituting (3.10) into (3.15),

$$\frac{\partial}{\partial C_i} \left(\frac{u_{\max}}{T_{\max}^*} \right) = \frac{T_{\max}^* \left(\frac{\partial u_{\max}}{\partial C_i} \right) - u_{\max} \left(\frac{\partial T_{\max}^*}{\partial C_i} \right)}{(T_{\max}^*)^2} = 0 \quad (3.16)$$

or

$$T_{\max}^* \left(\frac{\partial u_{\max}}{\partial C_i} \right) - u_{\max} \left(\frac{\partial T_{\max}^*}{\partial C_i} \right) = 0 \quad (3.17)$$

Substituting $u_{\max} = \omega^2 T_{\max}^*$ from equation (3.10)

$$T_{\max}^* \left(\frac{\partial u_{\max}}{\partial C_i} - \omega^2 \frac{\partial T_{\max}^*}{\partial C_i} \right) = 0 \quad (3.18)$$

Because T_{max}^* is never zero except in a trivial solution, the foregoing equation (3.18) may be divided through by it to yield the following more useful set of the minimizing equations

$$\frac{\partial}{\partial C_i} (u_{max} - \omega^2 T_{max}^*) = 0, (i = 1, 2, \dots, n) \quad (3.19)$$

This is a set of n simultaneous, linear, algebraic equations in the unknown C_i . However, the equations are homogeneous (zero righthand-sides). For a nontrivial solution, the determinant of the coefficient matrix is set equal to zero. The roots of the determinant are the n values of ω^2 . The lowest value of ω^2 is an upper bound approximation to the fundamental frequency, and the higher values are also upper bound approximations (usually less accurate) to the higher frequencies for the plate (Leissa and Qatu, 2011). If we have n constants, we obtain n homogeneous equations, $n-1$ equations can be solved to express $n-1$ constants in terms of one arbitrarily selected constant. These constants are used to get mode shape by considering the material property distribution function $f(x)$.

3.3.3 Galerkin Method

In this section the general idea of the Galerkin method from the mathematical point of view is given with application to the plate vibration problem (Ventsel and Krauthammer, 2001).

Let a differential equation of a given two dimensional boundary value problem be of the form,

$$L[W(x, y)] = p(x, y) \text{ in some two dimensional domain } \Omega \quad (3.20)$$

Where $W(x, y)$ is an unknown function of two variables and p is a given load term defined also in the domain Ω . The symbol L indicates either a linear or nonlinear differential operator. The function W must satisfy the prescribed boundary conditions on the boundary Γ of that domain. An approximate solution of the equation (3.20) is sought in the following form (Ventsel and Krauthammer, 2001),

$$W_N(x, y) = \sum_{i=1}^N \alpha_i f_i(x, y) \quad (3.21)$$

Where α_i are unknown coefficients to be determined and $f_i(x, y)$ are the linearly independent coordinate functions also called trial functions, which satisfy all the prescribed boundary conditions but not necessarily satisfy the equation (3.20). From calculus, any two functions

$f_1(x)$ and $f_2(x)$ are called mutually orthogonal in the interval (a, b) if they satisfy the condition.

$$\int_a^b f_1(x)f_2(x)dx = 0 \quad (3.22)$$

If a function $W(x, y)$ is an exact solution of the given boundary value problem, then the function $[L(W) - p]$ will be orthogonal to any set of functions. Since the deflection function $W_N(x, y)$ in the form of the equation (3.21) is an approximate solution of the equation (3.20), thus $[L(W) - p] \neq 0$, and it is no longer orthogonal to any set of functions. However, we can require that the magnitude of the function $[L(W) - p]$ be minimum. This requirement is equivalent to the condition that the above function should be orthogonal to some bounded set of the functions: first of all, to the trial functions $f_i(x, y)$. It leads to the following Galerkin equation.

$$\iint_A [L(W_N) - p]f_i(x, y)dxdy = 0 \quad (3.23)$$

Substituting for W_N from equation (3.21), we obtain,

$$\iint_A \left[L \left(\sum_{i=1}^N \alpha_i f_i(x, y) - p \right) \right] f_j(x, y)dxdy = 0, (j = 1, 2, \dots, N) \quad (3.24)$$

Introducing the residual error function $E(W_N)$, as follows,

$$E(W_N) = L \left(\sum_{i=1}^N \alpha_i f_i(x, y) \right) - p \quad (3.25)$$

Rewriting the above Galerkin equation in the form,

$$\iint_A E(\alpha_i, f_i(x, y); p)f_j(x, y)dxdy = 0; (j = 1, 2, \dots, N.) \quad (3.26)$$

The requirement in the above equation (3.26) is used as a condition for determining the coefficients α_i . Replacing the integral in the equation (3.26) by the sum of integrals, the following system of linear algebraic equations is obtained:

$$\begin{array}{l} a_{11}\alpha_1 + a_{12}\alpha_2 + \dots + a_{1N}\alpha_N = b_1 \\ \text{-----} \\ a_{N1}\alpha_1 + a_{N2}\alpha_2 + \dots + a_{NN}\alpha_N = b_N, \end{array} \quad (3.27)$$

Where,

$$a_{ij} = \iint_A L(f_i) \cdot f_j dx dy; b_i = \iint_A p \cdot f_j dx dy, (i, j = 1, 2, \dots, N.) \quad (3.28)$$

Solving equations (3.27), we can determine the unknown coefficients α_i . Which, in conjunction with the equation (3.21), gives the N-parameter Galerkin approximation of the equation (3.20). If $N \rightarrow \infty$, the Galerkin solution approaches the exact solution if the system of functions $f_1; f_2; \dots$ is complete and linearly independent.

3.4 Formulation of the Problem

To describe the free vibration of the plate with array of holes, need of the approximate solution techniques is apparent as mathematical complexity involved is more due to the variation of the material properties in the solid area and in the area occupied by hole. Equations describing free vibration of the rectangular homogeneous thin solid plate are simple and exact solutions are possible. But for the rectangular thin plates with the array of holes, solution becomes impractical due to the varying flexural rigidity. Most of the engineering applications do not involve simple solid rectangular plates. The perforated plates being not amenable by the exact solution techniques, one has to choose the approximate techniques for the solution of such problems. A satisfactory analytical solution first requires a suitable function to describe the variation of the material properties due to the perforations. The ratio of the thickness of the plate to its average lateral dimensions is taken not to exceed 1/20 to represent its fundamental vibration mode reasonably accurately with the classical thin plate theory.

In this thesis, problem of determining the fundamental frequency of free vibration of the perforated rectangular plate is studied in the two main categories.

1. The rectangular plates with the rectangular/square perforations
2. The rectangular plates with the circular perforations

3.4.1 The Rectangular Plates with the Rectangular/Square Perforations

For the analytical formulation of this type of the problem the Rayleigh's and Rayleigh-Ritz method with proper trial functions satisfying the given boundary conditions is used. These methods are applied to the following subcategories of the problem.

- a) *Plates with the rectangular/square perforations arranged in the rectangular/square array.*

For the solution of this type of the problem unit step functions are used to describe the variation of the material properties due to the perforations.

b) Plates with the rectangular/square perforations arranged in the staggered (triangular) arrays.

For the solution of this type of the problem unit step functions are used to describe the variation of the material properties by introducing expressions for phase differences due to the perforations.

c) Plates with the square perforations arranged in the square array.

For the solution of this type of the problem greatest integer functions are used to describe the variation of the material properties due to the perforations.

d) Moderately thick plates with the rectangular/square perforations arranged in the rectangular/square array.

For the solution of this type of the problem unit step functions are used to describe the variation of the material properties due to the perforations. Mindlin plate theory is used for the analytical formulation.

3.4.2 The Rectangular Plates with the Circular Perforations

The solution of this category of the problem is obtained by three methods. Perforation pattern considered is rectangular. According to the methods used for modeling, problem is further classified in to following subcategories.

a) Concept of the added concentrated negative mass to represent the hole

Equation of the plate vibration is obtained by substituting the inertia force for the holes in the equations of Galerkin formulation. Here perforations are considered as the concentrated negative mass.

b) Circular perforations replaced by the equivalent square perforations

In this approach circular perforations are replaced by equivalent square perforations and unit step functions are used to express the variation of the material properties due to the perforations. The Rayleigh's method is used to formulate the analytical model.

c) Determination of the modal constant expression for the fundamental frequency.

This is hybrid approach in which analytical formulation and experimental results are combined. In the Rayleigh's formulation the fundamental frequency values are taken from the experimental analysis. This problem is solved in reverse order by considering known experimental values of the fundamental frequency.

d) Use of the Heaviside function to exactly map the circular perforations to represent the material property variation.

In this approach material property variation function is formulated by using the Heaviside function. Heaviside function is exactly mapping the multiple circular perforations.

3.5 Validation of the Results Obtained by the Analytical Models

To access the accuracy and applicability of the analytical models formulated, the fundamental frequency results of the numerical analysis were compared with the FEM analysis results for the every specimen and the experimental results obtained for the representative specimens.

3.5.1 Validation by the Experimental Results of the Fundamental Frequency

Representative specimens of the perforated plates were constructed with the same perforation configuration as those analyzed numerically. The plates were securely mounted in a heavy frame to obtain the clamped all edges boundary condition. PCB Piezotronics Ltd., model number 086C03 Impact Hammer, PCB Piezotronics Ltd., model number 352C68 accelerometer and Larson and Davis 3000+ Vrite, dual channel signal analyzer were used to record the frequency response data at various locations on the plate. These data were transferred to a PC running the analysis software where the resonant frequencies of the vibration were determined and recorded.

3.5.2 Validation by the FEM Results of the Fundamental Frequency

The modal analysis is carried out by ANSYS 11 using Shell 63 element. Shell 63 has both bending and membrane capabilities. Both in-plane and normal loads are permitted. The element has six degrees of freedom at each node: translations in the nodal x, y, and z directions and rotations about the nodal x, y, and z axes. Meshing is done by free meshing with smart size option and quadrilateral elements are used. Mesh convergence for the FEM results is checked for the every specimen. This is checked by running different simulations. Final solution is chosen based on the mesh quality as well as mesh size. Thus converged solution is one with the lowest eigenfrequencies. It is assumed that the structure is formed of an isotropic homogeneous elastic material, i.e. Mild Steel with the material properties same as used in the numerical analysis.

3.6 Concluding Remark

For the formulation of the analytical models to determine the fundamental frequency of the perforated plates approximate methods are more suitable. These methods require

special functions to express the variation of the material properties. Also appropriate shape functions are to be chosen to represent the deflection of the plate's middle surface. Also based on the experimental results, it is possible to find an expression for the modal constant for the fundamental frequency. In this work analytical models formulated to determine the fundamental frequency of the perforated rectangular plates are classified in to the two broad categories, i.e. plates with the rectangular/ square perforations and the plates with the circular perforations. Table 3.1 gives the summary of the plate configurations for which the analytical models are formulated.

Table 3.1 Summary of the problems considered

Sr. no.	Type of problem/Approach of solution	Perforation type	Perforation pattern
Rectangular plates with the rectangular/square perforations			
1	Rectangular/square perforations arranged in the rectangular/square array	Rectangular/ Square	Rectangular/Square
2	Rectangular/square perforations arranged in the staggered (triangular) arrays	Rectangular/ Square	Staggered 60° and 45°
3	Square perforations arranged in the square array	Square	Square
Rectangular plates with the circular perforations			
4	Concept of added the concentrated negative mass to represent the hole	Circular	Rectangular/ Square
5	Circular perforations replaced by the equivalent square perforations	Circular	Rectangular/ Square
6	Determination of the modal constant expression for fundamental frequency.	Circular	Rectangular/ Square
7	Use of the Heaviside function to map circular perforations	Circular	Rectangular/ Square
Moderately thick rectangular plates with the rectangular/square perforations			
8	Rectangular/square perforations arranged in the rectangular/square array	Rectangular/ Square	Rectangular/Square

Chapter 4

Experimental Determination of the Fundamental Frequency

4.1 Introduction

The fundamental frequency results obtained by the experimental modal analysis are used to validate the analytical models developed. In this chapter detail of the experimental set up and the procedure of the experimentation are given. Procedure given here is uniformly followed for the testing of the specimens discussed in the further chapters of this thesis. For each of the representative plate specimen considered in the experiments boundary condition considered is clamped on all the edges. This boundary condition was applied as the analytical predictions of the fundamental frequency are calculated for the clamped all edges boundary condition.

4.2 Parameters of the Perforated Plate Specimens

In order to have sufficiently representative results, a representative specimen of the plates was selected in which the various parameters were varied, i.e. perforation size, perforation pattern, ligament efficiency. All the plates are made of the mild steel. The outer dimensions of all the specimens are 259 mm X 207 mm X 2 mm, but effective outer dimensions of the perforated area are 216 mm X 138 mm X 2 mm. All specimens are of the mild steel with aspect ratio $(b/a) = 1.564$. The material properties assumed for the plate are listed in Table 4.1. (Armenakas, 2006). The plate outer dimensions were kept constant so that all the plates could be supported in a single fixture frame manufactured to achieve clamped all edges boundary condition. Details of the geometric parameters of the perforated plate specimens tested experimentally are given in the respective chapters. Photo graphs of the perforated plates used in the experiment are also given in the respective chapters.

Table 4.1 Material properties assumed for the steel plate (Armenakas, 2006)

Sr. No.	Material property	Value
1	Young's modulus (E_o)	$2.1 \times 10^{11} \text{ N/m}^2$
2	Poisson's ratio (ν_o)	0.3
3	Density (ρ_o)	7850 kg/m^3

4.3 Details of the Fixture Used for Clamping the Plate Specimens

Figure 4.1 shows the schematic of the specimens used for the testing and the fixture plate. The margin with the holes, outside the effective area, is kept to clamp the specimens between two fixture plates to get the clamped-clamped boundary condition on all the four edges of the specimen. The test fixture mainly consists of the two rectangular plates of outer dimensions 259 mm X 207 mm X 9.2 mm. Both these fixture plates have central rectangular cut outs of dimension 216 mm X 138 mm, which are aligned concentrically one over the other. The test specimen with all four outside edges fixed was held centrally between these fixture plates. Figure 4.1 shows one of the two similar fixture plates with the central rectangular cut-out and holes, along circumference for bolting the plates firmly. These fixture plates, with the test specimen sandwiched, were clamped together by using the nut bolt assembly in the holes provided along the circumference of the fixture plates as shown in Figure 4.2, thus required boundary condition of all four outside edges fixed was achieved.

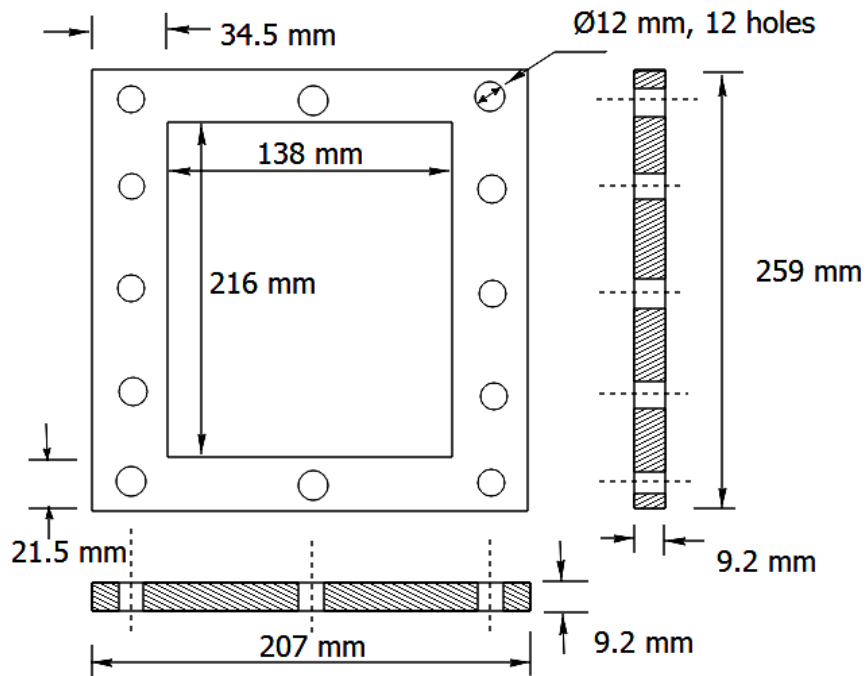


Figure 4.1 (a) Schematic of the fixture plate

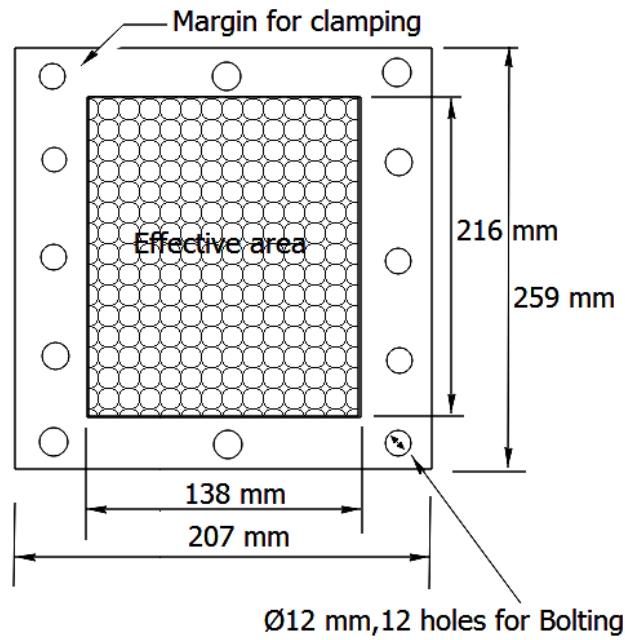


Figure 4.1 (b) Schematic of the 2 mm thick representative specimen

Figure 4.1 Schematic of fixture the plate and the representative specimen used for experimentation



Figure 4.2 The fixture and specimen



Figure 4.3 Experimental set up

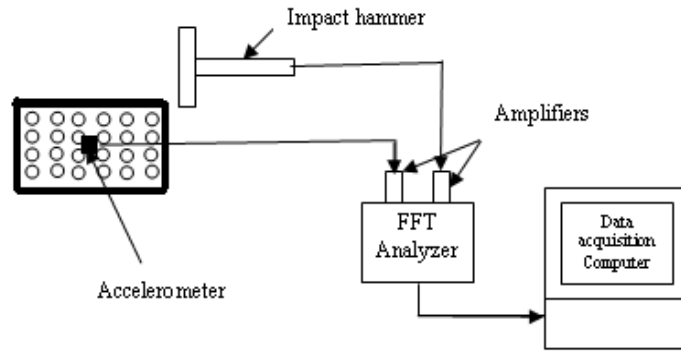


Figure 4.4 Schematic of the experimental set up

4.4 Experimental Set up and Procedure

Experimentation was carried with the help of two channel FFT analyzer, impact hammer and accelerometer (Harris, 2002; Larson and Davis Inc., 2008). Specifications of the instruments used are given in Appendix ‘C’. Figure 4.3 shows the experimental set up used for the testing and Figure 4.4 shows schematic of the experimental set up. The assembly of the fixture plates with the test specimen placed centrally between them was clamped firmly to the rigid foundation of a machine tool. For clamping the test fixture firmly to the rigid foundation, bolt heads were inserted in the horizontal **T** slots of foundation and were passed through the holes provided along the circumference of the fixture plates. Hexagonal nuts were tightened over the bolts for firmly holding the test fixture. Care was taken in applying uniform pressure at all the bolts with the help of torque wrench. Uniform torque of magnitude 28 N/m was applied to all the bolts for tightening (Fastenal Technical reference Guide, 2005) Four sampling points were chosen for mounting the accelerometer from driving point survey, such that node will not occur at these points. Fixed response method was used for taking the readings. The transfer function of each sampling point was calculated by the spectrum analyzer and was recorded for the sixteen impacts to get the final spectrum for the each specimen plate. Such experiments were repeated for ten times for each specimen plate. Final results of the natural frequencies for each specimen plate were mean values of the ten readings. Final values of the natural frequency are tabulated in the result tables. The weight of the accelerometer (Model: 352C68, PCB Co., USA) is 2 g. The approximate weight of the specimen ranges from 303.51g (specimen 6.15) to 467 g (full solid plate). The dynamic mass of accelerometer is much less than that of the plate so influence of the mass of the accelerometer on the dynamic behavior of the specimen can be neglected. A general rule is, the accelerometer mass should be less than one-tenth from the effective mass of the structure

to which it is attached (Wang and Lai , 2003; Baharin 2008, Baharin and Rahman, 2009; Harris, 2002)

4.5 Clamped All Edges Boundary Condition

Clamped all edges boundary condition is quite frequently used in the experiments. To achieve this boundary condition displacements and rotations at the edges were restricted. The realization of such a boundary condition in practice can't be perfectly achieved. However it is found from the reported literature that (Kaap, 1997; Baharin, 2008; Wang and Wereley, 2005; Wang and Lai 2003; Bellés and Pombo, 2007) attempts have been made to achieve clamped all edges boundary condition. Similar to the methods used in the above references a frame 259 mm X 207 mm was constructed to clamp the plate. The frame was made of cast iron and mass was also large and further plate and fixture both were bolted (with M12 bolts) to the machine tool base. Thus it prevented the frame moving together with the plate as shown in Figure 4.2 and 4.5. Further effects of spacing and number of bolts, fit of the bolts in the plate fixture assembly used for clamping, on the natural frequency were determined.

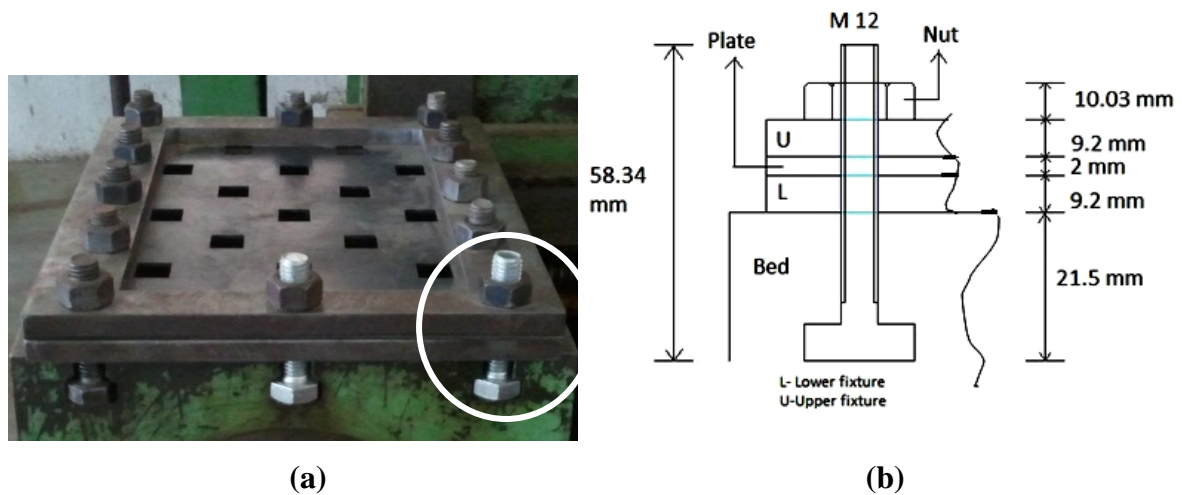


Figure 4.5 Diagram of the frame (side view) for the clamped boundary condition

4.5.1 Effect of Fit of the Bolts in the Plate-Fixture Assembly, On the Natural Frequency

In this exercise, we found out the effect that the size of the bolts or type of the fit obtained due to the clamping bolts will have on the natural frequency of the perforated plate. We achieved this by varying the dimensions of the clamping bolts. The solid rectangular plate was clamped to the machine bed sandwiched between two fixtures as shown in Figure 4.6. The fundamental frequency of the solid plate (138 mm x 216 mm x 2 mm) was obtained experimentally three times by using three sets of the clamping bolts one by one in each experiment. A set of 12 bolts were used at a time to secure plate-fixture arrangement to the

machine bed. Out of the three sets one set used was standard M12 coarse bolts where as we prepared two sets of the bolts by machining, each set with the different diameter of the bolt to obtain required fit. Details of the dimensions of the M12 coarse bolt are given in Table 4.2.

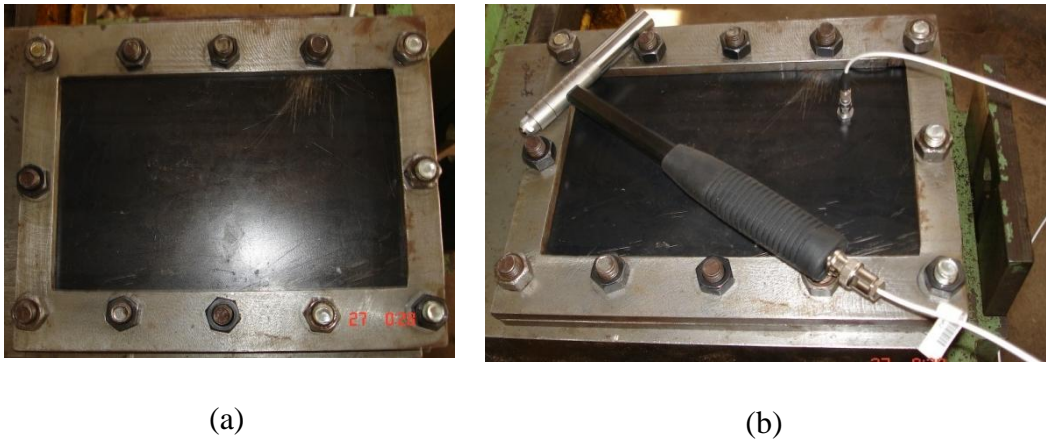


Figure 4.6 Solid plate specimen used in the experiments

Table 4.2 Details of the dimensions of M12 course bolt

Nominal Diameter, mm	Pitch, mm	Root radius, mm	Pitch diameter, mm
12	1.75	0.253	10.863

Using the above dimensions and tolerances, we obtained two different sets of the bolts machined to a length of 43.6 mm from bottom of the head, according to the following criteria:

1. Normal Running fit-Difference of 30 to 50 μ
2. Loose running fit-Difference of 80 to 100 μ

The Nominal diameter obtained for the individual criteria are:

Table 4.3 Details of the nominal diameter dimensions of the bolts for three sets

Set	Type of fit	Nominal Diameter, mm
Set1	Interference	12
Set2	Normal running fit	11.45
Set3	Loose running fit	11.40

4.5.2 Results and Discussions

The rectangular solid plate of thickness 2 mm having effective dimensions 138 mm x 216 mm was tested experimentally to find the fundamental frequency by using each set of the bolts given in Table 4.3. Figure 4.6 shows the specimen plate used in the experiments.

Experiments were performed three times using one set of the bolts at a time and following the procedure given in the section 4.4. Figure 4.7 shows the FRF (Frequency response Function) obtained from one of the experimental run for solid plate clamped with the Set1 Bolts. Results obtained are tabulated in Table 4.4.

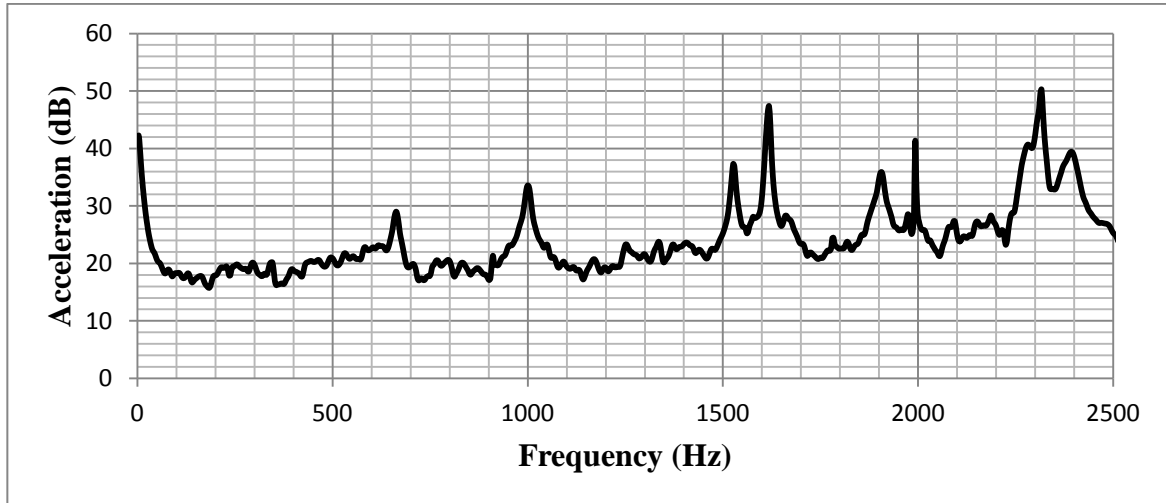


Figure 4.7 Frequency response Function (FRF) obtained with the Set1 Bolts

Table 4.4 Fundamental frequency results for the solid rectangular plate

Sr. No.	Set of bolts	Fundamental Frequency(Hz)	Absolute error(Hz)
1	Set1	663.071	-
2	Set2	659.898	3.173
3	Set3	659.898	3.173

Thus from the fundamental frequency results it is found that the effect of fit of the bolts on the fundamental frequency obtained is negligible. It gives maximum discrepancy of 0.47% in the results obtained. For the Set 1 bolts the fundamental frequency obtained is more by 3.172 hertz compared to other as it closely resembles the required boundary condition of the clamped all edges. Hence in all the experimental tests M12 coarse bolts with Interference fit are used i.e. the Set 1 bolts.

4.5.3 Effect of the Spacing and the Number of Bolts Used To Clamp the Plate-Fixture Assembly, On the Natural Frequency

We analyzed effect of the bolt spacing (Number of bolts) used for clamping the fixture, on the natural frequency of the plate. This effect was analyzed by conducting an experimental modal test on the solid plate of size 138 mm x 216 mm x 2 mm. The Solid plate

was tested three times with different arrangement of the bolt spacing in each test. The arrangements used for clamping the fixture are shown in Figure 4.8 to 4.10.

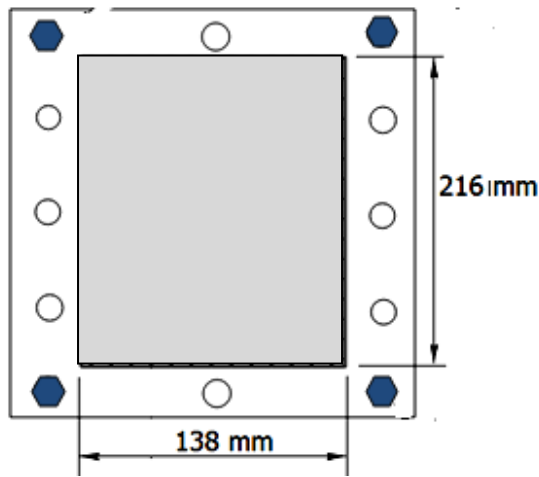


Figure 4.8 Bolt spacing arrangement first

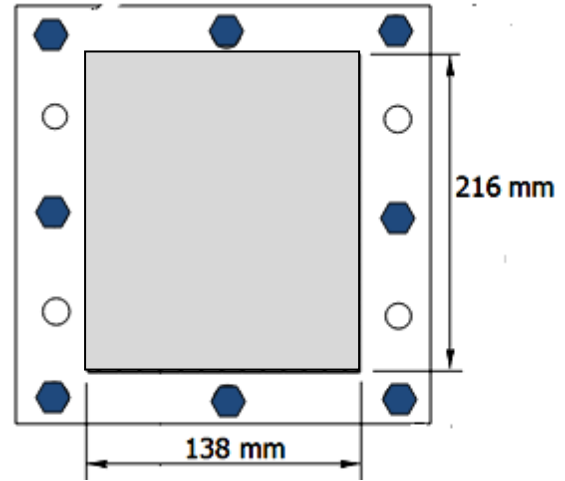


Figure 4.9 Bolt spacing arrangement second

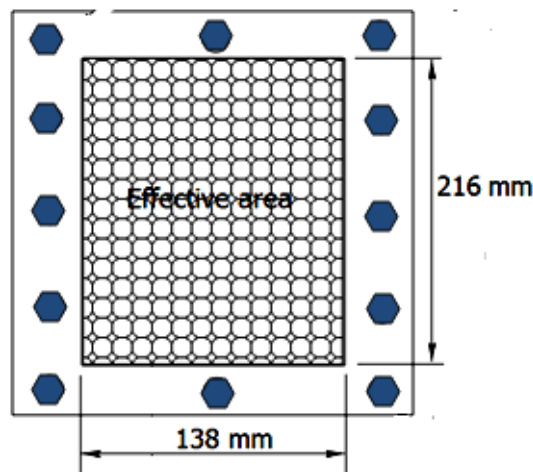


Figure 4.10 Bolt spacing arrangement third

In first arrangement as shown in Figure 4.8 only four bolts were used to clamp the plate at the four corners of the fixture. In this case spacing between the bolts is largest. Clamping arrangements second and third were obtained by eight and twelve bolts as shown in Figure 4.9 and Figure 4.10 respectively. In second arrangement one bolt was added on each side in between the two corner bolts giving intermediate spacing, whereas in third arrangement, on each larger side of the fixture two more bolts were added to get the five clamping bolts on each larger side. Due to the unavailability of the slots on the machine bed it was not possible to accommodate more than three clamping bolts on each of the small side of

the fixture. Thus we obtained three different clamped all edges arrangements to check the influence of the bolt spacing on the natural frequency of the plate.

4.5.3 Results and Discussion

Experiments were performed on the solid plate by following the procedure given in the Section 4.4. Results obtained from the experiment with each of the arrangements shown in Figure 4.8 to 4.10 are given in Table 4.5. Corresponding Frequency response functions are shown in Figure 4.11 to 4.13.

Table 4.5 Experimental natural frequencies with the different bolt spacing

Bolt spacing Arrangement	Experimental fundamental frequency ω_1,Hz	Analytical fundamental frequency ω_1,Hz	% Deviation
1	512.5	694.882	26.24
2	612.5		11.85
3	663.071		4.57

The experimentally obtained fundamental frequencies are compared with the analytical fundamental frequency obtained by the Rayleigh's method with shape function

$$W_1(x, y) = \left(x^2 - \frac{a^2}{4}\right)^2 \left(y^2 - \frac{b^2}{4}\right)^2 \quad (4.1)$$

It is observed that the bolt spacing influences the fundamental frequency significantly. From the Table 4.5, the bolt spacing arrangement first gives the maximum discrepancy in the results where as the bolt spacing arrangement third gives the minimum discrepancy of 4.57 % in the results. Thus as the bolts spacing decreased the fundamental frequency increased. Decreasing space between the bolts makes the plate more and more stiff which increases the strain energy of the plate, due to which the fundamental frequency goes on increasing. Thus to obtain close resemblance to the clamped boundary condition the bolt spacing should be minimum as possible. Due to the influence of the bolt spacing on the fundamental frequency we have used the bolt spacing arrangement as shown in Figure 4.10 in all the experiments.

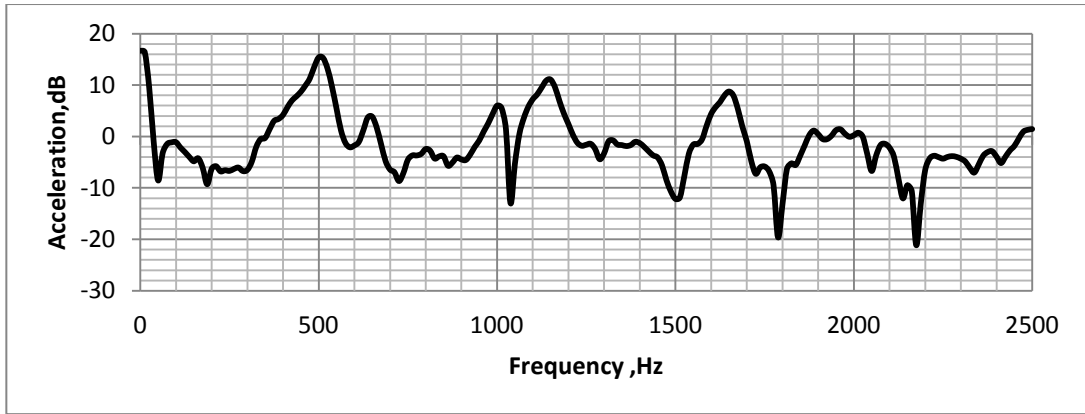


Figure 4.11 Sample frequency response function (FRF) obtained with the bolts spacing arrangement first

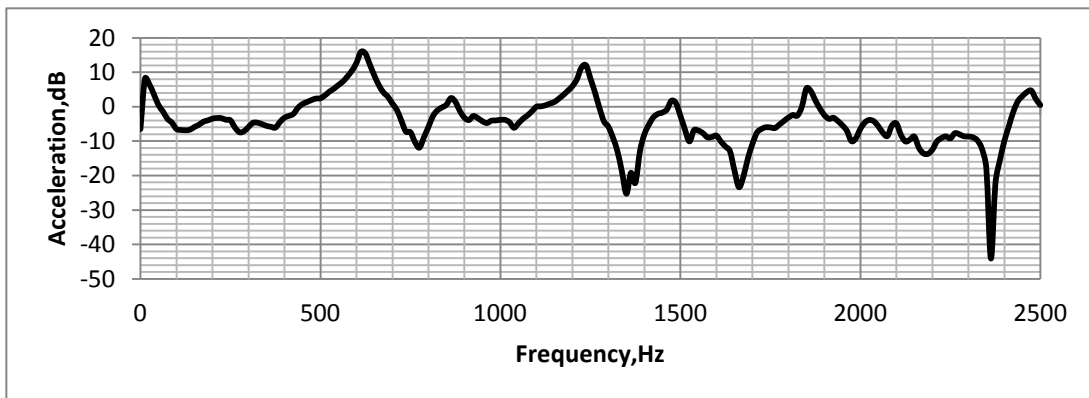


Figure 4.12 Sample frequency response function (FRF) obtained with the bolts spacing arrangement second

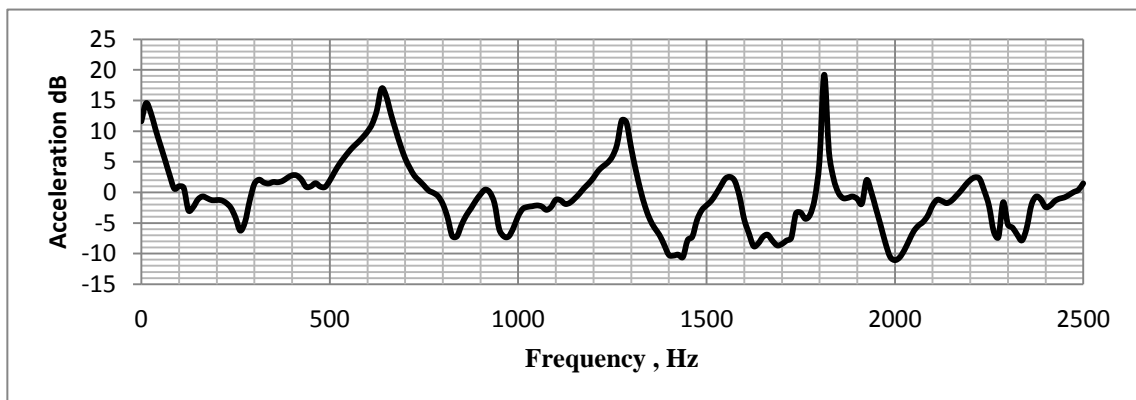


Figure 4.13 Sample frequency response function (FRF) obtained with the bolts spacing arrangement third

4.6 Effect of the Impact Location and the Hammer Tip on the Frequency Response Function (FRF)

4.6.1 Effect of the Impact Location:

This section discusses the effect of the impact location on the resulting frequency response function (FRF). While performing impact testing, the input impact location can have a very significant effect on the resulting frequency response function. For this study, solid rectangular plate is divided in to a grid of 10 x 10 points. Top diagonally symmetric portion with encircled points which has 15 node points is considered for study as shown in Figure 4.14 & 4.15. Points 1, 5, 12 and 15 were chosen for accelerometer positions and for each of the accelerometer position; excitation was given at the remaining three nodes. For example if accelerometer is at position 1 then excitation was given at the points 5,12 and 15.

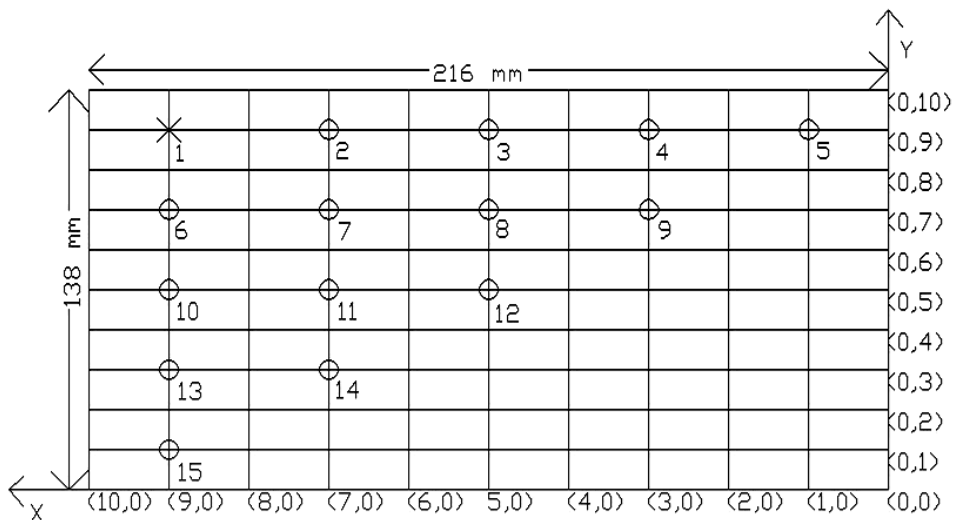


Figure 4.14 Layout of the experimental grid points on the plate



Figure 4.15 The experimental set up

The following two aspects were focused for the discussion:

1. Effect on the relative amplitude of the first three frequencies for the different hammer locations
2. Effect on the relative amplitude of the first three frequencies for the different accelerometer locations

The experimentation was conducted for analyzing above two aspects by using, roving excitation method i. e. excitation is roving and the response is fixed. The transfer function of each impact location was calculated by the spectrum analyzer (Spider-81 vibration controller system, Crystal Instruments) and was recorded for the eight impacts to get the final spectrum for each impact location. Such experiments were repeated for each point 1,5,12, and 15. Final results of the FRF for each point for the particular accelerometer location are given in Figures 4.16. The impact hammer and accelerometer used are the same as given in the section 4.4.

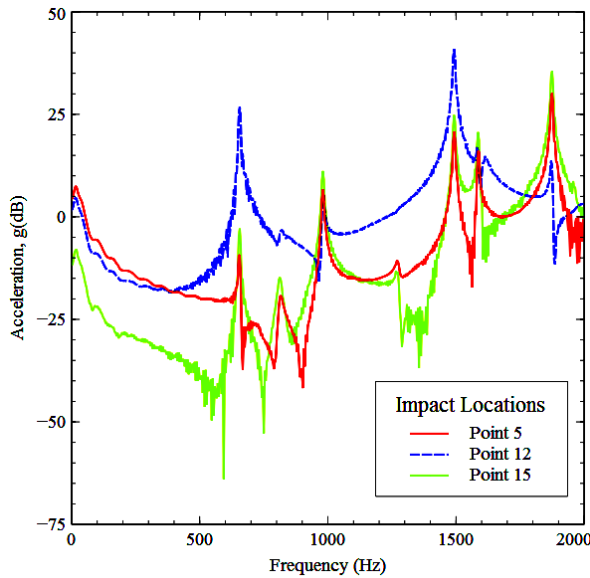
4.6.2 Results and Discussion

The FRF plots are obtained for the accelerometer locations at the point 1, 5, 12 and 15 and are given in Figure 4.16. For each accelerometer location the impact points are chosen at the three remaining nodes. Thus for the each accelerometer location three FRF's are obtained and are superposed as shown in Figure 4.16. These cases are presented here because effect of the accelerometer and the impact location on the amplitude of the resonance peaks in the FRF, is a very common problem during the impact testing.

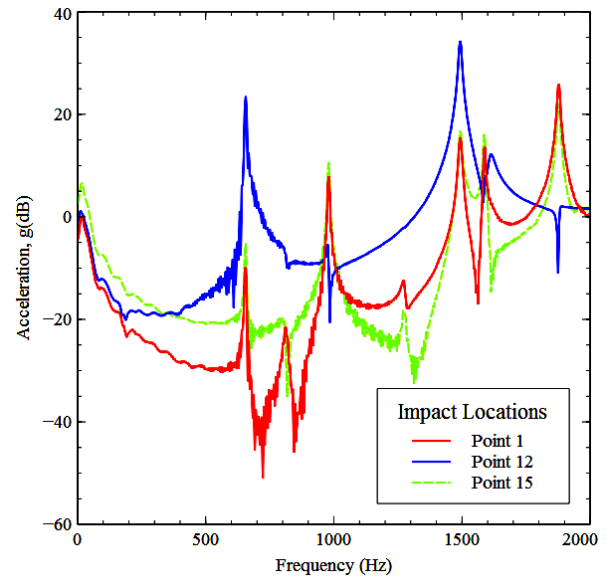
From the FRF's obtained it can be observed that, for a particular accelerometer location amplitude of the resonance peak depends on the impact location. It is also important to include sufficient points in the test to describe modes of the interest. If the excitation point has not been chosen carefully or if enough response points are not measured, then a particular mode may not be adequately represented. This can be observed for the accelerometer location at point 12 where the second frequency peak is not distinctive. This may be because of a node at point 12 for mode 2. Thus at times it may become necessary to include more than one excitation location in order to adequately describe all of the modes of the interest. The frequency responses can be measured independently with single-point excitation or simultaneously with the multiple-point excitations.

It is observed that the response level tend to increase as the impact location moves towards a response transducer, or a response transducer moves towards the impact location, and tend to

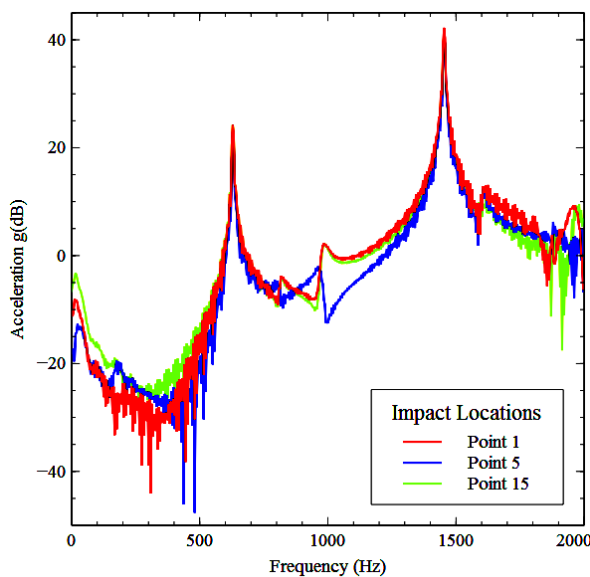
decrease as the impact location and the response transducer move further apart. In the following figures it appears that the impulse hammer hit location has, no effect on the eigenfrequency, yet a difference in amplitude of the eigenfrequencies is observed. The amplitude of the peak at each location describes the mode shape for the associated resonant frequency. The results indicate that for the first mode and the third mode, the fixed plate has maximum deflection at the middle.



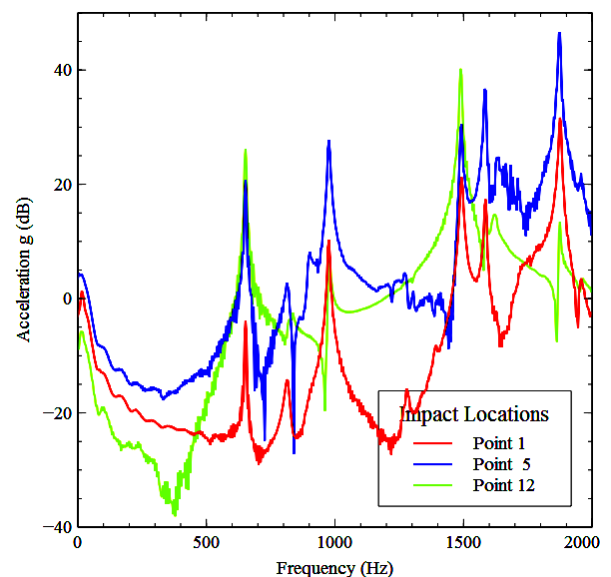
(a) FRF's for the accelerometer location at point-1



(b) FRF's for the accelerometer location at point -5



(c) FRF's for the accelerometer location at point -12



(d) FRF's for the accelerometer location at point -15

Figure 4.16 FRF's for different accelerometer locations on the plate

- **Some Key Observations:**

1. It can be noted that when the hammer position is at point-12 (centre of the plate) and the accelerometer location is varied, the overall amplitude of the FRF is maximum for the first and third resonant peak.
2. Also a common observation for all the roving locations is that for any particular FRF, the relative amplitude of the first three frequencies is as follows: 3rd Frequency > 1st Frequency > 2nd Frequency.
3. When the accelerometer is kept at Point-12, the FRF is almost the same irrespective of the hammer location.
4. More modes were excited when the impact was given at the corner positions compared to when it was given at the center position (Point-12).
5. Resonant peak amplitudes vary due to the inconsistency of the impact location whether it be not impacting the same location for each measurement or for not maintaining a consistent strike angle for the each measurement.
6. For each average that makes up the complete measurement, a very well controlled, precise impact excitation needs to be maintained.

4.6.3 Effect of the Impact Hammer Tip:

The selection of the hammer tip can have a significant effect on the FRF acquired. The impulse force excites all the resonances within its useful frequency range. The frequency content of the energy applied to the structure is a function of the stiffness of the contacting surfaces and, to a less extent, the mass of the hammer. The stiffness of the contacting surfaces affects the shape of the force pulse, which in turn determines the frequency content. It is not feasible to change the stiffness of the test object; therefore the frequency content is controlled by varying the stiffness of the hammer tip. (Agilent Technologies, 2001; Halversen, and David L. Brown,1977)

The effect of the hammer tip on the pulse and the force spectrum is illustrated in Figure 4.17 and Figure 4.18 respectively. The effect is studied for three types of tips metal, plastic and rubber. A solid rectangular plate was excited by using these tips one by one in three different tests. It is observed from the comparison of the pulse durations that the pulse duration for rubber tip is more where as for metal tip and the plastic tip pulse duration shows small variation i.e. slightly more for plastic tip. From Figure 4.18 it can be seen that if too soft a tip is selected then all the modes will not be excited adequately in order to obtain a

good measurement as in case of the rubber tip. The input power spectrum does not excite all of the frequency ranges of interest. Further it can be seen from input power spectrum of metal tip that harder the tip, the shorter the pulse duration and thus the higher the frequency content. Too hard a hammer tip can cause problems; energy is imparted to the structure beyond the frequency range of the interest and may overload the response (Avitabile, 2001). In all the experiments for the perforated plates we have used plastic tip as this tip excites the useful frequency range.

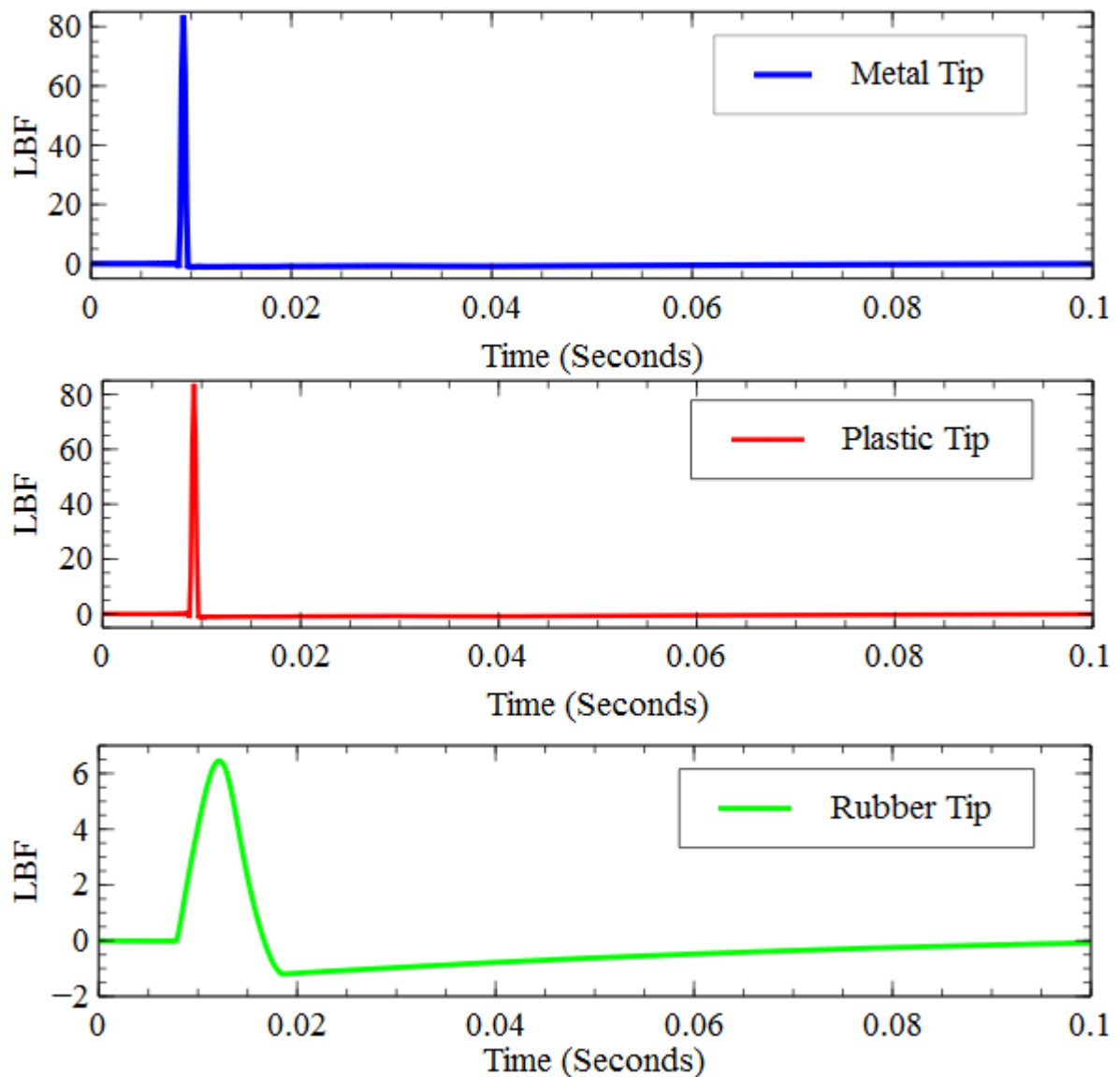


Figure 4.17 Force pulse with the different impact tips on the impact hammer

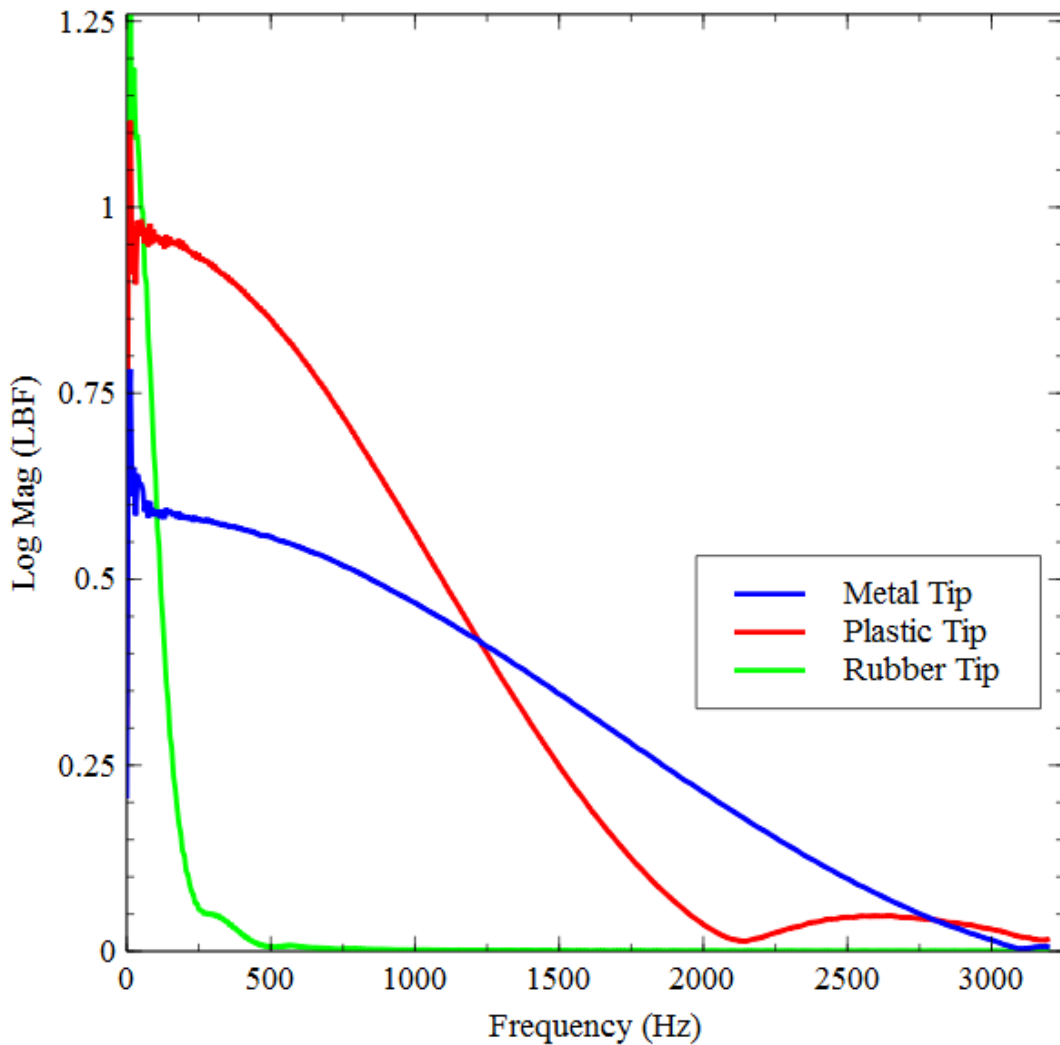


Figure 4.18 Force spectrums with the different impact tips on the impact hammer

4.7 Calculation of the Damping by Half Power Bandwidth Method

To calculate the damping ratio from the FRF, we have used half-power bandwidth method. In this method, first FRF amplitude is obtained. Corresponding to each natural frequency, there is a peak in the FRF amplitude, 3 dB down from the peak ,

(Peak amplitude / $\sqrt{2}$ for linear scale of amplitude) there are two points corresponding to the half power point, as shown in Figure 4.19. The more the frequency range between these two points, more the damping.

Vibration theory shows that (Rao, 1986; Thomson, 1997) the damping ratio is related to the sharpness of the peak of the magnitude plot. The damping ratio, ζ , can be determined by computing Q, i.e. quality factor defined as the resonant frequency divided by the bandwidth. Q is computed as:

$$Q = \frac{\omega_n}{\omega_2 - \omega_1} \quad (4.2)$$

The damping ratio is then given by

$$\zeta = \frac{1}{2Q} \quad \text{or} \quad \zeta = \frac{\omega_2 - \omega_1}{2\omega_n} \quad (4.3)$$

Where ω_n is the resonant frequency at the peak in Hz; ω_1 and ω_2 are the half power points at $\frac{A_{\max}}{\sqrt{2}}$ for linear scale of the amplitude or measured -3 dB down from the peak for log scale of magnitude as shown in Figure 4.19.

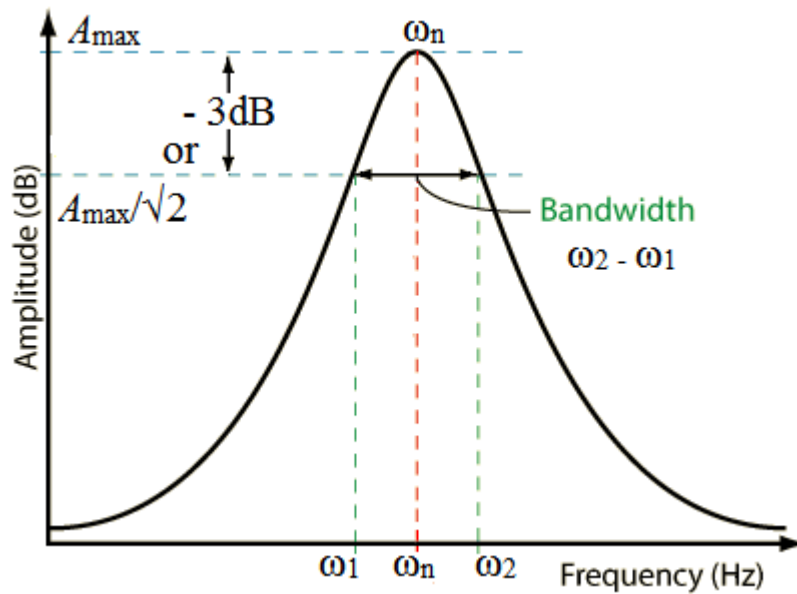


Figure 4.19 Half power bandwidth method

The damping factors (ζ) for the first two modes are calculated for each specimen plate tested experimentally. Results of these (ζ) are given in the Appendix “D” along with first two FEM and experimental frequencies. However damping factors for first two modes for the solid rectangular plate are given in Table 4.6 below.

Table 4.6 Damping factors for the first two modes of the solid plate specimen

ω_1 (Hz)		ζ_1	ω_2 (Hz)		ζ_2
Experi.	FEM		Experi.	FEM	
663.071	693.62	0.0105	974	1040.5	0.0069

It can be observed from the damping factors that the structure is lightly damped. Damping factor for first mode is 0.0105 and decreases in the sequence $\zeta_1 > \zeta_2$.

4.8 Concluding Remark

To validate the results obtained by the analytical models formulated in the forthcoming chapters, the experimental natural frequencies are used. Experimentation is carried out as explained in the section 4.4. Experimentation is carried out for one or two representative specimens only wherever possible, due to the limitations of the fixture dimensions.

Though the experimentation is carried out for the representative specimens, each of the specimens analyzed numerically is validated by comparing results with the results obtained from the FE simulation.

Section One

**Analytical Models to Determine the Fundamental Frequency of
the Rectangular Plates with the Rectangular/Square Perforations
(Chapter 5 and 6)**

Chapter 5

Analytical Models for the Rectangular Plate with the Rectangular and Square Patterns of the Perforations

5.1 Introduction

In this chapter the analytical models to determine the fundamental frequency of the perforated plate are formulated. The perforations considered are the rectangular / square whereas perforation patterns considered are the rectangular and square. The non homogeneity in the Young's modulus and the density due to the perforation is expressed by using the unit step functions and the greatest integer functions in the Rayleigh's Quotient. In the present analysis boundary condition considered is clamped at all edges. The perforated plate is considered as the plate with uniformly distributed mass and the holes are considered as the non homogeneous patches. The deflected middle surface of the plate is approximated by a function which satisfies the boundary conditions. Proposed models are validated by comparing the numerical analysis results with the Finite Element (FE) analysis and the experimental results.

5.2. Analytical Formulation

The fundamental frequency expression of a thin uniform thickness plate is formulated by the Rayleigh's principle (Leissa, 1969; Chakraverty, 2009). The Rayleigh's quotient for the fundamental frequency of the homogeneous thin plate is given by equation (3.11):

$$\omega^2 = \frac{\iint_R D_o \left[(\nabla^2 W_1)^2 + 2(1-\nu_o) \left\{ \left(\frac{\partial^2 W_1}{\partial x \partial y} \right)^2 - \left(\frac{\partial^2 W_1}{\partial x^2} \right) \left(\frac{\partial^2 W_1}{\partial y^2} \right) \right\} \right] dx dy}{\iint_R h \rho_o W_1^2 dx dy} \quad (5.1)$$

Where ω is the fundamental frequency, h is the uniform plate thickness, ρ_o is the density, ν_o is the Poisson's ratio, W_1 is the shape function, and R is the rectangular area over which integration is performed. D_o is the flexural rigidity, ∇^2 is the two-dimensional Laplacian operator. D_o and ∇^2 are given as,

$$D_o = \frac{E_o h^3}{12(1-\nu_o^2)}, \quad \nabla^2 = \frac{\partial^2}{\partial x^2} + \frac{\partial^2}{\partial y^2} \quad (5.2)$$

Where E_o is the modulus of elasticity.

The Rayleigh's quotient depends on the form of the function W_1 . The function $W_1(x, y)$ is a continuous function that approximately represents the shape of the plate's deflected middle surface and satisfies at least the kinematic boundary conditions and ω represents the natural frequency of the plate pertinent to the assumed shape function. Assume $\omega = \omega_1$ be its fundamental frequency.

5.3 Rectangular Plates with the Square/Rectangular Perforations Arranged In the Square/Rectangular Array

In the present analysis, square plate with the square perforations is considered as shown in Figure 5.1. The ligament efficiency η_l , considered for the perforation is, $(p / (d + p)) = 0.5$, where p is the ligament length (p_x or p_y) and d is the side length of the square perforation. Model in the present work does not consider any rotary inertia of the plate. To approximate the shape of the plate's deflected middle surface, function $W_1(x, y)$ used with the one term and the 5 terms is given as (Laura and Saffell, 1967; Szilard, 2004):

$$W_1(x, y) = \left(x^2 - \frac{a^2}{4}\right)^2 \left(y^2 - \frac{b^2}{4}\right)^2 \quad (5.3a)$$

The polynomial shape function $W_1(x, y)$ for a rectangular plate with the 5 terms is of the form (Laura, and Saffell, 2005)

$$W_1(x, y) = \sum_1^{n=5} c_i \left[x^{2n} - (a/2)^{2n} \right]^2 \left[y^{2n} - (b/2)^{2n} \right]^2 \quad (5.3b)$$

Where a and b are the side dimensions of the plate along x and y directions respectively.

The shape function $W_1(x, y)$ satisfies the following boundary conditions for the plate clamped on all the edges.

$$\left(\frac{\partial W_1(x, y)}{\partial x} \right)_{x=\pm a/2} = 0, \quad \left(\frac{\partial W_1(x, y)}{\partial y} \right)_{y=\pm b/2} = 0 \quad (5.4)$$

$$W_1(x, y)|_{x=\pm a/2} = 0, \quad W_1(x, y)|_{y=\pm b/2} = 0$$

From the equation (5.1) the Rayleigh's quotient depends on the material properties like density (ρ_o), modulus of elasticity (E_o), Poisson's ratio (ν_o). For a perforated plate as shown in Figure 5.1, the density (ρ), and modulus of elasticity (E) are changing along the surface of the plate with geometric pattern of the holes. The pattern of the variation of these parameters along the surface resembles that of the square waves. To evaluate the integrals involved in the

Rayleigh's quotient the density and the modulus of elasticity need to be expressed as a function of the cartesian co- ordinates x and y .

If the function $F(x, y)$ represents the variation of these parameters along the surface, then the density and the modulus of elasticity can be expressed as:

$$\begin{aligned}\rho &= \rho_0 F(x, y) \\ E &= E_0 F(x, y)\end{aligned}\quad (5.5)$$

where, E_0 and ρ_0 are the modulus of elasticity and the density for a homogeneous plate.

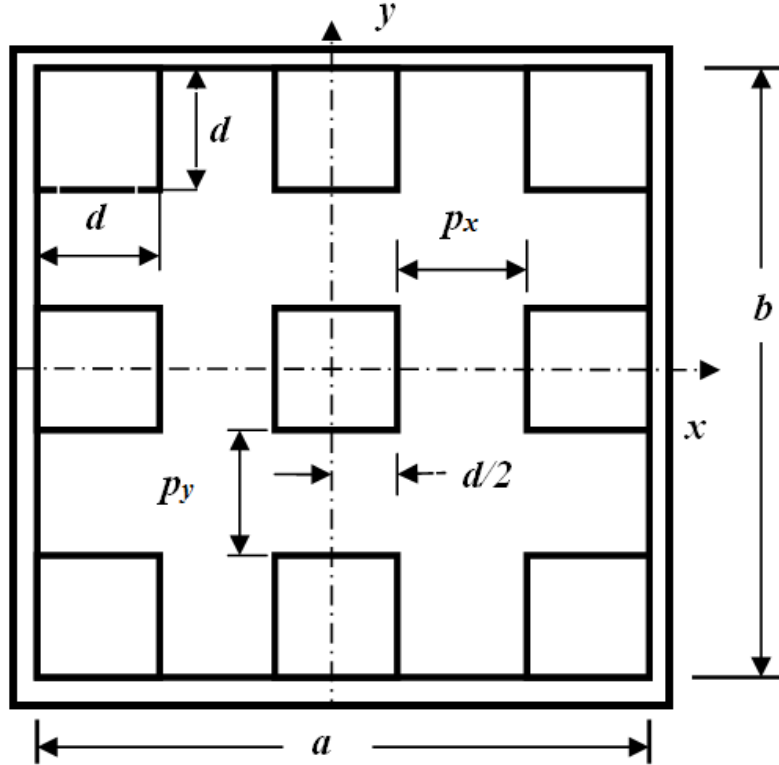


Figure 5.1 Coordinates of the perforated plate

Once the function $F(x, y)$ is constructed the integrals can be evaluated using above equations (5.1 to 5.3). The Rayleigh's quotient now becomes (Chakraverty, 2009):

$$\omega_1^2 = \frac{E_0 h^2}{12 \rho_0 (1 - \nu_0^2)} \frac{\iint_R F(x, y) \left[(\nabla^2 W_1)^2 + 2(1 - \nu) \left\{ \left(\frac{\partial^2 W_1}{\partial x \partial y} \right)^2 - \left(\frac{\partial^2 W_1}{\partial x^2} \right) \left(\frac{\partial^2 W_1}{\partial y^2} \right) \right\} \right] dx dy}{\iint_R F(x, y) W_1^2 dx dy} \quad (5.6)$$

For the function $F(x, y)$ to represent the variation of the density and the modulus of elasticity it must satisfy the following requirements.

$$F(x, y) = 0 \text{ in the region corresponding to a perforation} \quad (5.7)$$

$$F(x, y) = 1 \text{ otherwise}$$

The function $F(x, y)$ is constructed as per the geometry of the plates considered. To construct the function $F(x, y)$ we assume that the density at any point (x, y) is the superposition of the density along x direction and y direction, this superposition is also considered for the modulus of elasticity. The functions $f(x)$ and $g(y)$ represent variation of the density and the modulus of elasticity along x and y axes respectively. The Equations (5.9) and (5.10) shows the rectangular Heaviside function used to express the non homogeneity in the Young's modulus and the density of the plate due to the perforations. The functions $f(x)$ and $g(y)$ are formed by using the unit step functions and are superimposed to obtain the function $F(x, y)$.

The unit step as a function of a discrete variable n is given as:

$$H(n) = \begin{cases} 0, n < 0 \\ 1, n \geq 0 \end{cases} \quad \text{Where } n \text{ is an integer.} \quad (5.8)$$

$$f(x) = H(x - \frac{d}{2}) - H(x - \frac{d}{2} - p_x) + H(x - \frac{d}{2} - p_x - d) + ((H(-x - \frac{d}{2}) - H(-x - \frac{d}{2} - p_x) + H(-x - \frac{d}{2} - p_x - d)) \quad (5.9)$$

$$g(y) = H(y - \frac{d}{2}) - H(y - \frac{d}{2} - p_y) + H(y - \frac{d}{2} - p_y - d) + ((H(-y - \frac{d}{2}) - H(-y - \frac{d}{2} - p_y) + H(-y - \frac{d}{2} - p_y - d)) \quad (5.10)$$

where d is the side length of the square perforation, p_x and p_y are the ligament lengths in x and y directions respectively.

In the present analytical model a square plate having the square perforations is considered as shown in Figure 5.1. For the plate with $\eta_l = 0.5$, $p_x = p_y = d$ the above expressions for the $f(x)$ and $g(y)$ becomes as:

$$f(x) = H(x - \frac{d}{2}) - H(x - \frac{3d}{2}) + H(x - \frac{5d}{2}) + ((H(-x - \frac{d}{2}) - H(-x - \frac{3d}{2}) + H(-x - \frac{5d}{2})) \quad (5.11)$$

$$g(y) = H(y - \frac{d}{2}) - H(y - \frac{3d}{2}) + H(y - \frac{5d}{2}) + ((H(-y - \frac{d}{2}) - H(-y - \frac{3d}{2}) + H(-y - \frac{5d}{2})) \quad (5.12)$$

According to the set theory the Boolean operation of union of two sets A and B is represented by $A \cup B$ and their intersection is represented by $A \cap B$, where:

$$n(A \cup B) = n(A) + n(B) - n(A \cap B)$$

$$n(A \cap B) = n(A) \cdot n(B) \text{ for two independent sets } A \text{ and } B \quad (5.13)$$

The superposition of the $f(x)$ and $g(y)$ to obtain $F(x, y)$ is analogous to this Boolean operation of union as the functions $f(x)$ and $g(y)$ are independent. Using the above equations $F(x, y)$ for the square perforation pattern can be obtained by the relation:

$$F(x, y) = f(x) + g(y) - f(x).g(y) \quad (5.14)$$

The $F(x, y)$ thus obtained is used in the Rayleigh's quotient, equation (5.6) to obtain the fundamental frequency. These calculations were done for the plates of the different sizes.

5.4 Numerical Analysis

An analytical model developed in the section 5.3 is applicable to the rectangular perforated plates with the different side dimensions and having the rectangular/square perforations and, provided that the perforation pattern is rectangular or square and all the perforations are of the same size. A square plate with the simple geometry was considered for convenience of the computation. By virtue of the symbolic forms presented in this work, the method can be applied to the analytical studies of the perforated plates with the different boundary conditions. The numerical results have been computed for the five specimens listed in Table 5.1 and the fundamental natural frequencies are tabulated in Table 5.2. The fundamental frequencies are obtained by the Rayleigh's method using one term shape function and by using the Rayleigh-Ritz method with the 5 term shape function. The material properties considered for all the specimen plates analyzed are same as given in Table 4.1.

Table 5.1 Specimen parameters

Specimen No.	Plate Size (a mm x b mm)	Cutout Size (d mm x d mm)	h , (mm)	$p_x = p_y$ (mm)
5.1	400 x 400	80 x 80	2	80
5.2	500 x 500	100 x 100	2	100
5.3	600 x 600	120 x 120	2	120
5.4	700 x 700	140 x 140	2	140
5.5	800 x 800	160 x 160	2	160

5.5 Validation of the Approach

To verify the validity of the proposed model, modal analysis is carried out using the FEM, for clamped steel plates having 2 mm thickness and carrying nine holes at the positions shown in Figure 5.1. Parameters of the plate specimen considered in this study are shown in Table 5.1. Modal analysis is carried out by ANSYS 11 using Shell63 element. The converged solution of the eigenfrequencies is given in Table 5.2. Convergence summary is given in

“Appendix B” Table B.1. The material properties considered are same as used in the numerical analysis.

The numerical results obtained are also validated by comparing the results with the experimental natural frequencies.

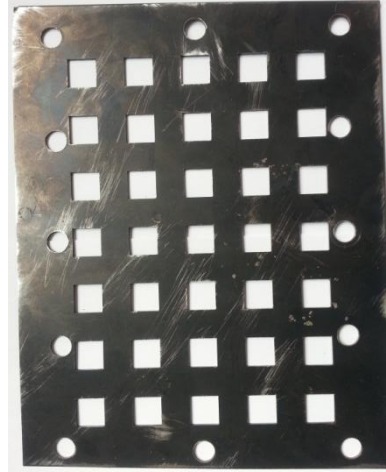


Figure 5.2 Perforated plate specimens no. 5.6 ($d = 16$ mm) tested experimentally

The experimental analysis was carried out for the one specimen with the square perforations of the size 16 mm. Specimen used for experimentation is shown in Figure 5.2. Thickness of the specimens is 2 mm. The fixture for performing experiments was as discussed in the chapter 4, section 4.3. Due to the size limitation of the fixture, experimental validation of the analytical results is done for the one plate with size 135 mm x 216 mm only as given in Table 5.3. The experimental result obtained is given in Table 5.3.

5.6 Results and Discussions

The proposed analytical model, for the plates with the square/rectangular holes, considers the effects of both the different holes and their locations on the frequency. This has been accounted by constructing the special function consisting of unit step function, to express the variation in the density and the Young's modulus. Figure 5.3 shows representative plot for the variation of the function $f(x)$ and $g(y)$ given by equations (5.11) and (5.12) for the plate of size 700 mm X 700 mm. This plot is a square wave depicting the actual variation of the material properties variation along x and y directions. Figure 5.4 shows the representative plot of the density for function $F(x,y)$ given by an equation (5.14) for the plate of size 700 mm X 700 mm. This plot resembles the actual perforated plate configuration where dark square patches shows the perforations.

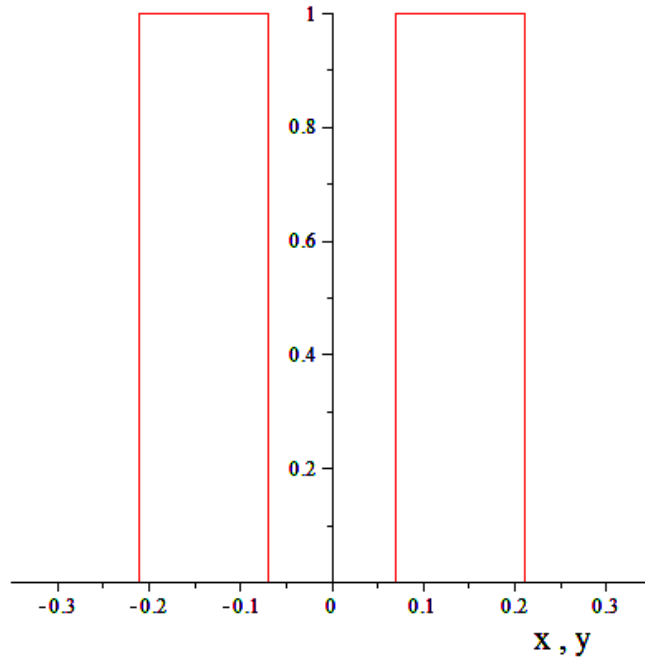


Figure 5.3 Plot of the unit step functions $f(x)$ and $g(y)$ for plate of size 700 mm X 700 mm

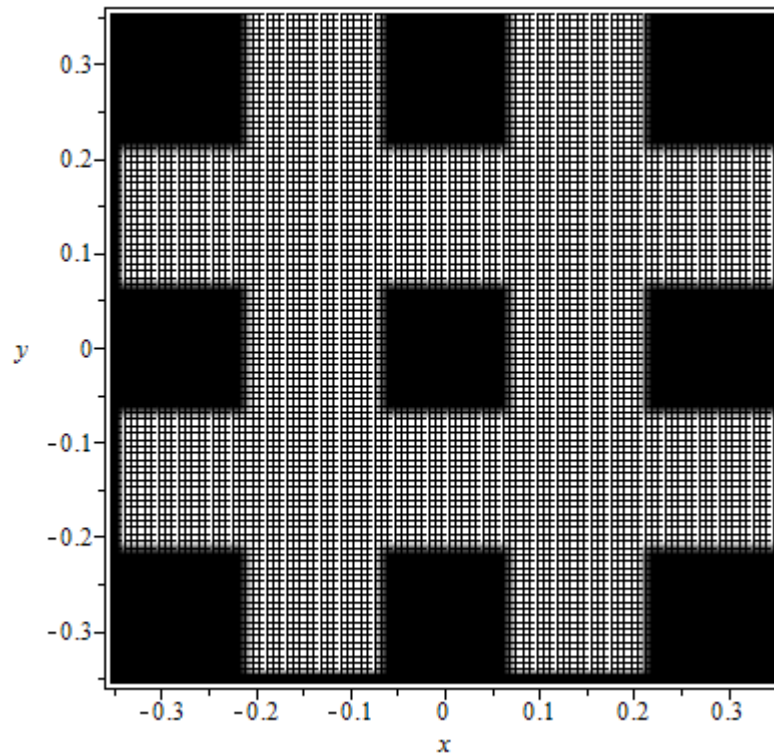


Figure 5.4 Plot of the functions $F(x,y)$ for the plate of size 700 mm X 700 mm

Comparison of the natural frequency of the first mode of vibration between the proposed analytical model and the FEM is given in Table 5.2.

Table 5.2 Comparison of the FEM and analytical results

Specimen No.	Fundamental frequency ω_1 , (Hz)			% Error	
	Analytical, Rayleigh (1 term shape function)	Analytical, Rayleigh-Ritz (5 term shape function)	FEM	1 Term & FEM	5 Term & FEM
5.1	102.269	101.0383	94.411	8.32	7.019
5.2	65.452	64.664	60.421	8.32	7.022
5.3	45.452	44.905	41.961	8.31	7.019
5.4	33.393	32.992	30.828	8.32	7.019
5.5	25.567	25.259	23.602	8.32	7.020

The agreement between the analytical approach and the finite element results is reasonably good. It is observed that the difference between the numerical and the FEM results gives systematic error of 8.32 % for one term shape function with the Rayleigh's method. Whereas these maximum differences in case of 5 term shape function using the Rayleigh-Ritz method is 7.022%. In numerical simulation mass matrix is formed using same shape function as used to generate stiffness matrix that is the two matrices are consistent with each other. Thus numerical simulation predicts higher values of the frequencies. It is observed that the analytical results obtained by the Rayleigh-Ritz method with 5 term shape function has 1.3% less error compared to the results from the Rayleigh's method with 1 term shape function.

Systematic error of 8.32 % and 7.019% occurs between the numerical and FEM results because of following reasons.

- 1) All the specimens are having same mass remnant ratio ($MRR = 0.64$) i.e ratio of the mass of the perforated plate to the mass of the solid plate of equal outer effective dimensions.
- 2) The mass remnant ratio depends upon the geometrical parameters such as specimen aspect ratio (a/b), perforation aspect ratio (d/d), thickness (h) of the specimen and ligament efficiency (ηl). All these geometrical parameters are identical for the specimens considered.
- 3) Due to the geometrical similarity of the specimens same amount of percentage (%) error occur between the numerical and the FEM results for each specimen, though absolute error is different.

This systematic error demonstrates that the analytical model as given, for the square plate with the square perforations having $\eta_l = 0.5$ gives results with same accuracy for the plates with geometrical similarity, but variation in the dimensions.

Table 5.3 Comparison of the experimental and analytical results

Spe. No.	Plate Size (<i>a</i> mm x <i>b</i> mm)	Cutout Size (<i>d</i> mm x <i>d</i> mm)	$p_x = p_y$ (mm)	ω_1 , (Hz)			% Deviation	
				Analy	Experi.	FEM	Analy & Exp	Analy & FEM
5.6	138 x 216	16 x 16	16	620.969	537.5	590.374	13.44	5.182

Table 5.3 shows comparison of the analytical, experimental and FEM results, error between the analytical and FEM results is 5.182% whereas error between the analytical and experimental results is 13.44%. This percent error is associated with the numerical difference of 83.469 Hz between analytical and FEM results. Thus error is more this could be due to the following discussed reasons.

5.6.1 Inferences About the Experimental Results

Results obtained by the experimental analysis differ from the results obtained by proposed method. Possible sources of the error could be as follows

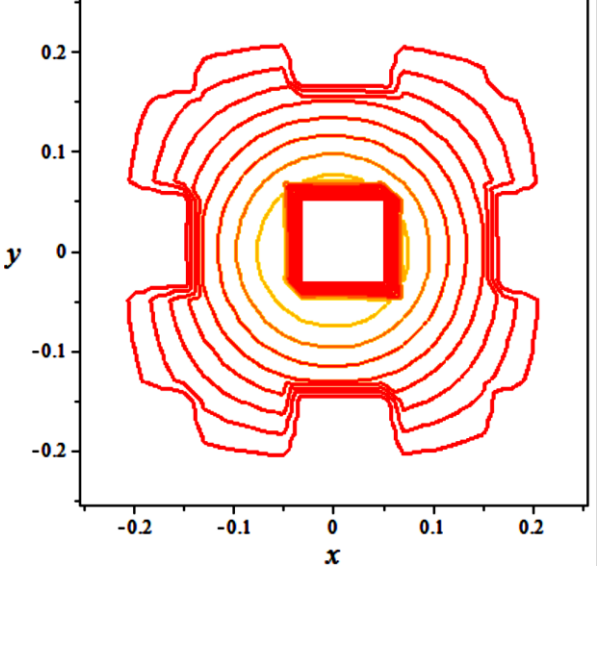
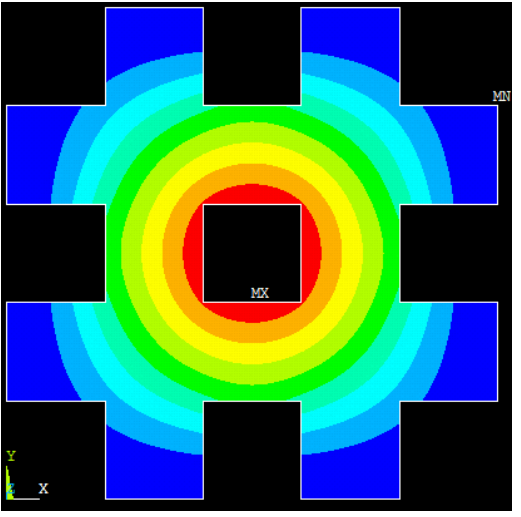
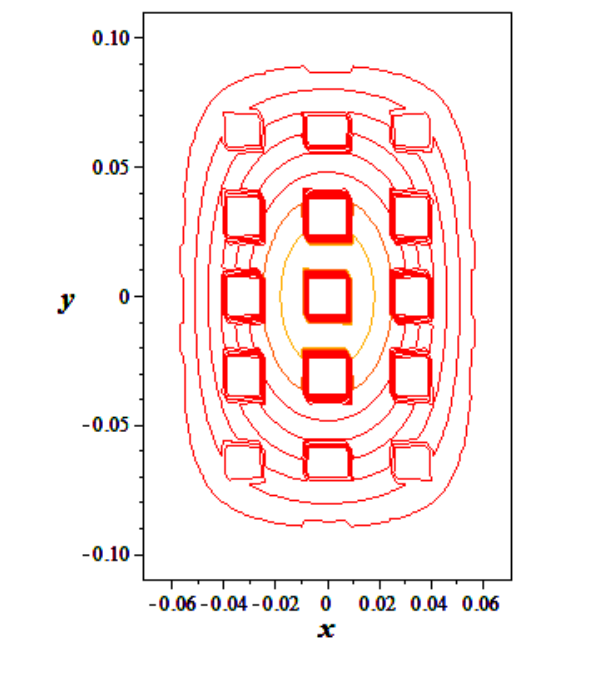
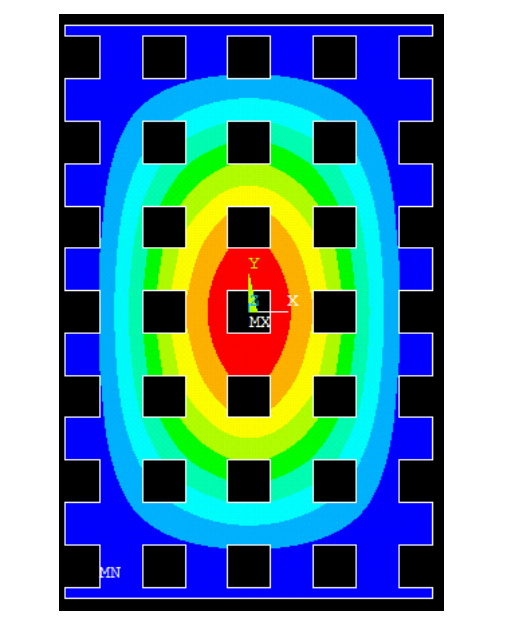
1. Except in very special situations boundary conditions can't be practically achieved. Following parameters can influence the fundamental frequency readings,
 - Spacing of the bolts on the fixture and their arrangement.
 - Dimensional inaccuracies in size of the fixture plates and specimen.
 - Clamping pressure of the bolts on the fixture.
 - Fit of the bolts inside the clamping fixture holes.
2. Environmental effects (dirt, dust, oil, and moisture).
3. Sensitivity values of the accelerometer and impact hammer are given for standard environmental condition, but these values change with change in temperature.
4. Cable noise generation, which may be generated when a cable is flexed, bent, struck, squeezed, or otherwise distorted.

5. Contamination of the cable connectors as a result of handling, the contamination can create low impedance between the signal path and ground.
6. Impact hammer double hits can also influence the fundamental frequency readings .Double hits occur when the hammer strikes the test item twice. Double hits render measurement errors. Double hits are difficult to avoid at measurement points.
7. Impact hammer off axis hits influences the measurements. It has following effects
 - Off axis hits result in reduced energy in the intended direction. This causes errors in measurement.
 - Off axis hits may excite modes(resonances) that would not normally be excited
 - The actual force that the test item experiences is less than the measured force that the load cell sees. The amplitude of the frequency response function will be too high.
8. In analytical modeling structure is assumed to be linear, isotropic, homogeneous and time invariant. Material may not exhibit such behavior practically.
9. An analytical solution neglect the rotary inertia terms and shear effects.
10. The analytical models are formulated for undamped natural frequency, but practically structural damping is always present in the system (Refer Table 4.6 and Appendix 'D' for damping values).
11. Additional mass effects of the accelerometer used to measure the response in the experiment.

5.6.2 Comparison of the Analytical and FEM Mode Shapes

Mode shape pattern obtained analytically for all the specimens are identical and are matching with those obtained from the FEM analysis. Table 5.4 shows the representative comparison of the analytical and FEM mode shapes contours for the Specimen no. 5.2 and 5.6. Analytical mode shapes are extracted from the Rayleigh-Ritz method with the shape function given by equation (5.3b).

Table 5.4 Comparison of the mode shapes obtained from analytical and FEM analysis

Analytical	FEM
Specimens no. 5.2 Dimensions 500 mm x 500 mm and $d = 100 \text{ mm} \times 100 \text{ mm}$	
 <p>The analytical mode shape for specimen 5.2 is shown as a series of concentric red contour lines. The central feature is a square hole. The contours are roughly square but have rounded corners and slightly irregular edges, indicating a higher-order mode. The x and y axes range from -0.2 to 0.2.</p>	 <p>The FEM mode shape for specimen 5.2 is a color-coded stress distribution. It shows a central square hole and four square cutouts at the corners. The stress is highest (red) at the center and lowest (blue) at the corners. The x and y axes are labeled, and a coordinate system is shown in the bottom left.</p>
Specimens no. 5.6 Dimensions 138 mm x 216 mm and $d = 16 \text{ mm} \times 16 \text{ mm}$	
 <p>The analytical mode shape for specimen 5.6 is shown as a series of concentric red contour lines. The central feature is a square hole, and there is a grid of smaller square holes. The contours are roughly rectangular with rounded corners. The x and y axes range from -0.10 to 0.10.</p>	 <p>The FEM mode shape for specimen 5.6 is a color-coded stress distribution. It shows a central square hole and a grid of smaller square holes. The stress is highest (red) at the center and lowest (blue) at the corners. The x and y axes are labeled, and a coordinate system is shown in the bottom left.</p>

5.7 Square Plates with the Square Perforations Arranged In the Square Array

The present section gives formulation for determining the fundamental frequency of the square plates with the square perforations with ligament efficiency $(h_r / (d + h_r)) = 0.5$ as shown in Figure 5.5. Boundary condition considered is all edges clamped. To express variations in the material properties due to the perforations greatest integer functions are used. To approximate the shape of the plate's deflected middle surface, function $W_I(x, y)$ used as given by equation (5.3a) and (5.3b).

$$W_I(x, y) = \left(x^2 - \frac{a^2}{4} \right)^2 \left(y^2 - \frac{b^2}{4} \right)^2 \quad (5.15a)$$

$$W_I(x, y) = \sum_1^{n=5} c_i \left[x^{2n} - (a/2)^{2n} \right]^2 \left[y^{2n} - (b/2)^{2n} \right]^2 \quad (5.15b)$$

The shape function $W_I(x, y)$ satisfies the following boundary conditions for the plate clamped on all the edges.

$$\left(\frac{\partial W_I(x, y)}{\partial x} \right)_{x=\pm a/2} = 0, \left(\frac{\partial W_I(x, y)}{\partial y} \right)_{y=\pm b/2} = 0, W_I(x, y)|_{x=\pm a/2} = 0, W_I(x, y)|_{y=\pm b/2} = 0 \quad (5.16)$$

Density and modulus of elasticity can be expressed as:

$$\begin{aligned} \rho &= \rho_0 F(x, y) \\ E &= E_0 F(x, y) \end{aligned} \quad (5.17)$$

where, E_0 and ρ_0 are the modulus of elasticity and density for a homogeneous plate.

Once the function $F(x, y)$ is constructed the integrals in the Rayleigh's quotient equation (5.3) can be evaluated. The function $F(x, y)$ represents the variation of the density and modulus of elasticity. For the function $F(x, y)$ to represent these parameters it must satisfy the requirements given by equation (5.7).

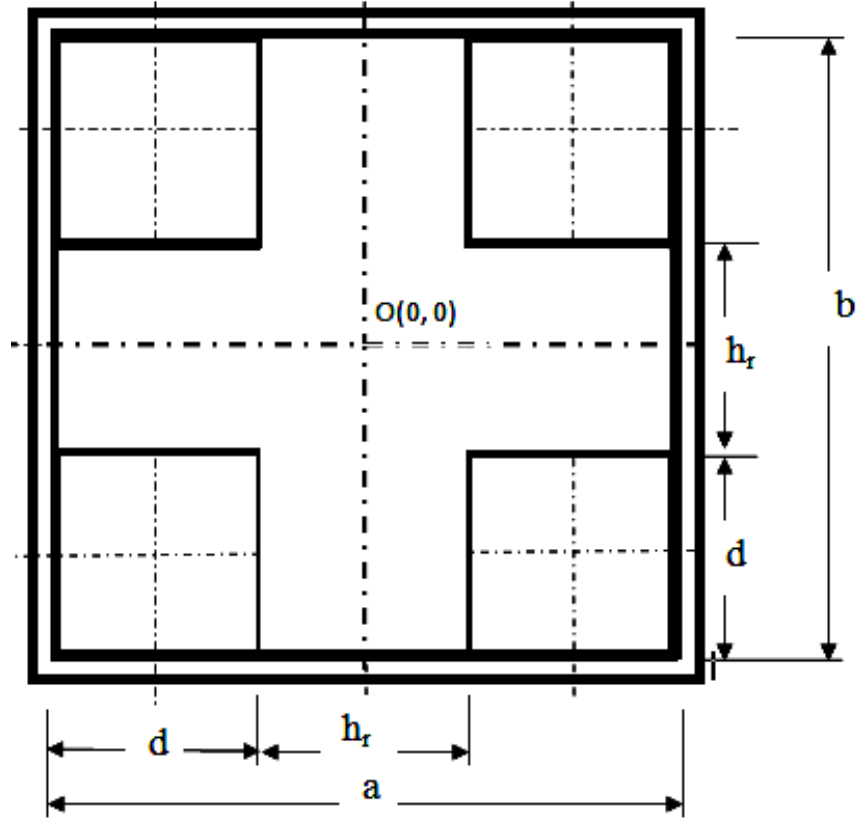


Figure 5.5 Orientation of the co-ordinates of the perforated square plate

The function $F(x, y)$ is constructed as per the geometry of the plates considered in Figure 5.5. To construct the function $F(x, y)$ we assume that the material property (Density and Young's modulus) at any point (x, y) is the superposition of the material property along x direction and y direction. The functions $f(x)$ and $g(y)$ represent variation of the material property along x and y axes respectively. The functions $f(x)$ and $g(y)$ are formed by using the greatest integer functions as given by equations (5.18) and (5.19). The functions $f(x)$ and $g(y)$ are superimposed to obtain the function $F(x, y)$.

$$f(x) = \text{floor} \left\{ 1 + \cos \left(\frac{3\pi x}{a} \right) \right\} \quad (5.18)$$

$$g(y) = \text{floor} \left\{ 1 + \cos \left(\frac{3\pi y}{b} \right) \right\} \quad (5.19)$$

$F(x, y)$ can be obtained by equation (5.14) given as:

$$F(x, y) = f(x) + g(y) - f(x)g(y) \quad (5.20)$$

$F(x, y)$ thus obtained is used in the Rayleigh's quotient equation (5.6) to obtain the fundamental frequency. Figure 5.6 shows the representative plot of the greatest integer function variation in x and y direction given by equation (5.18) and (5.19) for the specimen

with dimension 500 mm x 500 mm. Figure 5.7 shows the representative density plot of the greatest integer function $f(x, y)$ given by equation (5.20) in x and y direction for the specimen with dimension 500 mm x 500 mm.

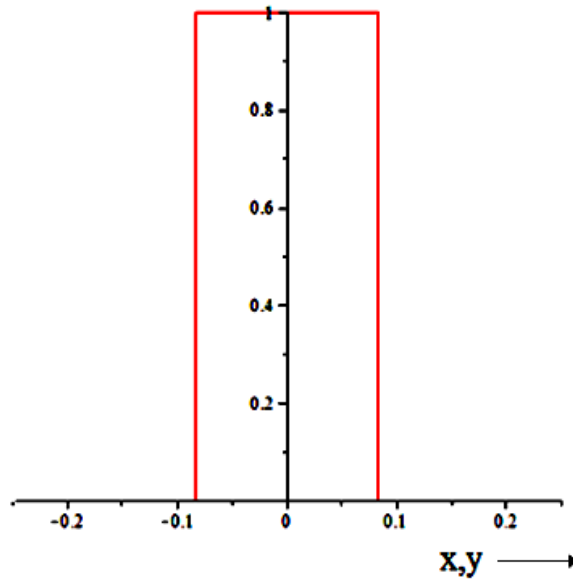


Figure 5.6. Plot of the greatest integer functions $f(x)$ and $g(y)$

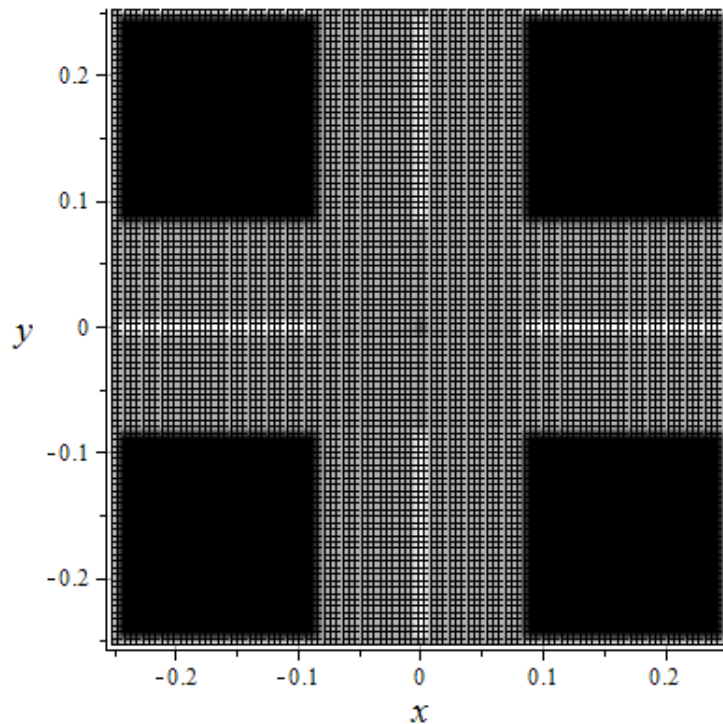


Figure 5.7. Density plot of the greatest integer function $f(x,y)$

Density plot of the function exactly depicts the geometry of the plate specimen. Thus variation of the material properties expressed by greatest integer functions given by equation (5.18) to (5.20) is a valid representation of actual variation.

5.8 Numerical Analysis

The model developed in the Section 5.7 is applicable to the square perforated plates with different side dimensions and having square perforation and, provided that the perforation pattern is also square and all the perforations of same size. To study applicability of the proposed model, Numerical analysis was carried out for clamped steel plates having 2 mm thickness and carrying the four holes at positions shown in Figure 5.5. The geometrical parameters and the effective outer dimensions of the plate specimen considered in this study are shown in Table 5.4 for the rectangular perforated plate. The material properties for all the specimen plates analyzed are as given in Table 4.1 except the Young's modulus which is taken as $E = 2 \times 10^{11}$ N/m². The numerical analysis is separately carried out for two shape functions given by equation (5.15a) and (5.15b) by using the Rayleigh and Rayleigh-Ritz method respectively.

5.9 Model Validation with the FEM Results

The validity of the proposed model has been verified by comparing the predictions with the FEM results. To investigate the vibration response, the FEM modal analysis is carried out for the clamped steel plate specimens having 2 mm thickness and carrying four holes with geometrical parameters given in Table 5.5. The FEM analysis is carried out using Shell63 element with ANSYS11. The converged FEM solution with the lowest eigenfrequencies is given in Table 5.5. Convergency summary is given in Appendix B, Table B.2.

Table 5.5 Specimen parameters

Specimen No.	Plate Size (<i>a</i> mm x <i>b</i> mm)	Cutout Size (<i>d</i> mm x <i>d</i> mm)	<i>h</i>, (mm)
5.8	400 x 400	133.33 x 133.33	2
5.9	500 x 500	166.66 x 166.66	2
5.10	600 x 600	200 x 200	2
5.11	700 x 700	233.33 x 233.33	2
5.12	800 x 800	266.66 x 266.66	2

5.10 Results and Discussions

Comparison between the FEM and numerically obtained natural frequencies of the plate for first mode is given in Table 5.6. All calculations have been performed for a clamped-clamped rectangular plate of 2 mm thickness.

Table 5.6 Comparison of the FEM and analytical results

Specimen No.	Fundamental frequency ω_1 , (Hz)			% Error	
	Analytical (1 term shape function)	Analytical (5 term shape function)	FEM	1 Term & FEM	5 Term & FEM
5.8	97.958	96.792	93.052	5.272	4.019
5.9	62.693	61.947	59.55	5.277	4.025
5.10	43.537	43.018	41.354	5.278	4.023
5.11	31.986	31.605	30.383	5.275	4.021
5.12	24.489	24.198	23.262	5.274	4.023

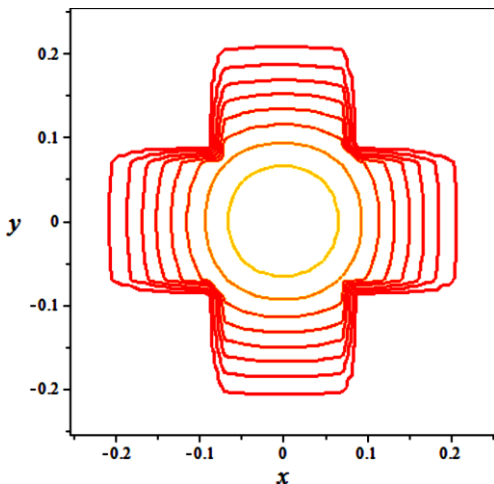
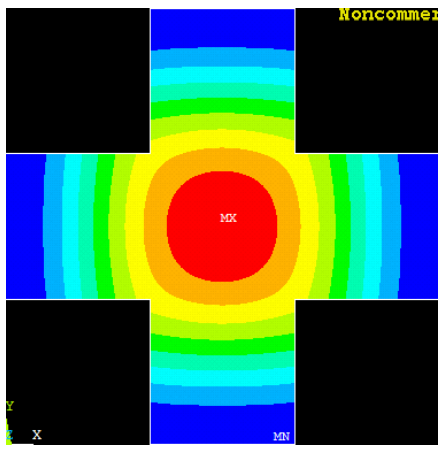
The agreement between the analytical approach and the finite element results is reasonably good when plate size increases. The maximum difference is of the order 5.278 % for case of 600 mm x 600 mm size thin plate when one term shape function is used. When the five term shape function is used with the Rayleigh-Ritz method maximum difference is of the order 4.025 % for case of 500 mm x 500 mm size thin plate. Thus when shape function given by equation (5.15b) is used error reduced by 1.25%. The improved performance of the proposed model, for the small holes as demonstrated in Table 5.6, is due to the fact that the effects of both the different holes and their locations on the frequency have been accounted by using the greatest integer functions. Variation in the density and Young's modulus due to holes is represented as a non homogeneity by constructing special function consisting of greatest integer function. Model in the present work does not consider any rotary inertia of the plate. A square plate with simple geometry was considered for convenience of the computation. By virtue of the symbolic forms presented in this work, the method can be applied to the analytical studies of the perforated plates with different boundary conditions.

5.10.1 Comparison of the Analytical and FEM Mode Shapes

Extracted mode shapes from the Rayleigh-Ritz method are compared to those of the finite element model (FEM) and are shown to have agreement between them. Contour plots

are compared in Table 5.7 for representative specimen no. 5.9. It can be observed that displacement pattern obtained analytically matches approximately with that obtained by the FEM analysis. Analytical mode shapes of the entire specimens shows identical displacement pattern as all the specimens are geometrically similar.

Table 5.7 Comparison of the analytical and FEM mode shapes

Analytical	FEM
Specimen no.5.9 Dimensions 500 mm x 500 mm and $d = 166.66$ mm x 166.66mm	
	

5. 11 Concluding Remarks

This work presents analytical models to estimate the fundamental frequency of the uniform thickness plates carrying square perforations in the square and staggered pattern. The effect of the nonhomogeneity in the Young’s modulus and density due to the holes on the natural frequency of the perforated plate has been modeled using unit step functions and the greatest integer functions. The Heaviside step function can be used to express the variation of the material properties of the perforated plates with different types of perforation pattern, whereas the greatest integer functions can be used to express the variation of the material properties of the perforated plates with square perforation pattern.

The material properties variation functions thus obtained can be used to determine the fundamental frequency of the plates using approximate techniques such as the Rayleigh’s and Rayleigh-Ritz method. The proposed models have been verified by comparing the numerical results with the FEM results. Also proposed approaches can be applied to the plates subjected to other boundary conditions with appropriate choice of the shape function to represent the deflection of the mid plane of the plate.

Chapter 6

Analytical Model for the Rectangular Plate with the Triangular Pattern of Perforations

6.1 Introduction

In this chapter an analytical model to determine the fundamental frequency of the rectangular plate with the staggered array of the perforations is formulated. Perforations considered are square / rectangular whereas the perforation pattern considered are 60° and 45° staggered, triangular. The variation of the material properties like density and the modulus of elasticity for a plate with a generalized staggered perforation pattern are expressed using the Heaviside step function in the Rayleigh's Quotient. In the present analysis boundary condition considered is clamped all edges. The perforated plate is considered as the plate with a uniformly distributed mass and the holes are considered as the non homogeneous patches as considered in the chapter 5. The deflected middle surface of the plate is approximated by a simple polynomial function which satisfies the boundary conditions. The fundamental frequency of vibration is determined by the numerical analysis from proposed approach for the different plate specimens varying in the effective outer dimensions and the perforation sizes. The results of the numerical analysis are validated by comparing results of the Finite Element Method modal analysis and the experimental results. It is found that results obtained from proposed approach are in reasonably good agreement with the results of the finite element analysis.

6.2 Clamped Rectangular Plates with the 60 ° Triangular Perforation Pattern

In this section the rectangular plates with the rectangular/square perforations arranged in a regular 60° triangular pattern are considered. As shown in Figure 6.1, the plate with edges of the effective lengths a and b along x and y axes respectively has the rectangular perforations of width d_x and d_y along x and y axes respectively. The centre to centre distance of the two adjacent perforations in the pattern in x and y directions are p_x and p_y respectively:

To evaluate the integrals involved in the Rayleigh's quotient, the density and the modulus of elasticity need to be expressed as a function of the x and y co-ordinates. If the

function $F(x, y)$ represents the variation of the material properties along the surface, then the density (ρ) and modulus of elasticity (E) can be expressed by equation (5.5)

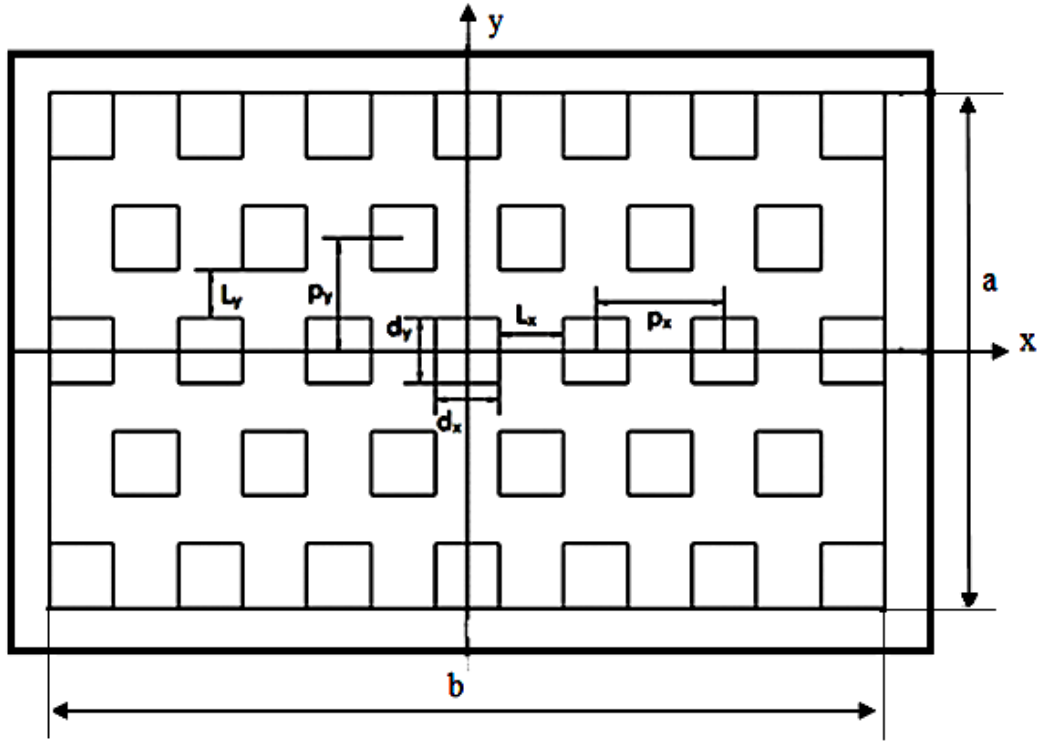


Figure 6.1 Generalized triangular perforation pattern

Comparison of the geometry of plate with staggered perforation pattern as shown in Figure 6.1 and a square perforation pattern in the Figure 5.1 shows that alternate rows of the regular 60° triangular pattern are displaced with respect to the previous rows. This deviation from the square pattern can be interpreted as a phase difference and it can be incorporated into the material property function $F(x, y)$. To obtain the variation of the material properties for a plate with triangular perforation pattern, initially the function $F(x, y)$ for a square pattern is obtained and appropriate phase difference is introduced in the expressions for $f(x)$ and $g(y)$. If φ_1 and φ_2 represent the phase difference to be introduced in the density or Young's modulus functions, as a result of the rows displaced. The resultant density or Young's modulus in x direction becomes $f(x-\varphi_1)$ and the resultant density or Young's modulus in y direction becomes $g(y-\varphi_2)$. Thus for a staggered pattern from equation (5.14) we have:

$$F(x, y) = f(x - \varphi_1) + g(y - \varphi_2) - f(x - \varphi_1) \cdot g(y - \varphi_2) \quad (6.1)$$

The functions $f(x)$, $g(y)$, $\varphi_1 = \varphi_1(y)$ and $\varphi_2 = \varphi_2(x)$ are obtained using the Heaviside unit step function. These functions are expressed as a series of rectangular pulses which represent the material property variations along the x and y axes respectively. From Figure 6.1 it can be

seen that the alternate rows of the perforations along x direction are shifted by distance $p_x/2$ and the perforations along y direction are shifted by distance p_y . Thus, the phase difference φ_1 and φ_2 are $p_x/2$ and p_y respectively for the alternate shifted rows of the perforations and zero otherwise. The expressions for φ_1 and φ_2 can be obtained using the Heaviside step function with amplitudes $p_x/2$ and p_y respectively. Considering the geometry of the plate shown in Figure 6.1, the function $f(x)$ for the central row of the perforations along x axis can be expressed as:

$$\begin{aligned}
f(x) = & H\left(x - \frac{d_x}{2}\right) - H\left(x - L_x - \frac{d_x}{2}\right) + H\left(x - L_x - \frac{3d_x}{2}\right) \\
& - H\left(x - 2L_x - \frac{3d_x}{2}\right) + H\left(x - 2L_x - \frac{5d_x}{2}\right) - H\left(x - 3L_x - \frac{5d_x}{2}\right) \\
& + H\left(x - 3L_x - \frac{7d_x}{2}\right) - H\left(x - 4L_x - \frac{7d_x}{2}\right) + H\left(x + L_x + \frac{d_x}{2}\right) \\
& - H\left(x + \frac{d_x}{2}\right) + H\left(x + 2L_x + \frac{3d_x}{2}\right) - H\left(x + L_x + \frac{3d_x}{2}\right) \\
& + H\left(x + 3L_x + \frac{5d_x}{2}\right) - H\left(x + 2L_x + \frac{5d_x}{2}\right) \\
& + H\left(x + 4L_x + \frac{7d_x}{2}\right) - H\left(x + 3L_x + \frac{7d_x}{2}\right) + \dots
\end{aligned} \tag{6.2}$$

Similarly the function $g(y)$ for a central column of the perforations along y axis in a square pattern can be expressed as:

$$\begin{aligned}
g(y) = & H\left(y - \frac{d_y}{2}\right) - H\left(y - L_y - \frac{d_y}{2}\right) + H\left(y - L_y - \frac{3d_y}{2}\right) \\
& - H\left(y - 2L_y - \frac{3d_y}{2}\right) + H\left(y - 2L_y - \frac{5d_y}{2}\right) - H\left(y - 3L_y - \frac{5d_y}{2}\right) \\
& + H\left(y + L_y + \frac{d_y}{2}\right) - H\left(y + \frac{d_y}{2}\right) + H\left(y + 2L_y + \frac{3d_y}{2}\right) \\
& - H\left(y + L_y + \frac{3d_y}{2}\right) + H\left(y + 3L_y + \frac{5d_y}{2}\right) - H\left(y + 2L_y + \frac{5d_y}{2}\right) + \dots
\end{aligned} \tag{6.3}$$

The above expressions for $f(x)$ and $g(y)$ are valid for a square pattern. The phase difference to be introduced in these expressions is a function of x and y co-ordinates ($\varphi_1 = \varphi_1(y)$ and $\varphi_2 = \varphi_2(x)$). The expressions for phase difference can be obtained as follows:

$$\varphi_1(y) = \frac{p_x}{2} \left\{ \begin{array}{l} H\left(y - p_y + \frac{d_y}{2}\right) + H\left(y - p_y - \frac{d_y}{2}\right) \\ + H\left(y + p_y - \frac{d_y}{2}\right) + H\left(y + p_y + \frac{d_y}{2}\right) + \dots \end{array} \right\} \quad (6.4)$$

$$\varphi_2(x) = p_y \left\{ \begin{array}{l} H\left(x - \frac{d_x}{2}\right) - H\left(x - p_x + \frac{d_x}{2}\right) + H\left(x - p_x - \frac{d_x}{2}\right) \\ - H\left(x - 2p_x + \frac{d_x}{2}\right) + H\left(x - 2p_x - \frac{d_x}{2}\right) - H\left(x - 3p_x + \frac{d_x}{2}\right) \\ + H\left(x + p_x - \frac{d_x}{2}\right) - H\left(x + \frac{d_x}{2}\right) + H\left(x + 2p_x - \frac{d_x}{2}\right) \\ - H\left(x + p_x + \frac{d_x}{2}\right) + H\left(x + 3p_x - \frac{d_x}{2}\right) - H\left(x + 2p_x + \frac{d_x}{2}\right) + \dots \end{array} \right\} \quad (6.5)$$

The generalized expressions for $f(x)$, $g(y)$, $\varphi_1(y)$ and $\varphi_2(x)$ are evaluated as an infinite series. These can be truncated to finite number of terms depending upon the dimensions and the geometry. These expressions can be written in a compact form as follows:

$$\varphi_1(y) = d \left\{ \sum_{M=3}^2 \left(H\left(y - \frac{(4M+2)\sqrt{3}-1}{2}d\right) - H\left(y - \frac{(4M+2)\sqrt{3}+1}{2}d\right) \right) \right\} \quad (6.6)$$

$$\varphi_2(x) = \sqrt{3}d \left\{ \sum_{M=7}^6 \left(H\left(x - \frac{(4M+1)d}{2}\right) - H\left(x - \frac{(4M+3)d}{2}\right) \right) \right\} \quad (6.7)$$

$$f(x - \varphi_1) = \sum_{M=8}^6 \left(H\left(x - \frac{(4M+1)d}{2} - \varphi_1\right) - H\left(x - \frac{(4M+3)d}{2} - \varphi_1\right) \right) \quad (6.8)$$

$$g(y - \varphi_2) = \sum_{M=4}^2 \left(H\left(y - \frac{(4\sqrt{3}M+1)d}{2} - \varphi_2\right) - H\left(y - \frac{((4M+4)\sqrt{3}-1)d}{2} - \varphi_2\right) \right) \quad (6.9)$$

$$F(x, y) = f(x - \varphi_1) + g(y - \varphi_2) - f(x - \varphi_1) \cdot g(y - \varphi_2) \quad (6.10)$$

The function $F(x, y)$ for a generalized staggered pattern can be obtained from equation (6.10) using the above equations (6.6) to (6.9). This function can be used in equation (5.6) to compute the fundamental frequency of the plates having staggered perforation pattern.

6.3 Numerical Analysis

An analytical model developed in Section 6.2 is applicable to the rectangular plates with the regular 60° staggered arrays of the rectangular perforations provided all the perforations are of the same size. Analytical model developed is based on the thin plate theory thus does not consider effects of the rotary inertia. Proposed model can be applied to

Since the perforations are square shaped we get the following relations for the dimensions shown in Figure 6.2.

$$\begin{aligned} d_x = d_y = d, p_x = 2d, L_x = (p_x - d) = d, p_y = \sqrt{3}d, \\ L_y = (p_y - d) = (\sqrt{3} - 1)d, a = 5d, b = (2\sqrt{3} + 1)d \end{aligned} \quad (6.11)$$

The unit cell, shown in Figure 6.2 represents a basic unit of a regular 60° staggered pattern. The whole pattern can be obtained by repeating this unit cell all over the surface. The variation of the density and modulus of elasticity is obtained using equation (6.10) by incorporating the relations given in equation (6.6) to (6.9). The density plot of the function $F(x, y)$ obtained is shown in Figure 6.3. The density plot resembles the geometry of the plate considered. The dark area represents the region where $F(x, y) = 0$ which is the region corresponding to a perforation. The density plot shows that $F(x, y)$ is a valid representation of the variation of the material properties of the plate.

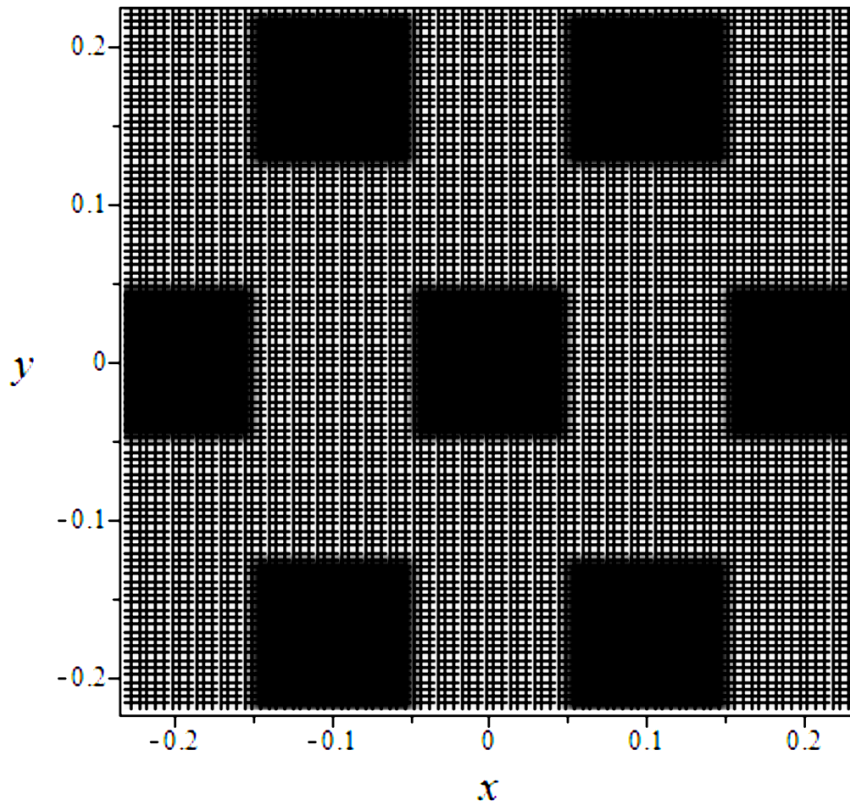


Figure 6.3 Density plot of the function $F(x, y)$

The function $F(x, y)$ obtained as above by equation (6.10) and $W_1(x, y)$ from equation (5.3) is used in the Rayleigh's quotient given by equation (5.3) to obtain the fundamental frequency. The numerical analysis is done for the rectangular plates of the different side dimensions ranging from 10 mm to 100 mm with the geometry as shown in Figure 6.2.

6.3.2 Analysis of the Plates with Fixed Outer Dimensions and Varying the Perforation Size

In this analysis clamped rectangular plates with the square perforations in a regular 60° staggered pattern and having fixed effective outer dimensions $a = 216 \text{ mm}$, $b = 138 \text{ mm}$ and thickness $h = 2 \text{ mm}$ are considered. Size of the square perforations considered for each specimen is different. Thus for each specimen, different numbers of perforation holes are obtained. The mass remnant ratio (MRR) which is the ratio mass of the perforated plate to the mass of the homogeneous plate with the same effective outer dimensions is calculated for each specimen as follows:

$$MRR = \frac{a \times b - N \times d^2}{a \times b} \quad (6.12)$$

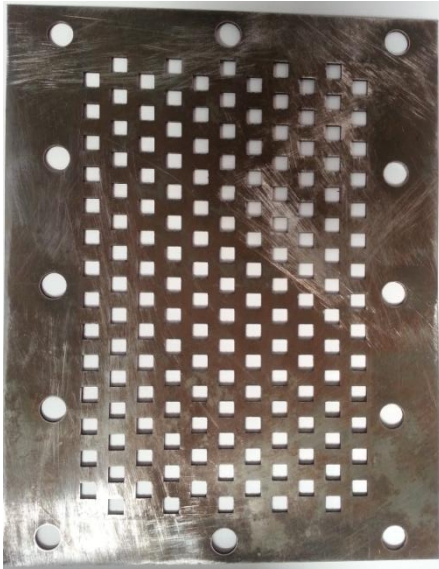
Where N is the ratio of total perforated area to area of a single perforation and d is the size of each square perforation. The specimens considered have square perforations; therefore the relations in equation (6.11) are applicable in this analysis. When all the perforations are included within boundary of effective outer dimensions N becomes equal to total number of the holes.

The function $F(x, y)$ given by equation (6.10) is obtained from equations (6.6) to (6.9) and $W_1(x, y)$ from equation (5.3) is used in the Rayleigh's quotient given by equation (5.6) to obtain the fundamental frequency of each specimen. Numerical calculations were done for the plate specimens with different size of the perforations, followed by validation of the numerical results. The results of the numerical analysis have been tabulated in Table 6.1 and 6.2.

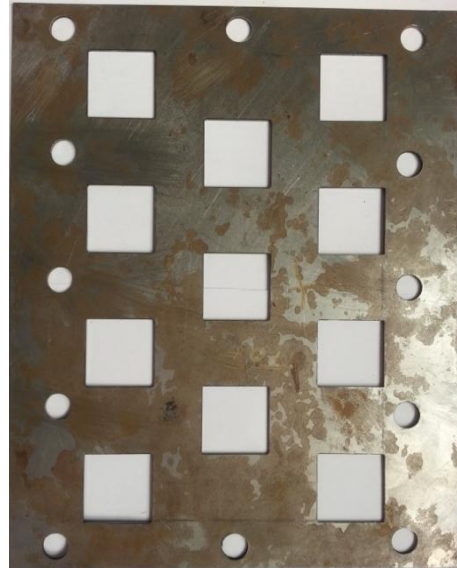
6.4. Validation of the Approach

To validate the results obtained by the numerical analysis, FEM modal analysis of the same plate specimens was carried out using ANSYS 11. The thickness ($h = 2\text{mm}$) and material properties of the plates considered for the finite element analysis are same as those considered for the numerical analysis given by equation (5.25). Modal analysis was carried out using Shell 63 as the element type. The analysis was repeated with successive refinement in the mesh until convergence was obtained. Summary of the convergence is given in Appendix "B" Table B.3 and B.4. Table 6.1 and 6.2 shows the fundamental frequency results obtained from the numerical analysis as well as the FE modal analysis.

The numerical results obtained are also validated by comparing results with the experimental natural frequencies. An experimental analysis was carried out for the two specimens with the square perforations of size 7.33 mm and 30.86 mm respectively. Specimens used for the experimentation are shown in Figure 6.4. Specimen's thickness is 2 mm. The experimental results obtained are given in Table 6.3.



Specimen No. 6.14($d = 7.33$ mm)



Specimen No. 6.15($d = 30.86$ mm)

Figure 6.4 Perforated plate specimens with the staggered pattern tested experimentally

6.5 Results and Discussion

Table 6.1 shows the results of the numerical as well as the FEM modal analysis for the plates with a single unit cell of 60° staggered perforations. Comparison between the results of the numerical and finite element analysis (FEA) shows that the fundamental frequency obtained using the proposed approach is higher than that obtained by the FEM. All the specimens tabulated in Table 6.1 are geometrically similar. Thus the mass remnant ratio MRR (0.65359) is same for each specimen. Therefore the proposed approach gives result with nearly same accuracy for each specimen. In this analysis a systematic error in the range 8 to 9 % is observed for the range of the perforation sizes considered. From the Table 6.1 it is observed that, as the perforation size becomes larger, frequency decreases. According to Sun choi et al., (1998) this occurs, as the stiffness drops more rapidly than mass and due to this frequency decreases. Table 6.2 shows the results of the numerical as well as FE modal analysis for the plates with fixed outer dimensions and the variable perforation size. The mass remnant ratio for each plate specimen considered is different. The distribution of the mass

and thus the stiffness for each specimen is different. No inference can be drawn from the results as particular trend for variation in the fundamental frequency is not observed. This is because dimensions of the perforation for each specimen are chosen so as to perfectly accommodate all the perforations within the effective outer dimensions.

Table 6.1 Results of the numerical and FE analysis for the plates with a single unit cell of 60° staggered perforation pattern

Specimen No.	Perforation Size, d (mm)	Plate size (a mm x b mm)	Frequency ω_1 by FEM modal analysis (Hz)	Frequency ω_1 by numerical analysis (Hz)	% Error
6.1	10	50 x 44.64102	6657.000	7269.251	9.197
6.2	20	100 x 89.28203	1664.300	1817.312	9.193
6.3	30	150 x 133.9230	739.660	807.694	9.198
6.4	40	200 x 178.5641	416.070	454.328	9.195
6.5	50	250 x 223.2051	266.280	287.630	8.017
6.6	60	300 x 267.8461	184.920	199.823	8.059
6.7	70	350 x 312.4871	135.860	146.814	8.063
6.8	80	400 x 357.1281	104.020	112.404	8.060
6.9	90	450 x 401.7691	82.185	89.326	8.689
6.10	100	500 x 446.4102	66.570	72.435	8.810

Table 6.2 Results of the numerical and FE analysis for the plates with the fixed outer dimensions

Specimen No.	Perforation Size, d (mm)	No. of perforations, N	MRR	Frequency ω_1 (Hz) by FEM	Frequency ω_1 (Hz) by numerical analysis	% Error
6.11	7.330	159	0.7134	607.150	671.168	10.544
6.12	12.71	54.7223	0.7034	601.020	650.907	8.300
6.13	30.86	11	0.6486	586.740	621.966	6.003

From comparison of the FEM and numerical analysis results given in Table 6.1 and Table 6.2 it is observed that, for all specimen the fundamental frequency values obtained by the numerical analysis are higher than values obtained by the FEM analysis. This is because frequency values depend upon type and the form of the shape function chosen. In present analysis only one term approximation is used for shape function which results in higher values of the fundamental frequency obtained by numerical analysis. The approximate representation of the deflection of the plate given by equation (5.3) is used for the ease of computations involved in the analysis. For the specimen 6.11 from Table 6.2 percent error between the FEM and numerical results is 10.544% but actual numerical difference between the results is 64.018 Hz which is significant.

Table 6.3 Results of the numerical and experimental analysis for the plates with the fixed outer dimensions

Specimen No.	Perforation Size, d (mm)	No. of perforations, N	MRR	Frequency ω_1 (Hz) by Experimental analysis	Frequency ω_1 (Hz) by numerical analysis	% Deviation
6.14	7.330	159	0.7134	575	671.168	14.32
6.15	30.86	11	0.6486	545	621.966	12.37

6.5.1 Inferences about Experimental Readings

Results of the experimental analysis are given in Table 6.3. One of the sample frequency response function (FRF) plot is given for each of the two experimentally tested specimens. Figure 6.5 and Figure 6.6 shows the sample FRF for the specimen 6.14 and specimen 6.15 respectively. It is observed that the maximum discrepancy between the numerical and experimental natural frequency is 14.32% for specimen 6.14 and 12.37% for specimen 6.15. Actual numerical difference between the FEM and numerical analysis results is 96.168 and 76.966 for specimen 6.14 and 6.15 respectively. This large numerical difference may be due to the possible sources of the error as discussed in Section 5.6.1. Comparison of the FEM and experimental results gives discrepancy of 5.29% and 7.11% for the specimens 6.14 (or 6.11) and 6.15(or 6.13) respectively.

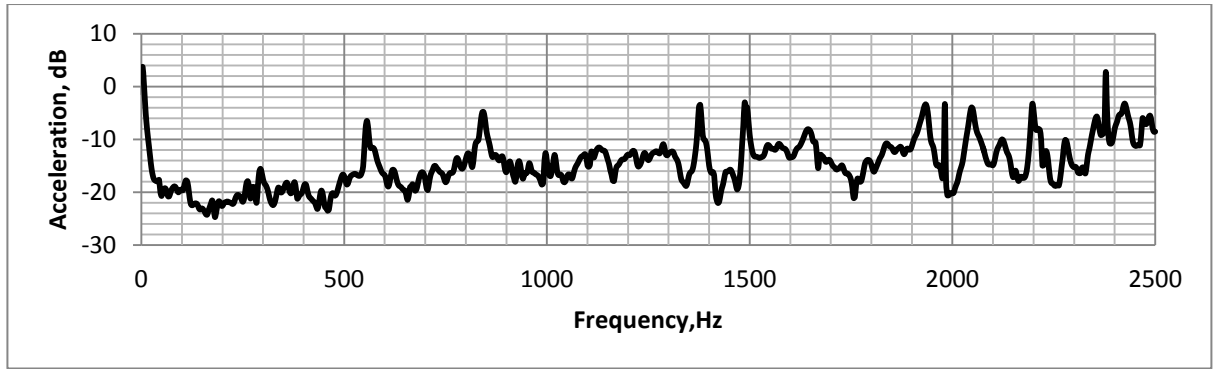


Figure 6.5 Frequency response function for the Specimen no. 6.14 ($d = 7.33$ mm)

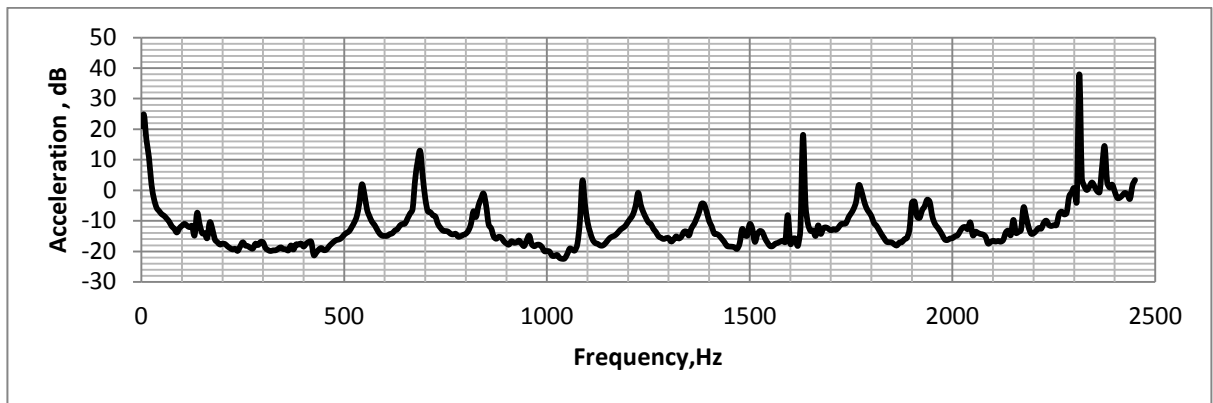


Figure 6.6 Frequency response function for the Specimen no. 6.15 ($d = 30.86$ mm)

6.5.2 Comparison of the Analytical and FEM Mode Shapes

Contour plots of the mode shapes obtained analytically and by the FEM are compared in Table 6.3a and Table 6.3b. The Table 6.3a shows representative mode shape for the specimen 6.10 with a unit cell of the staggered 60° pattern given in Table 6.1. Analytical and the FEM Modes for the specimens 6.1 to 6.10 are similar as shown in Table 6.3a. The Table 6.3b shows comparison of the analytical and FEM modes for the specimens with fixed outer dimensions given in Table 6.2. Comparison in Table 6.3a and Table 6.3b shows agreement between the analytical and FEM mode shapes for the fundamental frequency.

Table 6.3a Comparison of the analytical and FEM mode shapes for unit cell of 60° staggered perforation pattern

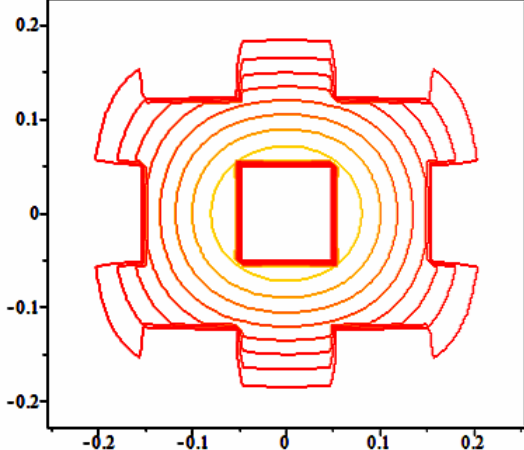
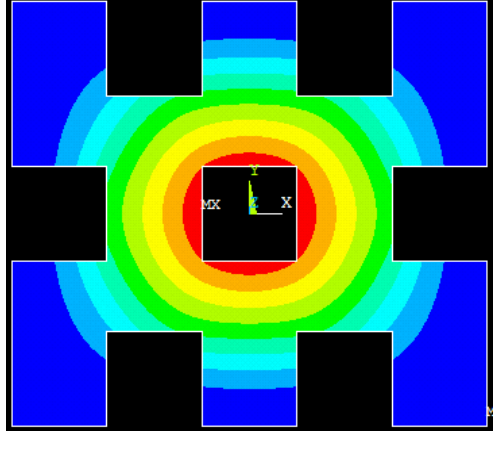
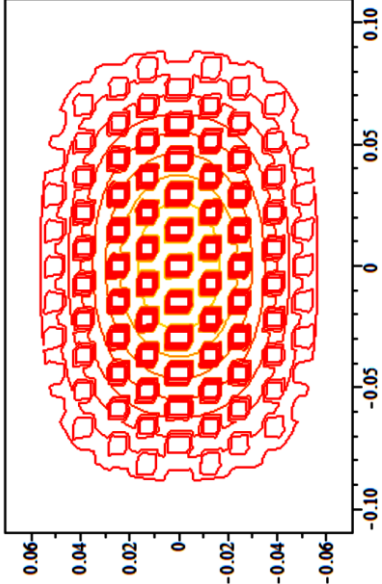
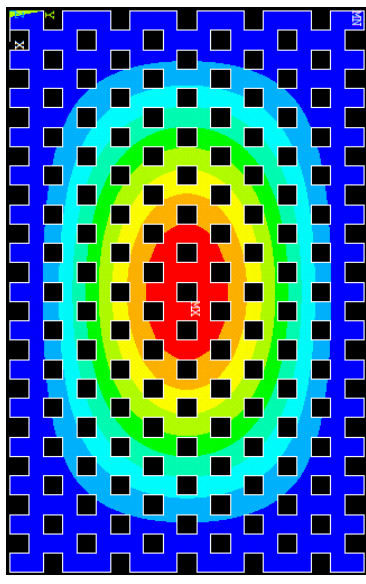
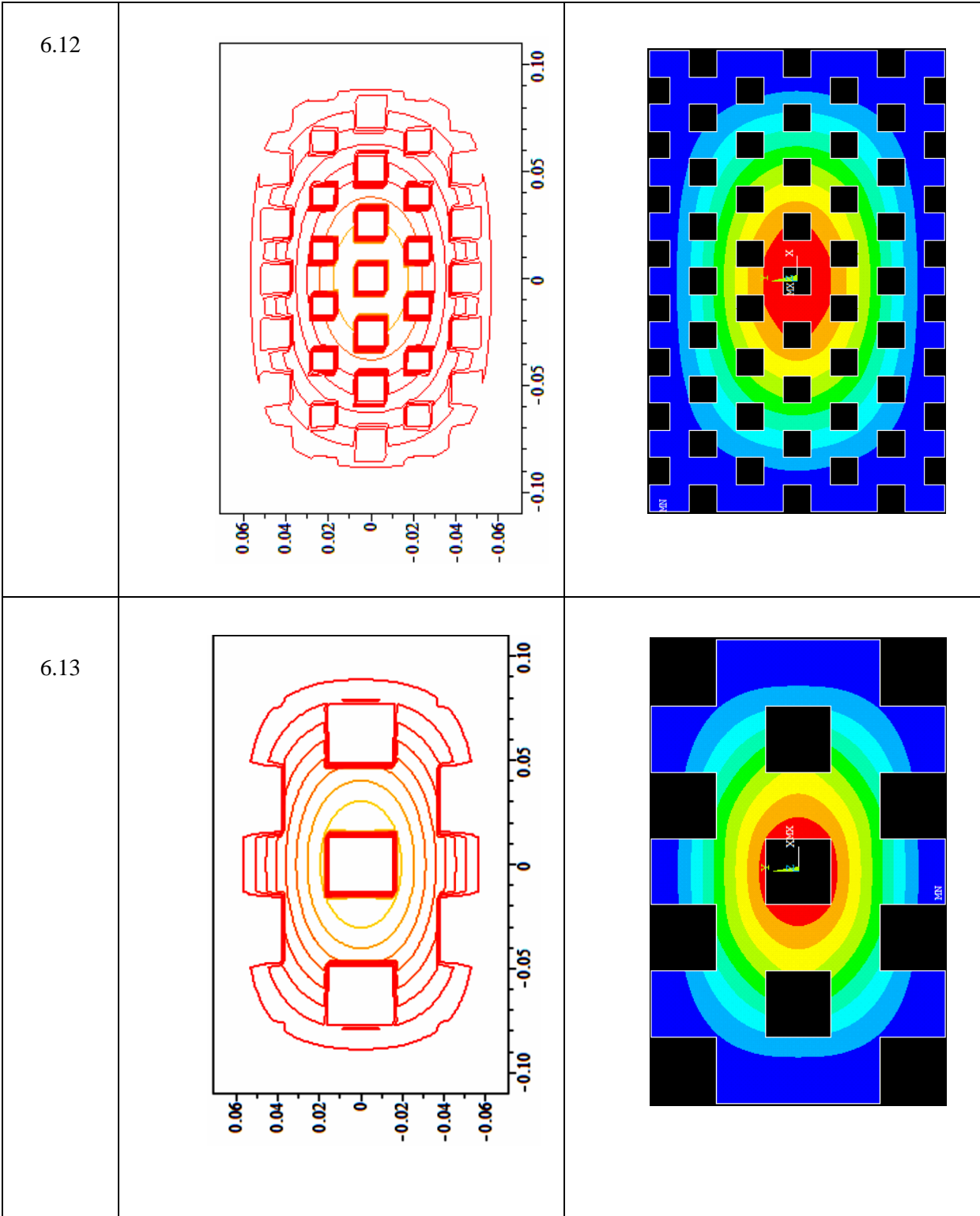
Speci. No.	Mode shapes	
	Analytical	FEM
	Specimens with the dimensions (138 mm x 216 mm)	
6.10		

Table 6.3b Comparison of the analytical and FEM mode shapes for the plates with the fixed outer dimensions

Speci. No.	Mode shapes	
	Analytical	FEM
	Specimens with the dimensions (138 mm x 216 mm)	
6.11		



6.6.2 Construction of the Material Property Variation Function

The function $F(x, y)$ represents the variation of the density and modulus of elasticity then for the perforated plate the density and modulus of elasticity can be given by equation (5.5). For the function $F(x, y)$ to represent these parameters it must satisfy the requirement given by equation (5.7). If $f(x)$ represents the variation in x direction and $g(y)$ represents variation in y direction. Then superimposing these functions will give the resultant density and Young's modulus at any point (x, y) for square pattern.

For a square pattern we have from equation (5.14),

$$F(x, y) = f(x) + g(y) - f(x) \cdot g(y) \quad (6.13)$$

If we consider the geometry of the plates with 45 degree staggered pattern we observe that alternate rows of the pattern are displaced with respect to the previous rows. This deviation from the square pattern can be interpreted as a phase difference and it can be incorporated into the density and modulus of elasticity function. If $\varphi 1$ and $\varphi 2$ represent the phase difference to be introduced in the density functions as a result of the rows displaced, the resultant density in x direction becomes $f(x - \varphi 1)$ and the resultant density in y direction becomes $g(y - \varphi 2)$. Thus for a staggered pattern we have from equation (6.1).

$$F(x, y) = f(x - \varphi 1) + g(y - \varphi 2) - f(x - \varphi 1) \cdot g(y - \varphi 2) \quad (6.14)$$

First the individual functions along the x axis and y axis are computed separately. Appropriate phase difference is introduced in the functions so as to consider the phase shift in the alternate rows. To construct the functions along the individual axes we represent the variation as a series of pulses constructed using the Heaviside step function. From the geometry of plate given in Figure 6.4 material is present in between the intervals $x \in \{-7d/2, -d/2\}, \{d/2, 7d/2\}$ and similarly for $y \in \{-7d/2, -d/2\}, \{d/2, 7d/2\}$. So the resultant property variation function can be given as:

$$H\left(t - \frac{d}{2}\right) - H\left(t - \frac{7d}{2}\right) + H\left(t + \frac{7d}{2}\right) - H\left(t + \frac{d}{2}\right) \quad (6.15)$$

This expression can be written in a compact form as:

$$\sum_{M=-1}^0 H\left(t - \frac{(8M + 1)d}{2}\right) - H\left(t - \frac{(8M + 7)d}{2}\right) \quad (6.16)$$

The function representing the phase difference in the property variation function can be obtained from the fact that alternate rows of a square pattern are shifted by a distance $2d$ to

get the 45 degree staggered pattern. Thus for the particular geometry considered we have the phase difference equal to $2d$ when we have $y \in \{-5d/2, -3d/2\}, \{3d/2, 5d/2\}$ and similarly for $x \in \{-5d/2, -3d/2\}, \{3d/2, 5d/2\}$. Thus the function for the phase difference can be obtained as a series of pulses of amplitude $2d$ which can be given by the following expression:

$$H\left(t - \frac{3d}{2}\right) - H\left(t - \frac{5d}{2}\right) + H\left(t + \frac{5d}{2}\right) - H\left(t + \frac{3d}{2}\right) \quad (6.17)$$

This expression can be written in a compact form as:

$$\sum_{M=-1}^0 H\left(t - \frac{(8M+3)d}{2}\right) - H\left(t - \frac{(8M+5)d}{2}\right) \quad (6.18)$$

Thus we get the following expressions for $\phi_1, \phi_2, f(x), g(y)$ and $F(x, y)$ respectively.

$$\phi_1 = \sum_{M=-1}^0 \left(H\left(y - \frac{(8M+3)d}{2}\right) - H\left(y - \frac{(8M+5)d}{2}\right) \right) \quad (6.19)$$

$$\phi_2 = \sum_{M=-1}^0 \left(H\left(x - \frac{(8M+3)d}{2}\right) - H\left(x - \frac{(8M+5)d}{2}\right) \right) \quad (6.20)$$

$$f(x) = \sum_{M=-1}^0 \left(H\left(x - \frac{(8M+1)d}{2} - \phi_1\right) - H\left(x - \frac{(8M+7)d}{2} - \phi_1\right) \right) \quad (6.21)$$

$$g(y) = \sum_{M=-1}^0 \left(H\left(y - \frac{(8M+1)d}{2} - \phi_2\right) - H\left(y - \frac{(8M+7)d}{2} - \phi_2\right) \right) \quad (6.22)$$

Density plot of the function $F(x, y)$ is given for the specimen plate with the side dimensions $a = b = 90$ mm and the square perforation size is 10 mm in Figure 6.5.

To determine the fundamental frequency the Rayleigh's method discussed in section (3.3.1) of the thesis is used. $F(x, y)$ obtained in by equation (6.14) is used to obtain the energy expressions.

The Rayleigh's quotient now becomes, as given by equation (5.6) from thesis.

$$\omega_1^2 = \frac{E_0 h^2}{12 \rho_0 (1 - \nu_0^2)} \frac{\iint_R F(x, y) \left[(\nabla^2 W_1)^2 + 2(1 - \nu) \left\{ \left(\frac{\partial^2 W_1}{\partial x \partial y} \right)^2 - \left(\frac{\partial^2 W_1}{\partial x^2} \right) \left(\frac{\partial^2 W_1}{\partial y^2} \right) \right\} \right] dx dy}{\iint_R F(x, y) W_1^2 dx dy} \quad (6.23)$$

6.7 Numerical Analysis and Validation

Numerical analysis is carried for the five specimens with the different sizes of the square perforations ranging from 10 mm to 30 mm. Thickness of the plate considered is 2 mm for each specimen. The material properties considered are $E_o = 2.1 \times 10^{11}$ N/ m², $\nu_o = 0.3$, $\rho_o = 7850$ kg/ m³. For each specimen the fundamental frequency is obtained by the Rayleigh's method. The shape function $W(x, y)$ is given by equation (6.24). Only First term approximation is considered for the Rayleigh's method. Shape function $W(x, y)$ satisfies clamped boundary condition on all edges.

$$W(x, y) = C_1 \left(x^2 - \left(\frac{a}{2} \right)^2 \right)^2 \left(y^2 - \left(\frac{b}{2} \right)^2 \right)^2 \quad (6.24)$$

For validation the FEM modal analysis of the same specimens was done using ANSYS (Element type: Shell 63) using the same material properties as used in the numerical analysis. Comparison of the results by both the methods is given in Table 6.4.

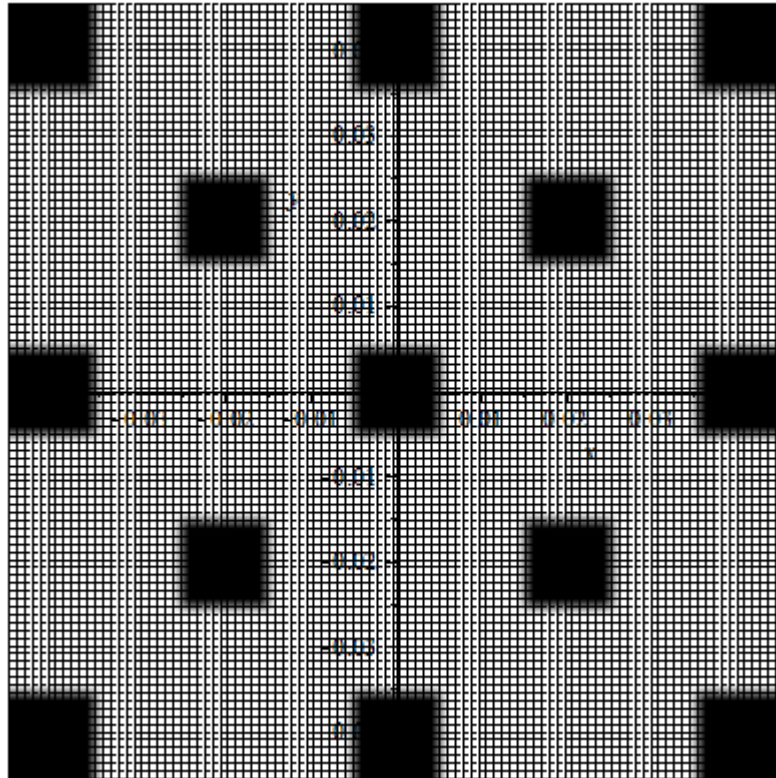


Figure 6.5 Density plot of the function $F(x, y)$ for the 45° staggered pattern

6.8 Results and Discussion

Table 6.4 Numerical and FEM analysis results for the 45° staggered pattern

Speci. No.	Plate size, (mm ×mm)	Hole Size (mm x mm)	ω_1 , (Hz)	ω_1 , FEM (Hz)	%Error
			Numerical <i>Rayleigh</i>		<i>Rayleigh & FEM</i>
6.16	90 × 90	10 × 10	2057.548	2030.4	1.337
6.17	135 × 135	15 × 15	914.465	902.42	1.334
6.18	180 × 180	20 × 20	514.387	507.62	1.333
6.19	225 × 225	25 × 25	329.841	324.91	1.517
6.20	270 × 270	30 × 30	229.493	225.62	1.716

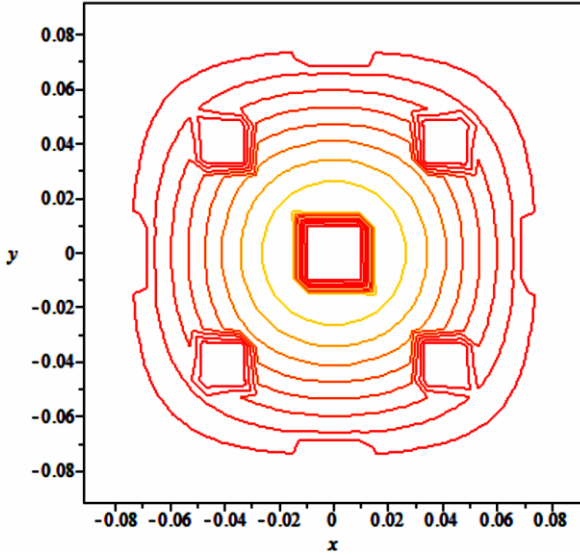
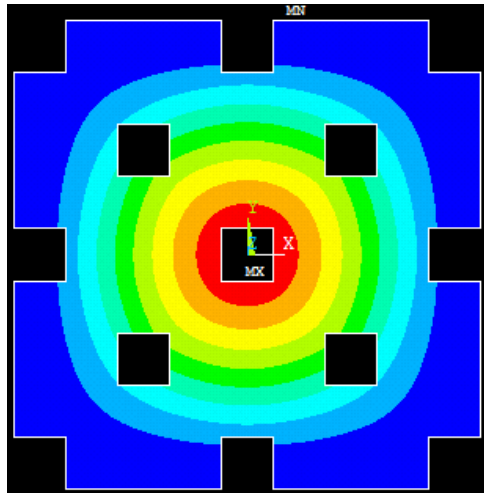
The agreement between the numerical and FEM results is reasonably good; differences are mainly due to the use of approximate methods and limitations of the Heaviside function used. The procedure developed in this approach is straightforward and allows for immediate solution. We found computation time is exceptionally good with one term of the shape function. The function $f_j(x, y)$ can be slightly extended beyond the actual domain, which will not change the maximum potential and kinetic energy as integrals will be calculated over actual domain i.e. $x \in \{-a/2, a/2\}$ and $y \in \{-b/2, b/2\}$. This helps greatly in reducing computation time.

The expressions obtained for the material property variation function in both the cases can be extended to the plates with similar geometry and the different outer dimensions. The material property variation function which is used for a plate with staggered pattern seems to be computationally less effective when more number of terms are used in the shape function and solved by the Rayleigh's - Ritz method. It involves the computation of the phase difference at each point which itself is a function of the position of the point; and then this phase difference is further used to compute the density along the individual axes. These values of density are then superimposed to give the resultant density at point. Thus we have used the Rayleigh's quotient and only one term approximation to minimize the complexity and the number of computation steps and the results can be obtained within few seconds. One term approximations are readily obtained and provide a good estimate of the fundamental frequency as seen from Table 6.4.

6.8.1 Comparison of the Analytical and FEM Mode Shapes

Contour plots of the mode shape obtained from the analytical method are compared with that obtained from the FEM analysis in Table 6.5. The specimens numerically analyzed are geometrically similar hence representative comparison is shown for the specimen 6.18. From comparison of the mode shapes it is observed that both the analytical and FEM modes are in agreement with each other.

Table 6.5 Comparison of the analytical and FEM mode shapes for a unit cell of 60° staggered perforation pattern

Analytical	FEM
Specimen no.6.18 Dimensions 180 mm x 180 mm and $d = 20$ mm x 20 mm	
	

6.9 Concluding Remark

The Heaviside step function can be used to express the variation of material properties of the perforated plates with the staggered array of perforation pattern. An approach presented here is an extension of the approach proposed in the chapter 5. An analytical model formulated in present work is more versatile, as the same model is applicable to the plates with the staggered and rectangular/square array of the rectangular/square perforations. If the expressions for phase difference in the equations governing the variation of the material properties for a staggered pattern are set to zero, the resultant expressions obtained for the material properties are valid for a rectangular pattern. The material properties variation functions thus obtained can be used to determine the fundamental frequency of the plates using approximate techniques such as the Rayleigh's method. Also proposed approach can be

applied to the plates subjected to the other boundary conditions with appropriate choice of the shape function to represent the deflection of the mid plane of the plate.

Section Two

**Analytical Models to Determine the Fundamental Frequency of
the Rectangular Plates with the Circular Perforations**

(Chapter 7, 8, 9 and 10)

Chapter 7

The Concentrated Negative Mass Approach

7.1 Introduction

The work given in this chapter is concerned with the vibration analysis of the perforated rectangular plates with the rectangular perforation pattern of the circular holes. Free vibration of the perforated plate with the rectangular perforation pattern of the nine circular perforations is studied. Boundary condition used for the plate is clamped on all four edges. In the current approach the Galerkin method is used for determining the fundamental frequency of the rectangular perforated plate with the rectangular perforation pattern of the circular holes. The perforated plate is considered as a plate with a uniformly distributed mass and holes are considered as concentrated negative masses. The deflected surface of the plate is approximated by the cosine series which satisfies the boundary conditions. Ten specimens are analyzed numerically with different perforation diameters to obtain the fundamental frequency. To validate the proposed model the FEM and experimental results have been used. The comparisons show that the analytical model predicts the natural frequencies reasonably well for the holes of small size.

Percentage error in the fundamental frequency obtained by comparing the numerical and FEM results is plotted against ratio of the plate area (A) to the perforation hole area (A_p). For the variation of the percent error in the fundamental frequency, trend line is established by regression analysis. Further from the equation of the trend line limiting condition in terms of the ratio of the plate area (A) to the perforation hole area (A_p) is established, to obtain accuracy in the fundamental frequency is obtained. Present analytical model is thus useful for predicting accurately the fundamental frequencies of wide range of the small size perforation geometries, for the rectangular plates with the rectangular perforation pattern for all edges clamped support condition.

7.2 Analytical Formulations

7.2.1 Equation of the Motion for an Isotropic Rectangular Plate

The Galerkin method is applied to the plate vibration problems (Ventsel and Krauthammer, 2001) to get the equation of motion. The partial differential equation

governing the free transverse vibration of an isotropic thin plate with dimensions a , b shown in Figure. 7.1, is (Ventsel and Krauthammer, 2001),

$$D\left(\frac{\partial^4 w}{\partial x^4} + 2\frac{\partial^2 w}{\partial x^2}\frac{\partial^2 w}{\partial y^2} + \frac{\partial^4 w}{\partial y^4}\right) + \rho h \frac{\partial^4 w}{\partial t^2} = 0 \quad (7.1)$$

$$D\nabla^2\nabla^2 w(x, y, t) + \rho h \frac{\partial^4 w}{\partial t^2}(x, y, t) = 0 \quad (7.2)$$

Where h is the uniform plate thickness, ρ is the density, w is the transverse displacement, and D is the flexural rigidity, ∇^2 is two-dimensional Laplacian operator. D and ∇^2 are given as

$$D = \frac{Eh^3}{12(1-\nu^2)}, \quad \nabla^2 = \frac{\partial^2}{\partial x^2} + \frac{\partial^2}{\partial y^2} \quad (7.3)$$

Where E is the modulus of elasticity and ν is the Poisson's ratio.

To solve equation (7.2) and obtain $w(x, y, t)$ in general, the following solution can be assumed

$$w(x, y, t) = (A \cos \omega t + B \sin \omega t)W(x, y) \quad (7.4)$$

This is separable solution of the shape function $W(x, y)$ describing the modes of the vibration and some harmonic function of time; ω is the natural frequency of the plate vibration which is related to the vibration period T by the relationship,

$$\omega = 2\pi / T \quad (7.5)$$

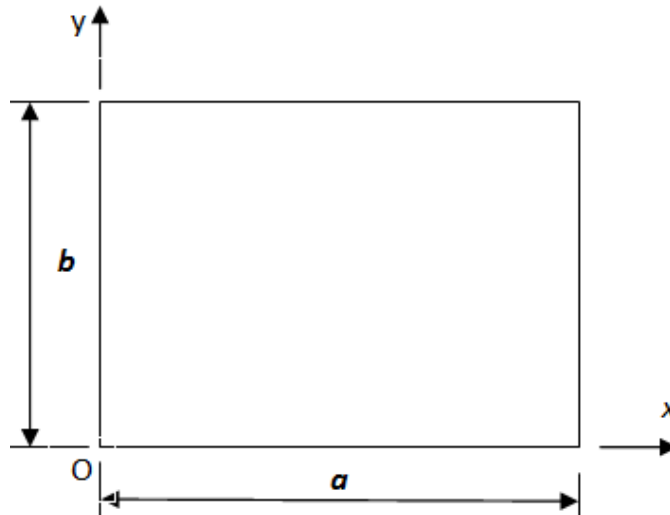


Figure 7.1 Rectangular plate co-ordinates

Introducing equation (7.4) in to equation (7.2) we get,

$$D\nabla^2\nabla^2w(x, y) - \omega^2 \rho h W = 0 \tag{7.6}$$

The shape function satisfying the boundary conditions for the rectangular plate with dimensions a and b is assumed in the form of series as below.

$$W(x, y) = \sum_{i=1}^n C_i W_i(x, y) \tag{7.7}$$

Where, C_i are unknown coefficients.

Now following the general procedure of the Galerkin method the unknown coefficients C_i can be determined from the orthogonality conditions.

For the plate problem vibration given by equation (7.6), the orthogonality conditions together with the equation (7.7) result in equation (7.8) as given below

$$\iint_A (D \sum_{i=1}^n C_i \nabla^2 \nabla^2 W_i - \omega^2 \rho h \sum_{i=1}^n C_i W_i) W_k dx dy = 0; k = 1, 2, \dots, n \tag{7.8}$$

The above conditions when implemented numerically leads to the Galerkin system of linear algebraic equations of the form

$$\begin{aligned} a_{11}C_1 + a_{12}C_2 + \dots &= 0 \\ \dots & \\ a_{n1}C_1 + a_{n2}C_2 + \dots &= 0, \end{aligned} \tag{7.9}$$

Where

$$a_{ik} = a_{ki} = \iint_A [D\nabla^2\nabla^2W_i - \omega^2 \rho h W_i] W_k dx dy \tag{7.10}$$

This system of homogeneous equations has a nontrivial solution if its determinant $\Delta(\omega)$ made up of the coefficients a_{ik} is equal to zero. Therefore we obtain n^{th} order characteristic equation for determining the natural frequencies as,

$$\Delta(\omega) = 0 \tag{7.11}$$

This equation will have an infinite number of solutions which constitute the frequency spectrum for the given plate. In general, the frequencies will depend on two parameters: m and n ($m = 1, 2, \dots$; $n = 1, 2, \dots$). For each frequency ω_{mn} , there is a corresponding shape function $W(x, y)$, which on the basis of the homogeneous equations, is determined by a constant multiplier (which can be assumed as being equal to unity).

7.2.2 Determination of the Fundamental Frequency of the Plates with the Circular Perforations

A rectangular plate with coordinate system $(O; x, y, z)$, having the origin O at one corner is considered as shown in Figure. 7.2 Co-ordinates of the plate clamped on all edges carrying circular holes. The displacement of an arbitrary point of coordinates (x, y) on the middle surface of the plate is denoted by w , in out-of-plane (z) direction. The boundary conditions considered here, are all edges clamped. Geometric parameters, hole diameter d is uniform for all perforations. The assumptions made in the following formulation are that transverse deflections are small so that the dynamic behavior of the plate is governed by the classical thin plate theory. Mass of the plate, (m) is considered as uniformly distributed with the nine concentrated negative masses denoted as ‘ $-M$ ’. The negative sign indicates that the concentrated mass ‘ $-M$ ’ cancels out the effect of the same amount of mass of the homogenous plate at the position of the cut-outs. This is an equivalent approach to apply the Galerkin method for the given perforated plate vibration problem. Analytical model in the present work does not consider any rotary inertia of the plate.

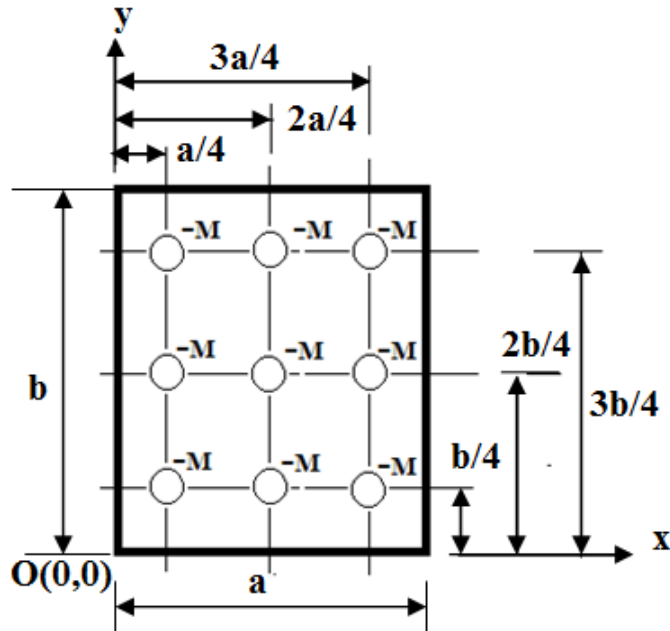


Figure 7.2 Co-ordinates of the plate clamped on all edges carrying circular holes

The middle surface displacement is approximated by using the shape function $W(x, y)$ in the form of a series, which satisfy the boundary conditions on the edges $x = 0$, $x = a$, and $y = 0$, $y = b$. Let us represent the shape function $W(x, y)$ for a rectangular plate with dimensions a and b in the form (Ventsel and Krauthammer, 2001),

$$W(x, y) = \sum_i \sum_k C_{ik} W_{ik}(x, y) \quad (7.12)$$

where C_{ik} are unknown coefficients representing the amplitudes of the free vibration modes and $W_{ik}(x, y)$ is the product of the pertinent eigenfunctions of the lateral beam vibrations.

$$W_{ik}(x, y) = F_i(x)F_k(y) \quad (7.13)$$

Which satisfy the prescribed boundary conditions on the edges $x = 0$, $x = a$, and $y = 0$, $y = b$. In equation (7.13) $F_i(x)$ and $F_k(y)$ represent the i th and k th modes of freely vibrating beams of spans a and b , respectively.

By applying the Galerkin method for determining the fundamental frequency, equation (7.10) can be modified for the coefficients a_{ik} of the Galerkin's system of equations, to the present problem, as follows (Ventsel and Krauthammer , 2001),

$$a_{ik} = a_{ki} = \iint_A [D\nabla^2\nabla^2 W_i - \omega^2 \rho h W_i] W_k dx dy - \sum M \omega^2 W_i W_k \quad (7.14)$$

The deflected surface of the vibrating plate is approximated by the series,

$$W(x, y) = \sum_{i=1}^{\infty} \sum_{k=1}^{\infty} C_{ik} (1 - \cos \frac{i2\pi x}{a})(1 - \cos \frac{k2\pi y}{b}) \quad (7.15)$$

This satisfies the boundary condition clamped all edges.

For the first approximation retaining only the first term in the expansion of equation (7.15) we obtain from equation (7.14),

$$a_{11} = \int_0^a \int_0^b [D(\frac{\partial^4 W_1}{\partial x^4} + 2 \frac{\partial^2 W_1}{\partial x^2} \frac{\partial^2 W_1}{\partial y^2} + \frac{\partial^4 W_1}{\partial y^4}) - m\omega^2 W_1] W_1 dx dy - \sum M \omega^2 W_1^2 \quad (7.16)$$

Introducing in equation (7.16) W_1 as below

$$W_1 = (1 - \cos \frac{2\pi x}{a})(1 - \cos \frac{2\pi y}{b}) \quad (7.17)$$

After simplification of equation (7.16) following expressions are obtained

$$D(\frac{12b\pi^4}{a^3} + \frac{12a\pi^4}{b^3} + \frac{8a\pi^4}{ab}) - m\omega^2(\frac{9ab}{4}) + 32M\omega^2 = 0 \quad (7.18)$$

$$\omega = \frac{-4\pi^2 \sqrt{-ab(-9mab + 128M)D(3b^4 + 3a^4 + 2a^2b)}}{a^2b^2(-9mab + 128M)} \quad (7.19)$$

7.3 Numerical Simulation

An analytical model developed in section 7.2.2 is applicable to the rectangular perforated plates with the different side dimensions, provided that the perforations are of the same size. By virtue of the symbolic forms presented in this work, the method can be applied to the analytical studies of the perforated plates with different boundary conditions. To estimate the sensitivity of the method for various cases of the hole sizes and plate sizes, the numerical analysis is carried out for the ten different plate specimens listed in Table 7.1. Third column of the Table 7.2 lists the ratio of the plate area (A) to the area of perforation hole (A_p).

$$A = a \times b \quad (7.20)$$

$$A_p = \frac{\pi d^2}{4} \quad (7.21)$$

Co-ordinates of the perforation centers (x mm, y mm) are given in Table 7.1. The material properties considered for all 2 mm thick specimen plates analyzed are as given in Table 4.1.

Table 7.1.Co-ordinates of the perforation centers

Specimen size (mm x mm)	Co ordinates of the perforation centers (x mm ,y mm)								
	a/4,b/4	a/4,2b/4	a/4,3b/4	2a/4,b/4	2a/4,2b/4	2a/4,3b/4	3a/4,b/4	3a/4,2b/4	3a/4,3b/4
138 x 216	34.5,54	34.5,108	34.5,162	69,54	69,108	69,162	103.5,54	103.5,108	103.5,162
276 x 432	69,108	69,216	69,324	138,108	138,216	138,324	207,108	207,216	207,324

7.4 Validation of the Proposed Approach

The proposed analytical model is validated by comparing the numerical analysis results with FE modal analysis results. The FE Modal analysis is carried out by ANSYS 11 using Shell 63 element. Parameters of the plate specimen considered in this study are shown in Table 7.2. Analysis is carried out for the clamped steel plates having 2 mm thickness and carrying nine holes at the positions shown in Figure.7.2. Mesh convergence for the FEM results is checked for every specimen. Thus converged solution is given in Table 7.3. Summary of the mesh convergence is given in Appendix “B”, Table B.5 and Table B.6.

The numerical results obtained are also validated by comparing results with the experimental natural frequencies. An experimental analysis was carried out for two specimens with circular perforations of diameter 5 mm and 10 mm respectively. The

specimens used for the experimentation are shown in Figure 7.3. Thickness of the specimens is 2 mm. The fixture for performing experiments was as discussed in the chapter 4, section 4.3. Due to the size limitation of the fixture, experimental validation of the analytical results is done for two plates only, as given in Table 7.3. The experimental results obtained are given in Table 7.3.



Specimen no.7.11 ($d = 5$ mm)



Specimen no.7.12 ($d = 10$ mm)

Figure 7.3 Perforated plate specimens used in the experiment

7.5 Results and Discussions

Comparison of the numerical and FEM natural frequencies of the plate specimens for first mode is given in Table 7.2. Last column of the Table 7.2 shows percentage error in the fundamental frequency values obtained by the numerical analysis and by the FEM analysis. The agreement between the analytical approach and the finite element results is within 7.5% when perforation size is small, $(A/A_p) = 168.683$. The maximum difference is of the order 25.33% especially for the specimen having $A/A_p = 35.932$. Figure.7.3 shows the variation of the percent error in the fundamental frequency with respect to (A/A_p) ratio. Dotted line shows the trend line for this variation. The power trend line clearly demonstrates the decrease in percentage error with increase in (A/A_p) ratio. An equation used to calculate the least squares fit through points for the trend line is,

$$\% Error = f \left(\frac{A}{A_p} \right)^g \quad (7.22)$$

In above expression f and g are constants. For the percentage error, (A/A_p) ratio data given in Table 7.2 values of the constants f and g are found to be 123.97 and - 0.51 respectively. Thus equation of the trend line shown in Figure 7.4 is,

$$y = 123.97x^{-0.51} \quad (7.23)$$

where y and x are values of percentage error and (A/A_p) ratio respectively.

R-squared value shown in Figure.7.4 is a correlation coefficient which reveals how closely the estimated values for the trend line correspond to actual data.

$$R^2 = 0.9371 \quad (7.24)$$

It is observed that the percent error increases above 10%, when the (A/A_p) ratio goes below the value 139.238. Thus present approach has limitation in predicting the value of the fundamental frequency, as it is based on the basic assumption of the concentrated negative mass. It is found that the error in the fundamental frequency is of order of 5% when ratio of the area of the plate (A) to the area of single perforation (A_p) is 542.017. As size of the perforation increases, present approach deviates more. Further from Table 7.2 it is observed that for the specimens of different configuration but having approximately the same (A/A_p) ratio analytical model gives results with similar accuracy (Specimen 7.1, 7.6 and 7.2, 7.7).

Table 7.2 Fundamental frequency results of the numerical and FE simulations

Specimen No.	d (mm)	(A/A_p)	ω , Numerical (Hz)	ω , FEM (Hz)	% Error
Specimens with dimensions (138 mm x 216 mm)					
7.1	5	1518.154	718.63	693.38	3.64
7.2	10	379.5384	729.04	693.85	5.07
7.3	15	168.6837	747.46	695.97	7.40
7.4	25	60.72615	817.34	710.17	15.09
7.5	30	42.17094	878.60	724.94	21.20
Specimens with dimensions (276 mm x 432 mm)					
7.6	10	1518.154	179.65	173.37	3.62
7.7	20	379.5384	182.26	173.46	5.07
7.8	25	242.9046	184.29	173.65	7.13
7.9	50	60.72615	204.33	177.53	15.10
7.10	65	35.93263	230.04	183.55	25.33

Comparison of the numerical and experimental natural frequency for the first mode is given in Table 7.3. Last column of the Table 7.3 shows percentage error in the fundamental

frequency values obtained by the numerical analysis and by the experimental analysis. The agreement between the analytical approach and the experimental results is reasonably good when perforation size is small. As demonstrated in Table 7.2 and Figure 7.4 variation of the percent error in the fundamental frequency with (A/A_p) ratio, is due to the fact that the effects of both the different holes and their locations on the frequency have been accounted.

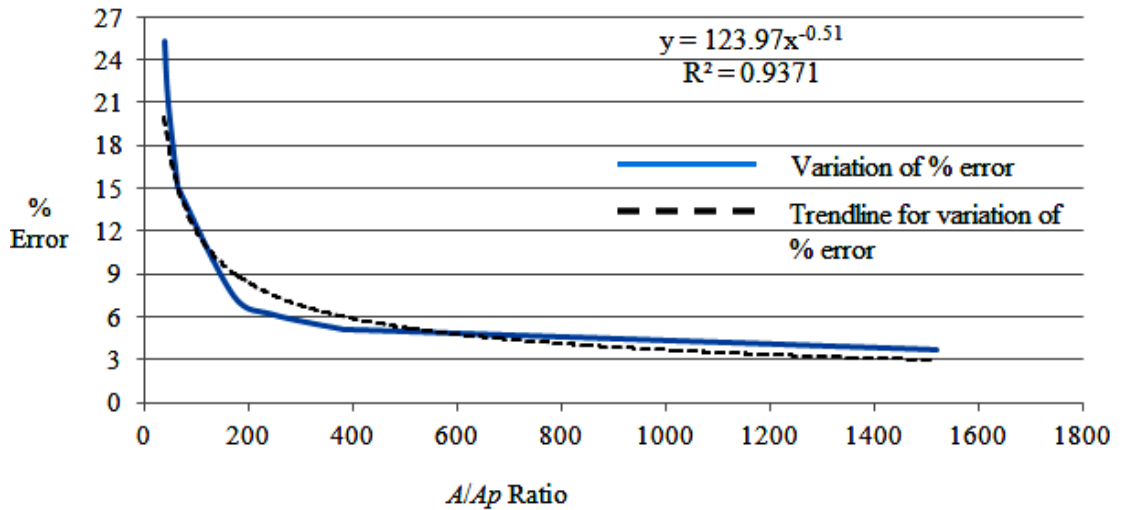


Figure 7.4 Variation of the percent error in the fundamental frequency with A/A_p ratio

Table 7.3 Fundamental frequency results of the numerical and experimental analysis

Specimen No.	d (mm)	(A/A_p)	ω , Numerical (Hz)	ω , Experimental (Hz)	% Deviation
Specimens with dimensions (138 mm x 216 mm)					
7.11	5	1518.154	718.63	650	9.5
7.12	10	379.5384	729.04	637	12.62

Experimentally obtained natural frequencies are compared with the numerical results obtained from the proposed model. Table 7.3 shows the comparison of these results. Figure 7.5 and Figure 7.6 shows the sample FRF obtained experimentally for the specimen 7.11 and 7.12 respectively. It is observed that the discrepancy between the numerical and experimental results is 9.5% for the specimen 7.11 and 12.62% for specimen 7.12. Thus it shows that as the perforation size increases results obtained by the proposed method deviates more. This occurs because as perforation size increases it changes the stiffness also significantly, but proposed model considers only change in/reduction in the mass or kinetic energy but not in the strain energy thus deviation between the numerical and experimental fundamental frequencies

becomes more. Further possible reasons for the deviation of the experimental results are as discussed in the Chapter 5, Section 5.6.1.

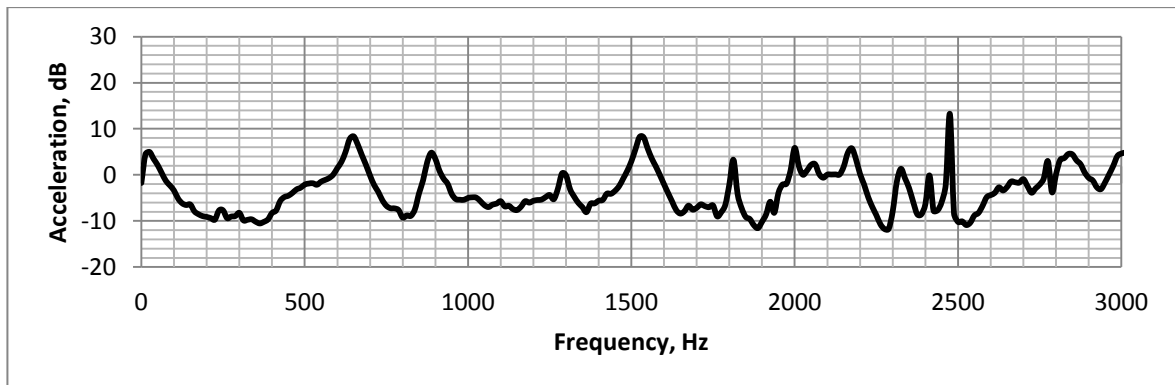


Figure 7.5 Frequency response function for the Specimens no. 7.11 ($d=5$ mm)

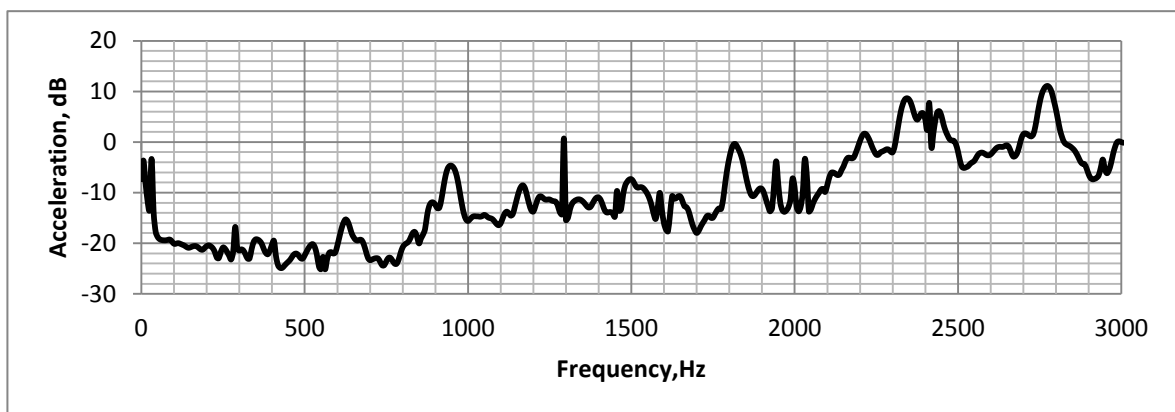


Figure 7.6 Frequency response function for the Specimens no. 7.12 ($d=10$ mm)

7.6 Concluding Remarks

This chapter presents an analytical model to estimate the fundamental frequency of the uniform thickness plates carrying circular perforations in the rectangular pattern. The effect of perforation on the natural frequency of the plate has been modeled using concept of the concentrated negative mass in the Galerkin method. The proposed model has been verified by comparing the numerical results with the FEM and experimental results. It is found that the error in the fundamental frequency is of order of 5% when ratio of the area of the plate (A) to the area of single perforation (A_p) is 542.017. It is found that the error in the fundamental frequency is more when the perforation size increases. Thus, the fundamental frequency of perforated plate can be obtained for small size of the perforation by a proper choice of the plate parameters and shape function depending on the boundary condition.

Chapter 8

An Equivalent Square Perforation Approach

8.1 Introduction

In this chapter an analytical models to determine the fundamental frequency of the perforated plate with the circular perforation is formulated. The circular perforations which are arranged in the rectangular array are replaced by an equivalent square hole and the non homogeneity in the Young's modulus and density due to an equivalent square perforation is expressed by using the unit step function. An analytical formulation is based on the Rayleigh-Ritz method. This approach is extension of the approach given in chapter 5 to the plates with the circular perforations. In present analysis the rectangular perforation pattern is considered for the plates with all edges clamped boundary condition. The perforated plate is considered as plate with uniformly distributed mass and the holes are considered as non homogeneous patches. The deflected middle surface of the plate is approximated by a two term polynomial function which satisfies the boundary conditions. Proposed approach is validated by comparing results with the Finite Element Method (FEM) modal analysis.

8.2. Analytical Formulation

8.2.1 Concept of an equivalent Square Hole for the Circular Perforation

Circular hole can be replaced by a square hole of same area with centre of the square same as the centre of the circular hole. Consider a circular hole of radius r_c as shown in Figure 8.1.

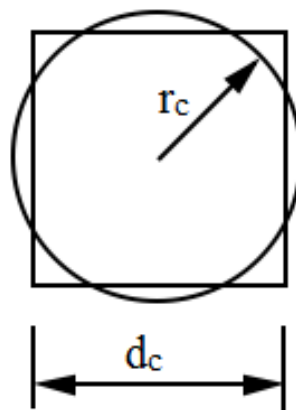


Figure 8.1 An equivalent square hole for the circle of radius r_c

Area of the circular perforation having radius r_c is given as,

$$A_c = \pi r_c^2 \quad (8.1)$$

For a square perforation of the side length d_c , area can be given as,

$$A_c = d_c^2 \quad (8.2)$$

For an equivalent square perforation, from equation (8.1) and (8.2)

$$d_c^2 = \pi r_c^2 \quad (8.3)$$

Thus for an equivalent square perforation the side dimension d_c can be given as,

$$d_c = r_c \sqrt{\pi} \quad (8.4)$$

8.2.2 Formulation of the Function to Express Non-Homogeneity in the Material Properties of the Plates with the Circular Perforations

A rectangular plate with coordinate system ($O; x, y, z$), having the origin O at one corner is considered as shown in Figure 8.2. Co-ordinates of the plate clamped on all edges carrying the circular holes are a and b along x and y axis respectively. The displacement of an arbitrary point of coordinates (x, y) on the middle surface of the plate is denoted by W , in out-of-plane (z) direction. The boundary conditions considered here, are all edges clamped. Geometric parameters of the perforated plate r_c i.e. the radius of hole is uniform for all the perforations arranged in the rectangular array. The assumptions made in the following formulation are that transverse deflections are small so that the dynamic behavior of the plate is governed by the classical thin plate theory. Equivalent square holes replacing the circular holes are shown with the side dimension as d_c . This concept of an equivalent square hole is used to apply the, unit step functions to express the non-homogeneity in the material properties. The Rayleigh-Ritz method for the plate vibration problem discussed in section (3.3.2) is used for the given perforated plate vibration problem. An analytical model in the present work does not consider any rotary inertia of the plate.

The function $F(x, y)$ represents the variation of the density and modulus of elasticity due to the equivalent square perforations. For the function $F(x, y)$ to represent these parameters it must satisfy the following requirements as given by equation (5.7).

$$\begin{aligned} F(x, y) &= 0 \text{ in the region corresponding to a perforation} \\ F(x, y) &= 1 \text{ otherwise} \end{aligned} \quad (8.5)$$

The function $F(x, y)$ is constructed as per the geometry of the plates considered with the equivalent square perforations. To construct the function $F(x, y)$ we assume that the density at any point (x, y) is the superposition of the density along x direction and y direction, this superposition is also considered for the modulus of elasticity.

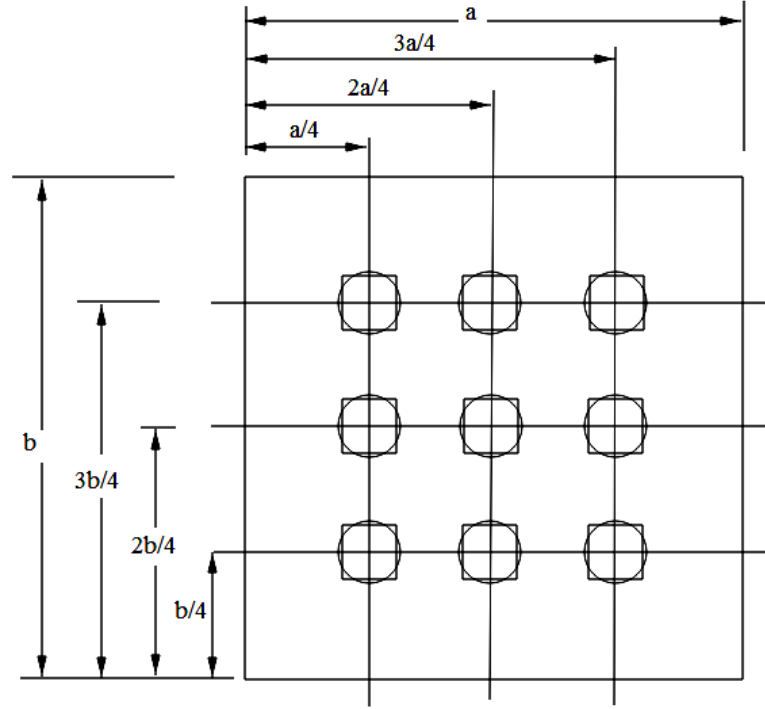


Figure 8.2 Orientation of the perforated plate with equivalent square perforations.

The functions $f(x)$ and $g(y)$ given by equation (8.7) and (8.8) represent variation of the density and modulus of elasticity along x and y axes respectively. Equations (8.7) and (8.8) show the rectangular Heaviside function used to express the non homogeneity in the Young's modulus and density of the plate due to the perforations. The functions $f(x)$ and $g(y)$ are formed by using the unit step functions and are superimposed to obtain the function $F(x, y)$ as given by equation (5.7) and (8.9).

The unit step as a function of a discrete variable n is given as:

$$H(n) = \begin{cases} 0, & n < 0 \\ 1, & n \geq 0 \end{cases} \quad \text{Where } n \text{ is an integer.} \quad (8.6)$$

$$\begin{aligned} f(x) = & H(x) - H\left(x - \left(\frac{a}{4} - \frac{dc}{2}\right)\right) + H\left(x - \left(\frac{a}{4} + \frac{dc}{2}\right)\right) - H\left(x - \left(\frac{2a}{4} - \frac{dc}{2}\right)\right) \\ & + H\left(x - \left(\frac{2a}{4} + \frac{dc}{2}\right)\right) - H\left(x - \left(\frac{3a}{4} - \frac{dc}{2}\right)\right) + H\left(x - \left(\frac{3a}{4} + \frac{dc}{2}\right)\right) \end{aligned} \quad (8.7)$$

$$\begin{aligned}
g(y) = & H(y) - H\left(y - \left(\frac{b}{4} - \frac{dc}{2}\right)\right) + H\left(y - \left(\frac{b}{4} + \frac{dc}{2}\right)\right) - H\left(y - \left(\frac{2b}{4} - \frac{dc}{2}\right)\right) \\
& + H\left(y - \left(\frac{2b}{4} + \frac{dc}{2}\right)\right) - H\left(y - \left(\frac{3b}{4} - \frac{dc}{2}\right)\right) + H\left(y - \left(\frac{3b}{4} + \frac{dc}{2}\right)\right)
\end{aligned} \tag{8.8}$$

For center origin of the plate above equations can be written as

$$\begin{aligned}
f(x) = & H\left(x - \frac{dc}{2}\right) + H\left(x - \left(\frac{a}{4} - \frac{dc}{2}\right)\right) - H\left(x - \left(\frac{a}{4} + \frac{dc}{2}\right)\right) \\
& + \left(H\left(-x - \frac{dc}{2}\right) + H\left(-x - \left(\frac{a}{4} - \frac{dc}{2}\right)\right) - H\left(-x - \left(\frac{a}{4} + \frac{dc}{2}\right)\right) \right)
\end{aligned} \tag{8.7a}$$

$$\begin{aligned}
g(y) = & H\left(y - \frac{dc}{2}\right) + H\left(y - \left(\frac{b}{4} - \frac{dc}{2}\right)\right) - H\left(y - \left(\frac{b}{4} + \frac{dc}{2}\right)\right) \\
& + \left(H\left(-y - \frac{dc}{2}\right) + H\left(-y - \left(\frac{b}{4} - \frac{dc}{2}\right)\right) - H\left(-y - \left(\frac{b}{4} + \frac{dc}{2}\right)\right) \right)
\end{aligned} \tag{8.8a}$$

Using the above equations $F(x, y)$ for a square perforation pattern can be obtained by the relation,

$$F(x, y) = f(x) + g(y) - f(x)g(y) \tag{8.9}$$

Plots of the functions $f(x)$ and $g(y)$ are shown in Figure 8.3 and Figure 8.4 respectively when origin is at lower left corner as shown in Figure 8.2. The Figure 8.6 and Figure 8.7 show plots of the functions $f(x)$ and $g(y)$ when origin is at the centre of the plate. The nature of the plots of $f(x)$ and $g(y)$ is same as the rectangular waves with amplitude unity. The density plot for the function $F(x, y)$ (for $a = 276$ mm, $b = 432$ mm and $r_c = 25$ mm) shown in Figure 8.5 and Figure 8.8 for corner and center origin respectively. The density plot of the function $F(x, y)$ resembles the geometry of the plate considered. The dark area represents the region where $F(x, y) = 0$ which is the region corresponding to the perforation. The density plot indicates that $F(x, y)$ is a valid representation of the density and elastic modulus variation for the plate.

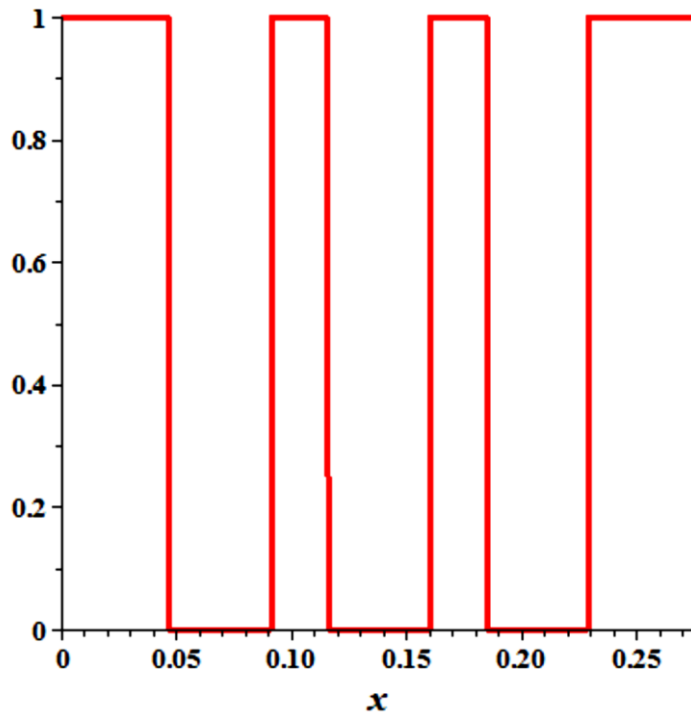


Figure 8.3 Plot of the function $f(x)$ for the specimen 276 mm x 432 mm with $r_c = 25$ from equation (8.7)

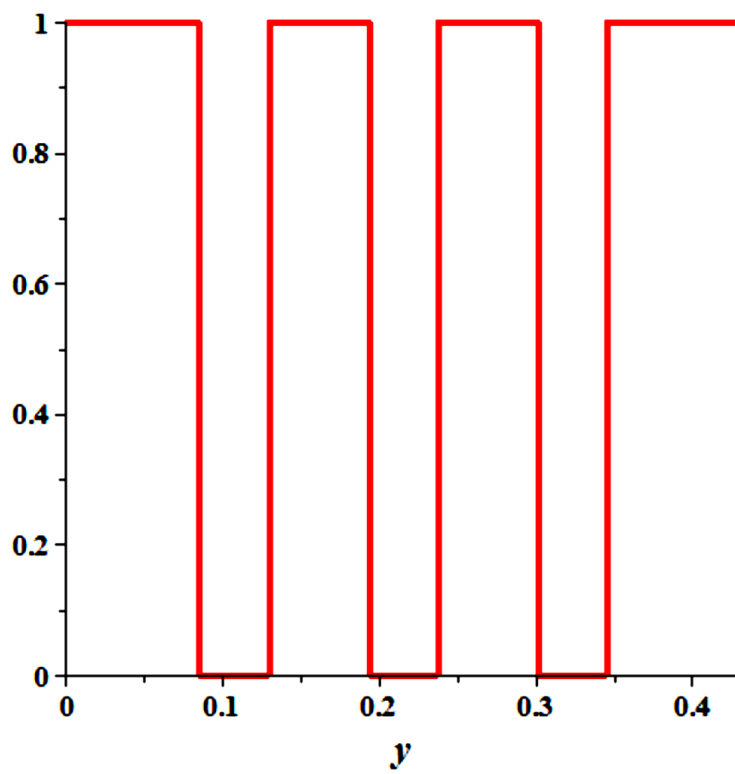


Figure 8.4 Plot of the function $g(y)$ for the specimen 276 mm x 432 mm with $r_c = 25$ from equation (8.8)

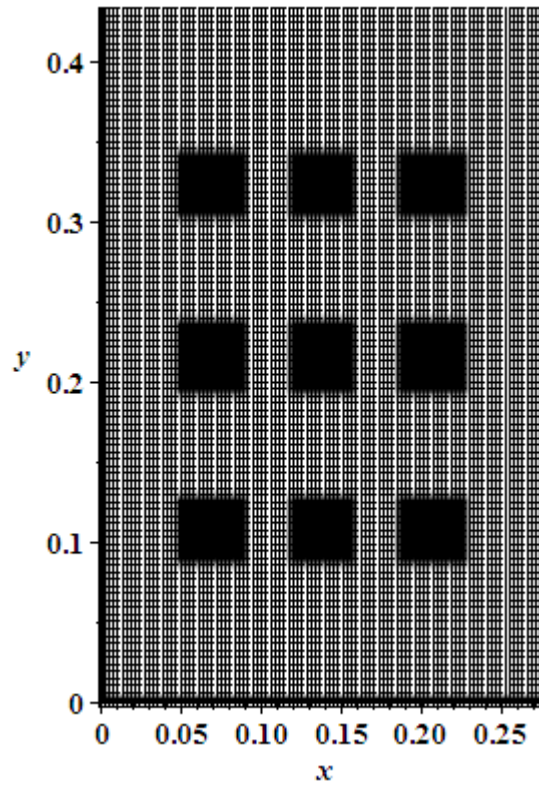


Figure 8.5 Density plot of the function $F(x, y)$ for the specimen 276 mm x 432 mm with $r_c = 25$ with corner origin

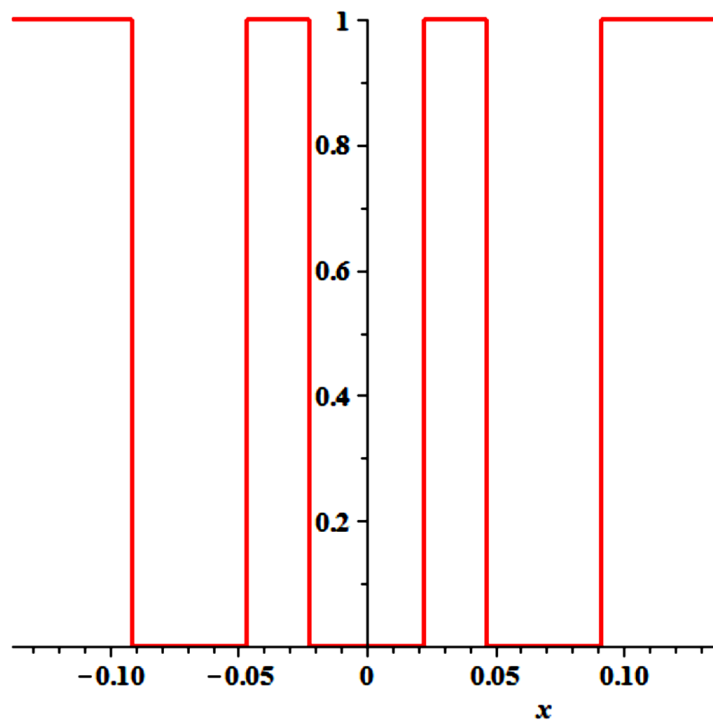


Figure 8.6 Plot of the function $f(x)$ for the specimen 276 mm x 432 mm with $r_c = 25$ from equation (8.7a)

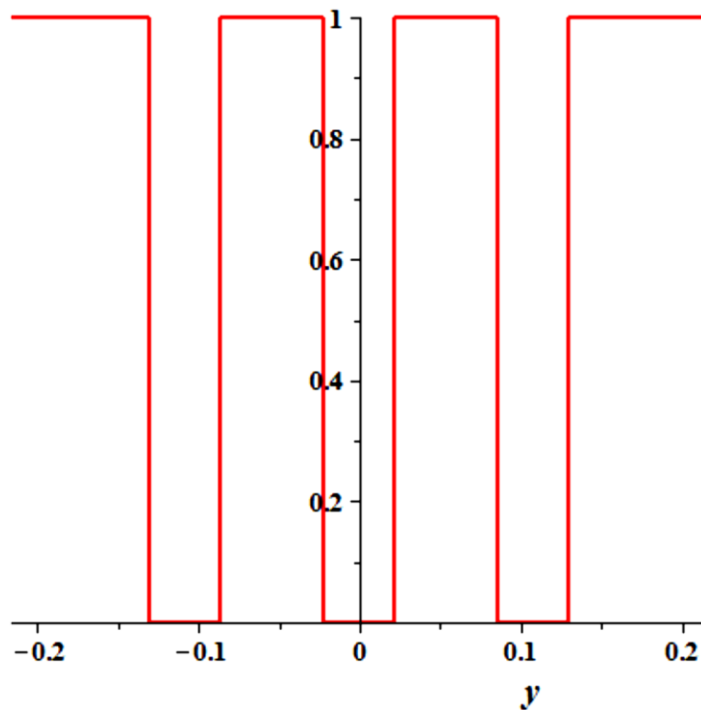


Figure 8.7 Plot of the function $g(y)$ for the specimen 276 mm x 432 mm with $r_c = 25$ from equation (8.8a)

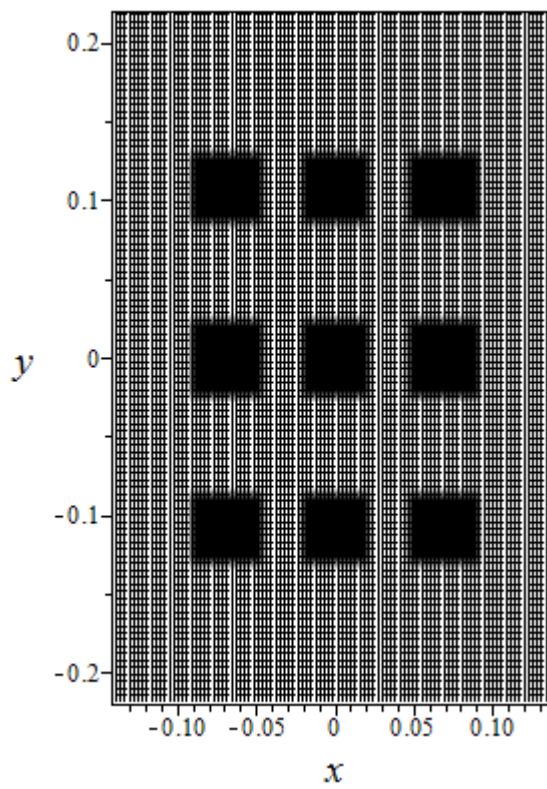


Figure 8.8 Density plot of the function $F(x, y)$ for the specimen 276 mm x 432 mm with $r_c = 25$ with center origin

8.2.3 Determination of the Fundamental Frequency of the Plates with the Circular Perforations

To determine the fundamental frequency the Rayleigh's-Ritz method discussed in section (3.3.2) is used (Leissa and Qatu, 2011; Chakraverty, 2009). The Rayleigh's-Ritz method is based on the maximum Kinetic energy and maximum Strain energy of the plate. The function $F(x, y)$ obtained in section (8.2.2.) is used to obtain the energy expressions given as below.

Maximum value of the Kinetic Energy is given as,

$$T_{\max} = \frac{1}{2} \omega_1^2 \int_0^a \int_0^b F(x, y) [h\rho W^2(x, y)] dx dy \quad (8.10)$$

The maximum Strain Energy is given as,

$$u_{\max} = \frac{1}{2} \int_0^a \int_0^b F(x, y) D [(\nabla^2 W)^2 + 2(1-\nu) \left\{ \left(\frac{\partial^2 W}{\partial x \partial y} \right)^2 - \frac{\partial^2 W}{\partial x^2} \frac{\partial^2 W}{\partial y^2} \right\}] dx dy \quad (8.11)$$

The middle surface displacement W in above expressions is approximated by using the shape function $W(x, y)$ in the form of a series, which satisfy the clamped boundary conditions on the edges $x = 0, x = a,$ and $y = 0, y = b$ as given by equation (5.4).

Let us represent the shape function $W(x, y)$ for a rectangular plate with dimensions a and b in the form,

$$W(x, y) = \sum_{i=1}^n C_i \phi_i(x, y) \quad (8.12)$$

where C_i are the unknown coefficients representing the amplitudes of the free vibration modes and $\phi_i(x, y)$ is the product of the pertinent eigenfunctions of the lateral beam vibrations.

Each of the ϕ_i in above equations satisfies at least the geometric boundary conditions. The geometric boundary conditions for the plate are those imposed on the displacements and slopes.

For clamped all edges the two term deflection function W , is considered as (Johri and Johri, 2011),

$$W(x, y) = \left[C_1 \left(\frac{x}{a} \right)^2 \left(\frac{y}{b} \right)^2 \left(1 - \frac{x}{a} \right)^2 \left(1 - \frac{y}{b} \right)^2 + C_2 \left(\frac{x}{a} \right)^3 \left(\frac{y}{b} \right)^3 \left(1 - \frac{x}{a} \right)^3 \left(1 - \frac{y}{b} \right)^3 \right] \quad (8.13)$$

In order to apply the Rayleigh-Ritz procedure, the maximum Strain energy must be equal to the maximum Kinetic energy i.e.

$$\delta(u_{\max} - T_{\max}) = 0 \quad (8.14)$$

$$T_{\max} = u_{\max} \quad (8.15)$$

From equation (8.10) and (8.11)

$$\omega^2 = \frac{u_{\max}}{T_{\max}^*} \quad (8.16)$$

where $T_{\max}^* = \frac{T_{\max}}{\omega^2}$ is the integral over the plate area without the frequency.

To use the Rayleighs-Ritz method u_{\max} and T_{\max} expressions are formulated in terms of C_i and ϕ_i , and then the frequency is minimized with respect to C_i . Thus C_i are determined so as to obtain the best upper bounds for the fundamental frequency. The frequency minimizing equations are,

$$\frac{\partial(\omega^2)}{\partial C_i} = 0, (i = 1, 2) \quad (8.17)$$

Substituting (8.17) into (8.18), following set of minimizing equations can be obtained.

$$\frac{\partial}{\partial C_i} (u_{\max} - \omega^2 T_{\max}^*) = 0, (i = 1, 2) \quad (8.18)$$

This is a set of 2 simultaneous, linear, algebraic equations in the unknown C_1 and C_2 . For a nontrivial solution, the determinant of the coefficient matrix is set equal to zero. The roots of the determinant are the 2 values of ω^2 . The lowest value of ω^2 is an upper bound approximation to the fundamental frequency.

The above explained analytical method can be extended to the different shape function having more number of terms. In the present study a higher degree polynomial function with 5 terms is also considered (Laura, and Saffell, 2005). This function needs co-ordinate system having origin at the centre of the plate and is given by equation (8.19).

$$W(x, y) = \sum_1^{n=5} c_i \left[x^{2n} - (a/2)^{2n} \right]^2 \left[y^{2n} - (b/2)^{2n} \right]^2 \quad (8.19)$$

The material property distribution function $F(x, y)$ in equation (8.9) is formulated by equation (8.7a) and (8.8a). An energy expression given by equation (8.10) and (8.11) are integrated for $x = -a/2$ to $x = a/2$, and $y = -b/2$ to $y = b/2$. Frequency minimization equation (8.18) in this case gives the set of 5 simultaneous, linear, algebraic equations in terms of the

unknowns $C_1 \dots C_5$. Which can be solved to get the fundamental frequency and with known frequency further mode shapes can be extracted.

8.3 Numerical Simulation

To estimate the sensitivity of the proposed approach for various cases of the perforation sizes and the plate sizes numerical simulation is carried out. The numerical simulation is carried out separately for each specimen with the two different shape functions given by equation (8.13) and (8.19). All the plate specimens analyzed numerically have thickness of 2 mm. Total ten specimens with different sizes of the uniform perforations arranged in the rectangular array are considered for the numerical simulation. Two sets of the plates are analyzed; first set of the plates is having outer effective dimensions as 138 mm x 216 mm and second set of the plates is having outer effective dimensions as 276 mm x 432 mm. The diameter of the perforation in first set varies over range 5 mm to 30 mm where as in second set it varies over range 10 mm to 65 mm. The side dimensions of the equivalent square perforations for range of the circular holes considered is given in Table 8.1. The material properties considered for all the specimen plates analyzed numerically are same as given in Table 4.1.

8.4 Validation of the Proposed Approach

The proposed analytical model is validated by comparing the numerical analysis results with the FEM and experimental analysis results. The FEM Modal analysis is carried out for each specimen by ANSYS 11 using Shell 63 element. The parameters of the plate specimen considered in this study are shown in Table 8.1. An analysis is carried out for the clamped steel plates having 2 mm thickness and carrying the nine holes at positions shown in Figure 8.2. Mesh convergence results for the every specimen are tabulated in Appendix “B”, Table B.5 and Table B.6. The converged solution is given in Table 8.1. It is assumed that the structure is formed of an isotropic homogeneous elastic material, i.e. mild Steel with the material properties same as used in numerical analysis (Table 4.1).

An experimental analysis was carried out for the two specimens with the circular perforations of the diameter 5 mm and 10 mm respectively. The specimens used for experimentation are shown in Figure 7.3. The thickness of the specimens is 2 mm. The fixture for performing the experiments was as discussed in chapter 4, section 4.3. Due to the size limitation of the fixture, experimental validation of the analytical results is done for the

two plates only as given in Table 7.3. The experimental results obtained are given in Table 8.3.

8.5 Results and Discussion

The results obtained by proposed approach and the FEM modal analysis are tabulated in Table 8.1. Comparison between the results of FEM and numerical calculations shows that the frequency obtained by proposed approach is higher than that obtained by the FEM. This is because the frequency values depend upon the type and the form of the shape function chosen. In the present numerical analysis the shape functions with 2 and 5 term approximation are used. The approximate representation of the deflection of the plate given by equation (8.13) provides the ease of the computations involved in the analysis. Increasing the number of terms will increase the accuracy of the numerical results. This can be observed from Table 8.1. In this study size of the circular perforations considered for each specimen is different. The mass remnant ratio (MRR) which is the ratio of mass of the perforated plate to the mass of the homogeneous plate with the same effective outer dimensions is calculated for the each specimen as follows:

$$MRR = \frac{a \times b - N \times d_c^2}{a \times b} \quad (8.20)$$

where N is the total number of perforations.

From Table 8.1 it can be observed that the mass remnant ratio for the each plate specimen considered is different. The distribution of the mass and thus the stiffness for the each specimen is different.

Results obtained from the numerical analysis are reasonably in good agreement with the FEM results, for the plate having MRR more than or equal to 0.852. It is observed from the fundamental frequency results given in Table 8.1 that, as the MRR decreases error in the fundamental frequency obtained by proposed approach becomes more. It shows that the mass distribution pattern approximated by an equivalent square perforation deviates more from the actual mass distribution pattern due to the circular perforations. This deviation gives maximum error of 10% in the fundamental frequency obtained by the proposed approach for the plate specimens having MRR less than 0.852. For plate specimens having the MRR greater than 0.946 present approach give results with more accuracy with maximum discrepancy of 2.7 %. Thus present approach can be used for the plate specimens having the MRR greater than or equal to 0.852 with maximum error of 6-7%. Further it can be noticed

that with the proposed analytical model results obtained for the specimens having approximately same MRR but different geometrical parameters, accuracy in the results obtained is almost same (Specimen Nos.8.1 and 8.6, Specimen Nos.8.2 and 8.7, Specimen Nos.8.4 and 8.9).

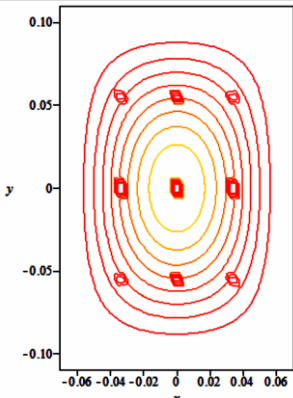
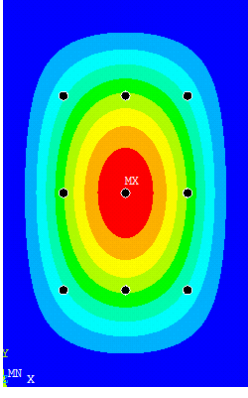
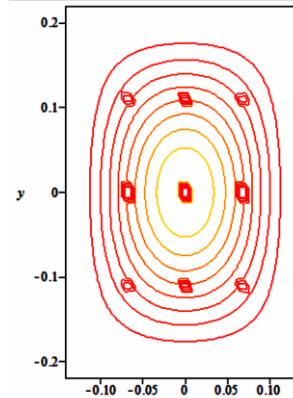
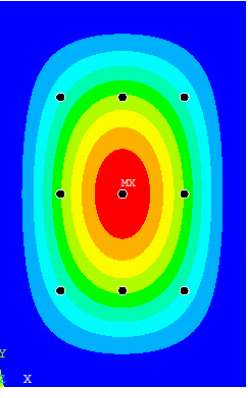
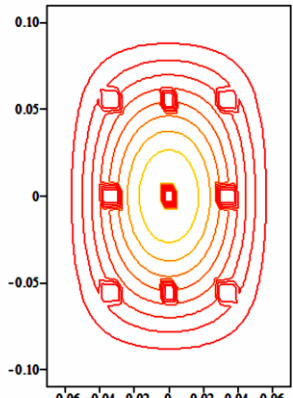
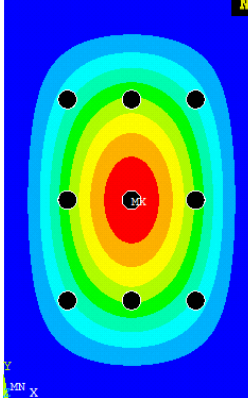
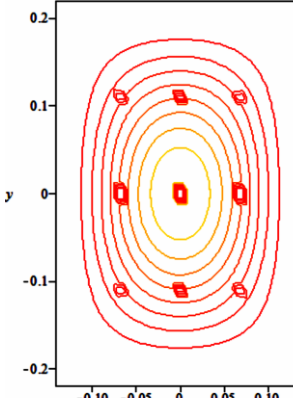
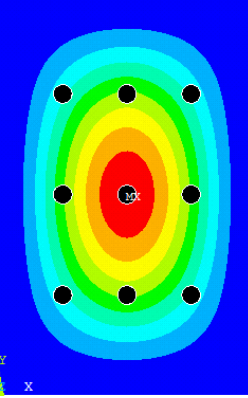
Table 8.1 Fundamental frequency results obtained by the numerical and FE simulations

Spe. No.	d_c (mm)	MRR	r_c (mm)	ω_1 , Numerical (Hz)		ω_1 , FEM (Hz)	% Error	
				2 Term $W(x, y)$	5 Term $W(x, y)$		FEM & 2 Term $W(x, y)$	FEM & 5 Term $W(x, y)$
Specimens with dimensions (138 mm x 216 mm)								
8.1	4.431	0.9940	2.5	696.790	696.688	693.38	0.391	0.377
8.2	8.862	0.9762	5	703.043	702.888	693.85	1.370	1.302
8.3	13.293	0.9466	7.5	714.042	713.744	695.97	2.701	2.553
8.4	22.155	0.8517	12.5	755.054	753.820	710.17	6.909	6.146
8.5	26.586	0.7865	15	802.215	787.522	724.94	10.354	8.632
Specimens with dimensions (276 mm x 432 mm)								
8.6	8.862	0.9940	5	174.197	174.172	173.37	0.477	0.462
8.7	17.724	0.9762	10	175.760	175.722	173.46	1.326	1.304
8.8	22.155	0.9629	12.5	176.975	176.922	173.65	1.914	1.884
8.9	44.311	0.8517	25	188.763	188.455	177.53	6.327	6.153
8.10	57.604	0.7495	32.5	203.390	202.442	183.55	10.809	10.292

8.5.1 Comparison of the Analytical and FEM Mode Shapes

Analytical modes shapes are extracted by using the five term shape function and contour plot are compared with the FEM mode shape contours plots. Table 8.2 shows the comparison of the mode shapes. It can be observed that though the analytical mode shapes are similar to the FEM, perforations are of square shape. This aspect gives slight variation and thus modes are not exactly identical. However the first mode of is same for all the cases, considered.

Table 8.2 Comparison of the analytical and FEM mode shapes

Specimen no	Mode shapes		Specimen no	Mode shapes	
	Analytical	FEM		Analytical	FEM
	Specimens with the dimensions (138 mm x 216 mm)			Specimens with the dimensions (276 mm x 432 mm)	
8.1			8.6		
8.2			8.7		

Specimen no	Mode shapes		Specimen no	Mode shapes	
	Analytical	FEM		Analytical	FEM
	Specimens with the dimensions (138 mm x 216 mm)			Specimens with the dimensions (276 mm x 432 mm)	
8.3			8.8		
8.4			8.9		

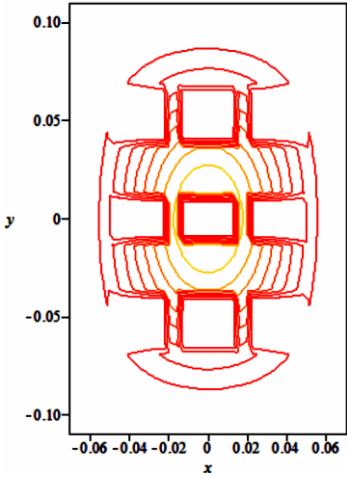
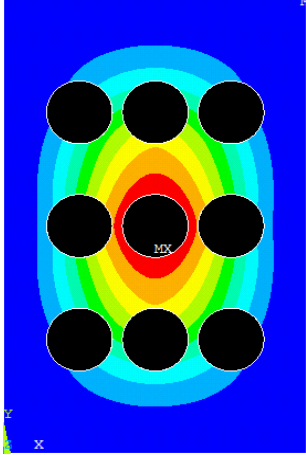
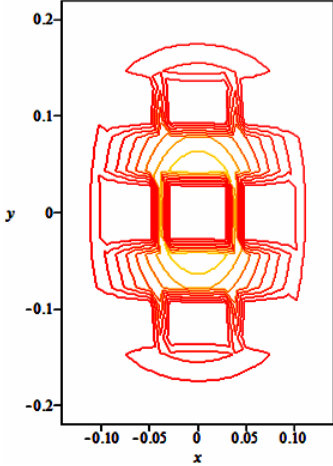
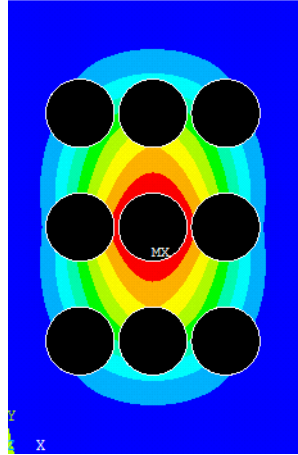
Specimen no	Mode shapes		Specimen no	Mode shapes	
	Analytical	FEM		Analytical	FEM
	Specimens with the dimensions (138 mm x 216 mm)			Specimens with the dimensions (276 mm x 432 mm)	
8.5	 <p>Analytical mode shape for specimen 8.5. The plot shows a cross-section with a central square hole and four side holes. The mode shape is represented by red contour lines. The x-axis ranges from -0.06 to 0.06, and the y-axis ranges from -0.10 to 0.10.</p>	 <p>FEM mode shape for specimen 8.5. The plot shows a cross-section with a central square hole and four side holes. The mode shape is represented by a color gradient from blue to red. The x-axis ranges from -0.06 to 0.06, and the y-axis ranges from -0.10 to 0.10.</p>	8.10	 <p>Analytical mode shape for specimen 8.10. The plot shows a cross-section with a central square hole and four side holes. The mode shape is represented by red contour lines. The x-axis ranges from -0.10 to 0.10, and the y-axis ranges from -0.2 to 0.2.</p>	 <p>FEM mode shape for specimen 8.10. The plot shows a cross-section with a central square hole and four side holes. The mode shape is represented by a color gradient from blue to red. The x-axis ranges from -0.10 to 0.10, and the y-axis ranges from -0.2 to 0.2.</p>

Table 8.3 Fundamental frequency results obtained by the numerical and experimental analysis

Specimen No.	d (mm)	(A/A_p)	ω , Numerical (Hz) ,2 Term $W(x, y)$	ω , Experimental (Hz)	% Deviation
Specimens with dimensions (138 mm x 216 mm)					
7.11/8.11	5	1518.154	696.790	650	6.71
7.12/8.12	10	379.5384	703.043	637	9.39

It is observed from the comparison of the experimental and numerical results that both results are within reasonable agreement. Maximum discrepancy of 9.39% occurs between the experimental and numerical fundamental frequency for the specimen 8.11, reasons for this discrepancy may be same as discussed in section Chapter 5, Section5.6.

8.6 Concluding Remark

In the present work an analytical model to determine the fundamental frequency of the perforated rectangular plate is formulated. The plates considered for study are having the rectangular array of the circular perforations. For modeling of the material property variation function due to the perforation, circular perforations are replaced by equivalent square perforations. With this approximation the Heaviside step functions are used to express the variation of the material properties of the perforated plate. Further analytical model to determine the fundamental frequency is formulated by using the Rayleigh's-Ritz method. The numerical analysis is carried out for the plate with all edges clamped boundary condition. From the comparison of the FEM and numerical analysis results it is found that the proposed approach can be used for the perforated plates with the MRR more than or equal to 0.852 with maximum error of 6-7% in the fundamental frequency. For the MRR greater than 0.946 present approach give results with more accuracy with maximum discrepancy of 2.7 %. Present approach can be equally applied to the perforated plates with other boundary conditions also.

Chapter 9

Determination of the Modal Constant for the Fundamental Frequency

9.1 Introduction

In this chapter, an expression for the modal constant of the fundamental frequency of the perforated plate is determined by the hybrid approach, combining the experimental and analytical methods. For calculating the modal constant the Rayleigh's formulation is used. The displacement solution is considered as a linear combination of the cosines. In the Rayleigh's formulation the fundamental frequency values are taken from the experimental analysis. This problem is solved in reverse order by considering the known experimental values of the fundamental frequency. Thus the modal constant expression for the fundamental frequency is found out. Proposed approach gives alternative method to the existing equivalent material properties approach. This modal constant can be directly used to calculate the fundamental frequency, by using the actual material properties instead of the equivalent material properties. In this work the perforation pattern considered is the rectangular with the circular perforations. The boundary condition considered is clamped-clamped. Thus proposed approach permits the ready determination of the reasonably good natural frequencies for a plate involving any combination of the ligament efficiency and the perforation diameter. To illustrate the applicability and accuracy of the approach, the Finite element method (FEM) analysis by ANSYS 11 and the experimental analysis results for the two plates within given test envelope and outside test envelope are presented.

9.2 Analytical Formulation

The fundamental frequency expression of a plate is formulated by the Rayleigh's principle as discussed in section (3.3.1). This formulation is carried out by considering the perforated plate as a solid plate with the same outer dimensions as, that of the perforated plate. Further, the Rayleigh's formulation for the fundamental frequency is modified with known value of the fundamental frequency obtained from an experimental modal analysis. Then actual geometrical parameters of the perforated plate are considered in the modified expression and rearranged to get an expression for the modal constant.

For constant thickness and the homogeneous plate, D , ρ and h are constant. Hence the Rayleigh's Quotient (Chakraverty, 2009) from equation (3.13),

$$\omega_{1s}^2 = \frac{D \int_0^a \int_0^b [(\nabla^2 W_1)^2 + 2(1-\nu)\{W_{1,xy}^2 - W_{1,xx}W_{1,yy}\}] dx dy}{h\rho \int_0^a \int_0^b W_1^2 dx dy} \quad (9.1)$$

where,

$$W_{1,xy} = \frac{\partial^2 W_1}{\partial x \partial y} \quad W_{1,xx} = \frac{\partial^2 W_1}{\partial x^2} \quad W_{1,yy} = \frac{\partial^2 W_1}{\partial y^2} \quad (9.2)$$

Equation (9.1) is called as the Rayleigh's Quotient and gives the fundamental natural frequency (ω_{1s}) of the solid plate.

From the equation (3.5) and for the orientation of the plate shown in Figure 9.1, assuming solution of the form,

$$W_1(x, y) = (A) \left[1 + \cos \frac{\pi x}{a} \right] \left[1 + \cos \frac{\pi y}{b} \right] \quad \text{Where,} \quad \left. \begin{array}{l} 0 \leq x \leq a \\ 0 \leq y \leq b \end{array} \right\} \quad (9.3)$$

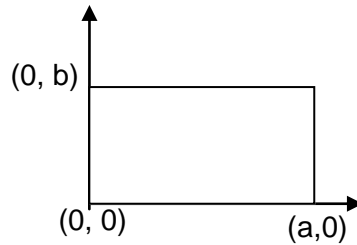


Figure 9.1 Co ordinates of the plate

9.2.1 Analytical Solution

The fundamental frequency ω_{1s} , is obtained by substituting equation (9.3) in equation (9.1) as follows

$$\omega_{1s}^2 = \frac{9D\pi^4}{h\rho a^4 b^4} \left[3(a^2 b^2) b^2 + (a^2 b^2) a^2 + 2a^2 b^2 + 2a^2 b^2 (1 - \nu^2) \right] \quad (9.4)$$

This, fundamental frequency equation is further modified by including the perforation parameters given by equation (9.11) to get the fundamental frequency (ω_{1p}) equation (9.14) for the perforated plate. The expression given by equation (9.1) is further modified by considering the geometrical parameters of the perforated plate to calculate values of the correction factor (A), from the known natural frequencies, obtained by an experimental analysis.

9.2.2 Geometry of the Perforated Plate with the Rectangular Perforation Pattern

From Figure 9.2, consider triangle ABC with area, (J)

$$J = \frac{L_h L_v}{2} - \left[\frac{\pi r^2}{4} + \frac{\pi r^2}{4} \right] = \frac{L_h L_v}{2} - \left[\frac{2\pi r^2}{4} \right] \quad (9.5)$$

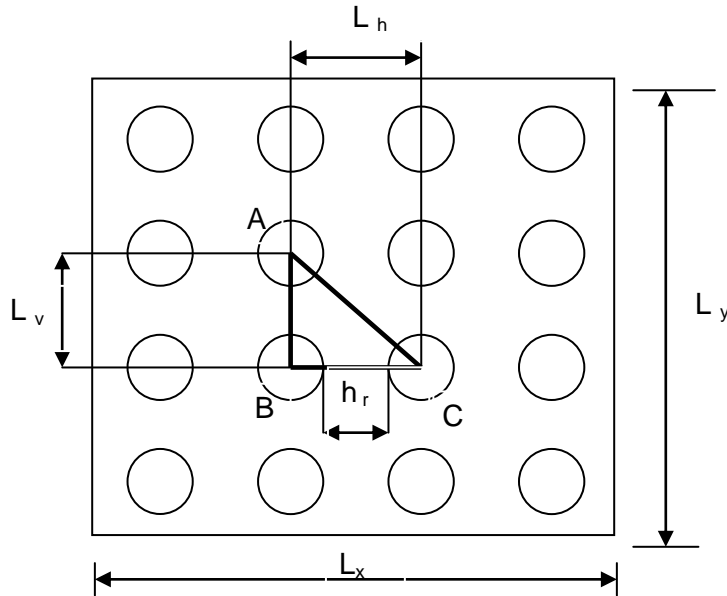


Figure 9.2 Geometry of the perforated plate

No. of triangular elements, N

$$N = 2 \left[\frac{L_x L_y}{L_h L_v} \right] \quad (9.6)$$

Total area of perforated plate, $K = J \times N$

$$K = L_x L_y - \frac{L_x L_y \pi r^2}{L_h L_v} \quad (9.7)$$

The Mass remnant ratio (*MRR*) is defined as ratio of the perforated plate area to the area of the full solid plate of the same outer dimensions. It can be expressed as,

$$MRR = K / (L_x L_y) \quad (9.8)$$

where ($L_x L_y$) is area of the full solid plate

$$MRR = 1 - \frac{\pi r^2}{L_h L_v} \quad (9.9)$$

$$MRR = \frac{ab}{ab} - \frac{ab \pi r^2}{ab L_h L_v} = 1 - \frac{ab \pi r^2}{ab L_h L_v} \quad (9.10)$$

Thus relation between the perforation parameters *MRR*, L_h , L_v , r and the plate dimensions a , b is

$$ab = \frac{(1 - MRR) L_h L_v ab}{\pi r^2} \quad (9.11)$$

The relation between the ligament efficiency, the pitch and the ligament width is:

$$\eta_l = \frac{(h_r)}{(d + h_r)} \quad (9.12)$$

$$\text{For case under study } L_h = L_v = (d + h_r) \quad (9.13)$$

9.3 Materials and methods

The fundamental frequency is obtained experimentally and by the FEM, for the four specimens with the configurations shown in Table 9.1. The Effective dimensions of the perforated area for all the specimens are 216 mm X 138 mm and the thickness of the plates is 2 mm. All the specimens are analyzed for the boundary condition clamped on all four edges. The correction factor is determined from equation (9.15) for each specimen from the values of the fundamental frequencies obtained from an experimental analysis.

Table 9.1 Details of the specimens analyzed

Specimen No.	η_l	Pitch ($d + h_r$), (mm)	h_r , (mm)	<i>MRR</i>
For $d = 6$ mm hole				
9.1	0.2	7.5	1.5	0.4973
9.2	0.6	15	9	0.874
For $d = 9$ mm hole				
9.3	0.4	15	6	0.7172
For $d = 12$ mm hole				
9.4	0.6	30	18	0.8743

9.3.1 Experimental Analysis

The clamping details and the experimental set up used in the experimental vibration analysis is same as discussed in section (4.3) and (4.5). The specimens are prepared for the ligament efficiency 0.2, 0.4 and 0.6 and the perforation diameters 6 mm, 9mm and 12 mm. Each specimen is tested ten times and average value of the fundamental frequency is obtained. Experimentation is carried out as per the procedure given in section (4.4). The outer dimensions of all the specimens are 255 mm X 213 mm X 2 mm, but the effective dimensions of the perforated area are 216 mm X 138 mm. All the specimens are of mild steel material with the aspect ratio $b/a = 1.565$. The material properties considered for all the specimens are same as given in Table 4.1. (i. e. $E = 2.1 \times 10^{11}$ N/m², $\nu = 0.3$, $\rho = 7850$ kg/m³).

9.3.2 FE Analysis

The experimental results are validated by comparing them with the FEM results. To determine the fundamental frequency of the specimens with configurations given in Table 9.1, modal analysis is carried out by using Shell63 element. The converged solution is given in Table 9.3. Details of the convergence are summarized in Table B.7, given in Appendix “B”. It is assumed that the structure is formed of an isotropic homogeneous elastic material, i.e. Mild

Steel. The material properties for all the specimen plates analyzed are same as given in Table 4.1.

9.4 Results and Discussion

Results obtained from the experimental runs conducted for the each specimen are tabulated in Table 9.2. The fourth column of the Table 9.2 shows mean values of the fundamental frequency for the respective specimen. The FE results and the experimental results are compared in Table 9.2. The FE results obtained for the fundamental frequency exceeds the experimental results, except for the first specimen. Maximum discrepancy is of 8% in the FEM and the experimental results.

An average value of the experimental fundamental frequency of the each specimen from Table 9.2 is used to calculate, the value of the correction factor (A) for the respective specimen.

Table 9.2 Natural frequencies of the fundamental mode by the FE and experimental analysis

Specimen No.	η_i	d , mm	Fundamental frequency ω_{1P} (Hz)		% Deviation
			FEM	Experimental	
9.1	0.2	6	546.52	590.7	8.083
9.2	0.6	6	650.33	616.2	5.248
9.3	0.4	9	612.65	571	6.798
9.4	0.6	12	637.9	587.6	7.885

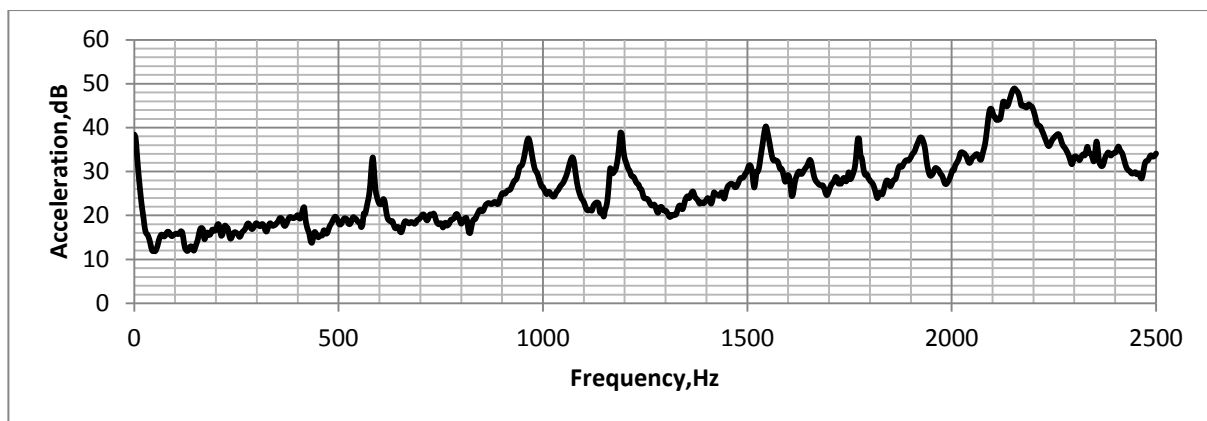


Figure 9.3 Sample frequency response function (FRF) obtained for the Specimen No. 9.1

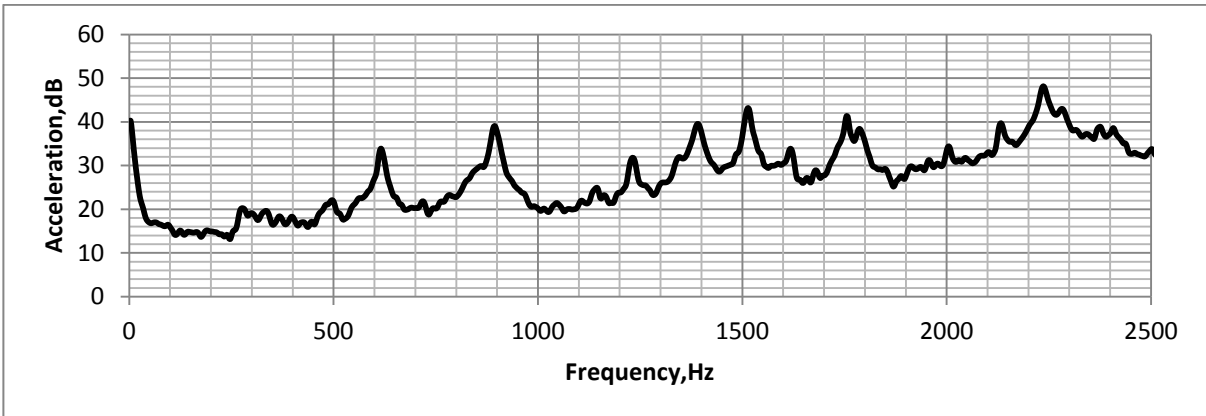


Figure 9.4 Sample frequency response function (FRF) obtained for the Specimen No. 9.2

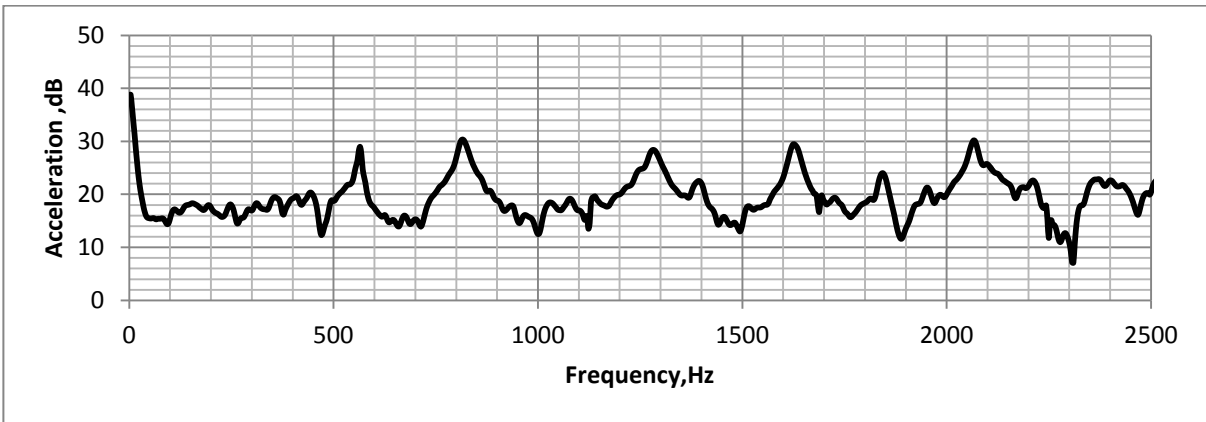


Figure 9.5 Sample frequency response function (FRF) obtained for the Specimen No. 9.3

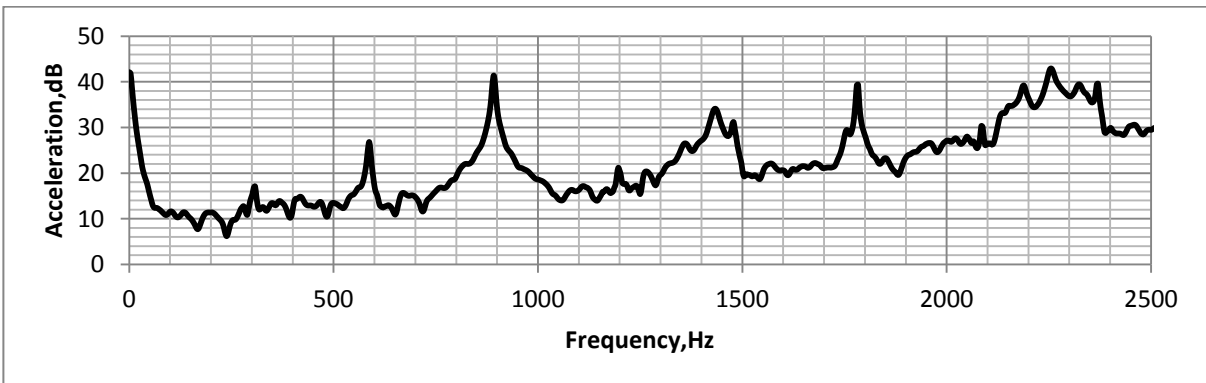


Figure 9.6 Sample frequency response function (FRF) obtained for the Specimen No. 9.4

9.4.1 Determination of the Modal Constant

The expression for the fundamental natural frequency of the solid plate given by equation (9.4) can be modified by considering the actual geometrical parameters of the perforated plate. The geometrical parameters of the perforated plate are related to the full solid plate dimensions by relation given in equation (9.11).

$$\omega_{1p}^2 = \frac{9D\pi^4}{h\rho \left[\frac{(1-MRR)L_h L_v ab}{\pi r^2} \right]^4} \left[3 \left[\frac{(1-MRR)L_h L_v ab}{\pi r^2} \right]^2 b^2 + \left[\frac{(1-MRR)L_h L_v ab}{\pi r^2} \right]^2 a^2 + 2 \left[\frac{(1-MRR)L_h L_v ab}{\pi r^2} \right]^2 (1-\nu^2) \right] \quad (9.14)$$

An expression in equation (9.14) can not be used directly to calculate the fundamental frequency of the perforated plate unless the correction factor is considered.

After simplification and considering the correction factor equation (9.14) becomes as follows

$$\omega_{1p}^2 = \frac{9D\pi^6 r^4}{h\rho \left[(1-MRR)L_h L_v ab \right]^2} \left[3b^2 + a^2 + 2 + 2(1-\nu^2) \right] (A) \quad (9.15)$$

Where, 'A' introduced as the correction factor. Values of the correction factor are calculated from equation (9.15), by using the fundamental frequencies determined experimentally, tabulated in Table 9.2. The correction factor values are tabulated in Table 9.3 for the different specimens. Equation (9.15) can be used for calculating the *fundamental frequency of the perforated plate* by substituting average value of the correction factor 'A', from Table 9.3.

Table 9.3 Values of the correction factor for the different specimens

Sr. no.	η_l	d, mm	MRR	L_h , mm	L_v , mm	ω_{IP} Expeiment	$\omega_{IP FEM}$	Value of 'A' 'Experimental'
1	0.2	6	0.4973	7.5	7.5	590.7	546.52	0.009099
2	0.6	6	0.8743	15	15	616.2	650.33	0.009906
3	0.4	9	0.7172	15	15	571	612.65	0.008504
4	0.6	12	0.8743	30	30	587.6	637.9	0.009007
Average Value of 'A' =								0.009129

A simple approximate formula for the fundamental natural frequency of the flexural vibration of the rectangular isotropic perforated plate is given as

$$\omega_{1p} \approx \sqrt{\frac{\lambda_{1p} D}{h \rho}} \quad (9.16)$$

where, λ_{1p} is called as the modal constant.

Thus modal constant λ_{1p} for the fundamental frequency is obtained from equation (9.15) & (9.16)

$$\lambda_{1p} = \left[\frac{9\pi^6 r^4}{[(1-MRR)L_n L_v ab]^2} [3b^2 + a^2 + 2 + 2(1-\nu^2)] (A) \right] \quad (9.17)$$

The modal constant (λ_{1p}) expression by considering an experimentally obtained value of the correction factor 'A' becomes as follows

$$\text{or } \lambda_{1Exp} = \left[\frac{9\pi^6 r^4}{[(1-MRR)L_n L_v ab]^2} [3b^2 + a^2 + 2 + 2(1-\nu^2)] (0.009129) \right] \quad (9.18)$$

An expression given by equation (9.18) can be used to calculate the modal constant λ_{1p} for the fundamental natural frequency of the perforated plates with the rectangular perforation patterns of the circular perforations, having different configurations.

9.5 Application and Accuracy of the Approach

The proposed approach is validated by additional experimental analysis and running the FEM simulations with ANSYS11. Configuration of the specimens is given in Table 9.4. The criteria's followed to select the plate dimensions in the analysis are

- 1) Validating the results of the proposed approach within the test envelope, i.e. the effective outer dimensions (a, b) same as the specimens given in Table 9.1.
- 2) Validating the results of the proposed approach outside the test envelope i.e. the effective outer dimensions, (a, b) different from the specimens given in Table 9.1.

The FEM analysis is carried out by using shell63 element for both the specimens. It is assumed that, the structure is formed of an isotropic homogeneous elastic material, i.e. mild

steel. The effective outside dimensions, thickness and the material properties of the first specimen analyzed are same as that used in the test envelope and within the fixture limit but configuration is different from the test envelope. However for the second specimen thickness and the material properties are same as that used in the test envelope but the effective outside dimensions (a , b) and the configuration is different from the test envelope.

Table 9.4 Comparison of the results obtained by the proposed approach with the experimental and FE simulation results

a , mm	b , mm	d , mm	η_l	$L_h = L_v$, mm	MRR	ω_{1P} With modal Constant(λ_{1Exp}), Hz	ω_{1P} From FEM Simulation, Hz	% Deviation
138	216	12	0.2	15	0.4973	590.82	563	4.94
550	860	50	0.6	125	0.87433	47.07	42	11.9

From comparison it is found that the results obtained for the first specimen from present the approach (9.18), vary from the FEM simulation results by 4.94% and for the second specimen by 11.9% respectively.

Thus results obtained from the proposed experimental modal constant (λ_{1Exp}) method are reasonably in good agreement with the FEM simulation results within the test envelope.

9.6 Concluding Remark

In the present work, an expression for the modal constant for the fundamental frequency of the perforated plate is determined. To establish this modal constant, experimental vibration data is used. A simple approximate formula for the fundamental natural frequency of the flexural vibration of the rectangular isotropic perforated plate is developed. The Rayleigh's method is used in combination with the experimental values of the natural frequency to establish the expression for the modal constant. The fundamental frequency calculated by using the proposed experimental modal constant (λ_{1Exp}) is in reasonably good agreement with the ANSYS result within the test envelope. Thus this approach provides alternative method to the equivalent elastic properties method of the perforated plate for finding the natural frequency.

Chapter 10

Plates with the Circular Perforations in the Rectangular Array

10.1 Introduction

In this chapter a rectangular plate with nine perforations is considered. All the perforations are circular with the same size arranged in the rectangular array. The material property distribution function $F(x, y)$ constructed by using the Heaviside function to map circular areas. The Rayleigh Ritz method is used to formulate an analytical model to obtain the fundamental frequencies. The shape function used is a polynomial. The numerical simulation is carried out for the eight specimens with different sizes of the uniform perforations. Two sets of the fundamental frequency results are obtained from the numerical simulation one for the single term shape function and other for the five terms of the shape function. Finally results are compared with those obtained from the FEM analysis.

10.2 Analytical formulation

A rectangular plate with coordinate system $(O; x, y, z)$, having the origin O at the center is considered as shown in Figure.10.1 which is similar to Figure.7.2 of the thesis. The displacement of an arbitrary point of coordinates (x, y) on the middle surface of the plate is denoted by w , in out-of-plane (z) direction. The boundary conditions considered here, are all edges clamped. The geometric parameters, the hole radius r is uniform for all the perforations. The assumptions made in the following formulation are that transverse deflections are small so that the dynamic behavior of the plate is governed by the classical thin plate theory. An analytical model in the present work does not consider any rotary inertia of the plate. The model is applicable to the rectangular perforated plates with the different side dimensions and having the circular perforation and, provided that all the perforations are of the same size.

The function $F(x, y)$ represents the variation of the density and modulus of elasticity due to the perforations. For the function $F(x, y)$ to represent these parameters it must satisfy the following requirements as given by equation (5.7).

$$\begin{aligned} F(x, y) &= 0 \text{ in the region corresponding to a perforation} \\ F(x, y) &= 1 \text{ otherwise} \end{aligned} \tag{10.1}$$

$$\begin{aligned}\rho &= \rho_0 F(x, y) \\ E &= E_0 F(x, y)\end{aligned}\tag{10.2}$$

Above equation is same as equation (5.5) of the thesis. Where ρ_0 and E_0 are the density and the Young's modulus of the homogeneous plate

The function $F(x, y)$ is constructed by using the Heaviside functions.

$$F(x, y) = f_j(x, y) - \left(\sum_{i=1}^9 f_i(x, y) \right)\tag{10.3}$$

Functions $f_i(x, y)$ and $f_j(x, y)$ are as follows,

$$f_i(x, y) = \text{Heaviside}\left(r^2 - (x - x_i)^2 - (y - y_i)^2\right)\tag{10.4}$$

Where x_i and y_i are the co-ordinates of the centre of i^{th} circular hole.

$$f_j(x, y) = \text{Heaviside}\left(\left(x + \left(\frac{a}{2}\right)\right)\left(x - \left(\frac{a}{2}\right)\right)\left(y + \left(\frac{b}{2}\right)\right)\left(y - \left(\frac{b}{2}\right)\right)\right)\tag{10.5}$$

The density plot of the function $F(x, y)$ for the plate specimen with dimensions 138 mm \times 216 mm and the perforation diameter 25 mm is shown in Figure10.2.

To determine the fundamental frequency the Rayleigh's-Ritz method discussed in section (3.3.2) of the thesis is used. The Rayleigh's-Ritz method is based on the maximum Kinetic energy and maximum Strain energy of the plate. $F(x, y)$ obtained in by equation (10.3) is used to obtain the energy expressions given as given by equations (8.10) and (8.11) where integral limits are from $x = -a/2, x = a/2$, and $y = -b/2, y = b/2$.

The middle surface displacement W in above expressions is approximated by using the shape function $W(x, y)$ in the form of a series given by equation (10.6) , which satisfy the clamped boundary conditions on the edges $x = -a/2, x = a/2$, and $y = -b/2, y = b/2$.

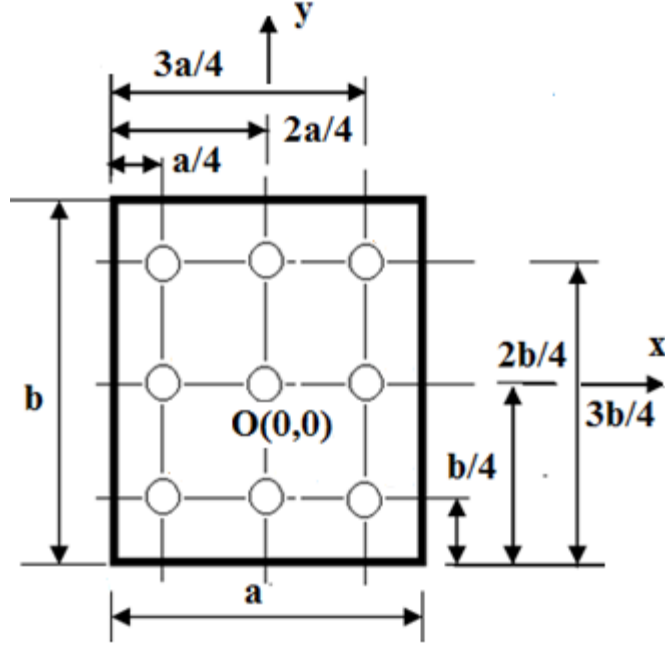


Figure 10.1 Co-ordinates of the plate clamped on all edges carrying circular holes

For clamped all edges the five term of deflection function W , is considered as (Laura, and Saffell, 2005),

$$W(x, y) = C_1 \left(x^2 - \left(\frac{a}{2} \right)^2 \right)^2 \left(y^2 - \left(\frac{b}{2} \right)^2 \right)^2 + C_2 \left(x^4 - \left(\frac{a}{2} \right)^4 \right)^2 \left(y^4 - \left(\frac{b}{2} \right)^4 \right)^2 + C_3 \left(x^6 - \left(\frac{a}{2} \right)^6 \right)^2 \left(y^6 - \left(\frac{b}{2} \right)^6 \right)^2 + C_4 \left(x^8 - \left(\frac{a}{2} \right)^8 \right)^2 \left(y^8 - \left(\frac{b}{2} \right)^8 \right)^2 + C_5 \left(x^{10} - \left(\frac{a}{2} \right)^{10} \right)^2 \left(y^{10} - \left(\frac{b}{2} \right)^{10} \right)^2 \quad (10.6)$$

To use the Rayleighs-Ritz method u_{\max} and T_{\max} expressions are formulated in terms of C_i and ϕ_i , and then the frequency is minimized with respect to C_i . Thus C_i are determined so as to obtain the best upper bounds for the fundamental frequency. The frequency minimizing equations are from equations (8.17) and (8.18),

$$\frac{\partial(\omega^2)}{\partial C_i} = 0, (i = 1, 2..5) \quad (10.7)$$

Substituting (10.7) into (10.8), set of minimizing equations can be obtained.

$$\frac{\partial}{\partial C_i} (u_{\max} - \omega^2 T_{\max}^*) = 0, (i = 1, 2..5) \quad (10.8)$$

This is a set of 5 simultaneous, linear, algebraic equations in the unknown C_1, C_2, C_3, C_4 , and C_5 . For a nontrivial solution, the determinant of the coefficient matrix is set equal to zero.

The roots of the determinant are the values of ω^2 . The lowest value of ω is approximation to the fundamental frequency.

10.3 Numerical Analysis and Validation

All the plate specimens analyzed numerically have thickness of 2 mm. Ten specimens with the different sizes of uniform perforations arranged in the rectangular array are considered for the numerical simulation. Two sets of the plates are analyzed; first set of the plates is having outer effective dimensions as 138 mm x 216 mm and second set of the plates is having outer effective dimensions as 276 mm x 432 mm. The diameter of the perforation in first set varies over the range 5 mm to 30 mm where as in second set it varies over the range 10 mm to 65 mm. The material properties considered for all the specimen plates analyzed numerically are $E_o = 2.1 \times 10^{11}$ N/ m², $\nu_o = 0.3$, $\rho_o = 7850$ kg/ m³.

Validation of the results is done by comparing the FEM Modal analysis (Using ANSYS, Shell 63 element) results which are given in Table 10.1. The parameters of the plate specimen considered in this study are shown in Table 10.1.

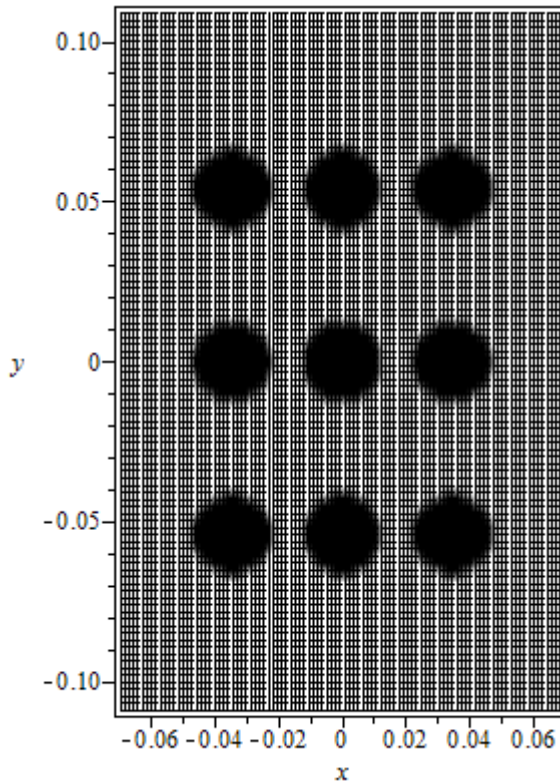


Figure 10.2 Density plot of the function $F(x, y)$ for the specimen size 138 mm \times 216 mm and $d = 25$ mm

10.4 Results and Discussion

The numerical analysis and FEM analysis results are compared in Table 10.1. The numerical analysis results are obtained by considering the one term and five term approximation of the shape function given by equation (10.6). The agreement between the numerical and FEM results is reasonably good, differences are mainly due to the use of the approximate methods and limitations of the Heaviside function used. The procedure developed in this approach is straightforward and allows for immediate solution. We found computation time is exceptionally good. The function $f_j(x, y)$ can be slightly extended beyond the actual domain, which will not change the maximum potential and kinetic energy as integrals will be calculated over the actual domain i.e. $x \in \{-a/2, a/2\}$ and $y \in \{-b/2, b/2\}$. This helps greatly in reducing computation time.

Table 10.1 Numerical and FEM analysis results

Specimen No.	r (mm)	$\omega_{1One\ term}$, Numerical (Hz) One term shape function	$\omega_{1Five\ term}$, Numerical (Hz) Five term shape function	ω_1 , FEM (Hz)	% Error ω_1 , FEM and $\omega_{1One\ term}$	% Error ω_1 , FEM and $\omega_{1Five\ term}$
Specimens with dimensions (138 mm x 216 mm)						
10.1	2.5	695.726	695.490	693.38	0.338	0.304
10.2	5	696.617	696.356	693.85	0.398	0.361
10.3	7.5	697.560	697.271	695.97	0.228	0.186
10.4	12.5	699.617	699.259	710.17	-1.485	-1.536
10.5	15	700.739	700.339	724.94	-3.338	-3.393
Specimens with dimensions (276 mm x 432 mm)						
10.6	5	173.931	173.872	173.37	0.323	0.289
10.7	10	174.154	174.089	173.46	0.400	0.362
10.8	12.5	174.270	174.201	173.65	0.357	0.317
10.9	25	174.904	174.814	177.53	-1.479	-1.529
10.10	32.5	175.331	175.225	183.55	-4.477	-4.535

The expression obtained for the material property variation function can be extended to the plates with similar geometry and the different outer dimensions. Table 10.1 shows that with this approach for MRR more than 0.851 error is less than 1.5%. It can be concluded from above results that by using the proposed approach one may get maximum error of -4.477% where the hole size is significantly large compared to the plate size i.e. ratio of the plate area to the perforation hole area is 35.932. This approach offers solution to the vibration problems for a wide spectrum of the perforated plates as the plates with the non-uniform diameter perforations can also be modeled.

10.4.1 Comparison of the Analytical and FEM Mode Shapes

Contour plots of the mode shapes obtained from the analytical method and FEM are compared in Table 10.2. Analytical mode shapes are obtained by considering the five term shape function as given by equation (10.6). It is observed that displacement pattern of the analytical mode shapes is in close agreement with that of the FEM.

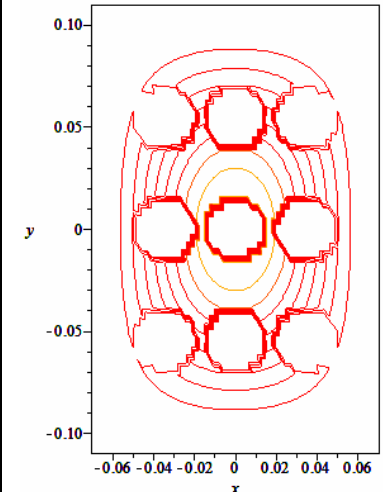
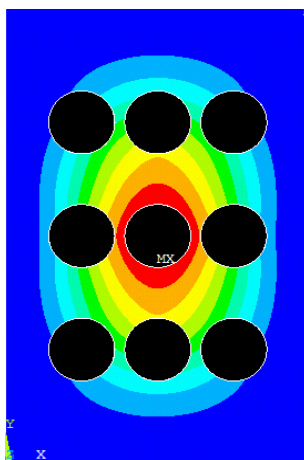
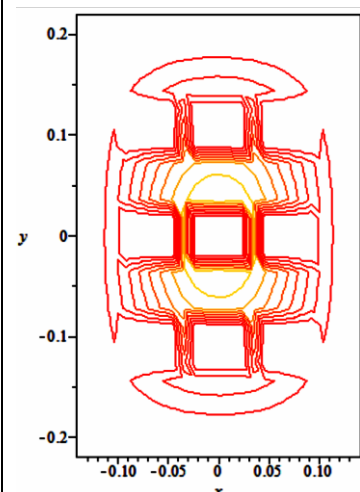
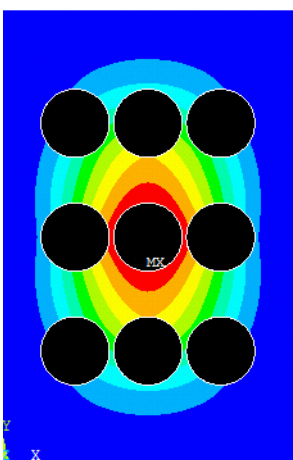
10.5 Concluding Remark

The approach in this chapter presents how the array of circular multi-perforations in a plate structure can be modeled in the vibration problems of a plate structure. It has provided a simple single expression for the exact bidirectional material property variation given by an equation 10.3. Further this model can easily handle the variation in the size of the perforations. This approach gives results with discrepancy less than 1.5% for MRR more than 0.851. Maximum error of -4.477% obtained for the specimen having ratio of the plate area to the perforation hole area equal to 35.932.

Table 10.2 Analytical and FEM mode shapes

Specimen no	Mode shapes		Specimen no	Mode shapes	
	Analytical	FEM		Analytical	FEM
	Specimens with the dimensions (138 mm x 216 mm)			Specimens with the dimensions (276 mm x 432 mm)	
10.1			10.6		
10.2			10.7		

Specimen no	Mode shapes		Specimen no	Mode shapes	
	Analytical	FEM		Analytical	FEM
	Specimens with the dimensions (138 mm x 216 mm)			Specimens with the dimensions (276 mm x 432 mm)	
10.3			10.8		
10.4			10.9		

Specimen no	Mode shapes		Specimen no	Mode shapes	
	Analytical	FEM		Analytical	FEM
	Specimens with the dimensions (138 mm x 216 mm)			Specimens with the dimensions (276 mm x 432 mm)	
10.5			10.10		

Section Three

Analytical Models to Determine the Fundamental Frequency of the Moderately thick Plates with the Circular Perforation (Chapter 11)

Chapter 11

Vibration Analysis of the Mindlin Perforated Plates

11.1 Introduction

This chapter presents extension of the approach presented in chapter 5 to the Mindlin plates. Work in this chapter presents the numerical calculations of the natural frequencies for elastic perforated rectangular plates with variable width to thickness ratios. The boundary conditions considered is all edges clamped condition. The material property variation in two directions of the plate due to the perforations is taken in same form by superposition as given in the chapter 5 Equation (5.14). The first-order shear deformation plate theory of the Mindlin has been applied to the plate analysis. The solution is obtained by the Rayleigh Ritz method. Free vibrations of the rectangular thick plates are analyzed by varying the width to thickness ratio. The numerical examples demonstrate the applicability of the present method. The results obtained by both the classical thin plate (CPT) and Mindlin (MPT) plate theories are compared with those obtained by the FEM analysis.

11.2 Theoretical formulation for the Mindlin Plate

Consider an isotropic, elastic, perforated rectangular plate of length a , width b , modulus of elasticity E , Poisson's ratio ν and the shear modulus $G = E[2(1+\nu)]$. The plate is of constant thicknesses in the z -direction, with the thickness h (see Figure 10.1). The edges of the plate are assumed to be clamped. The origin of the coordinate system is set at the centre plate as shown in Figure 11.1. The problem at hand is to determine the fundamental frequency of vibration for such a rectangular plate. In present analysis, the square plate with the square perforations is considered, same as shown in Figure 5.1. The ligament efficiency η_l , considered for the perforation is, $(p / (d + p)) = 0.5$, where p is the ligament length (p_x or p_y) and d is the side length of the square perforation. The natural frequencies of the plates are determined via the Ritz method using the Mindlin plate theory. The effects of the rotary inertia, and the transverse shear deformations, which cannot be considered in the Kirchhoff theory, become significant in thick plates. The simplest one is the first-order shear deformation plate theory (FSDT) that is famous as the Mindlin theory (MPT). (Mindlin, 1951; Shufrin, Eisenberger, 2006). This approach extends the kinematic assumptions of the CPT by releasing the restriction on the angle of the shearing deformations (J.N. Reddy, 1999;

C.M. Wang et. al., 2000). In the Mindlin plate theory, it is assumed that a plane originally normal to the plate middle surface remains straight but not generally normal to the middle surface after deformation, and hence a shear correction factor is introduced. Thus the Mindlin plate theory is suitable for the moderately thick plates. The three fundamental, independent quantities involved in MPT are the transverse deflection W and the two cross-sectional rotations ψ_x and ψ_y . (Liew, Hung and Lim, 1995). Maximum strain energy U_{max} and the maximum kinetic energy T_{max} for the Mindlin Plate are given as (Karunasena, Kitipornchai and Al-Bermani, 1996; Liew, Wang, Xiang and Kitipornchai, 1998)

$$U_{max} = \frac{1}{2} \iint_A \left\{ D \left[\left(\frac{\partial \psi_x}{\partial x} + \frac{\partial \psi_y}{\partial y} \right)^2 - 2(1-\nu) \left[\frac{\partial \psi_x}{\partial x} \frac{\partial \psi_y}{\partial y} - \frac{1}{4} \left(\frac{\partial \psi_x}{\partial y} + \frac{\partial \psi_y}{\partial x} \right)^2 \right] \right] + \kappa^2 Gh \left[\left(\psi_x + \frac{\partial w}{\partial x} \right)^2 + \left(\psi_y + \frac{\partial w}{\partial y} \right)^2 \right] \right\} dx dy \quad (11.1)$$

$$T_{max} = \frac{1}{2} \iint_A \rho h \omega^2 \left[W^2 + \frac{h^2}{12} (\psi_x^2 + \psi_y^2) \right] dx dy \quad (11.2)$$

Where, A = Area of the plate; $W(x,y)$ = Transverse deflection; ψ_x = Rotation about the y-axis; ψ_y = Rotation about the x-axis; ω = Angular frequency; ρ = Plate density per unit volume; D = Flexural rigidity of the plate = $Eh^3/[12(1 - \nu^2)]$; κ^2 is the shear correction factor. The transverse shear stresses are assumed as constant through the plate thickness in FSDT. Due to the fact that the transverse shear stresses are parabolic through the plate thickness (Wang, Reddy, Lee, 2000) shear correction factor is introduced to modify the transverse shear stresses. Mindlin (1951) pointed out that for an isotropic plate, the shear correction factor (κ^2) depends on the Poisson ratio ν and it may vary from $\kappa^2 = 0.76$ for $\nu = 0$ to $\kappa^2 = 0.91$ for $\nu = 0.5$. Shear corrections factor considered here is to be $\kappa^2 = 5/6 = 0.833$ which is commonly used for $\nu = 0.3$ (Wei, and Xiang, 2005; Zhou and Xiang, 2011).

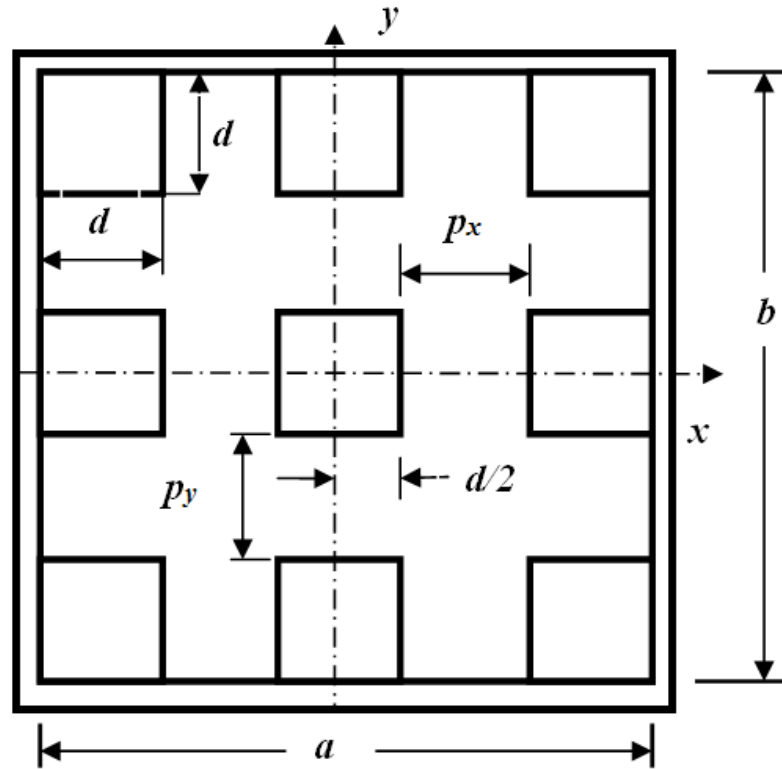


Figure 11.1 Geometry and the coordinate system of the perforated rectangular plate

11.3 Formulation for the material properties of the perforated Mindlin plate

If the function $F(x, y)$ represents the variation of the material properties along the surface, then the density and modulus of elasticity can be expressed as given by equation (5.5)

$$\rho = \rho_0 F(x, y) \tag{11.3}$$

$$E = E_0 F(x, y)$$

where, E_0 and ρ_0 are the modulus of elasticity and the density for a homogeneous plate.

The function $F(x, y)$ for the square perforation pattern can be obtained by the relation given by equation (5.14)

$$F(x, y) = f(x) + g(y) - f(x).g(y) \tag{11.4}$$

The functions $f(x)$ and $g(y)$ represent variation of the density and modulus of elasticity along x and y axes respectively. Equations (5.9) and (5.10) shows the rectangular Heaviside

function used to express the non homogeneity in the Young's modulus and density of the plate due to the perforations.

In present analytical model, the square plate having the square perforation is considered as shown in Figure 11.1. For the plate with $\eta_l = 0.5$, $p_x = p_y = d$ the above expressions for $f(x)$ and $g(y)$ becomes as given by equation (5.11) and (5.12):

$$f(x) = H(x - \frac{d}{2}) - H(x - \frac{3d}{2}) + H(x - \frac{5d}{2}) + ((H(-x - \frac{d}{2}) - H(-x - \frac{3d}{2}) + H(-x - \frac{5d}{2})) \quad (11.5)$$

$$g(y) = H(y - \frac{d}{2}) - H(y - \frac{3d}{2}) + H(y - \frac{5d}{2}) + ((H(-y - \frac{d}{2}) - H(-y - \frac{3d}{2}) + H(-y - \frac{5d}{2})) \quad (11.6)$$

11.4 Determination of the fundamental frequency of the perforated Mindlin plate

The Rayleigh-Ritz approximate procedure is employed to obtain the fundamental frequency of the Mindlin plates. The energy functional Π can be written in terms of strain energy and the kinetic energy of vibration as follow

$$\Pi = U_{\max} - T_{\max} \quad (11.7)$$

In the Ritz method, the displacement function, $\mathfrak{R}(x, y)$ is approximated by a finite linear combination of the trial functions in the form (Liew et al., 1998)

$$\mathfrak{R}(x, y) \approx \sum_{i=1}^m c_i \phi_i(x, y) \quad (11.8)$$

Where $\phi_i(x, y)$ are the approximate functions, which individually satisfy at least the geometric boundary conditions. By minimizing the energy functional Π with respect to each of the unknown coefficients c_i , a set of homogeneous equations is obtained as follows.

$$\frac{\partial \Pi}{\partial c_i} = 0; i = 1, 2, 3, \dots, m \quad (11.9)$$

The problem is reduced to the following eigenvalue and eigenvector problem:

$$([K] - \lambda^2 [M])\{c\} = 0 \quad (11.10)$$

Where $[K]$ is the stiffness matrix and $[M]$ is the mass matrix given as

$$[K] = \frac{\partial U}{\partial c_i}; [M] = \frac{\partial T}{\partial c_i} \quad (11.11)$$

The geometrical boundary conditions for clamped edges of the rectangular Mindlin plate can be expressed as (Liew et al., 1998)

$$\psi_x = 0, \psi_y = 0, W = 0 \quad (11.12)$$

The adopted admissible functions which satisfy above geometric boundary conditions for the deflection and rotations of the plate are given by equations (11.13) to (11.15)

The polynomial shape function $W(x, y)$ for a rectangular plate with 3 terms is of the form (Laura, and Saffell, 2005)

$$W(x, y) = \sum_1^{n=3} c_i \left[x^{2n} - (a/2)^{2n} \right]^2 \left[y^{2n} - (b/2)^{2n} \right]^2 \quad (11.13)$$

The one term trigonometric admissible functions for ψ_x and ψ_y that satisfies the required boundary conditions are taken as (Meera Saheb and Shasikanth, 2014),

$$\psi_x(x, y) = d_i \left[\sin \left(\frac{2\pi(x-(a/2))}{a} \right) \right] \left[1 - \cos \left(\frac{2\pi(y-(b/2))}{b} \right) \right] \quad (11.14)$$

$$\psi_y(x, y) = e_i \left[\sin \left(\frac{2\pi(y-(b/2))}{b} \right) \right] \left[1 - \cos \left(\frac{2\pi(x-(a/2))}{a} \right) \right] \quad (11.15)$$

Substituting equations (11.13) to (11.15) into equations (11.1) and (11.2) and then minimizing the energy functional Π with respect to the unknown coefficients leads to

$$([K] - \lambda^2 [M]) \begin{Bmatrix} \{c\} \\ \{d\} \\ \{e\} \end{Bmatrix} = 0 \quad (11.16)$$

Thus the fundamental circular frequency ω of the Mindlin plate is obtained by solving the generalized eigenvalue problem defined by equation (11.16).

11.5 Numerical Analysis

An analytical model developed in section 11.2 to 11.4 is applicable to the Mindlin rectangular perforated plates with the different side dimensions and having the rectangular/square perforation and, provided that the perforation pattern is rectangular or square and all the perforations are of the same size. By virtue of the symbolic forms presented in this work, the method can be applied to the analytical studies of the Mindlin perforated plates with the different boundary conditions. The numerical results for the fundamental frequency have been computed for the specimen with side dimension 500 mm x 500 mm and the perforation size 100 mm x 100 mm by varying the thickness of the specimen. Total 21 specimens are analyzed having the side length to thickness ratio (a/h) range from 5 to 250. The material properties considered for all the specimen plates analyzed are same as given in Table 4.1. (i. e. $E_o = 2.1 \times 10^{11}$ N/ m², $\nu_o = 0.3$, $\rho_o = 7850$ kg/ m³). Table 11.1. shows the geometrical parameters of the plate specimen considered in this study.

11.6 Results and Discussion

Results obtained from the numerical analysis for the different specimens with clamped all edges boundary conditions are given in Table 11.1. Results obtained from the MPT are compared with those obtained from the CPT and FEM. In Table 11.1 results are listed as ratio of the fundamental frequency obtained numerically to the fundamental frequency obtained by the FEM and last column gives ratio of the MPT and CPT results. Results obtained from the CPT are by using the Rayleigh Ritz method with same the shape function $W(x, y)$ as given by equation (11.13) but with the number of terms (n) equal to 5. Results from the FEM analysis are obtained with Shell 63 element by running ANSYS simulations. For all the specimens analyzed number of elements and nodes used for the converged solution are 48368 and 49264. The fundamental frequency results obtained by the MPT, CPT and FEM are plotted and are shown in Figure 11.2 for all the specimens.

From the result Table 11.1 and Figure 11.2 it is observed that discrepancy in the results obtained by the MPT and FEM exceeds 21% as the a/h ratio increases more than 33.333 i.e. for the plate thickness less than 0.015 m. Hence results are plotted for the a/h ratio from 5 to 33.333 and are shown in Figure 10.3. Further it is observed that the error between the CPT and FEM results remains constant for all the specimens and it is 6.92 % it can be observed from Figure 10.3 curves for the CPT and FEM results are similar with constant gap.

Error between the MPT and FEM as well as the MPT and CPT results varies with the a/h ratio. It shows influence of the plate thickness on the results obtained by the MPT. Results obtained by the MPT also depend upon the shear correction factor (κ^2), in present analysis this factor is taken as 5/6.

Table 11.1 Results obtained from the MPT, CPT and FEM

Specimen No.	Thickness (m)	a/h	Fundamental Frequency (Hz)		
			$\frac{\omega_{1(MPT)}}{\omega_{1(FEM)}}$	$\frac{\omega_{1(CPT)}}{\omega_{1(FEM)}}$	$\frac{\omega_{1(MPT)}}{\omega_{1(CPT)}}$
11.1	0.002	250	2.609	1.069	2.440
11.2	0.005	100	1.463	1.069	1.369
11.3	0.01	50	1.213	1.069	1.134
11.4	0.015	33.333	1.155	1.069	1.080
11.5	0.02	25	1.129	1.069	1.056
11.6	0.025	20	1.110	1.069	1.038
11.7	0.03	16.666	1.094	1.069	1.023
11.8	0.035	14.285	1.078	1.069	1.008
11.9	0.04	12.5	1.061	1.069	0.993
11.10	0.045	11.111	1.044	1.069	0.977
11.11	0.05	10	1.027	1.069	0.960
11.12	0.055	9.090	1.008	1.069	0.943
11.13	0.06	8.333	0.990	1.069	0.925
11.14	0.065	7.692	0.971	1.069	0.907
11.15	0.07	7.142	0.951	1.069	0.889
11.16	0.075	6.666	0.932	1.069	0.871
11.17	0.08	6.25	0.912	1.069	0.853
11.18	0.085	5.882	0.893	1.069	0.835
11.19	0.09	5.555	0.874	1.069	0.817
11.20	0.095	5.263	0.855	1.069	0.799
11.21	0.1	5	0.835	1.069	0.781

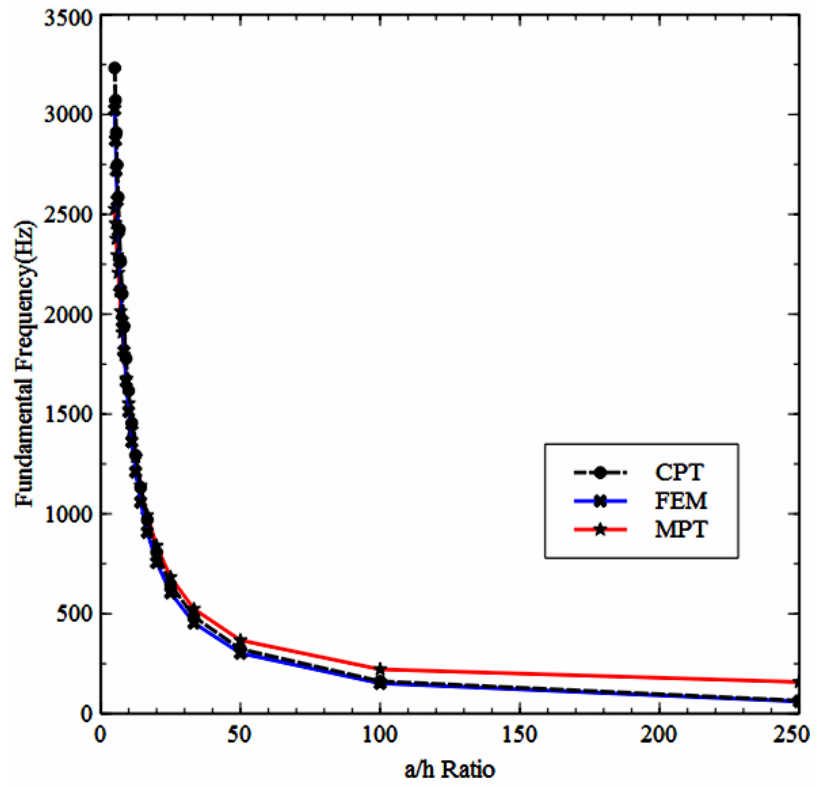


Figure 11.2 Results obtained from the MPT, CPT and FEM for all the specimens

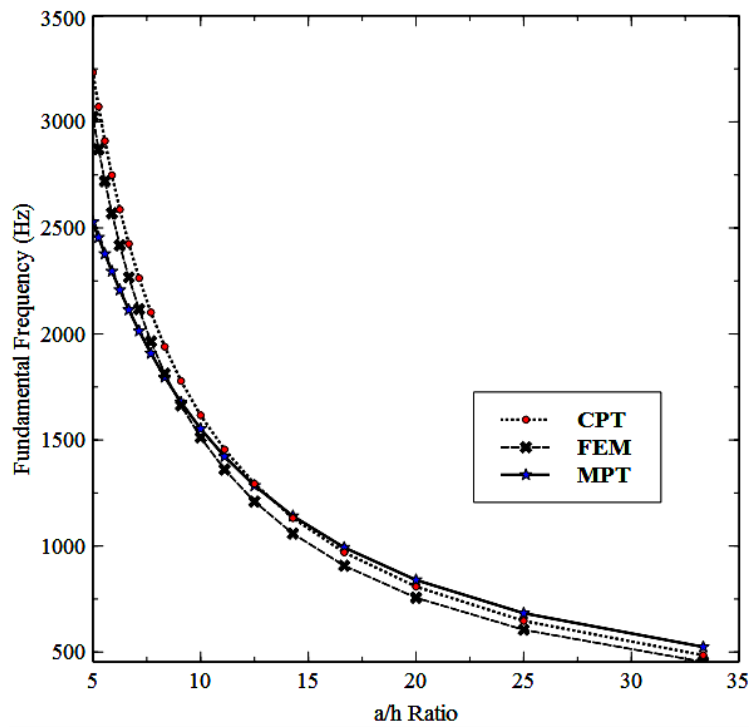


Figure 11.3 Results from the MPT, CPT and FEM for the specimens with $a/h \leq 33.333$

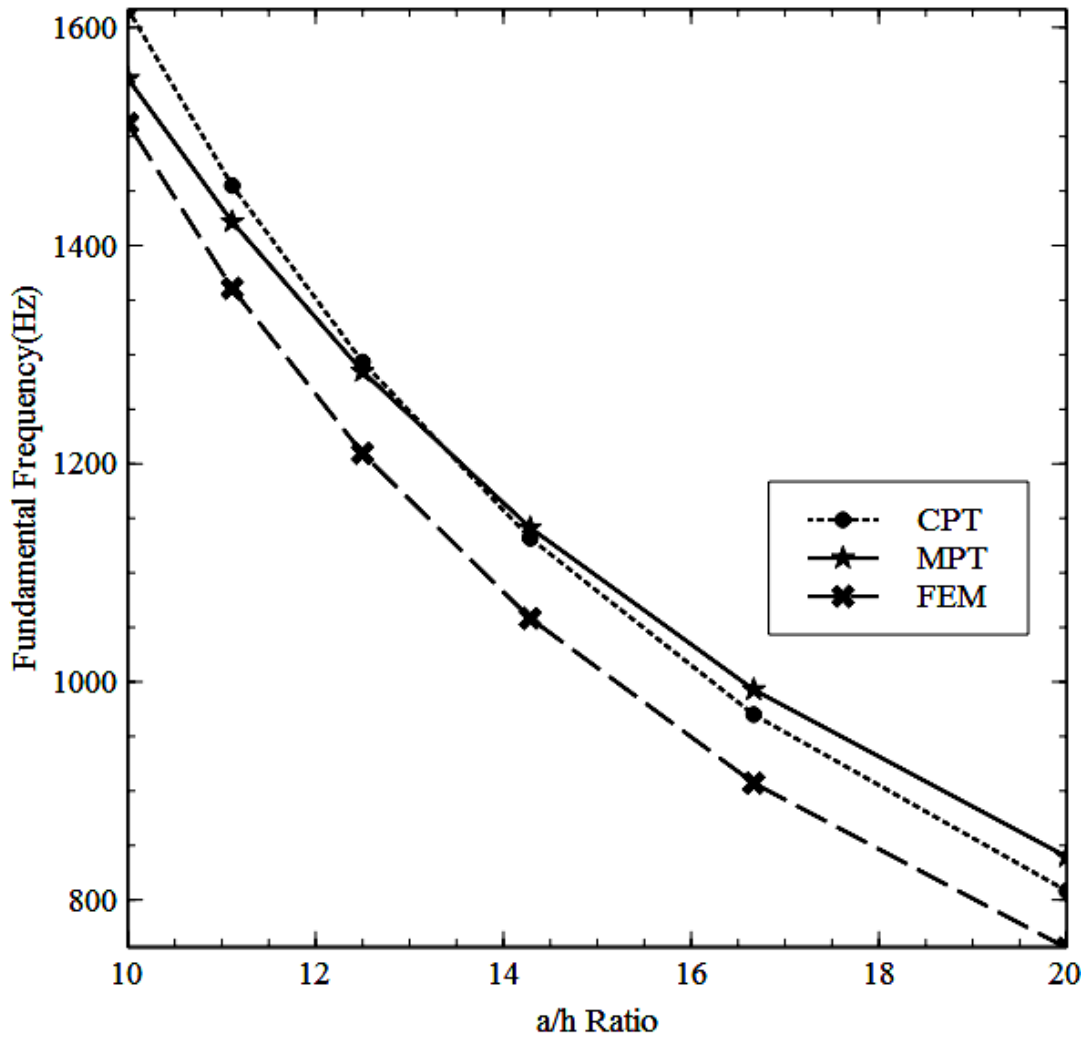


Figure 11.4 Results from the MPT, CPT and FEM for the specimens with $10 \leq a/h \leq 20$

From Figure 11.4 it is observed that the MPT over estimates the fundamental frequency values compared to the CPT and FEM results as the a/h ratio increases above 12.5 i.e the plate thickness values less than 0.04 m. The numerical difference between the fundamental frequency values goes on increasing as the a/h ratio increases above 12.5. Results from Table 11.1 shows that, discrepancy between the MPT and FEM results is less than 10% for $6.25 \leq a/h \leq 16.666$. The MPT gives discrepancy of the 15.56 %, 21.36%, 46.39% and 160.91% for the a/h ratio 33.333($h = 0.015$ m), 50($h = 0.01$ m), 100($h = 0.005$ m), and 250($h = 0.002$ m), compared to the FEM results. Further the fundamental frequency values from Table 11.1 shows that the CPT over estimates the results for the $a/h \leq 12.5$ than those obtained by the MPT and FEM. Thus for the perforated plates having the a/h ratio more

than 12.5, the CPT results can be preferred over the MPT results as error between the MPT and FEM increases above 6.19%.

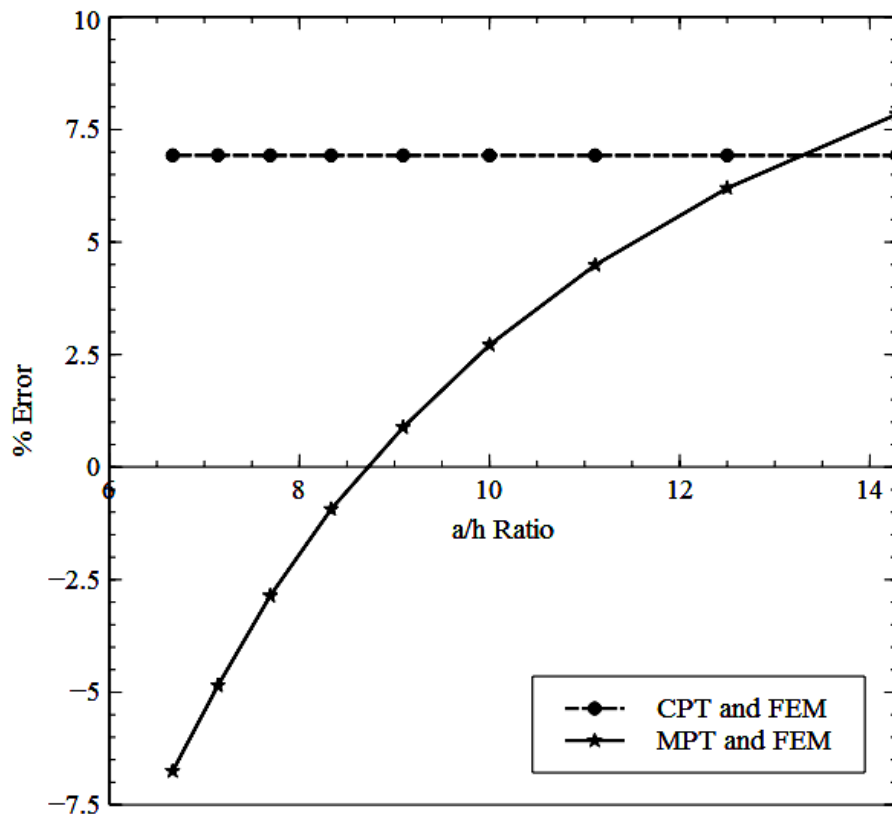


Figure 11.5 Plot of the % error vs. a/h ratio for the specimens with $6 \leq a/h \leq 14.285$

The plot of the percent error between the CPT and FEM results vs. a/h ratio and percent error between the MPT and FEM results vs. a/h ratio for the specimens with $6 \leq a/h \leq 14.285$ is shown in Figure 11.5. The percent error between the CPT and FEM results is constant and is shown by a straight line of constant slope i.e. parallel to the axis showing the a/h ratio values. This error is 6.92 percent. The numerical difference between the CPT and FEM results increases as the a/h ratio decreases below 12.5, though the percent error is constant.

From Figure 11.5 it can be seen that the percent error between the MPT and FEM results is below $\pm 5\%$ when $7.142 \leq a/h \leq 11.111$. Thus within this range results given by the MPT are reasonably good. For the a/h ratio 9.090 ($h = 0.055$ m) both the FEM and MPT results are matching with discrepancy of 0.88 %. Further it is observed that as the a/h ratio decreases below 9, the FEM over estimates the fundamental frequencies compared to the MPT and percent error becomes negative.

Comparison of the CPT and MPT results from last column of the Table11.1 shows that for $9.090 \leq a/h \leq 25$, error varies from - 0.689% for the specimen having the $a/h = 12.5$ to 5.310 % and -5.988% for the specimens having the $a/h = 25$ and 9.09 respectively. Thus within the range $9.090 \leq a/h \leq 25$ error between the MPT and CPT results is less than 6%.

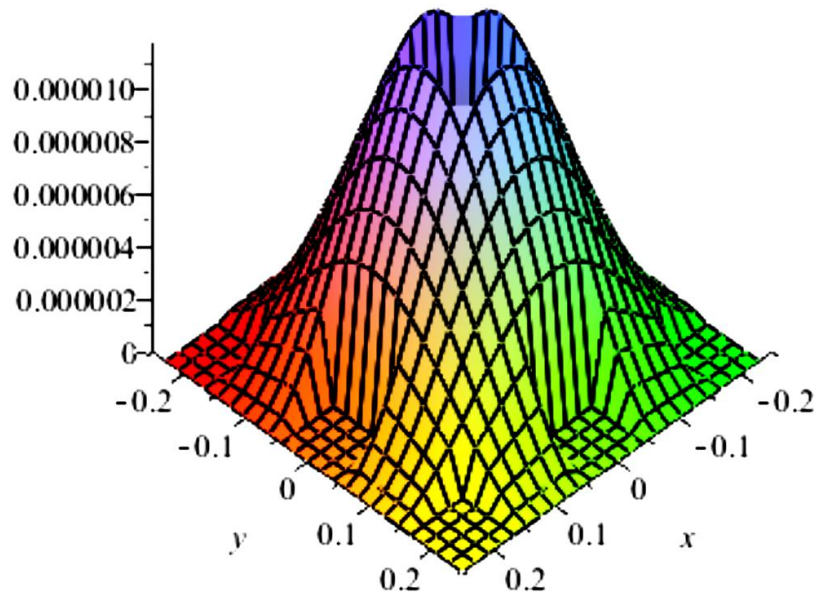


Figure 11.6 3D mode shape for the specimen 11.10 ($h = 0.045$ and $a/h = 11.111$)

Table 11.2 Mode shapes obtained from the MPT and FEM for the specimen 11.10

Spe. no	Mode shapes From MPT and FEM	
	Analytical, MPT	FEM
11.10		

11.5.1 Comparison of the Analytical and FEM Mode Shapes

It is observed that the mode shapes obtained from the MPT and FEM are similar for all the specimens. Representative deflection contour plots have been presented for the specimen 11.10 ($h = 0.045$ and $a/h = 11.111$) in Table 11.2 which shows the similarity of the modes. The 3D mode shape for the specimen 11.10 is shown in Figure 11.6. Also the mode shapes obtained from the CPT are matching with those obtained from the MPT.

11.6 Concluding Remark

In this study the applicability of the proposed approach for modeling of the material properties of the perforated plates has been confirmed for the Mindlin plate by comparison studies. A study has been conducted for the perforated plates with the different thickness to width ratios for the clamped boundary condition. It can be concluded that the effect of transverse shear deformation depresses the fundamental frequency significantly with decreasing the a/h ratio below 12.5. Thus within the range $7.142 \leq a/h \leq 11.111$ results given by the MPT are reasonably good because percent error between the MPT and FEM results is below $\pm 5\%$.

Chapter 12

Conclusions

12.1 Specific Contributions

The objective of this research is focused on the solution of the vibration problems of the perforated plates, and to validate all the analytical results with the FE simulations and experimental data. To this end, the original contributions of this study are:

1. Formulation of the analytical models to determine the fundamental frequency of the perforated plates by using the
 - Special functions to express variation of the material properties for thin plates.
 - Concept of replacing the small perforations by the negatively concentrated mass.
 - Concept of replacing the small circular perforations by the equivalent square perforations.
2. Development of the modal constant expressions to determine the fundamental frequency of the perforated plates with the rectangular array of the circular perforations.
3. Validations of the analytical models developed by comparing results of the numerical analysis with the FE simulations and experimental results for the representative specimens.
4. Formulation of the analytical model to determine the fundamental frequency of the perforated Mindlin (moderately thick) plate by using the unit step function to express variation of the material properties.

Thus goals of our research have been achieved. This is the first attempt of development of the analytical models for the multi-perforated plates to determine the fundamental frequency.

12.2 Conclusions

In this thesis, new analytical models of a perforated rectangular isotropic plate subjected to the transverse free vibrations have been proposed, based on the classical plate theory. Also one example is given for the moderately thick plates by using the Mindlin plate theory. Proposed models can be used to determine the fundamental frequency of the perforated plates. These models can be applied to the rectangular plates having the rectangular/triangular array of the square/rectangular and circular perforations. These

analytical models of the perforated plate provide alternate approaches to the well known equivalent material properties approach to determine the fundamental frequency. In particular, the analytical models are formulated for the clamped all edges boundary condition, and validated both experimentally and by the FE simulations, but models can be extended to other cases of the boundary conditions. Conclusions of the thesis are summarized into two categories.

i) The rectangular plates with the square/rectangular perforations

ii) The rectangular plates with the circular perforations

12.2.1 The Rectangular Plates with the Square/Rectangular Perforations

Under this category total five models are proposed. Four models are developed for the thin plates and one for moderately thick plates. The first two models are introduced to determine the fundamental frequency of plates with the rectangular/square array of the perforations. The third and fourth model is formulated for the plates having the staggered 60° and 45° array of the perforations. In all four models first, the functions are formulated to express the variations in the material properties due to the perforations. The special functions, Heaviside functions and greatest integer functions are employed for this purpose. Further these expressions are used in the approximate analytical methods to determine the fundamental frequency. The fifth analytical model in chapter 11 presents extension of the approach presented in the chapter 5 to the Mindlin plates.

- The first analytical model (Section 5.3) is developed for the plates having the rectangular array of the rectangular perforations. The Heaviside (Unit step) functions are used to express variation of the material properties. The numerical analysis is carried out for the plates with the square perforations arranged in the square array as a special case for the different specimens. From comparison of the FEM and experimental results with numerical results, it is found that this model gives maximum discrepancy of the order of 8.32% between the FEM and numerical results for single term shape function and 7.022% for five term shape function, where as between an experimental and numerical result, it is of the order of 13.44%.
- The second analytical approach (Section 5.7) given is applicable to the plates having the square array of the square perforations. The greatest integer functions are used to express variation of the material properties. The numerical analysis is carried out for

the five specimen and results are compared with the FEM results. The maximum discrepancy between the FEM and numerical results is of the order of 5.278% for single term shape function and 4.025% for five term shape function. Thus this model gives closer results compared to first model, but this approach is limited to the square array of the square perforations.

- The third and fourth analytical models (Section 6.2 and 6.6) proposed in this category are more versatile as these models are equally applicable to the rectangular /square and the staggered array of the perforations. The Heaviside (Unit step) functions are used to express variation of the material properties. Deviation from the square pattern (Introduced in first analytical model, Section 5.3) is interpreted as a phase difference and it is incorporated into the material property function $F(x, y)$. For 60° staggered pattern maximum discrepancy between the FEM and numerical results is of the order of 8 to 10.54% where as between the experimental and numerical results is 14.32%. The numerical results were found to be stable over broad range. For 45° staggered pattern maximum discrepancy between the FEM and numerical results is of the order of 1.716%. So we can conclude that model for 45° staggered pattern works better with proposed approach.
- The fifth analytical model is proposed for the moderately thick perforated plates. The Mindlin plate theory is used and the numerical calculations of the natural frequencies are presented for the rectangular plates with the variable width to thickness ratios. Within the range $7.142 \leq a/h \leq 11.111$ results given by the MPT are reasonably good because percent error between the MPT and FEM results is below $\pm 5\%$. Thus applicability of the approach for modeling of the material properties in thin plate models has been confirmed for the Mindlin plate by comparison studies.

12.2.2 The Rectangular Plates with the Circular Perforations

Under this category four models are developed. Out of the four, three models are formulated by using only the approximate analytical methods. Model given in the chapter 9 is a hybrid model which is combination of the analytical and experimental method. All the four models are developed for the rectangular perforation pattern but these models can be extended to the staggered array of the perforations.

- Formulation of the first analytical model (Section 7.2) is based on the concept of replacing the small perforations by the negatively concentrated mass. Thus inertia

force due to the hole is considered in the Galerkin formulation to obtain the fundamental frequency. This model yields results with good accuracy when the perforation size is small. It is found that the error in the fundamental frequency is of the order of 5% when ratio of the area of plate (A) to the area of single perforation (A_p) is 542.017.

- The second analytical model (Section 8.2) proposed gives good results from the point of view of the accuracy and computational time. This model is based on the concept of replacing the small circular perforations by the equivalent square perforations. Further the Heaviside step functions are used to express variations of the material properties. The numerical analysis is carried out for the ten specimens to get the fundamental frequency. From the comparison of the FEM and numerical analysis results it is found that the proposed approach is more suitable for the perforated plates with the MRR more than or equal to 0.852. When the MRR is in this range maximum error of 6-7% is observed in the fundamental frequency. The discrepancy between the FEM and numerical results is less than 2.56 % when (A/ A_p) is greater than 169. Thus for wide range of (A/ A_p) ratio this model gives reasonably good results.
- In third approach (Chapter 9) the modal constant expression for the fundamental frequency is proposed, which gives alternative method to the existing equivalent material properties approach. This modal constant can be directly used to calculate the fundamental frequency, by using the actual material properties instead of the equivalent material properties. In this approach experimentally obtained fundamental frequency is used in the Rayleigh's method to get an expression for the modal constant. Maximum discrepancy between the results obtained from the modal constant and the FEM is 11.9%.
- The fourth analytical model is given in Chapter 10 which is for array of the circular multi-perforations in a plate structure. It has provided a simple single expression for exact bidirectional material property variation. Further this model can easily handle the variation in the size of the perforations. The maximum error of the order of 0.338% to -4.477% is obtained for the specimens having the ratio of the plate area to the perforation hole area within the range 1518.154 to 35.932. This model gives very good agreement with the FEM results over broad range of the ratio of the plate area to the perforation hole area. Out of all the models developed this model gives the best results.

12.3 Note on the Accuracy of the Analytical Models Proposed

From a practical point of view almost any success by using the global admissible function methods depends on the selection of the functions. Increasing the number of terms “ n ” in the shape function increases the accuracy of the fundamental frequency but it worsen the higher ones as the number of terms used increases, thus we have confined ourselves to the fundamental frequency only. But the Ritz eigensolutions approaches the actual eigensolutions as $n \rightarrow \infty$ and the functions form a mathematically complete set (i.e., capable of representing any possible deflected shape of the beam) However, this increases greatly the problem complexity and computational time required. This means that a compromise must be made for a suitable choice of the function so that good convergence is assured while the necessary effort is kept within bounds. But, the fact that completeness guarantees convergence as the number of terms in the series approaches infinity is not particularly meaningful, because in deriving the approximate solutions the interest lies in convergence with as few terms as possible [Leonard Meirovitch, 2010]. When objective is to estimate the fundamental frequency of distributed parameter system one must choose a function resembling the first eigenfunction as closely as possible [Leonard Meirovitch, 2010]. Also none of the functions are unique and one may use his/her ingenuity to conceive functions best for the solution of the particular problem. It should be pointed out that the trial functions considered in our work are taken from standard references, testing them by trial and error, consider only few terms of the functions.

Thus in spite of above discussed limitations we show from proposed models that methods using global admissible functions can obtain reasonably good results without a great deal of computational effort. The shape Functions used provides a good estimate of the fundamental frequency. Few terms of the admissible functions in these cases suffice to yield results near the desired solution.

12. 4 Effect of Perforations on the Damping

Modal damping is calculated for first two modes, for all the specimens tested experimentally. Appendix “D” shows the values of the damping factors. Results show that plate specimens are lightly damped as damping factor values are less than 1.51% for all of the cases. For all the specimens damping factor for first mode is greater than second mode ($\zeta_1 > \zeta_2$). It can be seen that the damping factor values are slightly more for the perforated plates compared to the solid plate. No consistent effect on damping can be clearly observed, except

for specimen no. 9.1 to 9.4, where the ζ_1 and ζ_2 decreases with increasing MRR. As only representative specimens are analyzed experimentally no significant change in the extent of the variation of damping was observed. The noticeable differences can only be observed in damping values of specimen no.s 8.11/7.11 and 9.1. For these specimens perforation (circular) size is small compared to all other specimens. It can also be seen that due to small number of specimens analyzed, there is no significant change in the extent of the variation of the damping observed. The MRR of the perforated plate may not be the only factor that determines ζ_1 and ζ_2 . Both the shape and distribution of perforation may affect the damping coefficient; however, it is premature to conclude that the change in shape and distribution of perforation has marginal influence on the magnitude of the damping factor.

12.5 Recommendations for Future Research

The following are recommendations for future studies on the plates with the array of perforations.

- This study only considered the rectangular plates with the array of rectangular/square and circular openings. Future studies can consider different types of the plates and openings.
- This study only considered uniform thickness for the plates. Future studies can consider different types of the thickness variation such as linear, parabolic and exponential in one direction and bidirectional.
- This study only evaluated the fundamental frequencies for clamped all edges boundary condition. Future studies can investigate on the free vibration for a variety of different types of mixed boundary conditions.
- A future study could apply the thermal gradient on the plates with the array of perforations and study the free vibrations.
- Structural plates have a multitude of applications in the shipbuilding, aerospace, building and automobile industries. In these industries, complex real-life plate problems may need higher eigenfrequencies to be calculated rather than only the fundamental frequency. Theoretical foundations of the proposed approaches can be further extended to find out the higher eigenfrequencies by using properly chosen shape functions.

References

- [1] Agilent Technologies, The Fundamentals of Modal Testing, Application Note 243 – 3, 2001
- [2] Aksu G. and Ali R., Determination of dynamic characteristics of rectangular plates with cutouts using a finite difference formulation, *Journal of Sound and Vibration*, 44, pp. 147-158, (1976).
- [3] Ali R. and Atwal S. J., Prediction of natural frequencies of vibration of rectangular plates with rectangular cutouts, *Computers and Structures*, 12, pp. 819-823, (1980).
- [4] Altintas G., Effect of Mass Based Imperfections on Behavior of Linear Vibrating Plates Near Degenerate Modes, *Journal of Vibration and Control* 15(2) pp. 219–231, (2009).
- [5] Amabili M., Carra S., Experiments and simulations for large-amplitude vibrations of rectangular plates carrying concentrated masses, *Journal of Sound and Vibration* 331 (1) pp.155–166, (2012).
- [6] Amabili M., Geometrically nonlinear vibrations of rectangular plates carrying a concentrated mass, *Journal of Sound and Vibration* 329 (21) pp. 4501–4514, (2010).
- [7] Amabili M., Pellegrini M., Righi F., and Vinci F., Effect of concentrated masses with rotary inertia on vibrations of rectangular plates, *Journal of Sound and Vibration* 295 ,(1-2) pp.1–12, (2006).
- [8] Armenakas A. E., Appendix ‘A’ Mechanical properties of materials in: *Advanced Mechanics of Materials and Applied Elasticity*, CRC Press, Boca Raton, FL, (2006).
- [9] Avalos D. R. and Laura P.A.A., Transverse Vibrations of Simply Supported Rectangular Plates with Two Rectangular Cut Outs, *Journal of sound and vibration*, 267, pp. 967-977, (2003).
- [10] Avalos D. R., Larrondo H. A., Laura P. A. A., Rossi R. E., Transverse Vibrations of Simply Supported Rectangular Plates With Rectangular Cutouts Carrying An Elastically Mounted Concentrated Mass, *Journal of Sound and Vibration* 202(4) pp. 585-592,(1997).
- [11] Avitabile, Peter. "Experimental modal analysis." *Sound and vibration*, 35.1 , 20-31,(2001).
- [12] Azhari M., Shahidi A. R., and Saadatpour M.M., Local and post local buckling of stepped and perforated thin plates, *Applied Mathematical Modelling*, 29, pp.633-652, (2005).
- [13] Bellés, Patricia M., and José L. Pombo. "Experimental results of plates vibrations. Influence of boundary conditions." *sem-proceedings* (2007). <http://sem-proceedings.com/07s/sem.org-2007-SEM-Ann-Conf-s85p05-Experimental-Results-Plates-Vibrations.-Influence-oundary.pdf>

- [14] Bhattacharya A., and Venkat Raj V. , Yield Criterion for Thin Perforated Plates With Square Penetration Pattern, *Journal of Pressure Vessel Technology*, 126,pp. 169-175, (2004).
- [15] Bhattacharya A., Venkat Raj V., Peak stress multipliers for thin perforated plates with square arrays of circular holes, *International Journal of Pressure Vessels and Piping*, pp.379-388, (2003).
- [16] Boay C. G., Frequency Analysis of Rectangular Isotropic Plates Carrying A Concentrated Mass, *Computers & Structures* 56(I) pp. 39-48, (1995).
- [17] Britan A. , Karpov A. V., Vasilev E. I. , Igra O. , Ben-Dor G. , Shapiro E. , “Experimental and Numerical Study of Shock Wave Interaction with Perforate Plates ,” *Journal of Fluids Engineering* ,126,pp. 399-409, (2004).
- [18] Burgemeister K. A., Hansen C. H., Calculating resonance frequencies of perforated panels, *Journal of Sound and Vibration* 196(4) pp.387-399, (1996).
- [19] C.M. Wang, J.N. Reddy, K.H. Lee, *Shear Deformable Beams and Plates; Relationships with Classical Solution*, Elsevier, Amsterdam, 2000.
- [20] Chakraverty S., Jindal R., Agarwal V. K. Effect of non-homogeneity on natural frequencies of vibration of elliptic plates. *Meccanica*, Vol. 42, Issue 6, pp. 585 – 599, (2007).
- [21] Chakraverty S., Petyt M. Vibration of non-homogeneous plates using two-dimensional orthogonal polynomials as shape functions in the Rayleigh-Ritz method. *J. Mech. Eng. Sci.*, Vol. 213, Issue (C7), pp. 707-714, (1999).
- [22] Chakraverty S., *Vibration of plates*, First ed. CRC press Taylor & Francis Group, Boca Raton, pp. 56 – 135, (2009).
- [23] Chang C. N. and Chiang F. K., Vibration analysis of a thick plate with an interior cutout by a finite element method, *Journal of Sound and Vibration*, 125, pp. 477-486, (1988).
- [24] Choi S, Jeong KH, Kim T et al., Free vibration analysis of perforated plates using equivalent elastic properties. *Journal of the Korean Nuclear society* 30(5) pp.416-423, (1998).
- [25] Choi S., Jeong K. H., Kim T.W., Kim K.S., Park K. B. Free vibration analysis of perforated plates using equivalent elastic properties *Journal of the Korean Nuclear society*. Vol. 30, Issue 5, pp. 416-423, (1998).
- [26] Dumond, Patrick “Comparison of the assumed shape and finite element methods For a vibrating brace-plate system” *Proceedings of The Canadian Society for Mechanical Engineering Forum 2010,CSME FORUM 2010, Victoria, British Columbia, Canada,2010*

- [27] Duncan, J. P., & Upfold, R. W., Equivalent elastic properties of perforated bars and plates. *Journal of Mechanical Engineering Science*, 5(1), pp. 53-65, (1963).
- [28] Europerf, The advantages of perforated metals, European Perforators Association catalog, www.europerf.org (2013).http://www.europerf.org/data/files/advantages_en.pdf
- [29] Fastenal Technical reference Guide, 2005, Fastenal Company Engineering Department
- [30] Forskitt M., Moon J.R. And. Brook P. A., Elastic properties of plates perforated by elliptical holes, *Applied Mathematical Modeling* 15, pp.182-190, (1991)
- [31] Forskitt, M., Moon, J. R., & Brook, P. A., Elastic properties of plates perforated by elliptical holes. *Applied mathematical modeling*, 15(4), pp.182-190, (1991).
- [32] Grossi Ricardo O., Arenas Blanca Del V. and Laura P. A. A., "Free vibration of rectangular plates with circular openings," *Ocean Engineering*, 24, pp. 19-24, (1997).
- [33] Halvorsen, William G., and David L. Brown. "Impulse technique for structural frequency response testing." *Sound and Vibration* 11.11 ,8-21,(1977).
- [34] Harris C. M., Piersol A.G., *Shock and Vibration handbook*, 5th Edition, McGraw-Hill, New York, USA, (2002).
- [35] Harris, Cyril M. *Harris' shock and vibration handbook*. Vol. 5. New York: McGraw-Hill, 2002.
- [36] Hegarty R. F. and Ariman T., Elasto-dynamic analysis of rectangular plates with circular holes, *International Journal of Solids Structures*, 11, pp. 895–906, (1975).
- [37] Horvay G., Bending of honeycombs and perforated panels. *ASME Journal of Applied Mechanics*, 74, pp. 122–123, (1952)
- [38] Hou, Y., Wei, G. W. and Xiang, Y., DSC-Ritz method for the free vibration analysis of Mindlin plates. *Int. J. Numer. Meth. Engng.*, 62: 262–288., (2005). doi: 10.1002/nme.1186
- [39] Huang M., and Sakiyama T., Free vibration analysis of rectangular plates with variously shaped holes, *Journal of Sound and Vibration*, 226, pp. 769-786, (1999).
- [40] Hung M. Jo and Jo Jong Chull, Equivalent material properties of perforated plate with triangular or square penetration pattern for dynamic analysis, *Nuclear Engineering and Technology*, 38, pp. 689-696, (2006).
- [41] J.N. Reddy, *Theory and Analysis of Elastic Plates*, Taylor & Francis, Philadelphia, PA, 1999.
- [42] Jae-Kon Lee, Kim and Jin-Gon, An analytical study on prediction of equivalent elastic constants of perforated plate, *Journal of Mechanical Science and Technology*, 19, pp.2224-2230, (2005).

- [43] K.M. Liew, C.M. Wang, Y. Xiang and S. Kitipornchai, Chapter Five - Formulation in Skew Coordinates, In *Vibration of Mindlin Plates*, edited by K.M. LiewC.M. WangY. XiangS. Kitipornchai, Elsevier Science Ltd, Oxford, 1998, Pages 133-164, ISBN 9780080433417, <http://dx.doi.org/10.1016/B978-008043341-7/50006-6>.
- [44] Kaap D. L., *Dynamic Effective Elastic Constants for Perforated Plates with Square or Triangular Penetration Patterns*, M.S. Thesis, Department of Mechanical Engineering, University of Wisconsin-Madison, Madison, WI, (1997).
- [45] Kathagea K., Misiekb TH., Saal H., *Stiffness and critical buckling load of perforated sheeting*, *Thin-Walled Structures* 441223-1230(2006).
- [46] Kumar, Sanjiv, Rajiv Kumar, and Rakesh Sehgal. "Performance Analysis of Finite Element and Energy Based Analytical Methods for Modeling of PCLD Treated Beams." *Journal of Vibration and Acoustics-Transactions of The ASME* 134.3 (2012).
- [47] Kyeong-Hoon Jeong and Marco Amabili, *Bending vibration of perforated beams in contact with a liquid*, *Journal of Sound and Vibration*, 298, pp. 404-419, (2006).
- [48] L. Zhou, Y. Xiang, *Vibration Analysis of Mindlin Plates with Cracks by MLSElement Method*, *Procedia Engineering*, Volume 14, , Pages 1637-1644,(2011) ISSN 1877-7058, <http://dx.doi.org/10.1016/j.proeng.2011.07.206>.
- [49] Lal R., Dhanpati. *Effect of nonhomogeneity on vibration of orthotropic rectangular plates of varying thickness resting on pasternak foundation*. *Jl. Vibration and Acoustics, ASME*, Vol. 131, Issue 011007, pp.1- 9, (2009).
- [50] Lal R., Kumar Y., Gupta U. S., *Transverse vibrations of non-homogeneous rectangular plates of uniform thickness using boundary characteristic orthogonal polynomials*. *Int. Jl. Appl. Math and Mech.* Vol. 6, Issue14, pp. 93 – 109, (2010).
- [51] Lam K. Y. and Hung K. C., *Orthogonal polynomials and subsectioning method for vibration of plates*, *Computers and Structures*, 34, pp. 827-834, (1990).
- [52] Lam K.Y., Hung K.C. and Chow S.T., *Vibration analysis of plates with cutouts by the modified Rayleigh-Ritz method*, *Applied Acoustics*, 28, pp. 49-60, (1989).
- [53] Larson and Davis Inc., *ViRTe3000+ Real Time analyzer, Reference Manual*. Larson, (2008).
- [54] Laura P. A. A., Gutierrez R. H. *Transverse vibrations of orthotropic, nonhomogeneous rectangular plates*, *Fibre Science and Technology*, Vol. 21, Issue 2, pp.125 – 133, (1984).
- [55] Laura, Patricio A., and Bernard F. Saffell Jr. "Study of Small-Amplitude Vibrations of Clamped Rectangular Plates Using Polynomial Approximations." *The Journal of the*

- Acoustical Society of America 41.4A, 836-839, (2005).
- [56] Laura, Patricio A., and Bernard F. Saffell Jr. "Study of Small-Amplitude Vibrations of Clamped Rectangular Plates Using Polynomial Approximations." *The Journal of the Acoustical Society of America* 41.4A , 836-839,(2005).
- [57] Lee H.P., Lim S.P., and Chow S.T., Prediction of natural frequencies of rectangular plates with rectangular cutouts, *Computers and Structures*, 36, pp. 861-869, (1990).
- [58] Leissa A.W. Plate vibration research, 1976–1980pp. classical theory. *Shock and Vibration Digest*, Vol. 13, Issue 9, pp. 11 – 22, (1981).
- [59] Leissa A.W. Plate vibration research, 1976–1980pp. complicating effects. *Shock and Vibration Digest*, Vol. 13, Issue 10, pp. 19 – 36, (1981).
- [60] Leissa A.W. Recent research in plate vibrations pp. classical theory. *Shock and Vibration Digest*, Vol. 9, Issue 10, pp. 13 – 24, (1977).
- [61] Leissa A.W. Recent research in plate vibrations, 1981–1985. Part I. Classical theory. *Shock and Vibration Digest*, Vol. 19, Issue 2, pp. 11 – 18, (1987).
- [62] Leissa A.W. Recent research in plate vibrations, 1981–1985. Part II. Complicating effects. *Shock and Vibration Digest*, Vol. 19, Issue 3, pp. 10 – 24, (1987).
- [63] Leissa A.W. Recent research in plate vibrations. Complicating effects. *Shock and Vibration Digest*, Vol. 9, Issue 12, pp. 21 – 35, (1977).
- [64] Leissa A.W. *Vibration of Plates*. NASA SP-169, Washington, (1969).
- [65] Li Q.S., An exact approach for free vibration analysis of rectangular plates with line-concentrated mass and elastic line-support, *International Journal of Mechanical Sciences* 45 (4) pp. 669–685, (2003).
- [66] Liew K.M., Kitipornchai S., Leung A.Y.T. and Lim C.W., Analysis of the free vibration of rectangular plates with central cut-outs using the discrete Ritz method, *International Journal of Mechanical Sciences*, 45, pp. 941-959, (2003).
- [67] Liew, K. M., K. C. Hung, and M. K. Lim. "Vibration of Mindlin plates using boundary characteristic orthogonal polynomials." *Journal of Sound and Vibration* 182.1: 77-90, (1995).
- [68] Low K. H., Analytical and Experimental Investigation on A Vibrating Rectangular Plate With Mounted Weights, *Journal of Sound and Vibration* 160(1) pp. 111-121,(1993) .
- [69] Low K. H., Chai G. B. , Tan G. S., A Comparative Study of Vibrating Loaded Plates between the Rayleigh-Ritz and Experimental Methods, *Journal of Sound and Vibration* 199(2) pp. 285-297,(1997).

- [70] Low K. H., Chai G. B., Lim T. M. , Sue S. C., Comparisons of Experimental And Theoretical Frequencies For Rectangular Plates With Various Boundary Conditions and Added Masses, *Int. J. Mech. Sci.* 40(11) pp. 1119-1131,(1998).
- [71] Low K.H., An improved model for the frequency estimate of mass-loaded plates by a combined use of equivalent center mass and stiffness factors, *International Journal of Mechanical Sciences*, 43pp. 581-594,(2001).
- [72] M.G. Sainsbury, Q.J. Zhang, “The Galerkin element method applied to the vibration of damped sandwich beams”, *Computers & Structures*, Volume 71, Issue 3, Pages 239-256,(1999). ISSN 0045-7949, [http://dx.doi.org/10.1016/S0045-7949\(98\)00242-9](http://dx.doi.org/10.1016/S0045-7949(98)00242-9).
- [73] Meijers P., Ph.D. Thesis, University of Delft, Holland, Doubly periodic stress distributions in perforated plates (1967).
- [74] Meirovitch, Leonard. *Fundamentals of vibrations*. Waveland Press, 2010.
- [75] Mindlin, R.D., Influence of rotatory inertia and shear on flexural motions of isotropic, elastic plates. *Journal of Applied Mechanics*, ASME 18, 31–38, (1951).
- [76] Mishra D. M., Das A. K. Free vibrations of an isotropic nonhomogeneous circular plate. *AIAA Journal*, Vol. 9, Issue 5, pp. 963 – 964, (1971).
- [77] Monahan J., Nemergut P. J. and Maddux G. E., Natural frequencies and mode shapes of plates with interior cutouts, *The Shock and Vibration Bulletin*, 41, pp. 37-49, (1970).
- [78] Montgomery D. C., *Design and Analysis of Experiments*. 5th Edition. John Wiley & Sons, New York, (2004).
- [79] Mundkar G., Bhat R.B., and Neriya S., Vibration of plates with cutouts using boundary characteristics orthogonal polynomial functions in the Raleigh-Ritz method, *Journal of Sound and Vibration*, 176, pp. 136-144(1994).
- [80] New Metals, Inc., *Perforated Metal catalog*, <http://www.newmetals.com> (2013). <http://www.newmetals.com/PDF/perforated.pdf>
- [81] Nor Hatini Binti Baharin, Dec. 2008, *Effect Of Accelerometer Mass On Thin Plate Vibration*, A project report submitted in partial fulfillment of the requirement for the award of the degree of Master of Engineering (Mechanical), Faculty of Mechanical Engineering ,Universiti Teknologi Malaysia
- [82] O’Donnell W. J. Effective elastic constants for the bending of thin perforated plates with triangular and square penetration patterns, *Journal of Engineering for Industry*. Vol. 95, pp. 121 – 128, (1973).
- [83] O’Donnell W.J. Langer B.F., *Design of Perforated Plates*, *Journal of Engineering for*

- Industry, Trans. ASME 84, pp. 1-13, (1962).
- [84] O'Donnell, W. J., and Langer B. F., Design of perforated plates, ASME Journal of Engineering for Industry, Transactions of the ASME. Series B 84, pp. 307-320, (1962).
- [85] Ostachowicz W., Krawczuk M., Cartmell M., The location of a concentrated mass on rectangular plates from measurements of natural vibrations, Computers and Structures 80 (16-17) pp.1419–1428, (2002).
- [86] Pan M. Note on the transverse vibration of an isotropic circular plate with density varying parabolically. Indian Journal of Theoretical Physics, 24(4), pp. 179 – 182, (1976).
- [87] Paramsivam P., Free vibration of square plates with square openings, Journal of Sound and Vibration, 30, pp. 173-178, (1970).
- [88] Patil D.C., Gawade S.S. and Mali K.D., Dynamic response analysis of rectangular perforated plates with varying sizes of circular perforation holes. Inpp. 14th International congress on sound and vibration (ed. B Randall), Cairns, Australia, 9-12 July 2007.
- [89] Pedersen N. L., Optimization of holes in plates for control of eigenfrequencies, Journal of structural and multidisciplinary optimization, 28, pp. 1-10, (2004).
- [90] Rao B. P., V. Rao G., Raju, I. S., A perturbation solution for the vibration of inhomogeneous rectangular plates, Journal of Aeronautical Society of India, Vol. 28, Issue1, pp. 121–125, (1976).
- [91] Rao G. V., Rao B. P., Raju I. S., Vibrations of inhomogeneous thin plates using a high precision triangular element. J. Sound Vib., 34(3), pp.444 – 445, (1974).
- [92] Reddy J. N., Large amplitude flexural vibration of layered composite plates with cutout, Journal of Sound and Vibration, 83, pp. 1-10 (1982).
- [93] Rezaeepazhand J. and Jafari M., Stress analysis of perforated composite plates, Composite structures, 71, pp.463-468. (2005).
- [94] Romero G.G. , Alanís E.E. , Martínez C.C. , Nallim L.G. , Toledo M.W. , Álvarez L. , Vibration Analysis of Perforated Plates Using Time-Average Digital Speckle Pattern Interferometry, Experimental Mechanics ,50, pp.1013–1021, (2010).
- [95] Saheb, K. M., & Shasikanth, M. (2014). Large Amplitude Free Vibrations of Mindlin Square Plates using Coupled Displacement Field Method. International Journal of Current Engineering and Technology, Special Issue-2 ,683-686,(Feb 2014)
- [96] Sahu S. K. and Datta P. K., “Dynamic stability of curved panels with cutouts,” Journal of Sound and Vibration, 251, pp. 683-696, (2003).
- [97] Sinha Jyoti k., Singh Sandeep and Rama Rao A., Added mass and damping of submerged

- perforated plates, *Journal of sound and vibration*, 260, pp. 549-564 (2003).
- [98] Sivasubramonian B., Kulkarni A.M. and Rao G. V., Free vibration of curved panels with cutouts, *Journal of Sound and Vibration*, 200, pp. 227-234, (1997).
- [99] Sivasubramonian B., Rao G. V. and Krishnan A., Free vibration of longitudinally stiffened curved panels with cutouts, *Journal of Sound and Vibration*, 226, pp. 41-55, (1999).
- [100] Sobczyk K., Free vibrations of elastic plate with random properties -The eigenvalue problem, *Journal of Sound and Vibration*, 22(1), pp. 33 – 39,(1972).
- [101] Soler A. I. and Hill W. S., Effective bending Properties for stress analysis of rectangular tubesheets, *Journal of Engineering for Power* 99, pp.365-370, (1977).
- [102] Sunh Choi; Kyeong Hoon Jeong, TaeWan Kim, KangSoo Kim, KeunBae Park, Free vibration analysis of perforated plates using equivalent elastic properties, *Journal of the Korean Nuclear society* 30 (5), pp. 416-423,(1998).
- [103] Thomson, William. *Theory of vibration with applications*. CRC Press, (1996).
- [104] Tomar J. S., Gupta D. C., Jain N. C. Axisymmetric vibrations of an isotropic non-homogeneous circular plate of linearly varying thickness., 85(3), pp. 365 – 370, (1982).
- [105] Tomar J. S., Gupta D. C., Jain N. C. Vibration of non-homogeneous plates of variable thickness. *Journal of Acoustical Society of America*, 72(3), pp. 851– 855, (1982).
- [106] Tomar J. S., Gupta D. C., Jain N. C., Free vibrations of an isotropic non-homogeneous infinite plate of linearly varying thickness. *Meccanica, Journal of Italian Association of Theoretical and Applied Mechanics AIMETA*, Vol. 18, Issue 1, pp. 30 – 33, (1983).
- [107] Tomar J. S., Gupta D. C., Jain N. C., Free vibrations of an isotropic non-homogeneous infinite plate of parabolically varying thickness, *Indian J. Pure Appl. Math.*, 15(2), pp. 211– 220, (1984).
- [108] Tong Liu, Ke Wang, QI-WU Dong, and Min-Shan Liu, Hydro elastic natural vibrations of perforated plates with cracks, *Procedia Engineering*, 1, pp.129–133, (2009).
- [109] Ventsel E., Krauthammer T., *Thin Plates and Shells, Theory, Analysis, and Applications*, Marcel Dekker, Inc., New York, (2001).
- [110] Vinson, Jack R. *The behavior of thin walled structures beams, plates, and shells*. Springer, (1988).
- [111] W. Karunasena, S. Kitipornchai, F.G.A. Al-Bermani, Free vibration of cantilevered arbitrary triangular Mindlin plates, *International Journal of Mechanical Sciences*, Volume 38, Issue 4, April 1996, Pages 431-442, ISSN 0020-7403, [http://dx.doi.org/10.1016/0020-7403\(95\)00060-7](http://dx.doi.org/10.1016/0020-7403(95)00060-7).

- [112] Wang W.C., Lai K.H., Hybrid determination of equivalent characteristics of perforated plates, *Experimental Mechanics*, 43(2), pp.163-172, (2003).
- [113] Wang, C.M., Reddy, J.N., Lee, K.H., *Shear Deformable Beams and Plates: Relationships with Classical Solutions*. Elsevier, Oxford, UK., (2000).
- [114] Wang, G., Wereley, N. M., & Chang, D. C., Analysis of bending vibration of rectangular plates using two-dimensional plate modes, *Journal of aircraft*, 42(2), 542-550, (2005).
- [115] Watanabe O., and Koike T. , Creep-Fatigue Life Evaluation Method for Perforated Plates at Elevated Temperature, *Journal of Pressure Vessel Technology*, 128, pp. 17-24, (2006) .
- [116] Wu D. , Peddieson J. , Buchanan G. R. , Rochelle S.G. , Large axisymmetric deformations of elastic/plastic perforated circular plates, *Journal of Pressure Vessel Technology*, 125, pp. 357-364, (2003).
- [117] Wu J.S. , Luo S.S., Use of the Analytical-and-Numerical Combined Method in the Free Vibration Analysis of a Rectangular Plate with any Number of Point Masses and Translational, Springs *Journal of Sound and Vibration*, 200(2) pp.179-194,(1997).
- [118] Xu, Hongan, Jingtao Du, and W. L. Li. "Vibrations of rectangular plates reinforced by any number of beams of arbitrary lengths and placement angles." *Journal of Sound and Vibration* 329.18, 3759-3779, (2010).
- [119] Young P. G., Yuan J. and Dickinson S. M., Three dimensional analysis of the free vibration of thick rectangular plates with depressions, grooves or cutouts, *American Society of Mechanical Engineers Journal of Vibration and Acoustics*, 118, pp. 184-189, (1996).
- [120] Zhang Y., Eigenfrequency Computation of Beam/Plate Carrying Concentrated Mass/Spring, *ASME Journal of Vibration and Acoustics* 133(2) pp. 021006-1-10,(2011).

Appendix:A

Applications of Perforated Plates

- **Agriculture**
 - For bee hives
 - For grain dryers
 - For wine vat
 - For fish farming
 - For hammer mill screens
 - For silo ventilation
 - For sorting machines (screens and drums)
 - For threshing machine screens
 - For winnowing machine screens
 - For bent and folded perforated sheets as elements for conveyor belts
 - For stainless steel juice channels for wine presses

- **Brewing Industry**
 - For malting Floors
 - For hop Screen

- **Food Industry**
 - For vegetable and fruit presses
 - For cheese moulds
 - For baking trays
 - For cookers
 - For boilers
 - For frying ranges
 - For fruit & vegetable separators
 - For crushing machines
 - For coffee screens and pulpers
 - For tea sifters
 - For trays for vegetable and fruit dryers

- **Sugar and Distilling Industry**
 - For filters
 - For centrifuges
 - For diffuser lining
 - For elevator buckets
 - For sugar beet washers
 - For pulp presses

- **Chemicals**
 - For centrifuges
 - For drying machine baskets
 - For filters
 - For pulverizers
 - For perforated cathodes for electrolysis
 - Support tubes for filter industry

- **Electricity**
 - For base panels for distribution boards
 - For battery separator plates
 - For cable trays
 - For radiator covers
 - For water screens
 - For cable winding drums
 - For electronic switch cabinets with components made of perforated metal

- **Water Works**
 - For well screens
 - For filters

- **Gas Works**
 - For gas purifiers
 - For rotary and vibrating screens
 - For liquid gas burner tubes

- **Mines And Collieries**
 - For elevator buckets
 - For mine cages
 - For panels for dust extractors
 - For coal washing
 - For rotary and vibrating screens
 - For flocculation screens

- **Glue Manufacturers**
 - For bone screen

- **Glass Industries**
 - For glass reinforcement

- **Cement Industry**
 - For slurry screens

- **Paper Industry**
 - For filters
 - For paper paste diffuser floors
 - For washing and grading

- **Textile Industry**
 - For tannery machines
 - For yeing machines
 - For drying machines
 - For felt mills and textile printers

- **Steel Industry**
 - For cinder screens
 - For blast furnace screens

- **Shipbuilding Industry**
 - For embossed or perforated plates for floors, stairs and gangways
 - For filters
 - For cable trays

- For silencers
- **Automotive Industry**
 - For ventilation for tractor engine
 - For casing
 - For ventilation grid
 - For perforated tubes for sound isolation
 - For silencer for motorcycles
 - For flooring and running boards
 - For oil filters
 - For silencer tubes
 - For radiator grilles
 - For air filters
- **Mechanical Handling**
 - For sand dewatering buckets
 - For conveyor flight panels
- **Building Industry**
 - For embossed plates for floors and stairs
 - For folded and perforated plates for gangways and stairs
 - For decorative perforated or embossed or indented plates
 - For perforated pipe guards
 - For radiator covers
 - For sign-boards
 - For acoustic panels
 - For ventilation grilles
 - For decorative perforated benches or chairs
- **Building Architecture**
 - For façades made of perforated stainless steel sheets
 - For noise protection ceiling made of micro perforated aluminium sheets
 - For sunscreen slats for sun protection
- **Waste Disposal**
 - For electrical precipitator trays
 - For refuse screens
 - For screening and sorting drum for different kinds of recycling
- **Plating and Finishing**
 - For perforated dipping baskets
- **Quarries and Brick Making**
 - For drying trays
 - For elevator buckets
 - For roller mill runways
 - For oven trays
 - For rotary and vibrating screens
- **Railways**
 - For embossed floors
 - For embossed plates for containers and carriages
 - For embossed running boards
 - For ventilation grilles
 - For acoustic panels
 - For filters
 - For radiator covers
 - For luggage racks

- For spark arrestors
- **Cryogenics**
 - For beat diffuser screens
- **Printing Industry**
 - For copying machine drums

Appendix:B

FE Simulation Convergence Summary

Table B.1

Spec. No.	Plate Size (<i>a</i> mm x <i>b</i> mm)	Cutout Size (<i>d</i> mm x <i>d</i> mm)	$p_x = p_y$ (mm)	Simulation no.	No. of nodes	No. of elements	ω_1, (Hz)
5.1	400 x 400	80 x 80	80	1	3309	3086	94.533
				2	12788	12342	94.444
				3	50256	49364	94.411
5.2	500 x 500	100 x 100	100	1	3251	3028	60.496
				2	12556	12110	60.442
				3	109582	108306	60.421
5.3	600 x 600	120 x 120	120	1	3314	3091	42.016
				2	12808	12362	41.975
				3	50336	49444	41.961
5.4	700 x 700	140 x 140	140	1	3235	3011	30.865
				2	12492	12044	30.838
				3	49072	48176	30.828
5.5	800 x 800	160 x 160	160	1	3286	3063	23.631
				2	12696	12250	23.61
				3	49888	48996	23.602

Table B.2

Specimen No.	Plate Size (<i>a</i> mm x <i>b</i> mm)	Cutout Size (<i>d</i> mm x <i>d</i> mm)	Simulation no.	No. of nodes	No. of elements	ω_1, (Hz)
5.8	400x400	133.33 x 133.33	1	1016	931	93.197
			2	3893	3724	93.094
			3	8632	8379	93.065
			4	15233	14896	93.052
5.9	500x500	166.66 x 166.66	1	1081	996	59.627
			2	4153	3984	59.572
			3	9217	8964	59.557
			4	16273	15936	59.550
5.10	600x600	200 x 200	1	1049	964	41.407
			2	4025	3856	41.369
			3	8929	8676	41.359
			4	15761	15424	41.354
5.11	700x700	233.33 x 233.33	1	1033	948	30.423
			2	3961	3792	30.394
			3	8785	8532	30.386
			4	15505	15168	30.383
5.12	800x800	266.66 x 266.66	1	1041	956	23.292
			2	3993	3824	23.270
			3	8857	8604	23.264
			4	15633	15296	23.262

Table B.3

Spec. No.	Plate Size (<i>a</i> mm x <i>b</i> mm)	Perforation Size <i>d</i> (mm)	Simulation no.	No. of nodes	No. of elements	ω_1 (Hz)
6.1	50 x 44.64102	10	1	1497	1339	6676.9
			2	5672	5356	6662.3
			3	12525	12051	6658.6
			4	22056	21424	6657.0
6.2	100 x 89.28203	20	1	1497	1339	1669.2
			2	5672	5356	1665.6
			3	12525	12051	1664.7
			4	22056	21424	1664.3
6.3	150 x 133.9230	30	1	1498	1340	741.77
			2	5676	5360	740.22
			3	12534	12060	739.83
			4	22072	21440	739.66
6.4	200 x 178.5641	40	1	1497	1339	417.30
			2	5672	5356	416.39
			3	12525	12051	416.16
			4	22056	21424	416.07
6.5	250 x 223.2051	50	1	1519	1361	267.03
			2	5670	5444	266.48
			3	12723	12249	266.34
			4	22408	21776	266.28
6.6	300 x 267.8461	60	1	1498	1340	185.44
			2	5676	5360	185.06
			3	12534	12060	184.96
			4	22072	21440	184.92
6.7	350 x 312.4871	70	1	1510	1352	136.25
			2	5724	5408	135.96
			3	12642	12168	135.89
			4	22264	21632	135.86
6.8	400 x 357.1281	80	1	1497	1339	104.33
			2	5672	5356	104.10
			3	12525	12051	104.04
			4	22056	21424	104.02
6.9	450 x 401.7691	90	1	1478	1320	82.422
			2	5596	5280	82.248
			3	12354	11880	82.204
			4	21752	21120	82.185
6.10	500 x 446.4102	100	1	1519	1361	66.757
			2	5670	5444	66.620
			3	12723	12249	66.584
			4	22408	21776	66.570

Table B.4

Specimen No.	Plate Size (<i>a</i> mm x <i>b</i> mm)	Perforation Size, <i>d</i> (mm)	Simulation no.	Number of nodes	Number of elements	ω_1(Hz)
6.11	36.650 x 32.720	7.33	1	14639	12803	608.68
			2	20461	18301	607.40
			3	37547	34413	607.15
6.12	63.355 x 56.732	12.71	1	6563	5788	604.84
			2	24733	23147	601.82
			3	54471	52074	601.02
6.13	154.30 x 137.762	30.86	1	1433	1265	588.79
			2	5396	5058	587.30
			3	11887	11379	586.91
			4	20906	20228	586.74

Table B.5

Specimen No.	d (mm)	(A/A_p)	Simulation No.	No. of nodes	No. of elements	ω_1, (Hz)
Specimens with dimensions (138 mm x 216 mm)						
7.1	5	1518.15	1	2776	2476	692.95
			2	10479	9871	693.38
			3	40632	39408	693.48
7.2	10	379.538	1	2754	2457	694.00
			2	10390	9788	693.90
			3	40276	39064	693.85
7.3	15	168.684	1	2703	2394	695.74
			2	9890	9268	696.16
			3	38268	37016	695.97
7.4	25	60.7262	1	2072	1789	712.18
			2	7720	7146	710.62
			3	29720	28564	710.17
7.5	30	42.1709	1	1980	1691	727.23
			2	7372	6786	725.42
			3	28320	27140	724.94

Table B.6

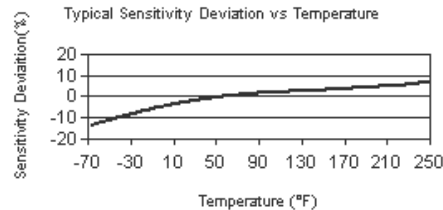
Specimen No.	d (mm)	(A/A_p)	Simulation No.	No. of nodes	No. of elements	ω_1, (Hz)
Specimens with dimensions (276 mm x 432 mm)						
7.6	10	1518.15	1	2768	2455	173.27
			2	10444	9810	173.36
			3	40492	39216	173.37
7.7	20	379.538	1	2718	2420	173.47
			2	10246	9642	173.47
			3	39700	38484	173.46
7.8	25	242.905	1	2535	2231	173.70
			2	9508	8892	173.66
			3	36740	35500	173.65
7.9	50	60.7262	1	2095	1814	177.93
			2	7813	7243	177.62
			3	30092	28944	177.53
7.10	65	35.9326	1	1807	1518	184.23
			2	6646	6060	183.70
			3	25408	24228	183.55

Table B.7

Specimen No.	η_l	Simulation No.	No. of elements	No. of Nodes	ω_1, Hz
Perforation diameter 6mm					
9.1	0.2	2	59185	70473	548.23
		4	81789	95200	547.7
		5	151382	170122	546.52
Perforation diameter 6mm					
9.2	0.6	1	14448	17697	653.45
		2	19356	31838	652.92
		3	25392	30534	652.13
		4	101565	111983	650.33
		5	129983	139998	650.55
Perforation diameter 9mm					
9.3	0.4	1	16040	19906	615.99
		2	23980	28978	614.6
		3	95956	106068	612.71
		4	113489	123066	612.65
		5	144268	156098	615.14
Perforation diameter 12mm					
9.4	0.6	1	2913	3582	645.08
		2	5350	6462	640.02
		3	6373	7644	639.68
		4	25377	27953	639.52
		5	47963	51259	637.93
		6	69921	73563	637.9

Appendix: C, Accelerometer Specifications, Model Number 352C68

Performance	ENGLISH	SI	Optional Versions (Optional versions have identical specifications and accessories as listed for standard model except where noted below. More than one option maybe used.)	
Sensitivity (±10 %)	100 mV/g	10.2 mV/(m/s ²)		
Measurement Range	±50 g pk	±491 m/s ²		
pk Frequency Range (±5 %)	0.5 to 10000 Hz	0.5 to		
10000 Hz				
Frequency Range (±10 %)	0.3 to 12000 Hz	0.3 to 12000 Hz		
Frequency Range (±3 dB)	0.2 to 20000 Hz	0.2 to		
20000 Hz Resonant Frequency	≥35 kHz	≥35		
kHz Phase Response (±5 °) (at 70°F Hz [21°C])	2 to 6000 Hz	2 to 6000		
Broadband Resolution (1 to 10000 Hz)	0.00016 g rms	0.0015 m/s ² rms		
Non-Linearity	≤1 %	≤1 %		
Transverse Sensitivity	≤5 %	≤5 %		
Environmental				
Overload Limit (Shock)	±5000 g pk	±49050 m/s ² pk		
Temperature Range (Operating)	-65 to +200 °F	-53 to +93 °C		
Base Strain Sensitivity	≤0.005 g/με	≤0.05 (m/s ²)/με		
Electrical				
Excitation Voltage	18 to 30 VDC	18 to 30 VDC		
Constant Current Excitation	2 to 20 mA	2 to 20 mA		
Output Impedance	≤300 ohm	≤300 ohm		
Output Bias Voltage	8 to 12 VDC	8 to 12 VDC		
Discharge Time Constant	0.8 to 2.4 sec	0.8 to 2.4 sec		
Settling Time (within 10% of bias)	<10 sec	<10 sec		
Spectral Noise (1 Hz)	60 μg/√Hz	588 (μm/sec ²)/√Hz		
Spectral Noise (10 Hz)	16 μg/√Hz	157 (μm/sec ²)/√Hz		
Spectral Noise (100 Hz)	5 μg/√Hz	49 (μm/sec ²)/√Hz		
Spectral Noise (1 kHz)	1.5 μg/√Hz	14.7 (μm/sec ²)/√Hz		
Physical				
Sensing Element	Ceramic	Ceramic		
Sensing Geometry	Shear	Shear		
Housing Material	Titanium	Titanium		
Sealing	Welded Hermetic	Welded		
Hermetic				
Size (Hex x Height)	9/32 in x 0.73 in	9/32 in x 18.5 mm		
Weight	0.070 oz	2.0 gm		
Electrical Connection Position	Top			
	Top Mounting Thread	5-40		
Male	5-40 Male			
Mounting Torque	8 to 12 in-lb	90 to 135 N-cm		



[5]

All specifications are at room temperature unless otherwise specified.

In the interest of constant product improvement, we reserve the right to change specifications without notice.

A - Adhesive Mount
 Supplied Accessory: Model 080A90 Quick bond Gel (for use with accelerometer adhesive mtg bases to fill gaps on rough surfaces) replaces Model 080A15

HT - High temperature, extends normal operation temperatures

Frequency Range (5 %)	5 to 10000 Hz	5 to 10000 Hz
Frequency Range (10 %)	3 to 12000 Hz	3 to 12000 Hz
Frequency Range (3 dB)	2 to 20000 Hz	2 to 20000 Hz
Broadband Resolution (1 to 10000)	0.0002 g rms	0.002 m/s ² rms Hz)
Temperature Range (Operating)	-65 to +250 °F	-54 to +121 °C
Discharge Time Constant	0.08 to 0.24 sec	0.08 to 0.24 sec
Spectral Noise (1 Hz)	75 μg/√Hz	736 (μm/sec ²)/√Hz
Spectral Noise (10 Hz)	25 μg/√Hz	245 (μm/sec ²)/√Hz

J - Ground Isolated

Frequency Range (5 %)	0.5 to 8000 Hz	0.5 to 8000 Hz
Frequency Range (10 %)	0.3 to 10000 Hz	0.3 to 10000 Hz
Frequency Range (3 dB)	0.2 to 16000 Hz	0.2 to 16000 Hz
Resonant Frequency	≥30 kHz	≥30 kHz
Electrical Isolation (Base)	≥10 ⁸ ohm	≥10 ⁸ ohm
Size (Hex x Height)	3/8 in x 0.75 in	3/8 in x 19.1 mm
	0.1 oz	2.8 gm

M - Metric Mount
 Mounting Thread M3 x 0.50 Male (M3 x 0.50 Male) Supplied
 Accessory: Model M080A15 Metric adhesive base, 0.31" hex x 0.125" thk, M3 x 0.50 thd, aluminum with insulating hardcoat finish replaces Model 080A15

W - Water Resistant Cable

Electrical Connector	Sealed Integral	Sealed Integral Cable
		Cable
Electrical Connection Position	Side	Side

Notes
 [1] Typical.
 [2] 200°F to 250°F data valid with HT option only. [3] Zero-based, least-squares, straight line method. [4] Transverse sensitivity is typically ≤ 3%.
 [5] See PCB Declaration of Conformance PS023 for details.



Supplied Accessories
 080A109 Petro Wax (1)
 080A15 Adhesive Mounting Base (1)
 ACS-1 NIST traceable frequency response (10 Hz to upper 5% point). (.)

Entered: ECB	Engineer: BAM	Sales: WDC	Approved: JJB	Spec Number:
Date: 12/12/2009	Date: 12/12/2009	Date: 12/12/2009	Date: 12/12/2009	8337



3425 Walden Avenue
 Depew, NY 14043 UNITED STATES
 Phone: 888-684-0013
 Fax: 716-685-3886
 E-mail: vibration@pcb.com Web site: www.pcb.com

Appendix:C, Impact Hammer Specifications, Model Number 086C03

<p>Performance</p> <p>Sensitivity (±15 %) Measurement Range Resonant Frequency Non-Linearity</p> <p>Electrical</p> <p>Excitation Voltage Constant Current Excitation Output Impedance Output Bias Voltage Discharge Time Constant</p> <p>Physical</p> <p>Sensing Element Sealing Hammer Mass Head Diameter Tip Diameter Hammer Length Electrical Connection Position Extender Mass Weight Electrical Connector</p>	<p>ENGLISH</p> <p>10 mV/lbf ±500 lbf pk ≥22 kHz ≤1 %</p> <p>20 to 30 VDC 2 to 20 mA <100 ohm 8 to 14 VDC ≥2000 sec</p> <p>Quartz Epoxy 0.34 lb 0.62 in 0.25 in 8.5 in Bottom of Handle 2.6 oz BNC Jack</p>	<p>SI</p> <p>2.25 mV/N ±2224 N pk ≥22 kHz ≤1 %</p> <p>20 to 30 VDC 2 to 20 mA <100 ohm 8 to 14 VDC ≥2000 sec</p> <p>Quartz Epoxy 0.16 kg 1.57 cm 0.63 cm 21.6 cm Bottom of Handle 75 gm BNC Jack</p>	<p>Optional Versions (Optional versions have identical specifications and accessories as listed for standard model except where noted below. More than one option maybe used.) T - TEDS Capable of Digital Memory and Communication Compliant with IEEE P1451.4 TLD - TEDS Capable of Digital Memory and Communication Compliant with IEEE 1451.4</p> <p>Notes</p> <p>[1] Typical. [2] See PCB Declaration of Conformance PS068 for details.</p> <p>Supplied Accessories</p> <p>081B05 Mounting Stud (10-32 to 10-32) (2) 084A08 Extender - Steel, 0.6" Diameter (1) 084B03 Hard Tip- Hard (S.S) (1) 084B04 Hammer Tip- Medium (White Plastic) (1) 084C05 Hammer Tip- Soft (Black) (2) 084C11 Hammer Tip- Supersoft (Red) (2) 085A10 Vinyl Cover For Medium Tip (Blue) (2) HCS-2 Calibration of Series 086 instrumented impact hammers (1)</p>										
 [2]													
<p><i>All specifications are at room temperature unless otherwise specified.</i> In the interest of constant product improvement, we reserve the right to change specifications without notice. ICP® is a registered trademark of PCB group, Inc.</p>													
<table border="1" style="border-collapse: collapse; width: 100%;"> <tr> <td style="padding: 2px;">Entered: LLH</td> <td style="padding: 2px;">Engineer: DJS</td> <td style="padding: 2px;">Sales: JJM</td> <td style="padding: 2px;">Approved: EB</td> <td style="padding: 2px;">Spec Number:</td> </tr> <tr> <td style="padding: 2px;">Date: 02/24/2010</td> <td style="padding: 2px;">Date: 12/08/2009</td> <td style="padding: 2px;">Date: 02/17/2010</td> <td style="padding: 2px;">Date: 02/17/2010</td> <td style="padding: 2px; text-align: center;">15273</td> </tr> </table>				Entered: LLH	Engineer: DJS	Sales: JJM	Approved: EB	Spec Number:	Date: 02/24/2010	Date: 12/08/2009	Date: 02/17/2010	Date: 02/17/2010	15273
Entered: LLH	Engineer: DJS	Sales: JJM	Approved: EB	Spec Number:									
Date: 02/24/2010	Date: 12/08/2009	Date: 02/17/2010	Date: 02/17/2010	15273									
<div style="display: flex; align-items: center;">  <div> <p>3425 Walden Avenue Depew, NY 14043 UNITED STATES Phone: 888-684-0013 Fax: 716-685-3886 E-mail: vibration@pcb.com Web site: www.pcb.com</p> </div> </div>													

Appendix:C

Larson and Davis, ViRT 3000+ ,FFT Analyser Specifications

Input		Digital Output and Control	
Measuring Range:	-10 to 172 dB SPL with proper transducer	Printer Output:	Centronics Parallel Port for use with HP compatible laser and Epson compatible dot matrix printers.
Impedance:	10 Gohm/0.5 pF with preamp 100 Kohm/60 pF direct input	Computer Interface:	RS-232 hi-speed parallel ports
Polarization Voltage:	0, 28, 200 VDC	I/O Port:	3 A/D inputs (0-5V) (8 bit); 2 optical input ports, 2 optical output ports
Connector:	5-pin miniature switchcraft or 7-pin LEMO	Analog Outputs	
Gain:	-30 to 90 dB in 10 dB steps	AC output:	5 volt full scale
Highpass/Lowpass Filters:	3-pole chebyshev	DC output:	0-5 volts
Highpass:	1 Hz, 20 Hz	Display Characteristics	
Lowpass:	10 kHz, 20 kHz	Internal LCD:	Flat panel, supertwist with anti-reflective treatment.
A-weight and C-weight Filters:	Meets ANSI S1.4-1983 Type 1, IEC651 Type 1, and IEC 804 Type 1	Backlighting:	Electroluminescent
Digital Characteristics		Contrast:	Adjustable from dark to full sunlight
Digitization:	16-bit A:D per channel	Size:	2.6 inches (6.60 cm) x 9.3 inches (23.62 cm)
Anti-aliasing:	Oversampled delta-sigma conversion offers anti-aliasing stopband rejection > 96 dB	Resolution:	128 X 489, with full graphics and alphanumeric
Detector:	Digital true RMS with 0.1 dB resolution	Environmental Specifications	
Dynamic Range:	> 80 dB (> 100 dB using WDR SLM)	Operating Temperature:	13 to 122 degrees F (-10 to 50 degrees C)
Amplitude Stability:	+/- 0.1 dB	Storage Temperature:	-13 to 158 degrees F (-25 to 70 degrees C)
Amplitude Linearity:	The greater of +/- 0.05 dB or +/- 0.005% of the maximum input signal	Relative Humidity (non-condensing):	90% max at 104 degrees F (40 degrees C)
Digital Averaging		Physical Characteristics	
Octave Bandwidths:	Linear Single: 0.0025 sec's to 278 hours Linear Repeat: 0.0025 sec's to 278 hours Exponential: 1/64 sec to 512 sec's, binary sequence BT/Exponential: 1 to 32,768 BT products, binary sequence, Exponential averaging BT/Lin: 1 to 32,768 BT products, binary sequence Linear averaging Linear single, linear repeat, exponential, exponential by N (number of spectra), Count single (number of spectra), Count repeat (number of spectra), Count manual (number of spectra, Manual accept)	Size:	11" wide X 7.75" high X 2.4 " thick
FFT Bandwidths:	Count repeat (number of spectra), Count manual (number of spectra, Manual accept)	Weight:	7.5 lb. (3.4 kg)
Memory		Power	
	780KB Standard Memory sufficient to store up to: 2976 1/3 octave spectra or 426 800-line FFT spectra	Internal	
Filters		Battery Power:	Removable NiCd pack supplied with 3000+
Octave and Fractional Octave:	1/1 and 1/3 octave real-time digital filters meeting or exceeding requirements for ANSI s1.11-1986 Type 0-AA and Type 1-D (user selectable), IEC 225, IEC 1260 Class 0 (3 Hz to 12.5 kHz), Class 1 (1 Hz to 20 kHz). Lower Frequency Limit of 1 Hz. Upper Frequency Limit of 20 kHz (2-channel)	Operating time:	4 hours (less with disk drive & sig. generator)
FFT:	100, 200, 400 line FFT analysis Maximum real-time frequency of 20 kHz (1 or 2 channels) 800 line FFT analysis (single channel only) to 20 kHz	Internal smart charger:	< 15 hours; external charger < 3.5 hours
Zoom Capability:	Real-time zoom X256 Buffered (non-real-time) Zoom X64 (1 channel) and X32 (2 channels)	External	
Time Domain Windows (FFT analysis):	Rectangular, Hanning, Flat-Top, ZeroPad, Impact and Exponential	Voltage range:	11-16 Vdc
Triggering:	Continuous (free-run), Digital remote (via interface), Frequency domain; level in selected frequency band Time domain; level in channel 1 (-99% to +99% full scale) Adjustable ch 1 delay (+/-), adjustable ch2 delay w/r to ch1 (+ only)	Typical current:	.75 Amp @ 12 V
		Connector:	5.5 mm x 2.5 mm coaxial power plug
		Optional System Configurations	
		2800-OPT 01	7-pin LEMO™ input connectors
		2800-OPT 10	Internal white and pink noise generator
		2800-OPT 11	Advanced internal digital signal generator
		2800-OPT 90-4	4 MB CMOS memory expansion module
		2800-OPT 225	Classification Lines
		2900-OPT 80	Sound Intensity
		2900-OPT 81	Maximum Length Sequence (MLS)
		Accessories	
		OPTIONAL:	Accelerometer: ICP® & charge coupled
		CCS008: Conforming soft case	TAC100: Tachometer
		CCS007: Carrying case for 3000+ and accessories	CBL117: RS232 serial computer interface cable
		3000-Stand: Holds 3000+ on a desktop	CBL126: Hi-speed parallel computer interface cable
		DVX003: External disk drive	CBL049: Connects the 3000+ to a cigarette lighter
		BAT007: Rechargeable NiCd	Software: RTAUTIL32 & DNA
		PSA013: External NiCd battery charger	
		2226: Twelve channel external microphone multiplexer	INCLUDED : Reference and training manuals
		PRM951-L2: ICP® accel. preamp, 2mA	EXC1.5 extension cable
		PRM951-L4: ICP® accel. preamp, 4mA	PSA003 or PSA004 power supply
		ADP012: Direct input adapter	CCS004 soft shell carrying case
		ADP006: BNC to 1/2 inch preamp adapter	1/8 inch phone plug
		ADP007: Microdot to 1/2 inch preamp adapter	3 amp spare fuse
		2260: Sound intensity probe	
		Microphone: 1/4, 1/2, and 1 inch condenser, 1/2" electret	

Appendix:C

The Spider-81 Vibration Controller System Specifications

Product Specifications:

- **Analog Inputs:** 8 BNC connectors per Spider-81 vibration test controller. Spider-81 and Spider-80X front-ends can be networked to form a 128 channel count system. Charge, voltage or IEPE, single-ended or differential, AC or DC coupling, 150 dBFS dynamic range, 24-bit A/D converters, range ± 20 volts, up to 102.4 kHz fs per channel, 8 BNC connectors per Spider-81 front-end.
- **Analog Outputs:** 2 BNC connectors per unit, 100 dB dynamic range, 24-bit A/D converters. ± 10 volts
- **Channel Phase Match:** Better than ± 1.0 degree up to 20 kHz among all channels
- **Peripherals:** 8 isolated DIO; 10 monitoring channels, LCD display with navigation buttons, RS-485, ground connection, abort contact switch, start and abort buttons
- **Dimensions:** 440 x 66 x 330 mm (WxHxD)
- **Weight:** 4.2 kg
- **Power:** Up to 18 watts during operation.
- **Computer Connections:** 100Base-T, RJ45 female connector supports connection to computer or network switch
- **Internal Memory:** Flash memory for data storage is 4 GB per unit
- **Operation Modes:** Connected to computer or stand alone Black Box mode.

Appendix: D

Damping factors obtained from the half power bandwidth method

Speci. No.	MRR	ω_1 (Hz)		ζ_1	ω_2 (Hz)		ζ_2	ω_3 (Hz)		ζ_3
		Experi.	FEM		Experi.	FEM		Experi.	FEM	
4.1(Solid)		663.071	693.62	0.0105	974	1040.5	0.0069	1492.187	1631.5	0.0047
Rectangular Perforation pattern circular perforations										
8.11/7.11		650	693.38	0.0148	972.656	1038.3	0.0114	1535.156	1623.3	0.0065
8.12/7.12		637	693.85	0.0106	929.687	1033.6	0.00757	1468.75	1605.9	0.0045
Rectangular Perforation pattern square perforations										
5.6		537.5	590.37	0.0118	831.25	896.02	0.00756	1306	1413.4	0.006
Staggered 60° perforation pattern square perforations										
6.14		575	608.64	0.0116	856.25	913.11	0.00766	1368	1429.4	0.0047
6.15		545	586.87	0.0114	868.75	911.50	0.00816	1268.8	1349.6	0.00656
Rectangular Perforation pattern circular perforations										
9.1		590.7	546.52	0.0151	954.949	828.88	0.0112	1191.714	1296.3	0.0125
9.2		616.714	650.33	0.0111	895.285	963.26	0.009	1393.714	1498	0.0052
9.3		571	612.65	0.0116	827.428	910.77	0.0100	1253.857	1416.5	0.0124
9.4		586.571	637.9	0.0111	891	976.04	0.00923	1435.143	1549.3	0.0052

List of Publications

1. Publications in International Journals Related to Thesis Work

- [1] Mali K.D., Singru P.M. (2012). An analytical model to determine fundamental frequency of free vibration of perforated plate by using unit step functions to express non homogeneity. *Journal of Vibroengineering* 14(3):1292-1298.
- [2] Mali K.D., Singru P.M. (2013). An analytical model to determine fundamental frequency of free vibration of perforated plate by using greatest integer functions to express non homogeneity. *Advanced Materials Research*, 622-623:600-604.
- [3] Mali K.D., Singru P.M. (2012). Determination of the fundamental frequency of perforated plate with rectangular perforation pattern of circular holes by negative mass approach for the perforation. *International Journal of Advanced Materials Manufacturing and Characterization* 1(1):105-109, ISSN-2277-3886.
- [4] Mali K.D., Singru P.M. (2013). An analytical model to determine fundamental frequency of rectangular plate having rectangular array of circular perforations". *Journal of Vibroengineering* 15(2):588-596.
- [5] Mali K. D., & Singru P. M. (2013). Determination of the fundamental Frequency of perforated rectangular plates: Concentrated negative mass approach for the perforation. *Advances in Acoustics and Vibration*, vol. 2013 .
- [6] Mali K.D., Singru P.M., Determination of modal constant for fundamental frequency of perforated plate by Rayleigh's method using experimental values of natural frequency. *International Journal of Acoustics and Vibration*.(Accepted)

2. Papers Presented at International Conferences Related to Thesis Work

- [1] Mali K.D., Singru P.M. "Determination of the fundamental frequency of perforated plate with rectangular perforation pattern of circular holes by negative mass approach for the perforation" Proceedings of the International conference on Materials, Processing and Characterization(ICMPC 2012), GRIET Hyderabad , Andra Pradesh, March 8-10, 2012.
- [2] Mali K.D., Joshi P.S., Singru P.M. "Free vibration analysis of simply supported rectangular plates with rectangular perforation pattern of square holes". Proceedings of the 57th congress of the Indian Society of Theoretical and Applied Mechanics (An international meet), held at Defence Institute of Advance Technology, Pune, on Dec. 17-20, 2012.

Brief Curriculum Vitae

Mr. Kiran D. Mali is currently a faculty at Dept. of Mechanical Engineering BITS-Pilani, K. K. Birla Goa Campus. He has completed his Masters Degree in Design Engineering, M.E.(Mech) Design Engg, from Shivaji University, Kolhapur in 2006. He joined BITS-Pilani, K K Birla Goa Campus in May 2007. His research areas include vibration analysis of structural components, experimental and analytical.

Dr. Pravin Singru is Associate Professor, Mechanical Engineering Department. He obtained his M. Tech. from IIT, Kharagpur and Ph.D. from Visvesvaraya National Institute of Technology, Nagpur. His doctoral thesis was on "Dynamic and Vibration Response of Pulleys of a Belt Drive". Dr. Singru has more than 22 years of teaching experience. He teaches courses in the area of Mechanics of solids, Kinematics and Dynamics of Machines, Vibrations & MEMS. Dr. Singru has been associated with BITS Pilani administration as Associate Dean Practice school at BITS Pilani, K K Birla Goa Campus, Member of selection committee for non-teaching staff, Faculty In charge (Workshop), Nucleus Member of Placement and Practice School Division, Member of Task Force for Mission 2012. He is actively involved in the curriculum redesign of Mechanical Engineering Program of BITS Pilani University. He has been guided six research scholars for their research leading to Ph.D. degree of the Institute. He has published more than 19 research papers in International Journals and 36 papers in National & International Conferences. He is reviewer of 5 International Journals. He has organized Indo-Russian work shop on Topical Problems in Solid Mechanics, sponsored by DST and Russian Academy of Sciences, Nov, 2008. He has delivered talks on invitation from various Institutions in India. Dr. Singru is Coordinator of National center for MEMS design with 30 lakhs grant. Under his leadership, department has received Rs. 80 lakhs grant from DST under FIST Scheme. He was organizing secretary of International Conference on Emerging Miniaturized Technology Micro to Nano (EMTM2N-2013), conducted in February 2013.